This is to certify that the

dissertation entitled
Rapid-Scanning Stopped-Flow Studies
of Tryptophanase
Activation/Deactivation by
Sudden Addition/Removal of
Potassium Ions
presented by

Iraj Behbahani-Nejad

has been accepted towards fulfillment
of the requirements for

____Ph.D.____ degree in __Chemistry__

James L. Dye

Ɉames L. Dye

Major professor

Date__October 20, 1987__

0-12771

RAPID-SCANNING STOPPED-FLOW STUDIES OF

TRYPTOPHANASE ACTIVATION/DEACTIVATION BY

SUDDEN ADDITION/REMOVAL OF POTASSIUM IONS

By

Iraj Behbahani-Nejad

AN ABSTRACT OF A DISSERTATION

Submitted to
Michigan State University
in partial fulfillment of the requirements
for the degree of

DOCTOR OF PHILOSOPHY

Department of Chemistry

1986

To My Wife, Lili

for her Everlasting Love

ACKNOWLEDGMENTS

ABSTRACT

RAPID-SCANNING STOPPED-FLOW STUDIES OF

TRYPTOPHANASE ACTIVATION ⁻ACTIVATION BY

SUDDEN ADDITION/REMOVAL OF POTASSIUM IONS

By

Iraj Behbahani-Nejad

Rapid scanning and fixed-wavelength stopped-flow spectrophotometry were used to study the activation/deactivation of tryptophanase by sudden addition/removal of potassium ions with the aid of a crown-ether or cryptand. Tryptophanase catalyzes α,β-elimination reactions of amino acid substrates, and requires activating monovalent cations, such as K^+, for catalytic activity. An additional requirement is a prosthetic group, pyridoxal-5'-phosphate (PLP) with which it covalently forms a Schiff's base. The active holoenzyme has absorption maxima at 337 nm and 420 nm, whose relative amplitudes depend on both pH and the monovalent cation activator used. A 420 nm absorption band also dominates the spectrum of the K^+-free (inactive) enzyme. An amino acid substrate or inhibitor, added to the active enzyme, forms a quinonoid by α-elimination, with an intense absorption maximum at ∿500 nm. For true substrates, β-elimination finally yields pyruvate and ammonia. With inhibitors, however, the reaction stops at the quinonoid.

Iraj Behbahani-Nejad

Two well known complexants of potassium ion, 18-crown-6 and cryptand [2.2.2], were used to suddenly reduce the concentration of free K^+ in an enzyme solution. In deactivation by 18-crown-6 at pH 8.70, a single exponential fit most of the absorbance change with a rate constant proportional to the square of the 18-crown-6 concentration. This strongly suggests that two K^+ ions per subunit are required for activation. In activation experiments at the same pH, even at saturating K^+ concentrations, only about 50% of the original absorbance at 337 nm was recovered although enzymatic activity was completely restored. This suggests that substrate or inhibitor, in addition to K^+, are required to completely reverse the deactivation brought about by depletion of potassium. The activation kinetics data showed that the growth of absorbance at 337 nm is triphasic at saturating K^+ concentrations, and quantitatively matches the decay at 420 nm after a small fast growth at this wavelength. The results suggest "kinetic anticooperativity" in the enzyme protomers upon binding potassium.

Tryptophanase activation and deactivation were also studied in the presence of L-ethionine, a competitive inhibitor of the enzyme. The decay of absorbance at 508 nm and growth at 420 nm upon deactivation were monophasic (95% of the change) and the 1st-order rate constant was inversely proportional to the square of the free K^+ concentration. This dependence again suggests that two K^+ ions per subunit are required for activation. The reverse process, however, was found to be triphasic at saturating K^+ concentrations. The data were again explained on the basis of kinetic anticooperativity in the binding of potassium ion to the enzyme.

Iraj Behbahani-Nejad

The method of weighted principal component analysis (PCA) was used to resolve the 3-dimensional data surface obtained by the scanning stopped-flow method. In the deactivation in the absence of ethionine (Chapter III), the absorbance-wavelength-time data surface was resolved into the spectral shapes and time courses of the independent components. Spectral shapes obtained by PCA for the 337 and 420 nm absorbers agree well with the reported assignments for the components of the enzyme. PCA analysis was also performed for the activation experiments (Chapters IV and V); however, only partial resolution was obtained due to an insufficient number of target absorbers.

TABLE OF CONTENTS

LIST OF TABLES

LIST OF FIGURES

xi

xiii

CHAPTER I

INTRODUCTION

A. A Brief Review on Catalysis by Pyridoxal-P and Pyridoxal-P

Enzymes

All living organisms use pyridoxal-phosphate (PLP vit. B_6), the
biochemically functional form of vitamin-B_6, to synthesize, degrade,
and interconvert amino acids. Although this versatile coenzyme en-
ables proteins to perform a class of different reactions such as race-
mization, transamination, decarboxylation, and α,β elimination reac-
tions (1,2), most of these processes depend on a common structural
and mechanistic principle. In addition, pyridoxal and pyridoxal-p
alone catalyze similar reactions in the complete absence of the enzymes
requiring this cofactor (3).

The reaction of pyridoxal-p with amino acids is generally believed
to occur through formation of a Schiff base intermediate between the
carbonyl group of pyridoxal-p and the α-amino group of amino acid
substrates (4,5,6,7) according to reaction (I.1): The specific role
of pyridoxal-p in the reaction is then to promote electron withdrawal
from the α-carbon of the bound amino acid leading to the cleavage of
the bonds, C^α-H(α-elimination), C^α-COO⁻ (decarboxylation), C^β-Y (β-
elimination and β-replacement) of this intermediate. In general,

1

$$R-\overset{\underset{\displaystyle Y}{|}}{CH}-\overset{\underset{\displaystyle NH_3^+}{|}}{\overset{\displaystyle H}{C}}-COO^-$$

(I.1)
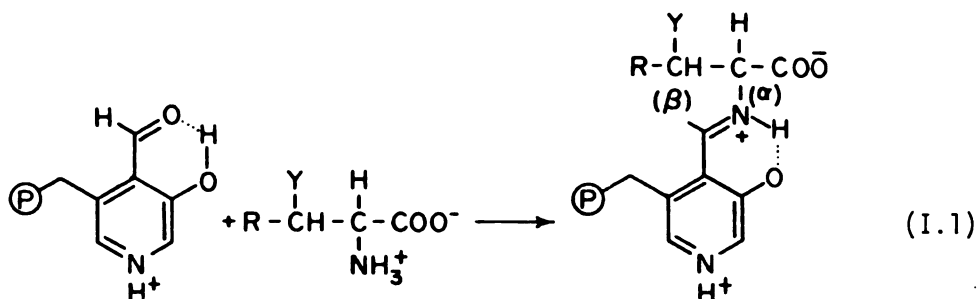
reactions occurring in the amino acid moieties of these Schiff bases
are influenced by two major factors: (1) The electron-withdrawing
effect of the pyridine ring, which may be further amplified by protona-
tion of pyridinium nitrogen in acidic solution; (2) The electron-with-
drawing effect of the azomethine nitrogen that contains a covalently
bound proton. This covalent bonding which is somewhat strengthened
by hydrogen-bonding to the adjacent carboxylate and phenolic oxygen,
exerts a strong electron-withdrawal effect on the carbon atoms adjacent
to the azomethine nitrogen, a factor which is believed to be respon-
sible for a large fraction of the catalytic effect observed in the
aldimine-type structure. Also because of the proximity of this (N-H)
covalent bonding to the α-carbon of the imino acid, the effect of this
electron-withdrawing group may be greater than that of the pyridine
ring.

The mode of binding of pyridoxal-p and its derivatives to proteins
has been investigated by a number of physiochemical techniques (8,9,
10). Although large differences in behavior exist among the various
B_6-dependent enzymes, in every PLP-dependent enzyme examined so far,

the ε-amino group of a lysine residue at the active site binds the co-
factor as a Schiff base (11,12,13). Treatment of a number of PLP
enzymes with sodium borhydride followed by enzymatic digestion has
led to the isolation of pyridoxal-lysine compound which strongly supports
this postulate (14,15,16,17,18). Very little, however is known about
the nature of the bonds formed between the other groups of the coenzyme
and the apo-enzymes.

Mechanism of Catalysis: A general mechanism for pyridoxal-p cata-
lyzed reactions was proposed independently by Snell (19) and Braunstein
(20) and was later supported by other studies (21,22). This mechanism
emphasizes the function of pyridoxal-p in weakening the sigma bonds
around the α-carbon of the bound amino acid because the conjugated pyri-
dine system acts as an electron-sink especially if the ring nitrogen
is protonated. Scheme I (Figure I.1) shows the probable reaction se-
quence for the diprotonated form of the Schiff base in the case of
labilization of the α-hydrogen for the α,β-elimination and β-replace-
ment reactions.

The first step in each case is formation of an aldamine Schiff base
(Structure I, Scheme I) between a substrate amino acid and pyridoxal-p
by transaldiminization reaction (I.1)(12). The next step in the reac-
tion sequence involves dissociation of the α-proton to give the inter-
mediate indicated by Structure II. The driving force for this reaction
is explained by the gain of delocalization energy upon formation of
the intermediate II due to the contribution of a quinonoid structure
resonance form which characteristically absorbs at around 500 nm (23).
Following the labilization step, the quinonoid Structure II can then
eliminate the β substituent to form a bound α-amino-acrylate Complex

Figure I.1. Reaction sequence of PLP-catalyzed α,β-elimination and β-replacement reactions.

5

(Scheme I)

Figure I.1.

III. The resulting unsaturated imine (III) can either add a different nucleophile than the one eliminated (β-replacement), or it can be converted to an α-imino acid (Structure IV, Scheme I). Since such imino acids are unstable in aqueous solutions, they subsequently undergo non-enzymatic hydrolysis to produce an α-keto acid and ammonia. It should be emphasized that the establishment of cationic character at substrate carbon β to nitrogen in intermediate III (resonance form of III in Scheme I) further facilitates α,β-elimination and β-replacement reactions.

What then is the function of the protein in catalysis? A "classical" answer to this question is that the enzymes provide a rate enhancement and specificity which is certainly unattainable in their absence in model system reactions. Their major functions perhaps include increased acid-base catalysis (a single base on the active site of aminotransferases facilitates the α-proton abstraction) (24,25), anchoring of the phosphate group of the coenzyme (26,27,28,29), and recognition of the correct reaction partners. Dunathan postulated that PLP enzymes orient the bond to be broken in the Schiff base complex orthogonal to the plane of the conjugated system, since this conformation of the breaking σ bond achieves maximal orbital overlap with the π system of the SB complex (30,31). The principle that bonds parallel to the π-plane are more labile than those not so aligned, has also been used by other workers (32). Later studies by Floss et al. (33,34) with model systems showed the non enzymatic rate of α-hydrogen exchange in pyridoxal Schiff bases is determined by the proportion of conformer having the C^{α}-H bond orthogonal to the π-system.

Therefore, it follows that the PLP-dependent enzymes control the reaction specificity by controlling the conformation about the $N-C^{\alpha}$ bond of the Schiff's base intermediate.

Several reviews of other aspects of this subject are available. Examples are the following: Metzler et al. (35,36,37) and Morozav et al. (38,39) on optical and luminescence properties and band shape analysis of vitamin-B_6 derivatives; Martel (4), Fasella (11) and Davis (40) on PLP reaction pathways; Perault et al. (23) on the electronic aspect of the PLP reactions; Dunathan (30,31) and Floss et al. (33,34) on the stereochemistry of PLP-catalyzed enzyme reactions.

B. Tryptophanase

The production of indole during protein decomposition has been known since the work of Nenki (41) and Kuhne (42) in 1875. The source of this compound, however, was unknown until Hopkins and Cole (43) showed in 1903 that it was produced by bacterial decomposition of the newly isolated (44) amino acid, tryptophan. In 1935, Happold and Hoyle (45) identified tryptophanase as the enzyme responsible for the production of indole in bacterial cells. Subsequent studies by Happold, Struyvenberg (46) and Wada (47) demonstrated that tryptophanase requires NH_4^+, K^+ or Rb^+ for enzymatic activity, and was inhibited by Na^+ or Li^+. In 1947, Wood, Gunsalus and Umbreit (48) discovered that tryptophanase also requires the coenzyme pyridoxal-phosphate and that indole, pyruvate and ammonia are formed in stoichiometric amount from L-tryptophan. Summarizing the data available by 1954 allows one to formulate the reaction catalyzed by crude, cell-free

preparations of tryptophanase as:

$$\text{L-Tryptophan} + H_2O \xrightarrow[\text{PLP, } NH_4^+]{\text{Tryptophanase}} \text{Indole} + \text{Pyruvate} + NH_3$$

$$(I.2)$$
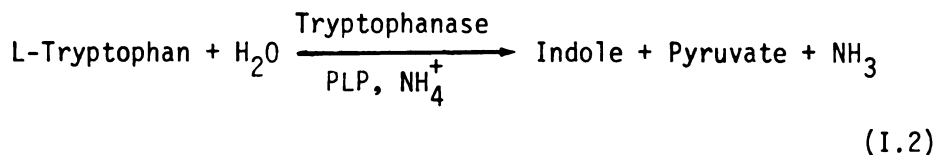
Early studies of this topic are reviewed by Happold (49) and
Wada (50) while a review by Snell (51) covers the studies up to
1975.

B.1. Enzyme Source

Tryptophanase is believed to play a catabolic role in metabolism,
perhaps by regulating the intracellular concentration of tryptophan
(51). Tryptophanase is present in very small amount in cells grown
without tryptophan, but it can be induced to comprise as much as
10% of the soluble cell protein (51,52).

In order to produce pure tryptophanase, free from tryptophan syn-
thetase, Newton and Snell (53) developed a constitutive strain of
Escherichia Coli called B/1t7A. This mutant lacks the genes for
tryptophan synthetase (54) and hence tryptophan for protein (trypto-
phanase) synthesis must be obtained by reversal of reaction I.2.
This strain produces large amounts of tryptophanase (up to 10% of
the soluble protein) under proper cultural conditions (55,57) and it
was first used by Newton and Snell (56) to obtain homogeneous crystal-
line tryptophanase.

B.2. Structural Properties

B.2.1. Subunit Structure - Tryptophanase (M_x = 220,000) from
E-Coli Blt7/A is a tetrameric enzyme composed of four identical sub-
units (58,59). The four subunit model of tryptophanase obtained from
hydrodynamic studies is also confirmed by electron micrographs of
the enzyme which show four subunits arranged in a square planar rather
than a tetrahedral configuration (59). From thermodynamic studies on
the dissociation of tryptophanase into its apoprotomers, Morino and
Snell (59,60) conclude that both hydrophobic and ionic forces are
important in maintaining the quaternary structure of apotryptophanase.
Dissociation of the enzyme into its subunits and the reverse process
are highly dependent on temperature, ionic environment, concentration.
pH, and the presence or absence of the coenzyme pyridoxal-P (59,60).
Snell and Goldberg showed that each subunit contains a single peptide
chain (61).

B.2.2. PLP Binding - Apotryptophanase is catalytically inactive
in the absence of added pyridoxal-phosphate (62). In the presence of
PLP, however, the apoenzyme binds one coenzyme moiety per subunit in
an azomethine linkage to an ϵ-amino group of a lysine residue at the
active site; that is, 4 pyridoxal-p are bound per molecule of native
tetrameric enzyme (58,63,64). The four binding sites appear to be
equivalent since only one major peptide containing the pyridoxal group
was found upon reduction of holotryptophanase (65,66). Similar to
other PLP dependent enzymes, the coenzyme can be resolved from the

holoenzyme by addition of penicillamine (59), cysteine (67) or high concentrations of ammonium salts (68), all of which form thiazolidine derivatives with pyridoxal-p.

Extensive ultracentrifugation studies on both holo- and apoenzymes by Snell and coworkers (59,69) showed that a large conformational change accompanies the binding of PLP by apotryptophanase. This conformational change results in a more compact structure such that the coenzyme becomes "locked" in the holoenzyme and increases its stability to denaturation by sodium dodecyl sulfate (59), heat (69,70) and changes in pH. Goldberg et al. (71,72) showed that fixation of the first two pyridoxal-p molecules to the apoprotomers results in a decrease in binding rate of the two remaining apoprotomers but each protomer, once saturated with the coenzyme, exhibits the same catalytic properties independent of the state of saturation of the surrounding protomers.

B.2.3. <u>Monovalent Cation Specificity</u> - The requirement of certain monovalent cations by some enzymes to express their optimum catalytic activity was reported over 40 years ago by Boyer and coworkers (73). Since that time, more than 60 different enzymes including tryptophanase have been found to require these ions (74,75). In some cases partial activity is observed while in other cases no activity is expressed in the absence of these cations. Extensive studies by Snell (56), Happold (49), and Wada (50) revealed that tryptophanase requires NH_4^+ or K^+ while Na^+ and Li^+ have essentially no activating effect. Tl^+ can also replace K^+ and has a greater affinity and Rb^+ also activates the enzyme but less effectively than K^+ (46).

Reviewing a number of studies of the activation of tryptophanase by monovalent cations, Snell (51) finds that both K^+ and Na^+ are equally effective in permitting the dissociation of tetrameric to dimeric apotryptophanase at low temperatures. This effect thus seems unlikely to serve as a basis for their markedly different catalytic effects. Toraya et al. (76) carried out gel filtration studies on the effect of various monovalent cations on the binding of the coenzyme and their relation to catalytic activity. They found that NH_4^+, K^+ and Rb^+, which are good activators, enhanced the binding constant for the coenzyme while enzyme in presence of the poor activators Na^+, Li^+ and Cs^+ showed a lower affinity for pyridoxal-p. The dissociation constant was >31 μM and 1.8 μM in the presence of Na^+ and K^+, respectively. They hence concluded that activating monovalent cations play an essential role in formation and maintenance of the firm binding of PLP to apoenzyme. This conclusion is also supported by the work of Happold (46) who showed that removal of K^+ ions from the holo-enzyme causes dissociation of the complex and that the coenzyme can then be removed by dialysis.

Suelter et al. (77) have shown that the activating constants for the various cations vary from 0.2 mM for NH_4^+ (most effective) to 54 mM for Li^+ (least effective). They suggested that lack of activity in previous studies in the presence of poor activators may be partially attributed to low cation concentrations rather than to intrinsic differences in pyridoxal-p binding. Their data show that 0.5 M Na^+ brings about nearly 50% of the activity observed with 0.1 M K^+.

Both Suelter (77) and Toraya et al. (76) point to the size of

monovalent cations as an interesting feature in catalysis. They
found that cations with ionic radii smaller than 1.3 Å or larger
than 1.5 Å (K^+ crystal ionic radius is about 1.35 Å) are poor acti-
vators. In light of this, they suggest that any monovalent cation
having an ionic radius near that of K^+ might bind to the appropriate
positions of the protein and bring about the alignment of the peptide
backbone into an optimum configuration so that proper orientation
of the reacting groups needed for efficient catalysis is achieved.
These studies, plus the fact that distinct spectral differences are
observed in the presence of K^+ vs. Na^+, demonstrate a general differ-
ence in the structure of tryptophanase and in the mode of binding
of pyridoxal-p in the two environments. A more compact structure
and tighter binding of pyridoxal-p in the K^+ environment is consis-
tent with these observations. Since the 3-dimensional structure of
a monovalent cation binding site of any enzyme has not been described
to date, however, this difference does not elucidate the molecular
basis for those dissimilarities.

In spite of the above discussion, the essential role played by
these cations in catalysis, that is whether they are directly in-
volved in catalysis, and/or they are simply required to affect the
3-dimensional configuration of the enzyme molecule in solution is not
yet known. Two separate studies by Suelter et al. (77,78), however,
point to the former case. Nuclear magnetic resonance studies of
pyruvate kinase, a monovalent cation dependent enzyme that catalyzes
phosphoryl transfer reactions, showed that thallium (Tl^+) binds within
4-8 Å of the divalent cation activator at the catalytic site (78),

indicating that it may participate in the catalytic process. A stoichiometry of 2 Tl$^+$ bound per subunit of tryptophanase, obtained by incorporation of radioactive thallium into the enzyme through dialysis (77), also supports a specific role for the cation rather than a non-specific conformational effect. In addition, the fact that most pyridoxal-p dependent enzymes that catalyze α,β-elimination reactions require monovalent cations for maximum activity whereas those catalyzing transamination do not, also supports the view that these cations are directly or indirectly involved in the catalytic process (74).

B.3. Spectral Properties

In the absence of pyridoxal-p, apotryptophanase has the spectrum of a simple protein with a maximum centered at 278 nm. Upon addition of PLP, two new absorption maxima centered at 420 nm and 337 nm appear, the relative amplitudes of which depend upon pH and the nature of the monovalent cation (59,65). Morino and Snell (65) demonstrated that at low pH values the 420 nm form of the enzyme predominated and as the pH was raised, absorbance at 337 nm increased at the expense of 420 nm absorbance. They described this change with pH by a single proton process titration curve.

Morino and Snell also showed that in the presence of non-activating monovalent cations such as Na$^+$ and imidazole (and in the absence of K$^+$ or NH$_4^+$), the enzyme (inactive) was entirely in a form also absorbing at 420 nm and that the spectrum did not change significantly between pH 7.0 and 9.0 (59). When K$^+$ replaced Na$^+$ as the cation, however, a dramatic change in the spectrum was observed in which

the 337 nm form became the dominant species at pH 8.0 (Figure I.2).
They attributed the 337 nm absorption to the active form of the enzyme
because this form predominated at pH values above 8.0 where the en-
zyme displays its maximum catalytic activity. The observation that
activating monovalent cations such as K^+ promoted the formation of the
337 nm form, was also consistent with this interpretation.

Model studies have shown that pyridoxal-p aldamines absorb in the
wavelength range of 440 nm - 430 nm (36,79,80). On the basis of these
model studies, Metzler et al. (37,40) suggested the structure in
Scheme II (Figure I.3) for the 337 nm and 420 nm forms. Since proton
action of Schiff's bases on the ring nitrogen has a minor effect on
both absorbance change and positions of absorption maxima, the state
of protonation at the pyridinium nitrogen for either structure I or
II in Figure I.3 is unclear.

Recent studies on tryptophanase spectral forms by June et al.
(81,82,83) demonstrated that interconversion of the 420 nm and 337
nm forms following a change in pH or monovalent cation over the range
of enzyme stability occurs in a complex fashion on the stopped flow
time scale. The authors performed the following three experiments:

    (a) An incremental drop in pH from 8.5 to 6.7; (pH DROP)

    (b) An incremental jump in pH from 7.4 to 9.3; (pH JUMP)

    (c) A sudden change in K^+ concentration from 0.1 $\underline{M}$ Na^+

        to equal .05 $\underline{M}$ Na^+ and K^+ at pH 8.0; (K^+ JUMP).

The major features of the pH-DROP and pH-JUMP experiments were
interpreted by June et al. in terms of 3 distinct time-dependent
phases:
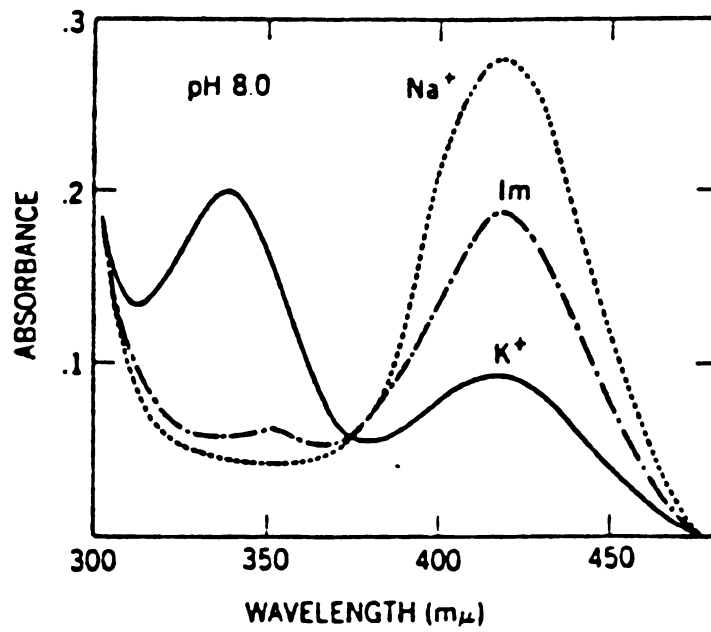
Figure I.2. Comparative effects of monovalent cations on the spectrum of holotryptophanase. [Taken from Reference (59).]
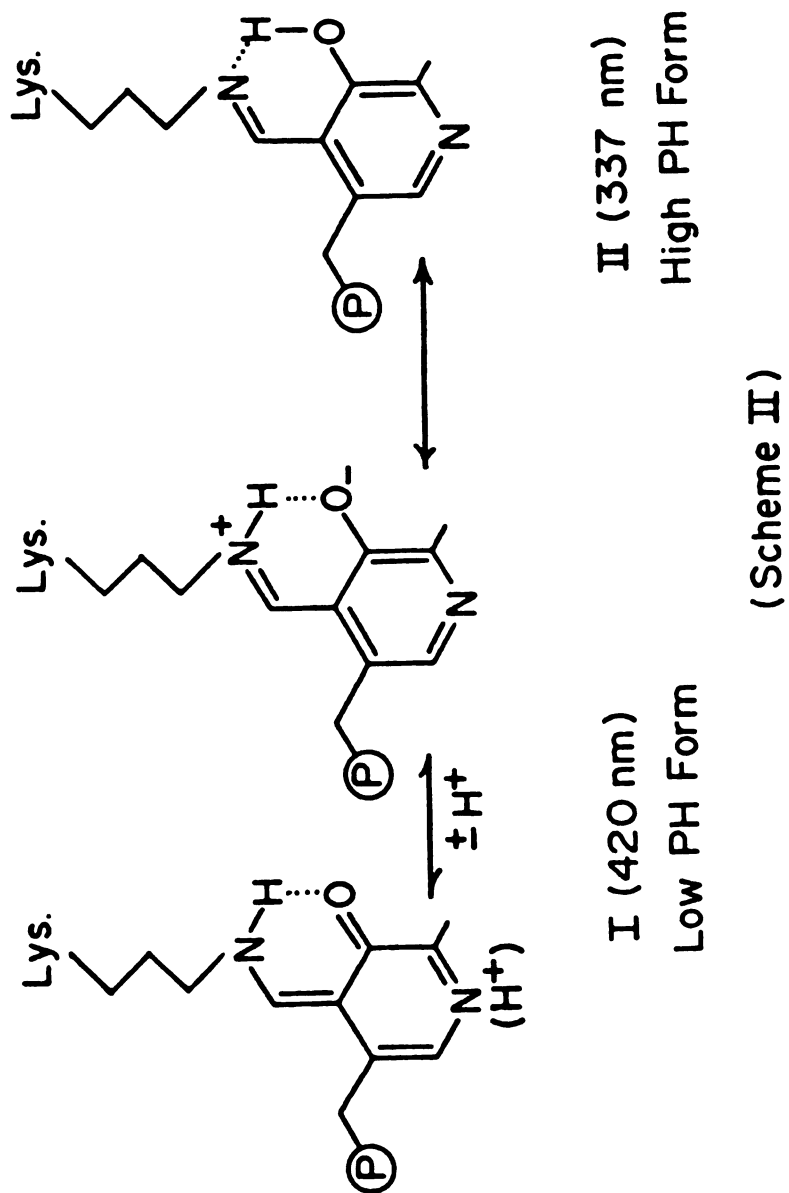
Figure I.3. Structures of 420 nm and 337 nm forms of tryptophanase suggested by Metzler et al. (37,40).

(1) An <u>abrupt</u> phase, which was complete in less than ∿6.5 msec (instrument dead time). The systematic changes observed at 295 nm were interpreted as fast protonation-deprotonation steps at the pyridinium nitrogen within the β and γ "manifolds". (Figure I.4)

(2) A <u>fast</u> 1st order conformational interconversion of 420 nm and 337 nm absorbances.

(3) A slow first order process involving growth at 355 nm coupled to two decays at 325- and 430-nm in the incremental PH JUMP, and decay at 355 nm with accompanying growth at 430 nm in the incremental pH DROP experiments.

Their K^+ JUMP experiment also showed slow conversion of the 420 nm peak to 337 nm absorption but the kinetics were not clean.

The results from these experiments led them to propose Scheme III (Figure I.4) involving enzyme forms E_α, E_δ, E_β, $E_\beta H^+$, E_γ and $E_\gamma H^+$. The E_α form (not shown) is predominant in the absence of activating monovalent cations and absorbs at 420 nm. E_β and $E_\beta H^+$ in the β manifold also absorb at 420 nm while those in the γ manifold, E_γ and $E_\gamma H^+$, absorb at 337 nm. The form E_δ absorbs at 355 nm. The structures giving rise to various absorptions shown in Scheme III were assigned by the authors on the basis of both model studies and studies on another pyridoxal-p dependent enzyme, namely asparate aminotransferase (28,37,84). Computed equilibrium distributions indicated that among the four species of the β and γ manifolds, $E_\beta H^+$ and E_γ predominate at low and high pH, respectively. Further details of their work appears in the references (81,82,83).
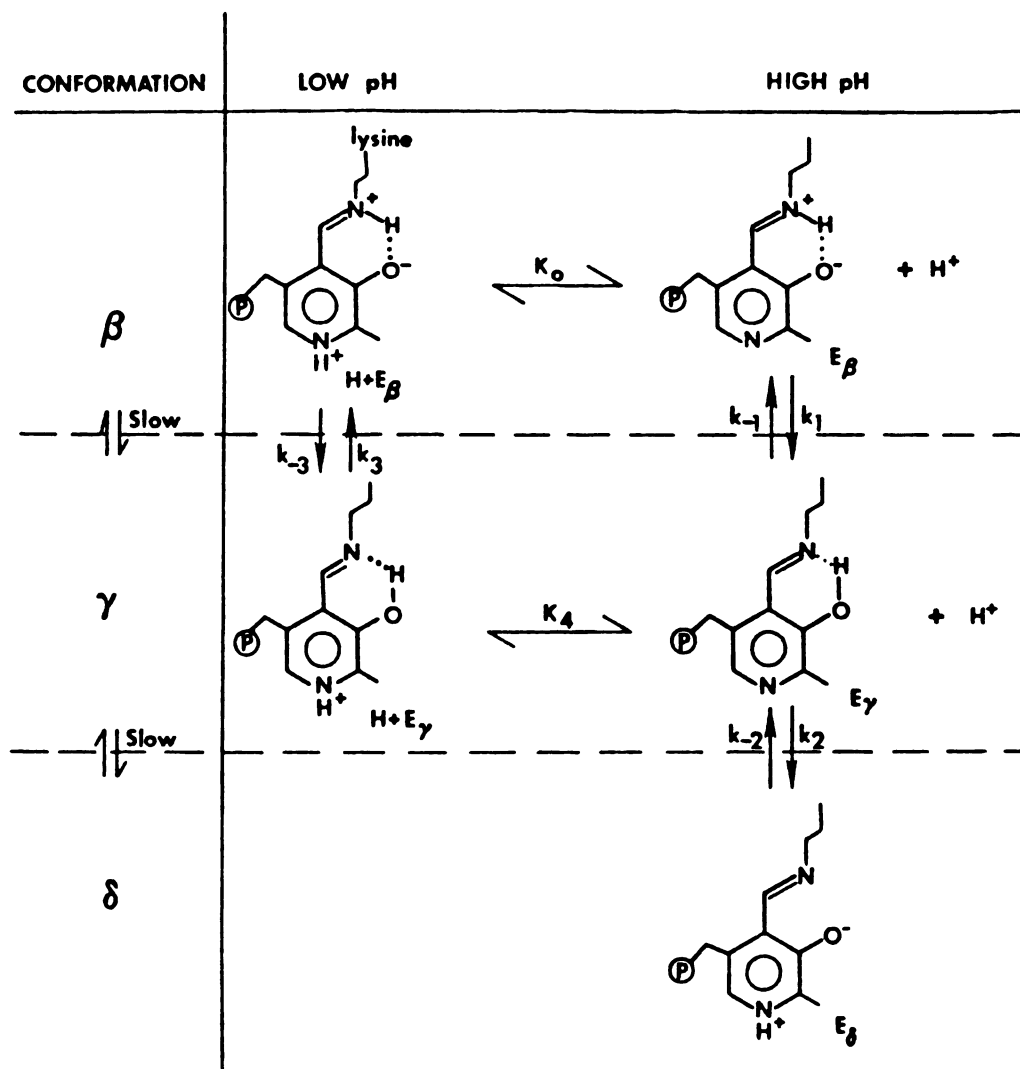
(Scheme III)

Figure I.4. Interconversion of tryptophanase spectral forms.

B.4. Catalytic Properties

Tryptophanase is one of a group of pyridoxal-p dependent enzymes which catalyzes a variety of α,β-elimination and β-replacement reactions (56,85,86). Following purification of the enzyme, Newton and Snell (56) were able to establish that not only tryptophan and tryptophan analogs but a variety of other β-substituted amino acids undergo α, β-elimination according to reaction I.3.

$$RCH_2CHNH_2COO^- + H_2O \xrightarrow{TP_{ase}} CH_3COCOO^- + RH + NH_3 \qquad (I.3)$$
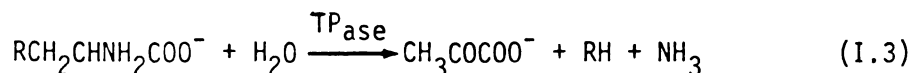
In addition, amino acids that serve as a substrate in reaction I.3, can also undergo a β-replacement reaction in the presence of indole to yield tryptophan according to reaction I.4.

$$Indole + RCH_2CHNH_2COO^- \xrightarrow{TP_{ase}} Tryptophan + RH \qquad (I.4)$$
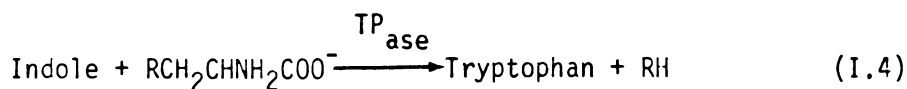
In fact, it is a reaction similar to (I.4) that permits an E-Coli B/1t7-A culture which lacks enzymes for tryptophan synthesis (such as tryptophan synthetase), but which contains a constitutive tryptophanase, to grow when supplied with indole.

B.5. Mechanism of Tryptophanase Catalysis

A mechanism for tryptophanase action consistent with all observations reported up to 1975 was outlined by Snell (51). In this mechanism (Scheme IV, Figure I.5) the exact ionic forms of both coenzyme

Figure I.5. Mechanism for tryptophanase catalyzed reactions. Taken
from Reference (83).
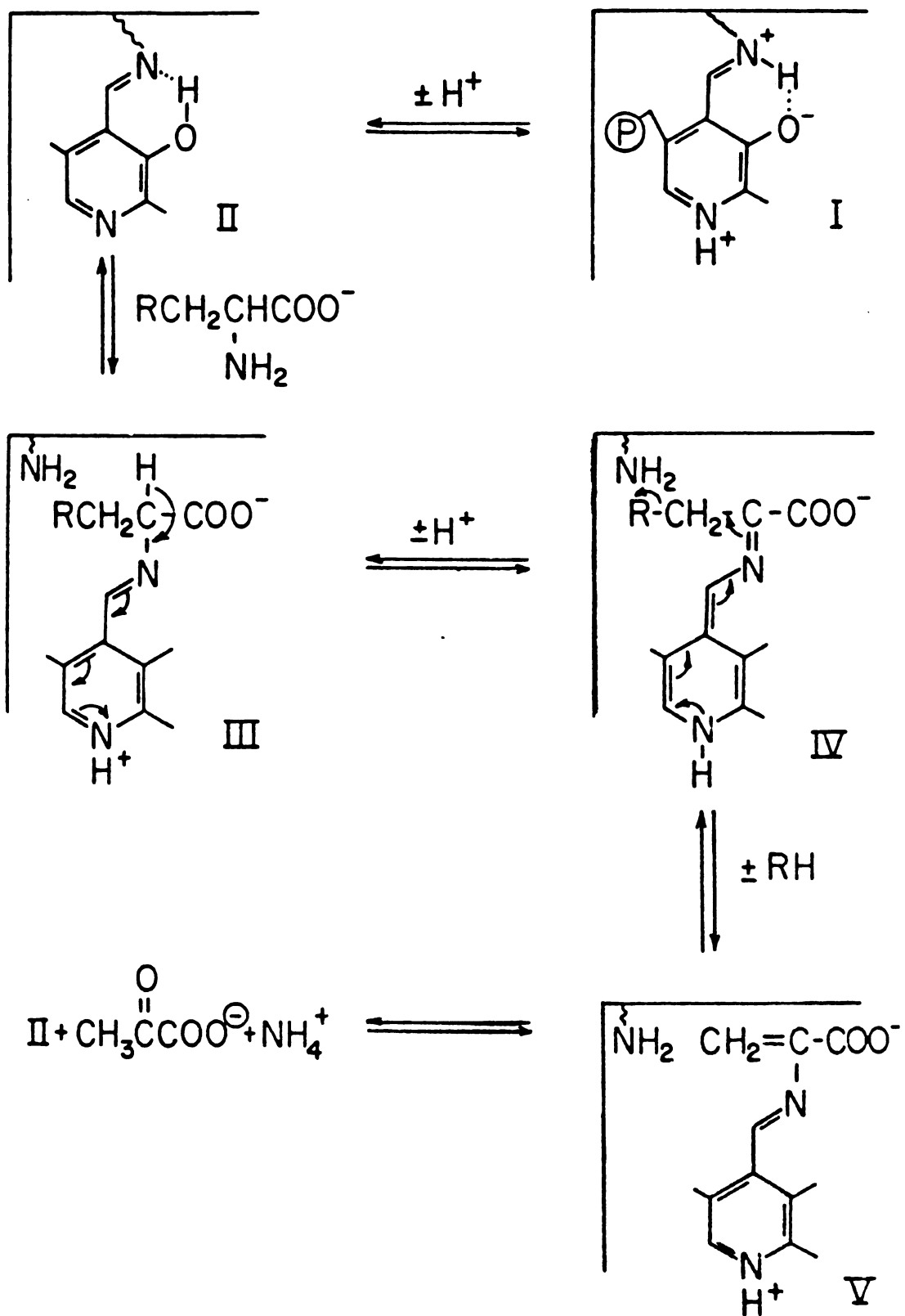
Figure I.5.

and substrate, as well as the catalytic groups of the apoenzyme which may contribute to the process are unknown.

The first step in this mechanism involves the conversion of the inactive form of the enzyme absorbing at 420 nm (Structure I, Figure I.5) to an active form II which absorbs at 337 nm. As described earlier, since the pH optimum of tryptophanase is near 8.5, it was assumed that the deprotonated form of the coenzyme (λ_{max} = 337 nm) is that which exhibits activity.

The second and third steps involve formation of the enzyme-substrate complex (Structure III, Figure I.5) via a transaldimination reaction, and the subsequent labilization of the α-hydrogen from the bound amino acid to form the quinonoid intermediate IV which has an intense absorption at ∿500 nm (65). The reaction with dead-end inhibitors (substrates which lack a labilizable β-substituent such as L-alanine and L-ethionine) stops here, but with trace substrates this absorption band disappears as substrate is depleted. Studies by Morino and Snell (65) on L-alanine and true substrates in the presence of D_2O and ^3H_2O indicated that the α-proton is labilized during quinonoid formation, and that for true substrates this labilization proceeds at a faster rate than elimination of the β-substituent. They thus concluded that elimination of the β-substituent of the substrate is the rate-limiting step. Later Suelter and Snell using s-orthonitrophenyl-L-cysteine (SOPC) as substrate in ^3H_2O, demonstrated that no tritium is incorporated into the unreacted SOPC. Based on this observation and the fact that no 500 nm absorbing species could be detected by a scanning stopped-flow study of the reaction with SOPC (87), they

concluded that loss of the α-proton was rate-limiting for the reaction with this substrate.

The fourth and fifth steps in Figure I.5 represent the elimination of the β-substituent of the substrate with formation of the enzyme-bound α-aminoacrylate complex (Structure V), and subsequent decomposition of this complex to yield pyruvate and ammonia along with regeneration of the active enzyme. Hillebrand et al. (88) also using SOPC as substrate, suggested that either α-iminopropionate or the carbinolamine of pyruvate are the immediate products of the SOPC degredation by tryptophanase. The intermediate then undergoes a non-enzymatic hydrolysis to yield pyruvate and ammonia.

In an effort to gain more information on the role played by monovalent cations in the mechanism, Suelter and Snell (77) studied the reaction of tryptophanase with the competitive inhibitor L-ethionine. They demonstrated that the absorption spectrum of holoenzyme in the absence of monovalent cations, plus or minus ethionine are nearly identical. However, the circular dichroic spectra of the same solutions were very different and are consistent with complex formation between the holoenzyme and ethionine. Upon addition of activating monovalent cations to the holoenzyme-ethionine complex, they observed a marked increase in absorption at 508 nm resulting from labilization of the α-proton that leads to formation of a quinonoid structure. They therefore concluded that ethionine interacts with the holoenzyme in the absence of monovalent cation, but does so in such a way that the 508 nm absorbing species is not formed. This observation clearly indicates that the cation exerts its effect by interacting directly

at or near the catalytic center rather than at some site on the protein surface which is distant from the active site. However, as discussed earlier, whether it participates directly in the catalytic process is still uncertain.

B.6. Kinetic Studies

To study the transient kinetics of quinonoid formation and correlate the rate of change of the enzyme to that of the product in tryptophanase reactions, June et al. (83,89) performed stopped-flow studies of tryptophanase catalysis with the inhibitors L-alanine and L-ethionine under various experimental conditions. Their results, in contrast to the conclusions of Morino and Snell (65), showed that the 420 - not the 337-nm form of the enzyme is the active form. They support this assignment by the following observations:

(1) The rate constant for disappearance of the 420 nm absorbance (18.0±2.2 Sec^{-1}) was the same as that of the fast phase of the biphasic growth of the quinonoid at 508 nm (15.0±1.2 Sec^{-1});

(2) The rate constant for disappearance of the 337 nm absorbance (0.56±0.08 Sec^{-1}) was the same as that of the slow phase of the quinonoid formation (0.63±.06 Sec^{-1}) and was essentially unaffected by the inhibitor concentration or the nature of the inhibitor, alanine or ethionine;

(3) The average rate constant for the slow phase obtained with ethionine (0.51±0.14 Sec^{-1}) and alanine (0.47±0.15 Sec^{-1}) agrees closely with the rate constant, 0.42 Sec^{-1}, for conversion of the

337 nm absorbance (γ form) to the 420 nm absorbance (β form) follow-
ing a rapid decrease in pH (82).

These results led them to conclude that the 337 nm form apparently
does not form quinonoid directly but is first converted to the 420
nm form by a conformational change before the α-proton of the amino
acid inhibitor is removed to form quinonoid (89). In addition, they
found that with deuterium at the α-position of alanine, the fast
phase of quinonoid growth slowed down while the slow phase remained
virtually unchanged. This was interpreted by the authors as indicat-
ing that the abstraction of the α-proton is the rate limiting step
of quinonoid formation while the slower phase reflects an enzyme
conformation change.

Based on these results and those from the incremental pH-JUMP
and pH-DROP studies (82,83), June et al. proposed Scheme V (Figure
I.6) as a mechanism for quinonoid formation. They also presented the
following additional factors as evidence supporting their proposed
mechanism:

(a) The effect of pH on quinonoid formation revealed that as
the pH was increased, the rate constant for the fast phase of
the biphasic quinonoid growth also increased while the relative
amplitude of the fast phase diminished. This supports their
previous suggestion that conformation β (420 nm form) is the one
poised for reaction, i.e., the active form of the enzyme.

(b) The rate constant for the fast phase of the quinonoid growth
exhibited a hyperbolic dependence on ethionine concentration,

$$H^+$$
$$+$$
$$\beta SH \rightleftharpoons EQ + H^+ \xleftarrow{K_{QH}} EQH^+$$
$$\Big\updownarrow Ks\beta$$

$$SH$$
$$+$$
$$\beta H^+ \xleftarrow{K_{\beta H}} \beta + H^+$$
$$\updownarrow K_{\beta\gamma}^{H} \qquad \updownarrow K_{\beta\gamma}$$
$$\gamma H^+ \rightleftharpoons \gamma + H^+$$
$$K_{\gamma H} \Big\{\updownarrow K_{\gamma\delta}$$
$$\delta$$
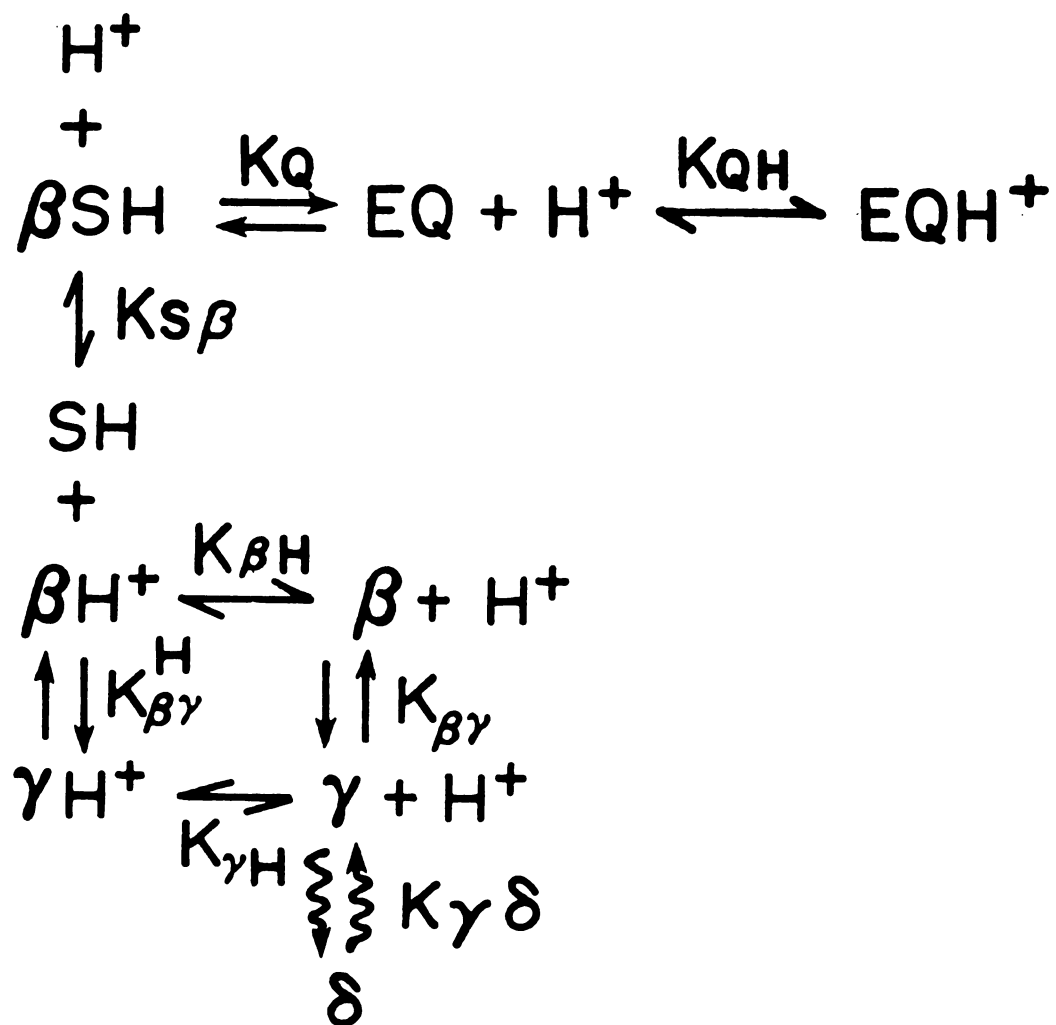
(Scheme V)

Figure I.6. Mechanism for the formation of quinonoid (EQ and EQH$^+$) from the competitive inhibitor, L-Ethionine (SH).

indicative of formation of the Michaelis complex SH;

(c) The rate constant for the slow phase of quinonoid growth appeared to be essentially constant over the range of ethionine concentrations used and comparable to that obtained with alanine. This again presents further support to the authors' previous proposal that k_2 reflects an enzyme conformational change.

Recent rate studies with the true amino acid substrate, S-benzyl-L-cysteine (SBC) are also in agreement with Scheme IV (90).

C.   Scanning Stopped-Flow Technique for the Study of Enzyme Reactions

Stopped-flow kinetics has been extensively used in the study of non-steady-state enzyme reactions at high enzyme concentrations. In a typical stopped-flow experiment, absorbance is monitored as a function of time at a certain wavelength.

Recent advances in computer-controlled data acquisition have made "scanning stopped-flow" practical for many enzymatic reactions (81,89 91-95). In Rapid Scanning Spectroscopy (RSS), a selected region of the electromagnetic spectrum is rapidly and repeatedly scanned while a spectrophotometric response such as absorbance or fluorescence is measured at a fixed number of wavelength "channels" across the spec-trum during each scan (96,97). If the time duration of each scan is short compared to the half-life of the reaction studied, the data can be regarded as a matrix $\underline{A}$ composed of N consecutive instantaneous spectra measured at P wavelength channels (98). The element A_{ij} of this matrix is then the spectrophotometric response measured at

wavelength channel i at the time of scan j.

The advantage of collecting this "time-wavelength-absorbance" surface for a spectral region rather than a fixed-wavelength experiment, is that the reacting enzyme, enzyme bound intermediates, substrates, and products may all be spectrophotometrically detectable in the same experiment. This obviously minimizes problems resulting from lack of reproducibility from one experiment to another and eliminates somewhat the problem of long time baseline drift.

In our laboratory a computer-interfaced rapid scanning stopped flow system has been successfully used for the studies on Cytochrome c oxidase (95,99), AMP-aminohydrolase (90) and tryptophanase (82,89. 100). Further details about the system including a historical background handling and performance of the system, and treatment of scanning stopped-flow data will appear in Chapter II.

D. Macrocyclic Complexing Agents for the Study of Tryptophanase Activation/Deactivation by Monovalent Cations

D.1. Structure and Properties

A large variety of naturally occurring macrocyclic antibiotics such as porphyrin, nonactin, and valinomycin and their unique ion binding and ion transport properties have been known for over fifty years. In 1964, Moore and Pressman (101) reported that valinomycin induces the transport of potassium ion through mitochondrial membrane by complexation. The biological activity of these compounds is believed to be related to their macrocyclic structure which consists

of a lipophilic exterior and a hydrophilic central cavity ringed with electronegative donor atoms (102). The macrocyclic nature of these compounds allows charged cations to bind in the central cavity, hence making the cation soluble in the lipid region of the membrane.

During the past two decades, a large number of synthetic macrocyclic compounds that contain multiple donor atoms capable of binding cations have been prepared and investigated. Many of these organic macrocyclic ligands possess very interesting and unusual ion binding properties. These chemicals are classified under two general classes:

(1) "Macrocyclic Crown-ethers", which were first synthesized by Pederson in 1967 (103,104) are cyclic polyethers whose trivial names indicate both the total number of atoms and the number of oxygen atoms in the ring. For example, 18-crown-6 or simply 18C6 contains a ring of 18 atoms, 6 of which are oxygen.

(2) "Cryptands", which were first synthesized by Lehn and coworkers in 1969 (105,106) are bicyclic diamines which have a 3-dimensional cavity for complexation of metal cations. The trivial name of this class denotes the number of oxygens in each of the polyether chains which bridge the two nitrogens. For example, Cryptand 222 or simply C_{222}, contains 2 oxygen in each strand. The structural formulas of cryptands and 18C6, a member of the first class, are shown in Figure I.7.

One of the most interesting features of these cyclic compounds is their ability to "selectively" bind various cations to form very strong complexes. Particularly interesting is the strong "affinity" and "selectivity" shown by the polyethers for alkali metal cations.

30
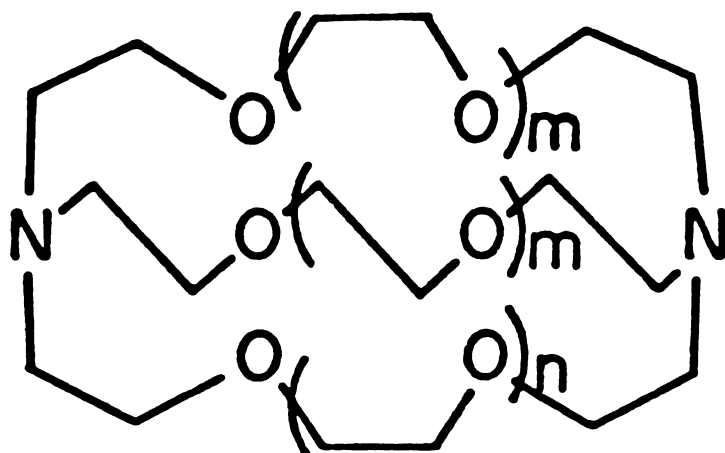
$$m = 0; \quad n = 1 \qquad (C211)$$
$$m = 1; \quad n = 0 \qquad (C221)$$
$$m = n = 1 \qquad (C222)$$
$$m = 1; \quad n = 2 \qquad (C322)$$
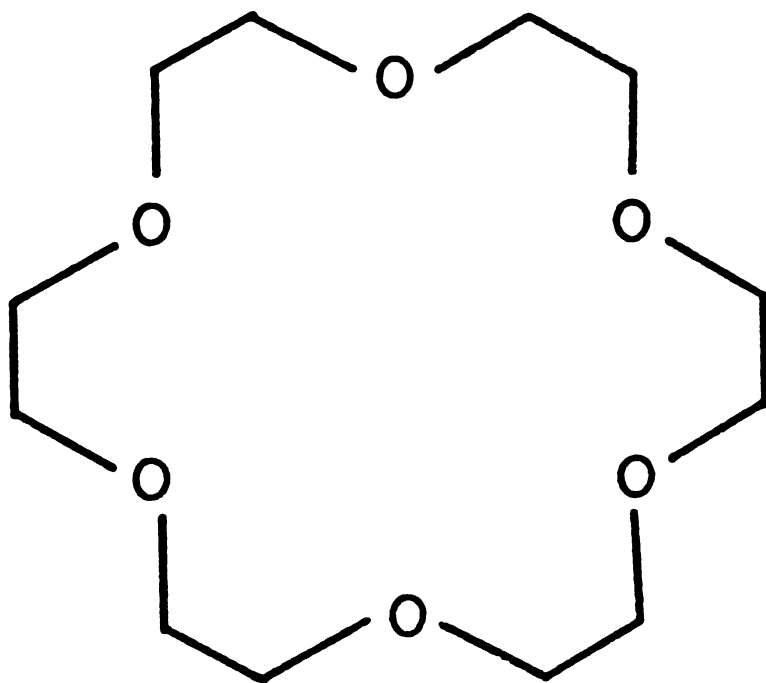
Figure I.7. Cryptand and 18-Crown-6 structural formulas.

Since the alkali metal ions are generally regarded as poor complex-ing cations, the cyclic polyethers appear to be the only neutral com-pounds (with the exception of macrocyclic antibiotics) to complex ap-preciably with these metals. This has resulted in their use as com-plexing agents to increase the solubility of alkali metals in amines and other solvents (108,109), and as models for carrier molecules in the study of ion transport phenomena in biological systems (110, 111,112).

D.2. Complexation

The cyclic polyethers form strong one to one (1:1) polyether: metal complexes with a large array of metal ions (110,113). Complexa-tion constants at least as high as 10^8 M^{-1} for complexes formed between cryptands and alkali metal cations are known (114,115). These com-plexes are generally assumed to consist of the metal ion bound in the cavity of the polyether ring (116). This "metal in the hole" picture has been substantiated by x-ray crystallographic studies of several of these complexes (117,118,119). The stable bonds in these systems have been attributed to ion-dipole interactions between the positively charged cation and the dipole created by the inwardly oriented oxygen atoms (113). The following factors are believed to influence the formation, stability, and selectivity of the macrocyclic ligand complexation:

(a) Relative size of cation and ligand cavity;

(b) arrangement of ligand binding sites;

(c)   type and charge of cation;

(d)   number and type of donor atoms.

Both 18-Crown-6 and C222 are selective for K^+ ion and form strong
1:1 complexes with this ion. Hence both of these compounds were
used during the course of this study.

CHAPTER II

EXPERIMENTAL METHODS

A. Materials

E-Coli B/1t7-A was grown in the Biochemistry Department at Michigan State University under conditions described elsewhere (2). Pyridoxal-5$\dot{}$phosphate (PLP), N-2-hydroxyethylpiperazine propane sulfonic acid (EPPS),N-N-bis(2-hydroxyethyl)glycine (Bicine), DL-dithiothreitol (DTT),ethylenediamine tetracetic acid (EDTA), and Sepharose 4B were obtained from Sigma Chemical Co. Potassium Epps (KEPPS), DEDTA, and K-Bicine were prepared by titrating the reagents with KOH. Ammonium Sulfate was Schwarz/Mann enzyme grade. 18-Crown-6- and Cryptand 222 were purchased from PCR, Inc., and were further purified before use (see B.4 in this Chapter). Tetramethyl ammonium chloride, $(CH_3)_4NCl$, obtained from Aldrich Chemical Company was recrystallized from n-propanol prior to use. $(CH_3)_4NOH$ was freshly prepared by passage of recrystallized $(CH_3)_4NCl$ through a Dowex-1-OH column. Cyanogen bromide, CNBr,and 1,7-diaminoheptane were obtained from Aldrich Chemical Co. Water used for the preparation of all solutions was double distilled. All other reagents were of analytical grade and were used without further purification.

B. Methods

B.1. Preparation of the 1,7-diaminoheptane Sepharose Column

The ligand 1,7-diaminoheptane was coupled to sepharose 4B after cyanogen bromide activation in a procedure adapted from that of Shaltiel and Er-el (120). Sepharose 4B is activated at pH 10.5-11.0 and 22° by the addition of 1 g of CNBr to 10 g (wet weight) of sepharose (121).

In the process, 24 grams of CNBr dissolved in 24 ml dioxane distilled over Na metal was added rapidly to 240 g of sepharose suspended in about 200 ml water as it was being stirred under the fume hood. The reaction was allowed to proceed for 8 minutes and the pH was maintained between 10.5-11.0 by addition of 5N NaOH. The pH tends to stabilize as the reaction proceeds. Activation was terminated by addition of crushed ice to the mixture. The activated gel was then filtered quickly and washed by ∿2 L. ice-cold deionized water and resuspended in about twice the settled volume of the gel (∿500 ml cold 0.1 $\underline{M}$ NaHCO$_3$ (pH 9.0). To this sepharose suspension, an equal volume of H$_2$O containing ∿120 g of 1,7-diaminoheptane at pH 9-9.5 was immediately added and the pH of the solution was readjusted to 9-9.5 with 6N HCl if necessary (in general, one needs 4 moles of ligand per mole of CNBr used for activation). The coupling reaction was allowed to proceed overnight at room temperature while the solution was gently swirled. Finally the gel was filtered and washed with water, 0.1 $\underline{M}$ NaHCO$_3$, 0.05 $\underline{M}$ NaOH, water, 0.1 $\underline{M}$ CH$_3$COOH, then water again. The alkyl-sepharose was stored at 4°C in aqueous suspension

in the presence of 0.02% sodium azide, Na_3N, to prevent growth of bacteria.

The sepharose column described above can be stored for months at 4°C and can be used repeatedly. It is regenerated with washes of 0.2 N KOH, H_2O, 0.2 N KOH, H_2O, 0.2 N HCl, H_2O, followed by adjusting the pH to 7.0 in water and finally washing with the column-equilibration buffer. The column has a high binding capacity and high flow rate (1-3 ml/min). The retention power of the column is assumed to involve hydrophic interactions between the hydrocarbon "arms" of the ligand and accessible hydrophobic pockets or regions of the enzyme and hence the method is referred to as "hydrophobic chromatography".

B.2. Preparation of Tryptophanase

Tryptophanase from E-Coli B/lt7-A was prepared as described by Watanabe and Snell (122) including the modification of Suelter et al. (123). Frozen wet cells of E-Coli (usually ∿30 g) suspended in 0.1 M potassium phosphate buffer at pH 7.0 were either sonicated with a Branson Sonic Oscillator or treated with a French Press to break the cells. During the preparation, all precipitation steps were carried out at 2-5°C by using an ice-bath. Whenever ammonium sulfate was added during the purification, the drop in pH from 7.0 was compensated for by addition of 10% ammonium hydroxide. With the exception of the dialysis buffer, all other buffers were made 0.1 mM in pyridoxal-p for enzyme stability. The dialysis buffer contained

20 μM pyridoxal-p. When apotryptophanase was desired, the holoenzyme was made 10 mM in DL-penicillamine and dialyzed at 4°C against a 90% ammonium sulfate saturated phosphate buffer at pH 7.0. During the preparation, the protein concentration was monitored by the Lowrey procedure (124).

The enzyme prepared in this way is 90-95% homogeneous and is stored in the apoenzyme form as a suspension under nitrogen in 90% saturated $(NH_4)_2SO_4$ buffer containing 10 mM DTT to preserve activity. Loss of activity upon long time storage was observed in some cases; however, retreatment of the apoenzyme with 10 mM DTT in a phosphate buffer at 50°C followed by precipitation restored the activity. A detailed description of the preparation procedure is given elsewhere (123).

B.3. Activity Assay of Tryptophanase

The activity of tryptophanase was measured spectrophotometrically by using the chromogenic substrate S-o-nitrophenyl-L-cysteine (SOPC). This compound was prepared according to the published method (125). Suelter et al. (123) have shown that SOPC absorbs maximally at 370 nm and undergoes α,β-elimination in the presence of tryptophanase according to Equation II.1:

$$O-NO_2C_6H_4SCH_2CHNH_2COO^- + H_2O \xrightarrow{\text{TP}_{ase}} O-NO_2C_6H_4S^- + CH_3COCOO^- + NH_4$$

(II.1)
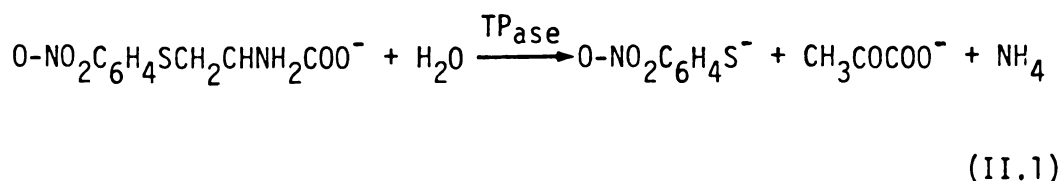
The reaction was monitored as a decrease in absorbance at 370 nm with $\Delta\epsilon$ = 1860 $\ell.mol^{-1}.cm^{-1}$. The assays were carried out in 50 mM

potassium phosphate buffer containing 50 mM KCl, 0.6 mM SOPC, pH 8.0 at 30°C. The activity, which is the number of moles of product formed per ml per minute, is calculated from the Equation II.2:

$$\text{Activity} = \frac{(\Delta O.D.)_{370} \times \text{Enz. Dilution Factor}}{1.86} \qquad (II.2)$$

The specific activity is calculated by dividing the activity by the protein concentration in mg/ml. The protein concentration was determined spectrophotometrically using $\varepsilon_{278} = 0.795$ $ml.mg^{-1}.cm^{-1}$ (65). Specific activity greater than 40 $\mu mole.min^{-1}.mg^{-1}$ is indicative of pure protein. Specific activity as high as 50-55 $\mu mol.min^{-1}.mg^{-1}$ is reported for the enzyme (82,83,present work).

B.4. Purification of the Complexing Agents

18-Crown-6 (or IUPAC: 1,4,7,10,13,16-hexaoxacyclooctadecane) was first recrystallized from warm acetonitrile as the crown-acetonitrile complex (126). The weakly bound acetonitrile was then removed from the crown by placing the crystals in a vacuum oven for several hours. The crown obtained by vacuum decomposition of the complex was then high vacuum sublimed with the apparatus shown in Figure (II.1). The impure crown was placed in the apparatus below the cup and was heated with an oil bath to 60-70°C while the cold inner tube was maintained at $\sim$-60°C with chilled N_2 gas. After completion of the sublimation, the purified crown was scraped from the walls of the inner tube as a white powder (M.P. 39-40°C) and was stored in the dark in a closed
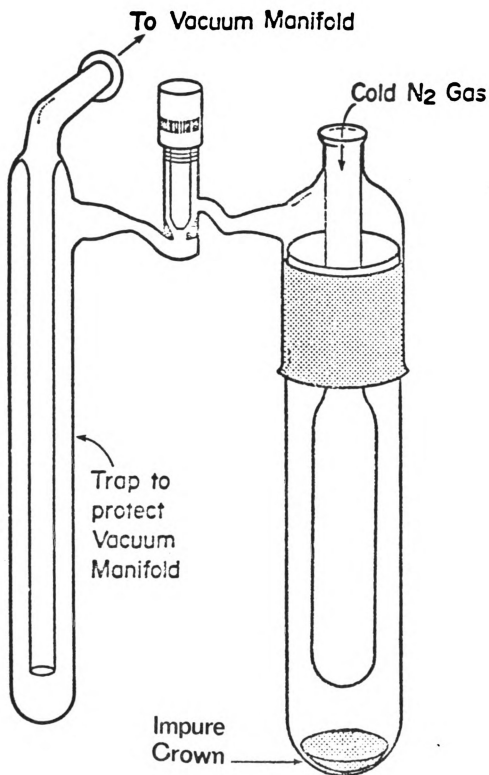
Figure II.1. Molecular distillation apparatus for purification of crown.

reservoir (extremely hygroscopic and light sensitive). Cryptand 222 (or IUPAC: 4,7,13,16,21,24-hexaoxa-1,10-diazabicyclo[8.8.8]hexa-cosane) was high-vacuum sublimed at 110°C by Dr. Long Dinh Le.

C. The Stopped-Flow Method

C.1. A Historical Background

A history of flow methods begins with the classical studies of continuous-flow by Roughton and co-workers (127) in 1923. They studied rates of chemical reactions by allowing the reactants to flow from large reservoirs into a mixer and then into a long tube. Con-centration-time profiles were obtained by observation of the absor-bance of the solution at various points along the tube. Some 17 years later, Chance (128) was the first to apply the continuous-flow method in the development of stopped-flow methods of analysis. Further modifications were later made by different workers including Crouch et al. (129), Malmstadt (130), Dye and Feldman (131), Dye et al. (92,96) in order to tailor the system for their particular needs. Essentially, the stopped-flow technique involves rapid and efficient mixing of the two reactants (milliseconds), stopping the flow, and monitoring the spectrophotometric response as the reaction proceeds. Modern stopped-flow systems are usually computer-interfaced for fast data acquisition.

C.2. The Rapid Scanning Stopped-Flow System

A thermostated, computer-interfaced, double beam rapid scanning stopped-flow system built by G. H. Ho (132) was used in this research. A block diagram of the system is shown in Figure II.2. The system utilizes a 1000 watt xenon arc lamp as the light source. The entire flow system is made up of inert material and is housed inside a water-tight bath capable of circulating water, thus allowing for the temperature-controlled experiments. Both the sample and reference cells are provided with two path-length options (1.86 cm and 0.20 cm). To assure complete mixing of reagents prior to observation, a quartz double four-jet mixing chamber is used.

In absorbance measurements, the light dispersed from the scanning monochromotor is transmitted through a beam splitting fiber optic to the observation and reference cells. Light from the cells is then brought to a pair of matched photomultiplier tubes by the use of similar fibers. The reference and sample photocurrents are next converted to absorbance and amplified by using an operational amplifier and the absorbance signal is stored on floppy disk in a PDP/8I computer. A detailed description of the system is given in the Ph.D. dissertations of G. H. Ho (construction of the flow system), N. Papadakis (133) and R. B. Coolen (134) (interface and software, synchronization of scans, and signal averaging scheme).

C.2.1. Scanning Mode - The system utilizes a Perkin-Elmer Model 108 scanning monochromotor which is capable of repeatedly scanning

Figure II.2. Block diagram of the computer interfaced scanning stopped-flow system.

42
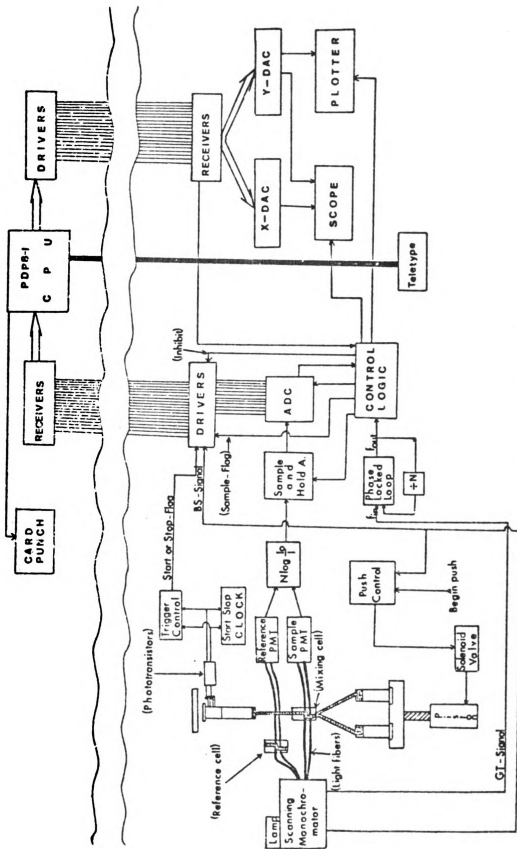
Figure II.2.

from 3 to 150 complete spectra per second. By using appropriate photo-multiplier tubes (PMT), a range of about 250 to 1200 nanometer (nm) of the electromagnetic spectrum can be scanned. As described earlier, the scanning mode is advantageous in the sense that it eliminates the need for several fixed-wavelength mode experiments which mini-mizes reproducibility problems and problems associated with long-time baseline drift.

C.2.2. Fixed-wavelength Mode - The scanning mode has two main disadvantages associated with it; (a) some noise is introduced by the nutating mirror of the monochromator, (b) reactions with half-lives of less than 50 mS (limited by the scan speed) are not suitable for kinetic studies in this mode (only 4 forward spectra can be col-lected in 50 mS at the 150 scan speed). These problems, however, are eliminated in the fixed wavelength mode. In this mode, the pro-gress of a reaction can be followed at any selected wavelength by manually setting the monochromotor to that particular wavelength. In this case reactions with half-lives in the order of the "dead-time" of the instrument (few msec) are possible to study (see C.2.4). In addition, the absence of noise introduced by the nutating mirror contributes to the enhancement of the signal-to-noise ratio (S/N).

C.2.3. Flow Velocity - In stopped-flow experiments, the flow of solutions should be fast enough to cause turbulence necessary for efficient mixing. The "flow velocity" is obtained by measur-ing the distance between the start and stop flags and the flow

time, which is the time required for the stopping syringe to travel this distance. A measure of turbulent flow is given by Reynolds' Number R (135):

$$R = dV \, \rho/\eta \qquad\qquad (II.3)$$

where d is the diameter of the tube in (cm), V is the flow velocity in (cm.sec^{-1}), ρ and η are the dynamic density and viscosity in (gcm^{-3}) and poise (g.cm^{-1}.sec^{-1}), respectively. For practical purposes, the range of Reynolds' number for efficient turbulent flow might be from 2000 to 2500, but it can be as low as 10 for jet-type mixers (135).

The critical velocity required to get turbulent flow for aqueous solution at 20°C is found to be V = 200/d, where d is in mm. Since 2 mm diameter tubes were used for construction of mixing and observation cells, the critical velocity is thus about 100 cm/sec. From the velocity profile of an aqueous solution as function of time, a flow velocity of about 550 cm/sec was calculated at ~40 psi pushing pressure for our system (90). This value (corresponding to R ~ 110) is well above the critical velocity of 100 cm/sec and thus assures us of turbulent flow.

C.2.4. <u>Dead Time</u> - The time required to transfer the solutions from the mixing chamber to the observation point and bring them to a complete stop is defined as the "dead time". It thus depends upon the mixing efficiency, stopping time, and the flow velocity for a

particular experiment. If the stopping time is very small and the mixing very efficient, then the dead time can be estimated from Equation (II.4):

$$t = V/U \qquad\qquad (II.4)$$

where V, the "dead volume" is the volume from the point of mixing to the end of observation window, and U is the average flow velocity in ml/sec. For our mixing and observation cells, the dead volume was calculated from physical measurements to be 0.048 and 0.121 ml for the short and long path lengths respectively (132). With our typical flow velocity of about 550 cm/sec ($\sim$18 ml/sec), a dead time of 2.7 mSec for the short path length, an$\overset{\cdot}{}$ 6.7 mSec for the long path length can be computed.

C.2.5. <u>Stopping Time</u> - The "stopping time" is the time required for the mixed solutions to come to complete rest after the flow has been stopped. It was measured by N. Papadakis (133) by studying the fast reaction;

$$Fe^{+3} (0.01\underline{M}) + SCN^{-} (0.01 \underline{M}) \rightarrow FeSCN^{2+} \qquad\qquad (II.5)$$

and monitoring the absorbance change at 455 nm. He found the stopping time to be reproducible and $\sim$0.5 mSec under the experimental pushing pressure.

C.2.6. Mixing Efficiency.- The mixing efficiency of the stopped-
flow sytem was tested by G. H. Ho (132) and N. Papadakis (133) with
the aid of a specific reaction. They mixed equal volumes of 0.2 mM
p-nitrophenolate and 0.1 mM hydrochloric acid and followed the ab-
sorbance change at 400 nm where the paranitrophenol absorbs. They
found the resultant absorbance to be a flat straight line. This in-
dicates the reaction which is diffusion-controlled (136), is over
by the time the mixed solutions reach the observation point (i.e.,
the instrument dead time, $\sim$7 msec). Such a result could not have
been obtained if complete mixing (100%) had not occurred prior to
observation. The same results were also obtained by F. Halaka (99)
and S. Elias (90) using different acid-base indicator reactions.

D. Data Collection, Calibration and Computer Graphics

The stopped-flow system is interfaced to a PDP 8/I computer for
data acquisition. The raw data are stored on floppy disks for later
calibration and analysis. The stored data can also be retrieved and
displayed on a Tektronix Model 610 storage-display scope connected to
a Tektronix Model 4601 hard-copy unit. This unit was used for visual
inspection, preliminary examination of the results, and production
of photocopies. This capability in the system allows the experimenter
to examine the results from an experiment during the performance or
anytime thereafter.

The calibration procedure for the system involves collection of
a set of neutral density filter spectra in order to calibrate the
absorbance values. The spectra of holmium oxide and didymium oxide

glass filters are also collected in order to calibrate the wavelength in intervals. Data stored on floppy disks, including the calibration data, are put on magnetic tapes and then transferred to the Michigan State University CDC750 computer where kinetic and principal component analysis are performed. Calibration of raw data was performed as described in Appendix E of the Ph.D. Dissertation of R. Cochran (98).

Two dimensional graphics of this work were obtained by using program MULPLT written by Dr. T. V. Atkinson at Michigan State University for the Chemistry Department PDP/11 computer. Computer programs to transfer calibrated stopped-flow data from the CDC 750 computer to the PDP/11 to be used in MULPLT, were written by Dr. F. Halaka and Dr. T. H. Pierce. Three dimensional plots were constructed by using program GEOSYS, available on the Michigan State University HAL routines.

E. Analysis of Scanning Stopped-Flow Data

Scanning stopped-flow experiments produce massive amounts of data. A general procedure for analyzing these data is as follows:

E.1. Rate Equations - Program KINFIT4

Finding the rate law(s) that fit the time course of a reaction progress curve is the first step in studying the kinetics of that reaction. KINFIT4, an existing general non-linear curvefitting computer program was used for this purpose. This program is a modified

version of the program KINFIT originally written by Dye and Nicely in 1971 (137). Individual or simultaneous multiple data sets can be fitted to integrated or differential equation(s) in order to find the "best" parameters that fit the experimental results. The program also computes the estimates of the marginal standard deviations, which include the effect of coupling among the adjustable parameters. A detailed description of the program is given elsewhere (137).

E.2. Weighted Principal Component Analysis (PCA)

An essential step in data analysis is to determine how many detectable species occur in a reaction. This information, coupled with the rate law results obtained from the first step, can lead one to propose and explain a plausible mechanism that accounts for the experimental facts about a particular reaction. The statistical method of Principal Component Analysis (PCA) is ideally suited for determining the number of light-absorbing species in a chemical reaction in rapid scanning wavelength kinetics experiments.

The method of PCA was developed by Cochran and Horne (138,139, 140) and is discussed in detail in Cochran's Ph.D. dissertation (98). The method was successfully used by Dr. F. Halaka in resolving the reduction of cytochrome $\underline{c}$ oxidase by MPH (99). Neither mechanistic assumptions nor any assumptions about the spectral shapes of light absorbing species are needed to apply PCA. The applicability of PCA requires only that the response at each wavelength channel be a linear function of the concentration of each detectable species (Beer's law).

Two kinds of principal component analysis are useful for kinetic experiments. Each requires only the matrix $\underline{A}$ (with proper weights), and each gives a lower bound estimate of $\underline{q}$; the number of independent detectable chromophores in the reaction. The first method, "Second moment matrix principal component analysis" or (M analysis), gives for q a lower bound estimate that is sensitive to the linear dependence of the concentrations of the detectable species. The second method, "sample covariance matrix principal component analysis" or (S analysis), gives for $\underline{q}$ an estimate that is sensitive to the linear dependence of the time-rates of the concentrations. The two estimates of $\underline{q}$ are not necessarily the same, and application of both methods enables one to discriminate between alternate mechanisms. The following example illustrates the application of M and S analyses, suppose:

$$A_1 \searrow$$
$$\searrow A_3 \qquad\qquad (II.6)$$
$$A_2 \nearrow$$
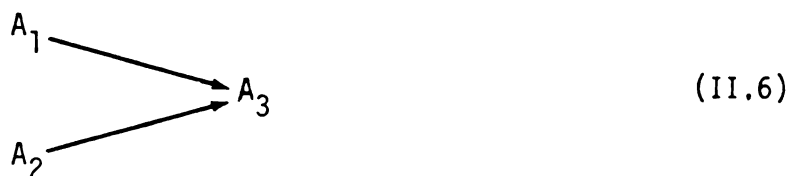
where A_1, A_2, and A_3 are three different absorbers. Application of M analysis to this mechanism would give $q_M = 3$, since there are three absorbers in the reaction and all three change concentration with time (notice that a linear relation between the concentrations does not exist). However, mechanism (II.6) has the constraint:

$$\frac{d[A_3]}{dt} = - \left(\frac{d[A_1]}{dt} + \frac{d[A_2]}{dt} \right) \qquad\qquad (II.7)$$

which says that the rate of one absorber depends upon the rates of the other two. Thus, for this example, application of S analysis would give $\underline{q}_S$ = 2, since there are only two absorbers whose concentrations change independently of one another during the reaction. The PCA procedure along with its application to this work will be discussed in more detail later in Chapter VII.

CHAPTER III

"TRYPTOPHANASE INACTIVATION BY SUDDEN REMOVAL"
OF K^+ WITH THE AID OF A CROWN-ETHER OR CRYPTAND

A. Introduction

Inorganic monovalent cations such as K^+, Na^+, or NH_4^+ play an important role in biological processes. For example, they act as cofactors in transport, charge carriers in nerve impulses, and activators of enzymes. The latter is the basis of our interest in these cations. Monovalent cation activated enzymes fall into two main classes; those that catalyze phosphoryl transfer reactions, and those that catalyze elimination reactions. The latter group includes a subgroup of pyridoxal phosphate-dependent enzymes that catalyze α,β-elimination reactions of α-amino acids. Tryptophanase from Escherichia Coli B/lt7-A is a member of such a group which also requires certain monovalent cations for catalysis (51).

The spectrum of active tryptophanase above 280-nm contains absorption maxima centered at 337 and 420 nm; their relative amplitudes are sensitive to the nature and concentration of monovalent cations and to pH (46,82). An absorption band at 420 nm dominates the spectrum of the inactive K^+-free enzyme.

A variety of experimental approaches are used to investigate the specific role of monovalent cations in maintaining the tryptophanase

51

structure as well as their mode of action in the catalytic processes.
For example, on the basis of spectroscopic and ultracentrifugal experi-
ments, Mornio and Snell reported differences between K^+- and Na^+-
tryptophanase in the sedimentation rate of the holoenzyme, in the af-
finity of the apoenzyme for pyridoxal-phosphate, in the spectrum of
the holoenzyme, and in the rate of recombination of the apoenzyme
with pyridoxal-phosphate (59,65). Suelter and Snell studied the
effect of different monovalent cations on the kinetic parameters,
K_m and V_{max}, when using SOPC as substrate. They showed that each
cation activates the enzyme, Li^+ being the least effective and am-
monium the best (77). Toraya et al. established that K^+ is absolutely
required for conversion of the apoenzyme-pyridoxal-phosphate complex
into the functional form (76). This was later supported by the work
of Suelter and Snell who showed that with ethionine as substrate, the
extent of formation of the quinonoid intermediate is linearly related
to the maximum velocity observed with each cation (77). Despite
these and a number of other studies on the subject, however, a de-
tailed study of the kinetics of activation and/or deactivation of
tryptophanase has not been reported to date. Studying the monovalent
cation activation of tryptophanase is made difficult by the following
observations: (1) it is difficult to replace K^+ with a less effective
cation such as Na^+ within a reasonable experimental time and simul-
taneously observe the changes because tryptophanase shows a greater
affinity for K^+ than for Na^+; (2) a suitable K^+-free medium in which
holotryptophanase remains stable for a period long enough to be ac-
tivated has not been investigated or reported.

In order to gain some insight into the mechanism of monovalent cation activation/deactivation of tryptophanase, we used the stopped flow system to change immediately the concentration of monovalent cation (K^+ in our case) and simultaneously follow the kinetics of the processes. For this purpose we took advantage of the selective ion binding properties of the two classes of macrocyclic compounds known as crown ethers and cryptands described in Chapter I. 1,4,7,10,13,16-hexaoxacyclooctadecane, referred to as 18-crown-6, 18-C_6 or simply crown in the text, and 4,7,13,16,21,24-hexaoxe-1,10-diazobicyclo[8.8.8]hexacosane, referred to as cryptand[2.2.2] or C_{222} (See Figure I.7 for structural formulas) are both well-known complexants for K^+ and were hence used in this study. This study made use of scanning and fixed-wavelength stopped-flow spectrophotometry. In a scanning experiment, digitized data are stored for the entire wavelength region spanned as a function of time. These data describe the kinetics of absorbance changes for every wavelength channels at essentially the same time. The deactivation process was followed spectrophotometrically by noting the changes in absorbance at 420 and 337 nm as a function of time, results of which are reported in this chapter.

B. Underline Experimental Section

Tryptophanase from Escherichia Coli B/1t7-A was prepared as described previously (123). Holoenzyme was prepared from stock apoenzyme by incubation in 25 mM K^+-Epps, pH 8.0, 1 mM EDTA, 0.2 M KCl,

20 mM dithiothreitol (DTT), and sufficient pyridoxal-p for 15 min at 50°C as suggested by Högberg-Raibaud et al. (63). Protein concentration was determined spectrophotometrically using ε_{278} = 0.795 ml·$mg^{-1} \cdot cm^{-1}$ (65). The enzyme had a specific activity of 50-55 ·mole· $min^{-1} \cdot mg^{-1}$ when assayed with 0.6 mM S-orthanitrophenyl-L-cysteine (SOPC) in 50 mM potassium phosphate, pH 8.0, 50 mM KCl, at 30°C (123). The activated enzyme was then extensively dialyzed while cold against three changes of 15 mM bicine buffer at pH 8.75, 3 mM KCl, 1 mM EDTA, 5 mM DTT, 5 μM PLP, with a total K^+ concentration of about 17 mM. When cryptand[2.2.2] was used, the buffer contained tetramethyl-ammonium ion (TMA) rather than K^+ for maintenance of ionic strength, and the initial pH was adjusted so that the pH after mixing with the enzyme solution would be 8.70. This pH was chosen in order to see a large change in absorbance upon activation/deactivation. The macro-cyclic crown ether, 18-crown-6, was recrystallized from acetonitrile as the crown-acetonitrile complex (126), vacuum dried, and sublimed under high vacuum for maximum purity. Cryptand[2.2.2] was also vacuum sublimed before use.

A computerized double-beam rapid scanning absorbance stopped-flow spectrophotometer (91,92,96) was used either in the scanning mode to collect up to 150 spectra/second in the region 300-500 nm or in the fixed wavelength mode to collect absorbance-time data at any desired wavelength. In either case, the stopped-flow system measures and stores data in progressive pairs of time points and their corresponding voltages. Through existing software programs

described elsewhere (98), each data pair was then converted to a calibrated absorbance and a corrected time. These constitute the final data used by KINFIT and PCA for all data fitting and analysis. Unless otherwise indicated, all stopped-flow concentrations are the final values after mixing. All experiments were carried out at the ambient temperature of $24 \pm 1°C$.

C. Studies and Results

C.1. Equilibrium Studies

In order to carry out the deactivation experiment with either $18-C_6$ or C_{222} properly, it was necessary to determine the effects of these reagents (if any) on the activity under assay condition as well as on the spectrum of tryptophanase. For this purpose, assay experiments were carried out under the same conditions at pH 8.0 with $18-C_6$ or C_{222} present at various concentrations in the assay mixture. The results showed that the activity is not affected by addition of $18-C_6$ as long as K^+ is present in excess. Cary 17 experiments also showed no significant effect due to presence of $18-C_6$ on the spectrum of the enzyme under the same conditions. However, in contrast to the absence of an effect of 18-Crown-6 on the enzyme activity when K^+ is present in excess, cryptand[2.2.2] decreased the activity by about one-third. This might be expected considering that cryptand[2.2.2] is a diamine and it is possible for it to interact with an ionizable group(s) on the protein near the active site and thus affect the activity. For this reason the effects of

different enzyme and cryptand[2.2.2] concentrations were not deter-
mined by the stopped-flow. Nevertheless, a single stopped-flow
experiment that used C_{222} was done in order to qualitatively compare
the results with those obtained with 18-crown-6.

C.2. Kinetic Studies

The deactivation process was studied as a function of the enzyme
concentration at a fixed concentration of $18\text{-}C_6$ and as a function
of 18-crown-6 concentration at a fixed concentration of the enzyme.
In all cases, the active enzyme at pH 8.70 was rapidly mixed in a
stopped-flow apparatus with a solution of 18-crown-6 which suddenly
reduced the concentration of free K^+ and thus caused the enzyme to
deactivate. Both scanning and fixed-wavelength experiments were per-
formed; however, kinetic analyses were usually done on data collected
in a fixed-wavelength mode. This is due to the fact that, in a fixed-
wavelength experiment, it is possible to collect more data points
for a particular wavelength under study than is possible in the scann-
ing mode because of computer memory limitations and the finite scan
speed.

The major overall process involves a decay of the 337 nm band of
the active enzyme and growth of the 420 nm band of the inactive
enzyme as expected from previous studies (81,82,89). These studies
showed that the active enzyme also has an absorption band at 420 nm
whose intensity relative to the 337 nm band is pH dependent. The
rate of interconversion of these two bands following pH jump and
drop experiments and their role in catalysis were also described.

Figure III.1 shows the overall changes in terms of initial and final spectra in a typical deactivation experiment.

C.2.1. Deactivation Process as a Function of the Enzyme Concentration- This experiment was carried out at the four enzyme concentrations indicated in Table I. In all cases the enzyme solution was pushed against a solution of the same buffer that contained 18-crown-6 with a final concentration of 148 mM (after mixing). This crown concentration is large enough to reduce the free K^+ concentration from about 17 mM originally present to a final value of 1.06 mM. The final value of K^+_{free} was calculated from an equilibrium constant of 115 M^{-1} reported for complexation of K^+ with 18-crown-6 in aqueous solutions (119), neglecting the amount of K^+ bound to the enzyme (K_D = 1.44 mM). Figure III.2 displays a 3-dimensional plot of the overall spectral changes from 300 to 500 nm that occur when a solution of 3.0 mg/ml tryptophanase is mixed with 148 mM 18-crown-6 (values after mixing). This wavelength region was chosen to insure simultaneous observation of the 337 nm γ form and the resulting 420 nm α form (inactive). The principal changes in absorbance shown in Figure III.2 are the decay of the active enzyme with maximal absorbance at 337 nm, and growth of the inactive band at 420 nm as expected. Figure III.3 displays, in two dimensions, selected difference spectra from Figure III.2 as a function of time, and Figure III.4 shows the overall time courses at the two maximal wavelengths.

58

Figure III.1. Initial and final spectra collected during deactivation of 3 0 mg/ml (55 µM) tryptophanase by 148 mM 18-crown-6 (after mixing) in 15 mM bicine buffer, pH 8.75. Spectra were collected by the stopped-flow system described in the experimental section. Cell pathlength = 1.85 cm (●) = initial spectrum, (*) = final spectrum.
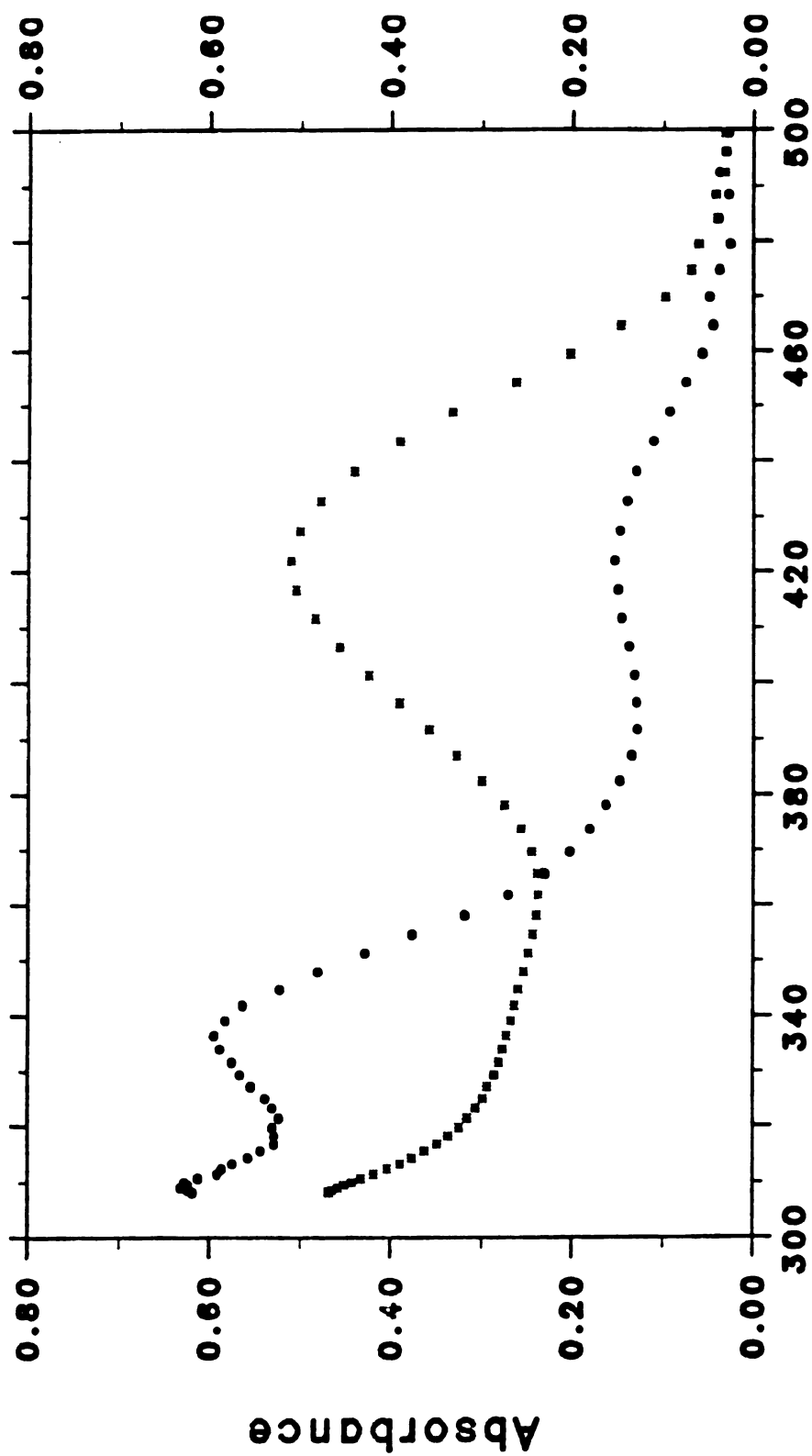
Figure III.1

Table III.1. Concentration of Various Species After Mixing in the K^+-Drop (deactivation) experiment.

Deactivation as f(E) $C_o^a = 148$ mM K^+_{free} (final) = 1.06 mM	Deactivation as $f(C_o)$ $E_o^b = 2$ mg/ml (36 μM)	
[ENZ], mg/ml	$[C_o]$, mM	K^+_{free} (final), mM
1.0 (18 μM)	60.0	2.70
1.5 (27 μM)	61.0	2.67
2.0 (36 μM)	76.0	2.13
3.0 (55 μM)	112.2	1.42
	148	1.06

$^a C_o$ is the total concentration of 18-crown-6.

$^b E_o$ is the total concentration of the enzyme.
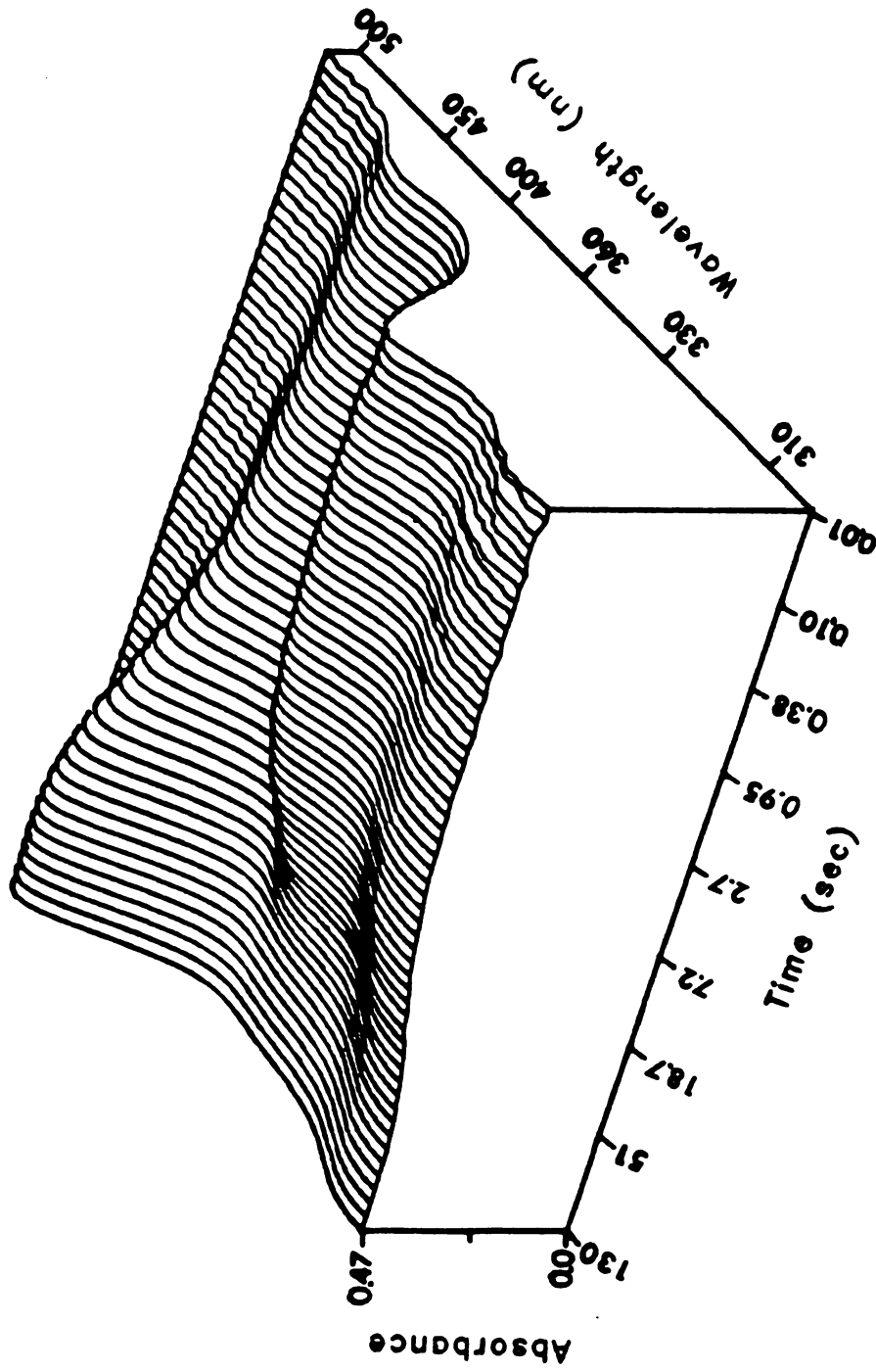
Figure III.2. Absorbance-time-wavelength surface in the 300-500 nm region for the deactivation of tryptophanase by 18-crown-6. Conditions are the same as in Figure III.1. (Cell path length = 1.85 cm, T = 24±1°C).
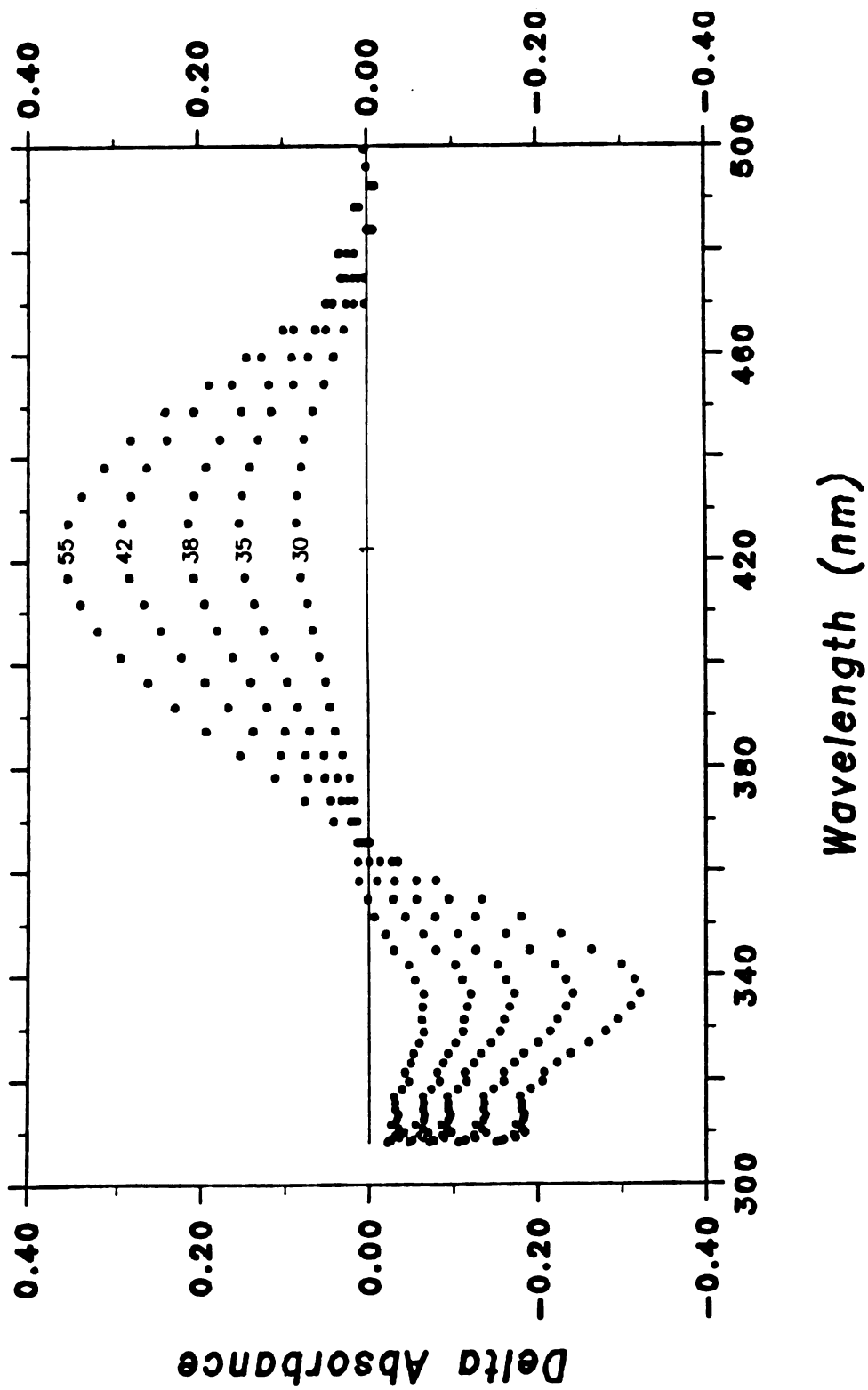
Figure III.3. Selected difference spectra constructed from Figure III.2 by subtracting the first spectrum from subsequent spectra. Times are: 30, 4 Sec; 35, 8 Sec; 38, 12.7 Sec; 42, 22 Sec; 55, 130 Sec.
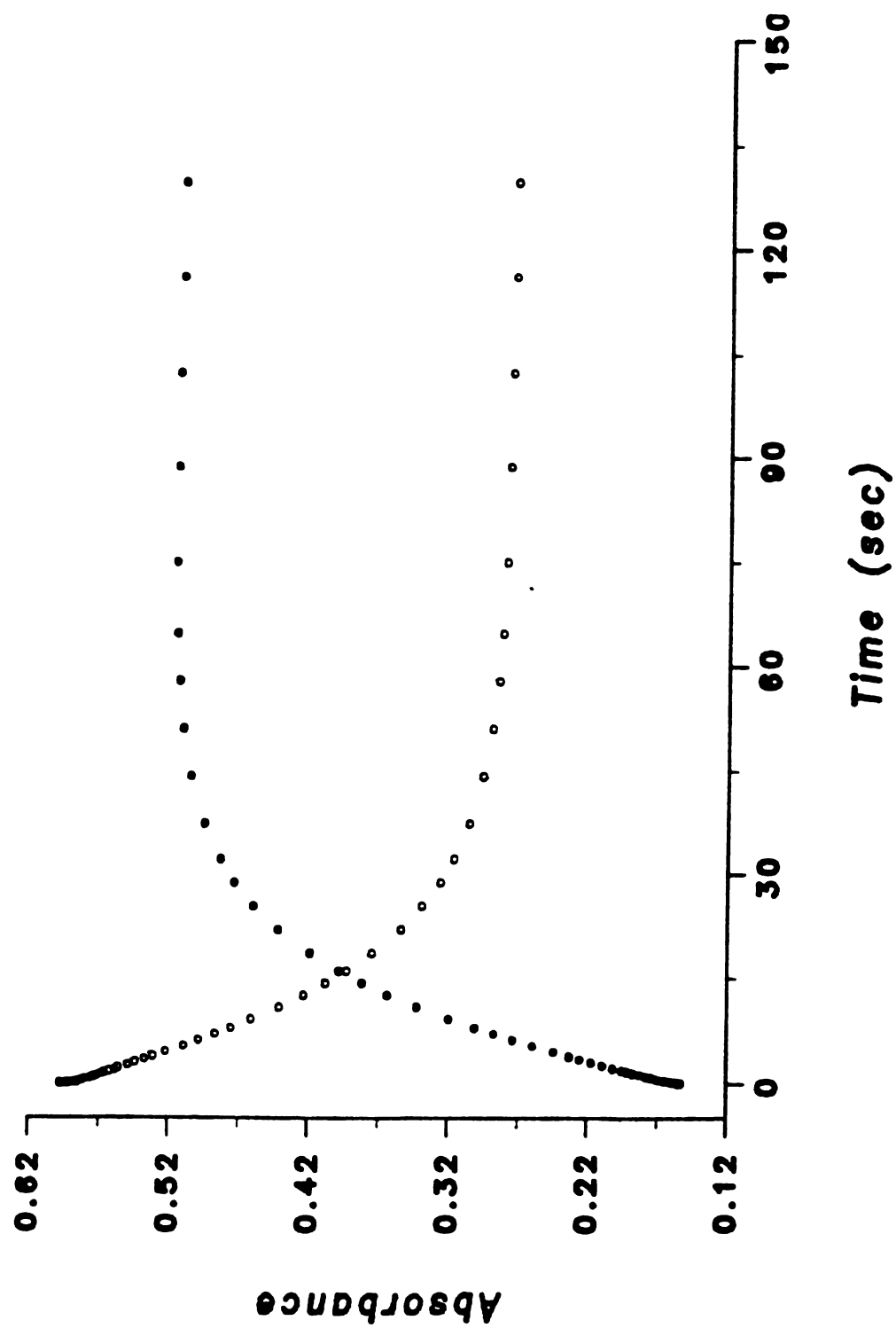
Figure III.4. Time dependence of absorbance at 337 (o) and 420 nm ( ) taken from the spectra shown in Figure III.2.

C.2.2. <u>Deactivation as a Function of 18-C$_6$ Concentration</u> - This experiment was carried out with an enzyme concentration of 2.0 mg/ml (36 μM) and five concentrations of 18-crown-6 (see Table III.1 for the concentrations used) in order to determine the effect of free K$^+$ on the rate of deactivation. In each case a solution of the enzyme in Bicine buffer at pH 8.70 was pushed against the same buffer to which had been added an amount of 18-crown-6 to give the final concentrations indicated in Table III.1. The overall changes of absorbance were the same as those shown in Figure III.2. Reducing the 18-crown-6 concentration, and hence increasing the free K$^+$ concentration, slowed down the effective rate of deactivation. For example, the process which is complete in less than two minutes in the presence of 148 mM 18-crown-6 is not completely over after about 3.5 minutes at the lowest crown concentration indicated in Table 1. Figure III.5 shows the effect of different 18-crown-6 concentrations on the kinetic profile at 337 nm.

C.2.3. <u>Results</u> - Detailed examination of the deactivation process showed five distinct temporal regions as indicated in Figure III.6

1. An "abrupt" change in absorbance occurred which was too fast to follow by the stopped-flow method. These changes occurred during the 7 mSec dead-time of the instrument (1.85 cm pathlength cell). The changes in spectra during this time were obtained by subtracting the enzyme spectrum at t = 0 obtained by mixing enzyme with buffer in the absence of 18-crown-6, from the first spectrum collected after mixing ($\sim$7-13 mSec). The changes in absorbance consisted of a
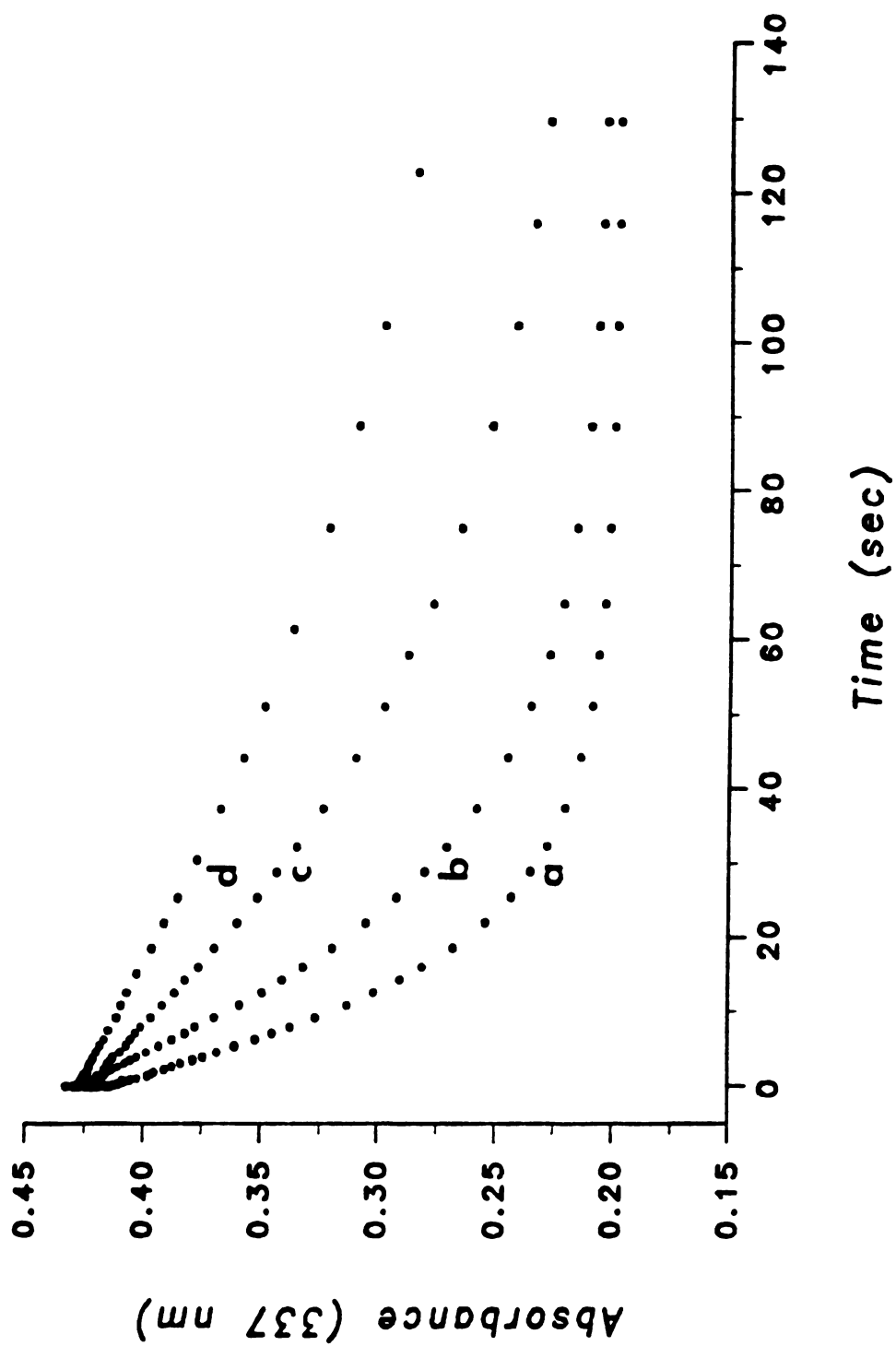
Figure III.5. Effect of various concentrations of 18-crown-6 on the rate of deactivation at 37 nm. Conditions are the same as in Figure III.1. (a) 148 mM Crown, (b) 112 mM Crown, (c) 76 mM Crown, (d) 60 mM Crown.

Figure III.6. Time dependence of absorbance change at 420 nm during the reaction of holo-tryptophanase in K^+-Bicine buffer at pH 8.75 with 18-crown-6. Concentrations are the same as in Figure III.1.
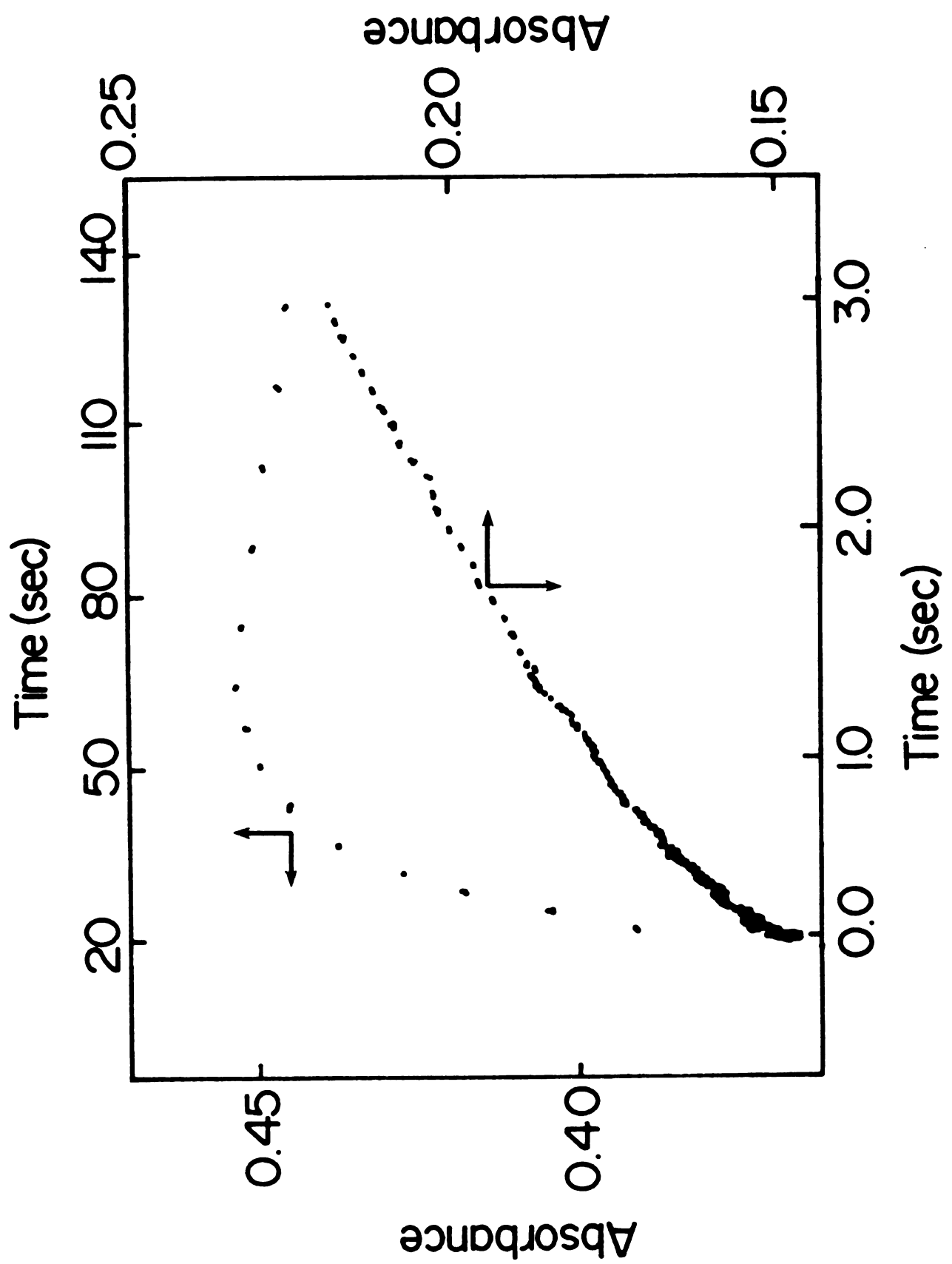
Figure III.6

generalized decrease in absorbance in the range of ∿325-360 nm with

a possible peak at ∿340 nm, and an increase in the range ∿300-315 nm

with a possible peak at ∿310 nm. The amplitude of this abrupt change

was proportional to the enzyme concentration ($\Delta A \approx 0.025$ per mg enzyme

at 310 nm) and was constant at all concentrations of 18-crown-6 in-

dicated in Table 1.

2. Following the abrupt changes a fast exponential change (burst)

was observed which consisted of a decay at 337 nm ($2.5 \pm 0.4\%$ of the

total change) and a growth at 420 nm ($3.9 \pm 0.3\%$ of the total change).

The burst occurred at all enzyme concentrations indicated in Table 1,

however, it was not detectable at low concentrations of 18-crown-6.

The apparent first-order rate constant for the changes in this

region at 337 and 420 nm were obtained by fitting the first three

seconds of the absorbance vs time data at each wavelength to equation

(III.1) by using the non-linear curve-fitting program KINFIT4 des-

cribed elsewhere (137).

$$A_{obs} = A(o) \mp \Delta A \exp (-k_2' t) \pm ct \{ \begin{array}{l} \lambda = 420 \text{ nm} \\ \lambda = 337 \text{ nm} \end{array} \} \qquad (III.1)$$

This equation combines the exponential change observed in this

region and the changes of the following region which   were found to

be linear. The 3rd-term in equation (III.1) accounts for the contri-

bution of the latter phase to the kinetic profiles at the two wave-

lengths. The adjustable parameters were A(o), the absorbance change

of the linear region extrapolated to time zero, $|\Delta A|$, the absolute

value of the change in absorbance between A_o (absorbance at t = 0)

and $A(o)$, C, the slope of the linear region, and k_2' the apparent first-order rate constant for the burst. Relatively small and random residuals were obtained for the computer fit of the data to equation (III.1) at both wavelengths. This fit indicates that the equation used adequately describes the data. Figure III.7 shows a computer fit of such data at 337 nm along with the residual plot for concentrations of 3.0 mg/ml and 148 mM of the enzyme and 18-crown-6, respectively. The rate constants thus obtained are tabulated in Table III.2. As the results indicate, the apparent 1st-order rate constant is essentially independent of wavelength and enzyme concentration. Since the burst disappears at the lower crown concentrations, the dependence of k_2' (if any) on the concentration of 18-crown-6 could not be determined.

3. The third temporal region of the deactivation process consisted of a linear decay at 337 nm or growth at 420 nm. This change occurred at all concentrations of both the enzyme and 18-crown-6. Inspection of the time courses at both wavelengths showed that this region lasts about 7 to 10 seconds in time, and so the data in this region were fitted to a linear function with KINFIT4 in order to determine the effect of the enzyme and 18-crown-6 on the rate (slope) of this change. Again, small and random residuals $(A_{obs}-A_{calc})$ were obtained for the fit, indicating that the proper equation was used. Tables III.3 and III.4 summarize the results of the analysis of this phase.

4. Most of the change in absorbance after $\underline{7}$ seconds ($67\pm4\%$ of the total change after the abrupt phase) occurs as a single exponential

Figure III.7. (A) Fit of the burst and linear phases for the
deactivation of tryptophanase by 18-C_6 by Equa-
tion III.1. X's are the experimental data points
and the solid line is the calculated curve.
Data collected in a fixed-wavelength mode. (B)
Residuals of the fit shown in (A). Residuals
are defined as A(calc)-A(obs). Conditions are
again the same as in Figure III.1.

Figure III.7
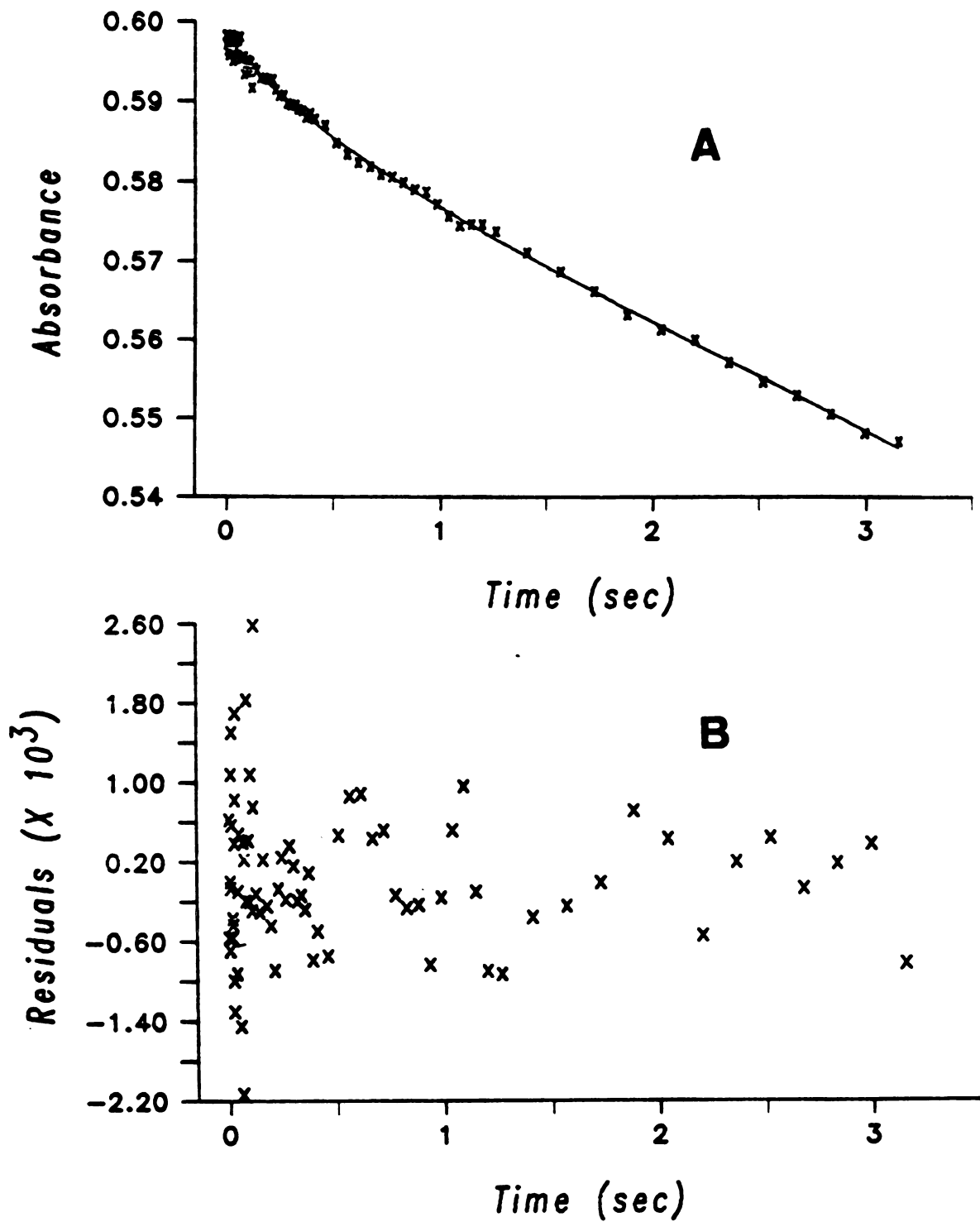
Table III.2. Analysis of the Burst Region of the Deactivation Process
            by 18-Crown-6 in Bicine Buffer, pH = 8.70, at 24±1°C.
            k_1' is the Observed 1st-order Rate Constant for the Process.

[E_0], mg/ml	$k_2' \pm \sigma^a$ S^{-1} (λ=337 nm)	$k_2' \pm \sigma^a$ S^{-1} (λ=420 nm)
3.0 (55 μM)	2.57± .60	2.14±.18
2.0 (36 μM)	2.80± .75	1.94±.23
1.5 (27 μM)	1.79± .50	1.85±.38
1.0 (18 μM)	2.80±1.05	1.77±.23

AVE = 2.2±.5 Sec^{-1}

[a]Marginal Standard deviation.

Each measurement is the average of two separate pushes.

Table III.3. Variation of the "Slope" of Linear Region of the Deactivation Process as a Function of the Enzyme Concentration at Fixed Crown Concentration of 148 mM. Conditions of the Experiment are Described in the Experimental Section.

$[E_0]$, mg/ml	Slope (337 nm) $\times 10^2 \text{ s}^{-1}$	Slope (420 nm) $\times 10^2 \text{ s}^{-1}$
3.0	$1.42 \pm .01$	$1.71 \pm .01$
	$1.40 \pm .01$[a]	$1.75 \pm .01$[a]
2.0	$.97 \pm .01$	$1.22 \pm .01$
	$.96 \pm .01$[a]	$1.21 \pm .01$[a]
1.5	$.73 \pm .01$	$.92 \pm .01$
	$.71 \pm .01$[a]	$.91 \pm .01$[a]
1.0	$.47 \pm .01$	$.61 \pm .01$
	$.44 \pm .01$[a]	$.59 \pm .01$[a]

[a]Separate pushes.

Table III.4. Variation of the "Slope" of Linear Region of the Deactivation Process as a Function of 18-Crown-6 Concentration at Fixed Enzyme Concentration of 2.0 mg/ml (36 µM). Conditions of the Experiment are Described in the Experimental Section.

$[C_0]$, mM	Slope (337 nm) $\times 10^2 \, s^{-1}$	Slope (420 nm) $\times 10^2 \, s^{-1}$
148.	.96 ±.01	1.212±.006
	.97 ±.01[a]	1.216±.007[a]
112.2	.583±.004	.773±.003
	.550±.006[a]	.778±.003[a]
76.0	.255±.005	.354±.003
	.278±.005[a]	.356±.002[a]
61.0	.154±.005	.225±.003
	.147±.005[a]	.222±.003[a]
60.0	.165±.003	.212±.003
	.140±.004[a]	.219±.004[a]

[a]Separate pushes.

decay (337 nm) or growth (420 nm). This phase was analyzed by simply choosing data points collected after ∿7 seconds and eliminating data points that occur in the very last slow process. Data for this phase were fit by a single exponential equation (III.2):

$$A_t = A_\infty \pm \Delta A \exp (-k_4' t) \qquad\qquad (III.2)$$

where A_∞, the absorbance at infinite time, ΔA, the total change in absorbance in this phase and k_4', the apparent 1st-order rate constant, were the three adjustable parameters. Figure III.8 represents a typical fit for this region at 337 nm, and Tables III.5 and III.6 list the values obtained for the rate constant, k_4', for this region. As indicated in Table III.5, the rate constants for this phase are practically independent of the wavelength and the enzyme concentration (except for a ∿20% decrease at the lowest enzyme concentration). It is important to note that the 420 nm band shows a slight but reproducible shift to shorter wavelengths during this time period. This shift was also reflected in the computer fit of the data at 420 nm as small but systematic deviations in the residuals at this wavelength. When the concentration of 18-crown-6 was varied, the residuals became smaller and more randomized at lower concentrations. This shift may imply that the 420 nm absorbing species produced at the end of the exponential stage is not the resting form of the inactive enzyme but that the final product has its peak at a shorter wavelength possibly around 382 nm.

5. Finally, a very slow exponential process following the
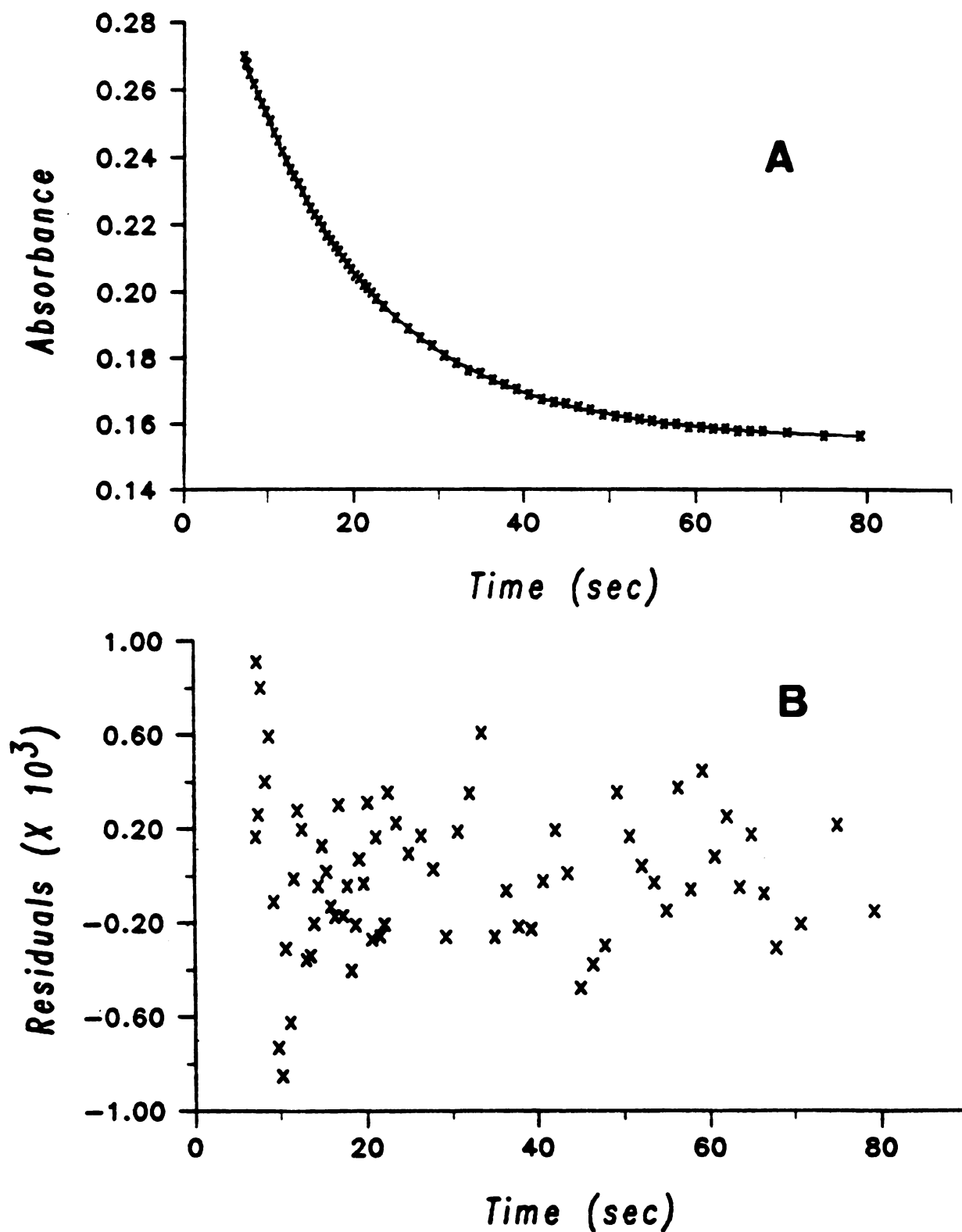
Figure III.8. Fit of the exponential region of the deactivation process by Equation III.2. Conditions are the same as in Figure III.1. Again X's are the experimental data points and the solid line is the calculated curve. (B) Residuals of the fit shown in (A).

Table III.5. Kinetic Parameters for the Exponential Region of the Deactivation Process as a Function of the Enzyme Concentration at Fixed Crown Concentration of 148 mM. t=24±1°C.

$[E_0]$, mg/ml	$k_4^!$ $(337) \times 10^2$ s^{-1}	$k_4^!$ $(420) \times 10^2$ $s^{-1}{}^a$
3.0	6.67±.02	7.51±.04
	6.77±.02[b]	7.71±.04[b]
2.0	6.61±.02	7.64±.04
	6.65±.02[b]	7.64±.04[b]
1.5	6.37±.03	7.44±.04
	6.10±.06[b]	7.45±.04[b]
	6.33±.06[c]	7.03±.06[c]
1.0	5.06±.03	6.15±.03
	5.33±.03[b]	6.00±.03[b]
	4.90±.03[c]	5.82±.08[c]

[a]Fit shows systematic deviations at this wavelength

[b]Duplicate pushes.

[c]Scanning file.

Table III.6. Kinetic Parameters for the Exponential Region of the De-
activation Process as a Function of 18-Crown-6 Concentra-
tion at a Fixed Enzyme Concentration of 2.0 mg/ml (36 μM).
See the text for conditions of the experiment. Results
are from duplicate pushes.

$[C_0]$, mM	$k_4'(337) \times 10^2$ s^{-1}	$k_4'(420) \times 10^2$ s^{-1} [a]
148	6.65±.02	7.64±.04
	6.61±.02	7.64±.04
112.2	3.69±.01	4.26±.02
	3.69±.01	4.27±.02
76.0	1.632±.004	1.96±.01
	1.657±.006	1.97±.01
61.0	.928±.005	1.166±.005
	.923±.003	1.183±.004
60.0	.920±.004	1.112±.004
	.904±.003	1.115±.003

[a]Again fit shows systematic and non-random residuals at this λ especially
at higher Crown concentrations.

1st-order exponential phase occurred at all enzyme concentrations (Table III.1). Changes in the spectra during this stage involve decays centered at $\sim$443 nm and $\sim$330 nm and a simultaneous growth centered at $\sim$382 nm as indicated in the difference spectra of Figure III.9 collected during this phase. The changes in absorbance were very small ($\sim$2.5% of the total change at 330 nm, $(\Delta A)_{382} \simeq 0.010$ O.D. at the highest enzyme concentration), essentially about 3 times the signal/noise ratio in a scanning experiment at $\sim$400 nm. When the data in this phase were fitted to a single exponential equation by KINFIT, the same values were obtained for the rate constant at each wavelength. The values thus obtained were $1.4\pm0.3 \times 10^{-2}$ Sec^{-1} at 382 nm (growth), $0.8\pm0.4 \times 10^{-2}$ Sec^{-1} at 443 nm (decay) and $1.6\pm0.9 \times 10^{-2}$ Sec^{-1} at 330 nm (decay). These values were calculated for data obtained at 112 and 148 mM 18-crown-6; the changes in absorbance at lower concentrations of 18-crown-6 were too small to permit a reasonable evaluation of the effect of concentration on the rate. The rate constants for regions 2 to 5 are summarized in Table III.7.

C.3. Kinetics of Deactivation by Cryptand[2.2.2]

The experiment with Cryptand[2.2.2], or simply C_{222}, was carried out in order to compare the results with those of 18-crown-6. Since K$^+$ forms a much stronger complex with C_{222} than with 18-crown-6 (binding equilibrium constant with K$^+$ is 8.70×10^5 M^{-1} for C_{222} compared to 115 M^{-1} for 18-C_6), a substantially lower concentration of C_{222} was required for this experiment. An enzyme concentration of 3.0 mg/ml
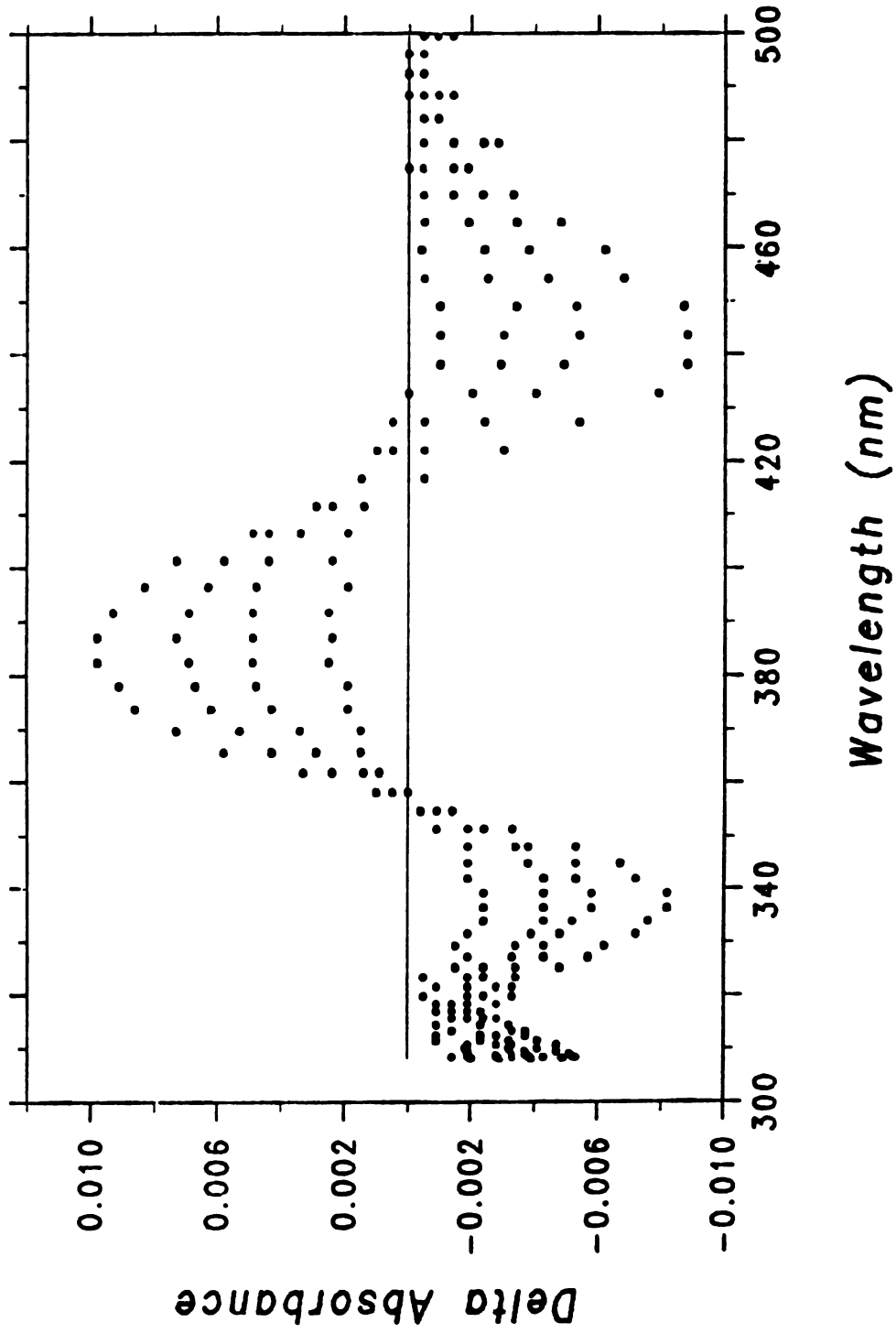
Figure III.9. Slow exponential changes occurring at the completion of the deactivation process (region 5). The spectra were constructed from those in Figure III.2 by subtracting the spectrum at the end of the exponential deactivation phase (region 4) from subsequent spectra.

Table III.7.   Summary of the Results of the "K$^+$ Drop" Experiments Described in the Text.

Nature of the process	Rate law	Rate constants (per second)	(nm)
Exponential burst (region 2)	$d(Abs)^o/dt = -k_2(Abs)$	$k_2 = 2.2 \pm 0.5$	(337 + 420)
Linear (region 3)	$d(E_{actual})/dt = -k_3(E_0)(C_0)^2$	$k_3 = 1.85 \pm 0.08\ M^{-2}$ $= 1.91 \pm 0.09\ M^{-2}$	(337) (420)
Exponential (region 4)	$d(Abs)/dt = -k_4(Abs)(C_0)^2$	$k_4 = 2.8 \pm 0.2\ M^{-1}$	(337)
Exponential (region 5)	$d(Abs)/dt = k_5(Abs)$	$k_5 = (1.4 \pm 0.3) \times 10^{-3}$ $= (0.8 \pm 0.4) \times 10^{-3}$ $= (1.6 \pm 0.9) \times 10^{-3}$	(382) (443) (330)

* (Abs) refers to difference in absorbance at time t and absorbance at the end of this process.

(55 µM) and a C_{222} concentration of ~16 mM (both before mixing) were used for this experiment. This concentration of cryptand was cal-culated to be large enough to reduce the concentration of free K^+ to 1.0 mM after mixing, so that the data could be compared with those obtained with 18-crown-6 at the same enzyme concentration. As men-tioned earlier, since C_{222} reduced the activity of the enzyme (even at concentrations much below 16 mM), the effects of enzyme and cryp-tand concentrations were not studied.

The general behavior with C_{222} was very similar to that obtained with $18-C_6$ except that no linear region was detected at this concen-tration of C_{222}. Similarly, the 420 nm band shifted slightly toward shorter wavelength as indicated in the difference spectra of Figure III.10 collected for this experiment. A generalized double-exponential equation (III.3) was used to fit the data at 337 and 420 nm;

$$A_t = A_\infty \pm \Delta A_1 \exp (-k_1't) \pm \Delta A_2 \exp (-k_2't) \qquad \text{(III.3)}$$

where A_∞, the absorbance at infinite time, ΔA_1 and ΔA_2, the changes in absorbance due to the two exponential phases, and k_1' and k_2', the observed first order rate constants for the two phases respectively, were the adjustable parameters. The equation seemed to describe the data relatively well. Figure III.11 represents the fit of the data at 420 nm to equation (III.3) along with the residual plot obtained for the fit, and Table III.8 shows the values obtained for the rate constants.

Comparison of the results with those of 18-crown-6 at the same

Figure III.10. Selected difference spectra collected during the reaction of tryptophanase with cryptand[2.2.2] in 15 mM TMA-BICINE buffer at pH 8.75. Concentrations are: [ENZ] = 3.0 mg/ml (55 M), [C222] = 15.8 mM (before mixing). Times are: 28, 6 Sec; 30, 9.3 Sec; 32, 12.7 Sec; 34, 18.7 Sec; 36, 25.5 Sec; 38, 37.5 Sec; 40, 51 Sec; 44, 102 Sec. Cell path length = 1.85 Cm, T = 24 ± 1°C.
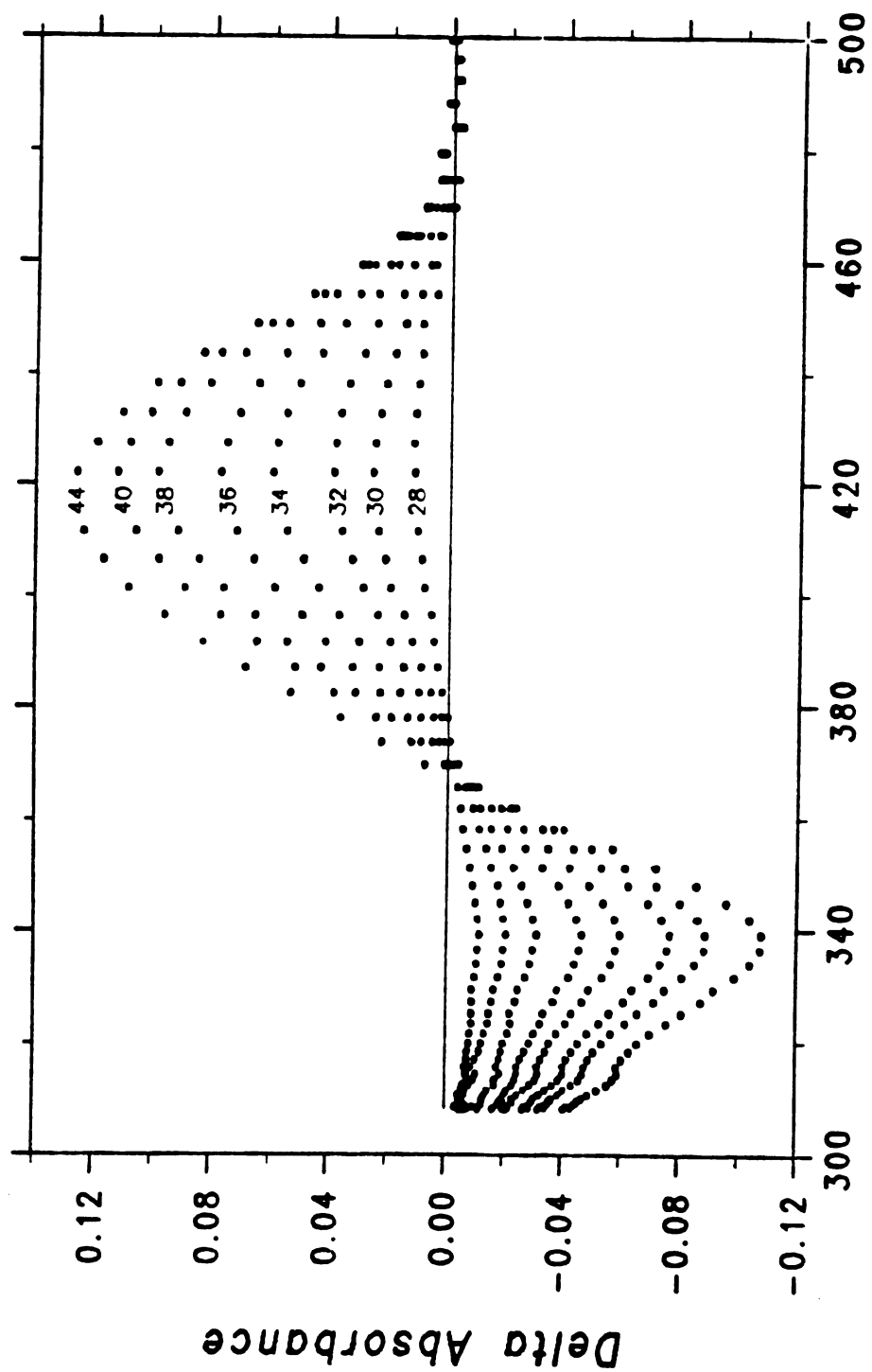
Wavelength (nm)

Figure III.10

Delta Absorbance
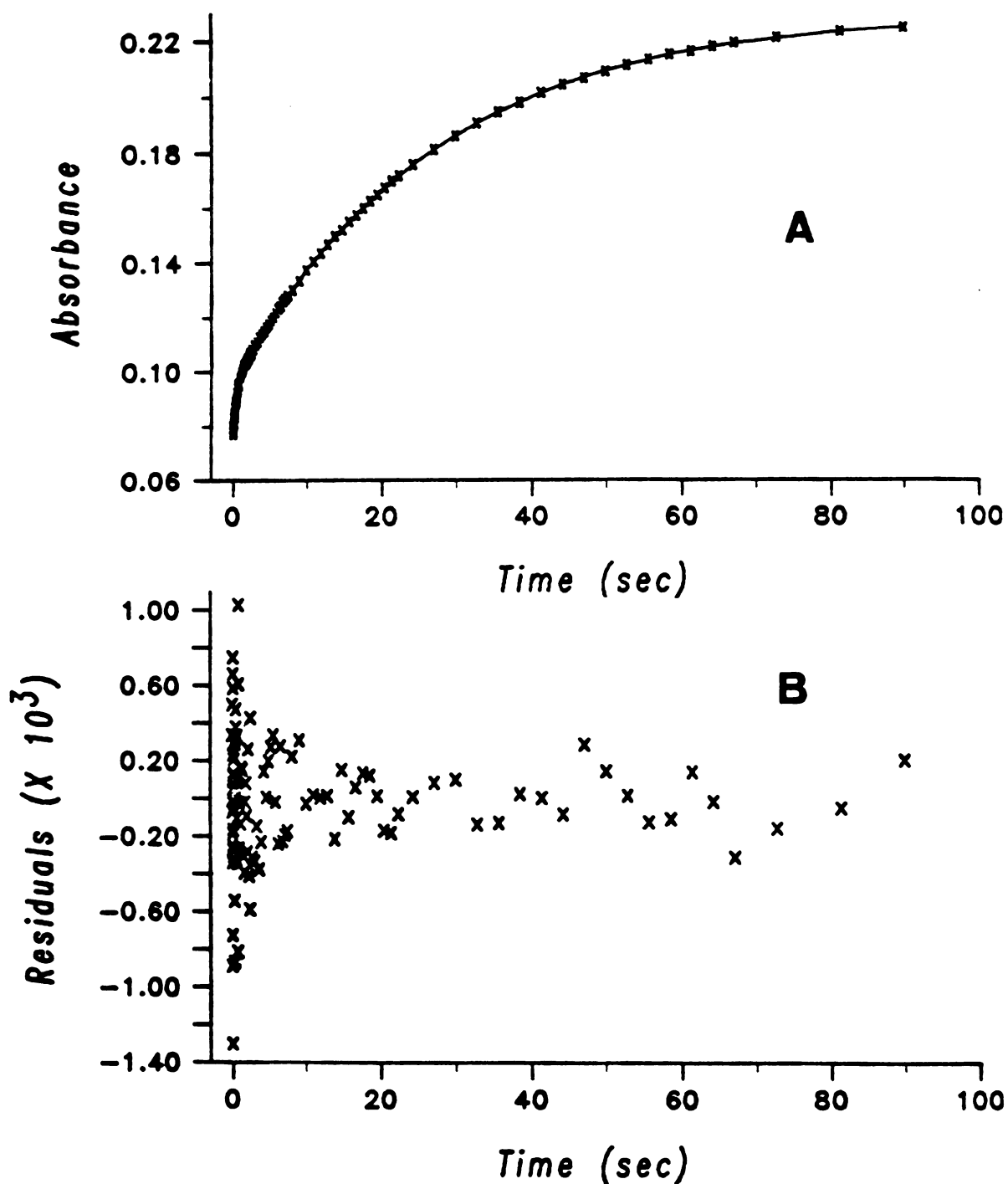
Figure III.11. (A) Fit of the overall absorbance change at 420 nm (subtracting the tail) for the deactivation of tryptophanase by C_{222} by the double exponential Equation III.3. Conditions of the experiment are the same as in Figure III.10. (B) Residuals of the fit shown in (A).

Table III.8. Kinetic Parameters at 337 and 420 nm for the Deactivation of Tryptophanase by Cryptand [2.2.2]. The data were fit to Equation III.3 in the text.

---Wavelength---	---Two Exponentials---	
I. 337 nm	$k_1'(S^{-1})$	$k_2'(S^{-1})$
	2.44 ± 0.28	$(2.96\pm0.01)\times10^{-2}$
	2.64 ± 0.29	$(2.90\pm0.01)\times10^{-2}$
II. 420 nm	1.72 ± 0.07	$(3.70\pm0.01)\times10^{-2}$
	2.09 ± 0.07	$(3.78\pm0.01)\times10^{-2}$
	AVE = 2.2 ± 0.4	

enzyme concentration (Tables III.2 for k_1' and III.5 for k_2') shows that k_1', the rate constant for the burst, is the same for both complexing agents, however, k_2' values are smaller in magnitude when C_{222} is used. This difference could be due to a buffer effect (Since TMA^+ is present in the C_{222} buffer) and/or an inhibiting effect of C_{222} on the enzyme similar to that observed in the assay measurements. Similar to the crown experiments, a very slow process also followed the second exponential phase with absorbance changes at the same wavelengths, i.e., decays centered at $\sim$440 and 330 nm, and a growth at 382 nm. Figure III.12 displays the spectral changes collected during this phase when C_{222} is used. Since at this cryptand concentration the changes were small and there were not sufficient data points to allow a reasonable computer evaluation of this phase, another experiment with a cryptand concentration of 30 mM (before mixing) was performed in order to analyze these changes. When the data were fit to an exponential equation with the KINFIT program, the same values were obtained again for the rate constant at each wavelength [$0.9 \pm 0.4 \times 10^{-2}$ Sec^{-1} at 382 nm (growth), $0.7 \pm 0.1 \times 10^{-2}$ Sec^{-1} at 335 nm (decay), and $1.03 \pm 0.03 \times 10^{-2}$ Sec^{-1} at 443 nm (decay)]. The values are practically the same as those obtained with 18-crown-6 and again seem to suggest that the 420 nm form produced is not the final product of the deactivation process. It should be mentioned here that cryptand [2.2.2] at the latter concentration completely deplets free K^+ and thus strictly speaking, the data here cannot be compared to a similar case for 18-crown-6.
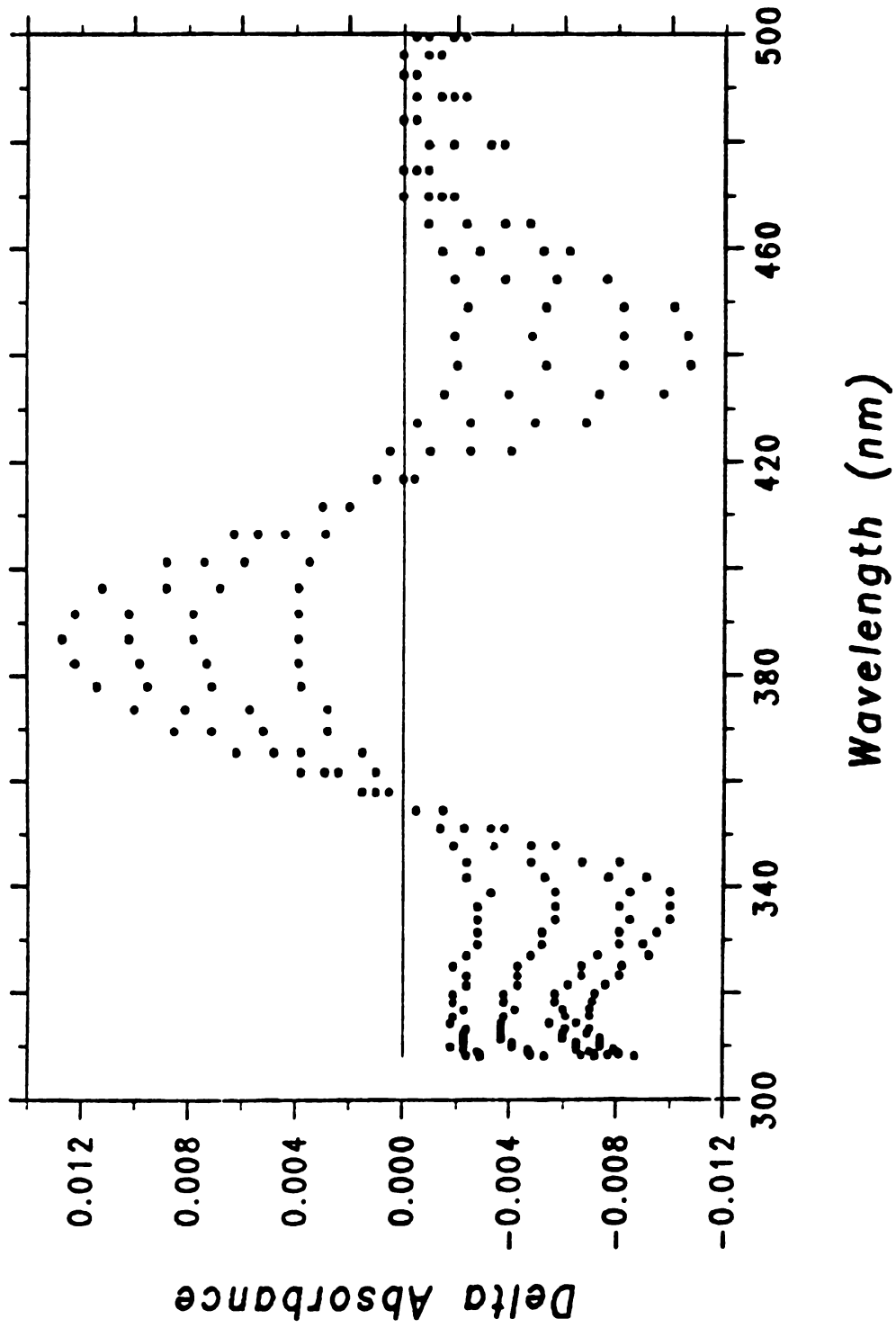
Figure III.12. Slow exponential changes occurring at the end of the reaction between trypto-
phanase and cryptand[2.2.2]. This figure is to be compared with Figure III.9
showing the same changes when 18-crown-6 is used.

D. Discussion and Conclusions

The kinetic studies of tryptophanase deactivation with the aid of 18-crown-6 or cryptand [2.2.2] provide some insights into the interconversion of the active to inactive enzyme. Inspection of the results presented in Tables III.3 and III.5 shows that the rate of deactivation is proportional to the total enzyme concentration and to the square of the 18-crown-6 concentration (see also Figure III.13) during the linear region of the process. If E_0 and C_0 are the initial concentrations of the total enzyme and 18-crown-6 respectively, then the rate of this process can be represented as

$$\frac{d(E_{active})}{dt} = -k_3(E_0)(C_0)^2 \qquad .$$

$$\text{(III.4)}$$

To find k_3 from the data presented in Tables III.3 and III.4, we can rewrite equation (III.4) in terms of absorbance such that

$$[\frac{d(E_{active})}{dt}]_{337} = \frac{1}{\varepsilon_{337} \cdot b} \frac{d(A)_{337}}{dt} = \frac{(slope)_{337}}{\varepsilon_{337} \cdot b} = k_3(E_0)(C_0)^2$$

$$\text{(III.5)}$$

Solved for k_3 equation (III.5) becomes

$$(k_3)_{337} = (slope)_{337}/\varepsilon_{337} \cdot b \cdot (E_0)(C_0)^2$$

$$\text{(III.6)}$$

Similarly at 420 nm we have
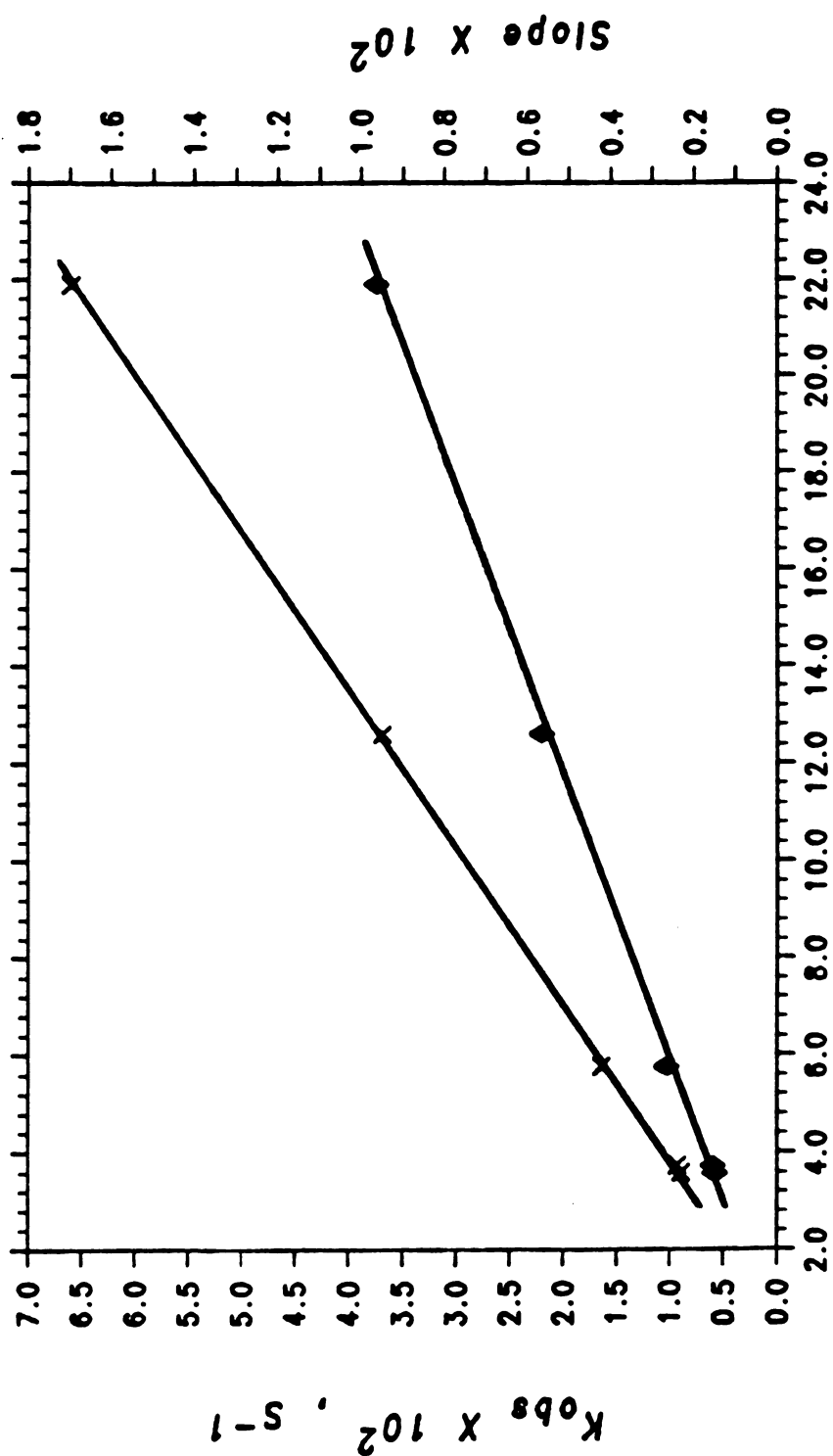
Figure III.13. Dependence of the apparent 1st-order rate constant for the exponential region of the deactivation process (x) and the slope of linear region ( ) of the process on the square of 18-crown-6 concentration.

$$(k_3)_{420} = (slope)_{420}/\varepsilon_{420} \cdot b \cdot (E_0)(C_0)^2 \qquad \text{(III.7)}$$

Values of 3500 $M^{-1} \cdot Cm^{-1}$ for ε_{337} and 4600 $M^{-1} \cdot Cm^{-1}$ for ε_{420} obtained from previous studies (82) and a cell path length of 1.86 Cm (b) were used. The rate constant k_3 was found to be 1.85±0.08 $M^{-2} \cdot Sec^{-1}$ at 337 nm and 1.91±0.09 $M^{-2} \cdot Sec^{-1}$ at 420 nm. We assumed that the extinction coefficient at 420 nm of the inactive species formed in the reaction is the same as that of the 420 nm active species. The fact that the same value of k_3 is obtained at 420 nm and 337 nm when using this assumption, might suggest that the coenzyme form which gives rise to the inactive 420 nm absorption is in fact similar in structure to the active 420 nm forms (E_β,$E_{\beta H^+}$ in Figure I.4) but is bound in such a way as to prevent direct interaction with groups necessary for catalysis at the active site.

The data obtained in the exponential region show that while the observed rate constant for this region is essentially independent of the enzyme concentration (Table III.5), it depends again on the square of the 18-crown-6 concentration (Table III.6, also Figure III.13). Similar dependence was also observed qualitatively when cryptand[2.2.2] was used. Thus, the rate equation for this region can be written as

$$\frac{d(Abs)}{dt} = -k_4(Abs)(C_0)^2 \qquad \text{(III.8)}$$

To find k_4, we used only data obtained at 337 nm (Table III.6) since the computer fit of the data at 420 nm during this time period showed small (10^{-4} to 10^{-3}) but systematic deviations due to a slight shift

of the 420 nm band to shorter wavelengths as indicated earlier. The results (excluding the lowest enzyme concentration) give a value of 2.8 ± 0.2 $M^{-2}\cdot Sec^{-1}$ for k_4. The systematic deviation at 420 nm may indicate that the change of absorbance at this wavelength is perhaps not due to a single process involving growth of the inactive 420 nm form but other slow processes involving species absorbing at or close to this wavelength may also be occurring during this time period. The fact that the residuals of the fit at this wavelength are greater in magnitude and are more systematic at higher concentrations of 18-crown-6 where the final slow changes (decay at 443 nm, growth at 382 nm) are observed, indicate that the latter process may be going on during this time region. In addition, one would expect that the 420 nm form of the active enzyme which is present to an extent of 15 to 20 percent at this pH (83), also converts into the inactive form(s) absorbing at the same wavelength and thus adds to the complexity of the analysis at this wavelength.

The mechanism of deactivation of tryptophanase by control of free K^+ concentration is complex and the results described indicate that multiple enzyme forms are probably involved. Since 18-crown-6 reacts with free K^+ very rapidly ($K_f = 4.3 \times 10^8$ $M^{-1}\cdot Sec^{-1}$) (148) we expect essentially instantaneous reduction in the free K^+ concentration in a K^+-drop experiment. The abrupt changes observed during the dead-time of the instrument are perhaps due to the immediate perturbation of the enzyme spectrum caused by sudden removal of potassium ions. Qualitatively similar changes have been observed earlier during the pH-drop experiments (83) which may indicate that sudden removal of

K^+ by crown or cryptand causes deprotonation of an amino group at or close to the enzyme active site resulting in an immediate "local" pH drop, thus perturbing the enzyme spectrum.

The changes observed in the exponential burst region (region 2) seem to suggest a perturbation in the equilibrium distribution of the 337 and 420 nm active species in favor of the 420 nm species before deactivation takes place. The apparent rate constant obtained for this region in both crown and cryptand cases, $k = 2.2 \pm 0.5$ Sec^{-1}, is similar to the observed fast first-order rate constant for the inter-conversion of the 337 and 420 nm forms, 1.41 Sec^{-1}, obtained by D. June (83) at a similar pH. In addition, the ratio of the magnitude of the absorbance change at 420 nm to 337 nm ($\Delta A_{420}/\Delta A_{337}$) compares favorably in both cases; being 1.32 in the pH change experiments and 1.47 in the deactivation experiments.

Zero-order kinetics are typically observed in surface catalysis where the concentration of the catalyst is very small. The zero-order decay observed here after the burst phase and before the onset of the first-order kinetics thus suggested catalysis by a minor species whose concentration is proportional to the total enzyme concentration. In the buffer system used for the experiment, the only species which may be available at very low concentration relative to the enzyme is pyridoxal-p. We expect a substantial change in the rate of deactivation as the concentration of PLP in solution is changed if it is involved as a catalyst for the conversion process. To check this, a similar experiment was performed at a substantially different PLP concentration (25 mM PLP). There was no effect on the rate of the

reaction, thus, eliminating the possibility of catalysis by PLP.
The zero-order process, however, may be explained qualitatively if
one considers that the deactivation occurs simultaneously with a
redistribution process involving the 337 and 420 nm forms. Recall
that the relative concentrations of these two forms had been altered
during the burst phase. The redistribution process may occur during
this time region (region 3) if one assumes that the potassium-crown
complex is released slowly from the enzyme. The release of the
(K^+C) complex would allow diffusion of the buffer into the enzyme
active site, thus, causing the described redistribution process.
This explanation is drawn from the fact that the magnitude of the
experimental absorbance change during the linear region is always
less than that calculated by using the exponential deactivation param-
eters (region 4) by a magnitude equal to that of the burst absorbance
change (region 2) at all concentrations in which a burst was detected.
However, the data could not be quantitatively accounted for by this
hypothesis in the absence of information about diffusion rates.

The second order dependence of the rate of deactivation on the
concentration of 18-crown-6 strongly suggests that two potassium ions
per subunit are required for activation, consistent with the binding
of two thallium(I) ions per subunit as reported earlier (77). The
slow exponential changes at the completion of the deactivation pro-
cess (region 5) observed with both 18-crown-6 and cryptand suggest
that the 420 nm species formed is not the final form of the inactive
enzyme. However, partial dissociation of pyridoxal-p from the enzyme
may also be occurring during this time region. Principal component

analysis (PCA) indicates the existence of at least three independent absorbers in the system. This and other PCA results will be discussed in Chapter VII.

CHAPTER IV

TRYPTOPHANASE ACTIVATION BY CONTROL
OF FREE K^+ CONCENTRATION - K^+ JUMP

As described in the previous chapter, there are two forms of holotryptophanase, a form that absorbs at 420 nm and one which absorbs at 337 nm. The latter form is observed only in the presence of activating monovalent cations such as K^+ and NH_4^+ and at sufficiently high pH values, while the former is dominant at low pH values. An absorption band at 420 nm also dominates the absorption spectrum of the K^+-free (inactive) enzyme. Thus, in order to study the kinetics of interconversion of the inactive enzyme conformer(s) into active conformer(s), one needs to prepare the enzyme in a medium that is free of activating monovalent cations, and keep it "stable" long enough to be reactivated by mixing with an activating cation. For this purpose, we first attempted to prepare the enzyme in the presence of tetramethylammonium chloride, $(CH_3)_4NCl$, and then mix it with a solution of K^+ ion to reactivate it. The following section describes the enzyme stability and spectral studies in the presence of $(CH_3)_4NCl$ done in search of finding a suitable medium for such an experiment.

A. Studies in the Presence of $(CH_3)_4NCl$

A.1. Methods

Tryptophanase from E-Coli B1t7/A was prepared as previously des-
cribed (123). An "11 x 2" cm Sephadex G-25 medium grade column was
used to prepare the enzyme in the presence of tetramethylammonium
ion. The column was packed and equilibrated with a $(CH_3)_4NCl$ buffer
containing 25 mM Epps, 50 mM $(CH_3)_4NCl$, 2 mM EDTA and 2 mM dithio-
threitol (DTT) titrated to pH 8.0 with tetramethylammonium hydroxide,
TMA-OH. The TMA-OH for the titration was prepared by passing 50 ml
of a 1 molar solution of recrystallized TMACl over a Dowex-1-OH column.
To prepare tryptophanase in the TMA-buffer, an aliquot of the apo-
enzyme precipitate in 90% saturated ammonium sulfate buffer at pH
7.0 was centrifuged, decanted, and the precipitate was dissolved in
0.1-0.15 ml of the activation buffer. The latter buffer contained
25 mM K^+-Epps, pH 8.0, 1 mM EDTA, 0.2 M KCl, and 20 mM DTT but no
pyridoxal-phosphate. The enzyme typically had a concentration of
$\sim$30 mg$\cdot$ml^{-1} at this stage, measured spectrophotometrically at 278 nm
with ϵ_{278} = 0.795 ml$\cdot$mg$^{-1}\cdot$cm^{-1} (65). This solution was then loaded
into a Sephadex column that had been preequilibrated with the TMA-
Epps buffer and was subsequently eluted with the same buffer. Frac-
tions which contained the enzyme were pooled for the experiments.
The apoenzyme had a typical concentration of 2 mg$\cdot$ml^{-1} at this
stage.

A.2. Stability Studies

The stability of tryptophanase in the presence of tetramethyl-ammonium ion was checked at different concentrations of pyridoxal-p and dithiothreitol (DTT) to find a suitable medium for the enzyme. Since pyridoxal-p absorbs in the same spectral region as the enzyme (maxima centered at 390 and 330 nm corresponding to the aldehyde and hydrated forms of pyridoxal-p, respectively), an "ideal" medium would be one in which no excess pyridoxal-p is present to interfer with the spectral forms of the enzyme. For this reason, the enzyme collected from the Sephadex column in the TMA-buffer was made equimolar in pyridoxal-p and then activated. The specific activity of the solution was then sampled at different times as a measure of the enzyme stability.

The results showed that tryptophanase in the TMA-buffer with the same PLP concentration as the enzyme and a DTT concentration of 2 mM is unstable and gradually looses activity; up to 65 percent in a period of 2 hours. To see whether the activity loss is due to dissociation of PLP from the enzyme, a two-fold excess of pyridoxal-p was added to the above solution which was then heated at 50°C to be reactivated. The resultant solution showed no gain of activity which suggests that PLP is not dissociated from the enzyme. However, when the same solution (no excess pyridoxal-p) which had lost 65 percent of its activity was made 20 mM in DTT (the reducing agent), the enzyme regained about 45 percent of its activity but again lost it with time. When the same partially deactivated enzyme solution was

reactivated in the presence of excess pyridoxal-p and DTT, the enzyme regained most of its activity and retained it for about five hours. Gradual loss of activity occurs at longer times. Thus, it seems that the activity loss of the enzyme in this system is at least partially due to oxidation of the -SH groups on the enzyme, essential for enzymatic activity, rather than dissociation of the coenzyme, pyridoxal-p. When the enzyme activity loss in the original solution was allowed to proceed for longer than 2-3 hours, the activity could not be recovered by addition of excess PLP and DTT. The results, therefore, showed that the $(CH_3)_4NCl$-buffer, containing 2 mM DTT and equinormal pyridoxal-p and enzyme, is not a suitable medium for keeping tryptophanase stable in the absence of activating monovalent cations.

Next, the stability of tryptophanase in the same buffer solution but in the presence of either excess pyridoxal-p (100 µM) or DTT (20 mM) was investigated. A 2.0 mg·ml^{-1} solution of the apoenzyme in the TMA buffer prepared as before was divided into three portions. The first solution was made equinormal in PLP (40 µM) but excess in DTT, the second solution excess in pyridoxal-p but low in DTT (2 mM) and the final portion was made with excess pyridoxal-p and DTT to be used as a control solution. All solutions were activated by heating in a 50°C water bath and their activities were subsequently monitored. The two former enzyme solutions gradually lost their activities; up to 80 percent in a period of five hours, while the control solution was stable during this time period. When excess pyridoxal-p was added to the first solution after the activity loss, the regain of activity was found to be consistently higher than that of the second solution

after addition of excess DTT. In neither case could the activity be fully recovered. (Specific activity under assay conditions was used to monitor the activity recovery.) The results suggest again, that loss of the enzyme activity in the absence of activating monovalent cations is at least partially due to oxidation of the -SH groups on the enzyme.

Finally, the stability of tryptophanase in the presence of TMA ion was investigated by preparing the holoenzyme first, followed by passing the solution through the Sephadex column. The enzyme was eluted with a similar TMA-buffer solution which contained 20 mM DTT. The results were similar. The enzyme lost 40 percent of its activity by passing through the column and an additional 20 percent activity loss occurred in a period of six hours. When such a solution (de-activated for less than 2 hours) was reactivated by addition of potassium ions, the enzyme regained and retained its activity. How-ever, if the activity loss proceeded for longer than six hours, full activity could not be restored upon addition of K^+ ions.

A.3. Spectral Studies

The stability of tryptophanase in the presence of tetramethyl-ammonium ion was also studied spectrophotometrically with a Cary 17 spectrophotometer. A 50 μM solution of apotryptophanase in a TMA-Epps buffer at pH 8.0 (2 mM DTT) was titrated with pyridoxal-p up to the stoichiometric point by successive additions of 5 $\mu\ell$ increments of a 2 mM PLP solution. Formation of the holoenzyme complex was followed by growth of the absorption band at 420 nm. The magnitude

of the absorbance change was found to be directly proportional to the concentration of pyridoxal-p in the solution as shown in Figure IV.1, which indicates a tight binding of pyridoxal-p to the enzyme in this system. No other changes occurred during the titration in the wavelength region scanned, 320-500 nm. Monitoring the holoenzyme spectrum after saturation with pyridoxal-p (50 μM) showed no significant decrease in absorbance at 420 nm which would be expected if pyridoxal-p slowly dissociated from the holoenzyme. This confirms the stability studies which showed that addition of excess PLP to the enzyme in this buffer cannot restore the lost activity.

A similar solution of apotryptophanase in the same TMA-Epps buffer was further titrated with pyridoxal-p to see whether the excess pyridoxal-p, which is required to restore the enzyme activity in the presence of excess DTT, remains free in solution. The titration was carried to 100 μM pyridoxal-p (two fold excess). The results were indicative of two binding sites for pyridoxal-p on the enzyme; a binding site which gives rise to an absorption band at 420 nm as indicated earlier (Figure IV.1) and a second site that yields an absorption band centered at 355 nm after completion of the first process. A difference spectrum, obtained by subtracting the spectrum at saturation of the first binding site (50 μM PLP) from the final spectrum (100 μM PLP), is shown in Figure IV.2. The spectrum of 50 μM pyridoxal-p in the same buffer is also shown for comparison. If the excess pyridoxal-p had remained free in the solution, the two spectra would be superimposable. The fact that they are different suggests the existence of a second set of binding sites on the enzyme for PLP, as
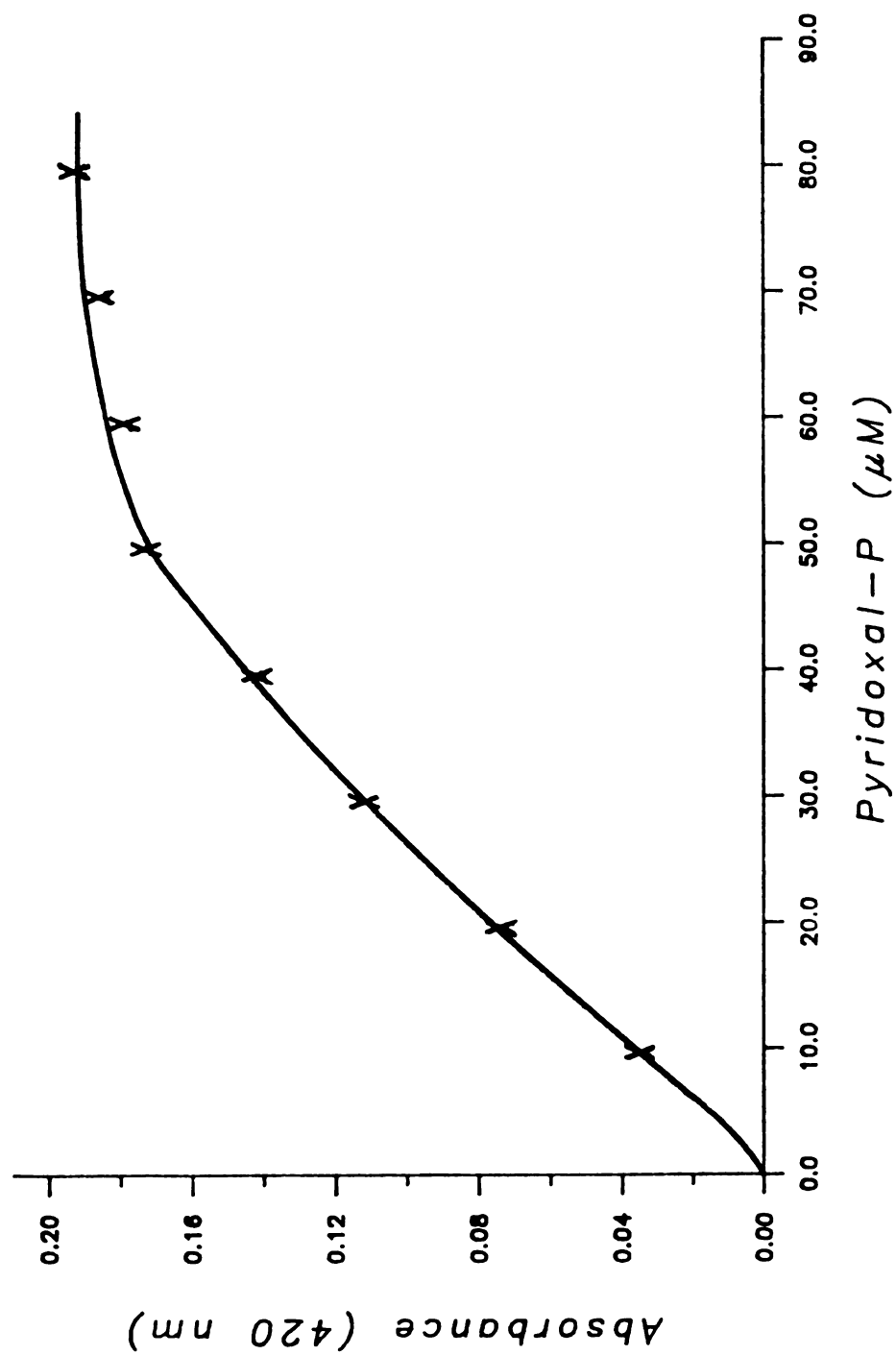
Figure IV.1. Dependence of the absorbance growth at 420 nm upon titration of apotryptophanase with pyridoxal-p in $(CH_3)_4NCl$-buffer at pH 8.0, 2.0 mM DTT. Concentration of the enzyme was 50 μM. Points after saturation (60-80 M pyridoxal-p) are obtained from a second titration.
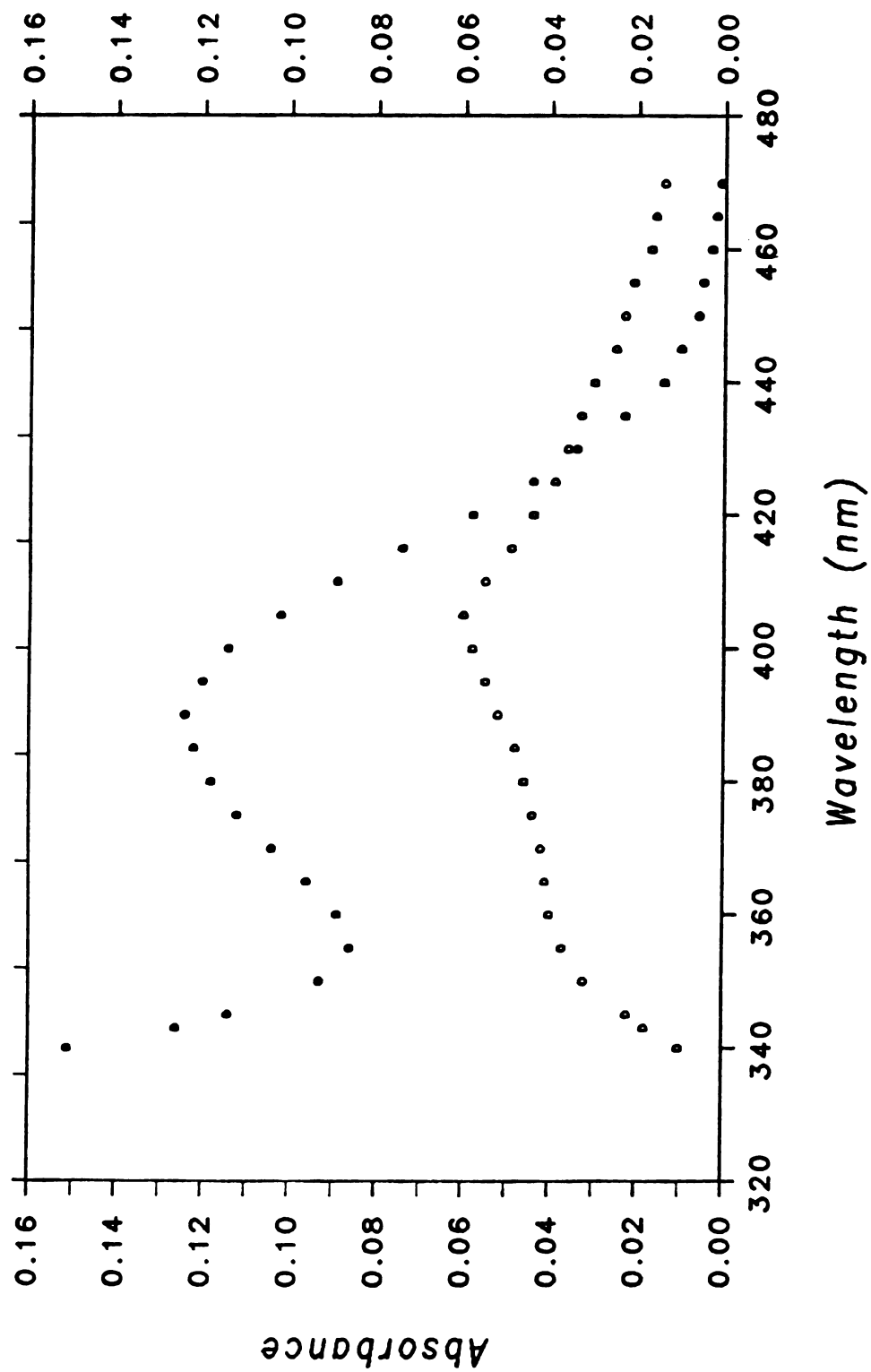
Figure IV.2.   (o) Difference spectrum obtained during titration of a 50 μM solution of apo-tryptophanase with excess pyridoxal-p, [enzyme (100 μM PLP)-enzyme (50 μM PLP)] in TMA-Epps buffer at pH 8.0.   (●) Spectrum of 50 μM PLP in the same buffer.

evidenced by the growth at 355 nm.

The stability and spectral studies clearly show that pyridoxal-p does not dissociate from the enzyme in the presence of tetramethyl-ammonium ion and 2 mM DTT. However, tryptophanase gradually loses activity probably due to partial oxidation of the -SH groups on the enzyme. The stability studies show that a $(CH_3)_4NCl$-buffer with both pyridoxal-p and DTT present in excess can be used to keep tryptophan-ase relatively stable in the absence of activating monovalent cations and, thus, might be employed in the reactivation kinetic studies. Further studies revealed, however, the following problems associated with such a buffer system:

1. Activation of tryptophanase in this buffer by addition of saturating amounts of potassium ions gives only small absorbance changes, $\Delta O.D. \simeq 0.012$ per mg of the enzyme at 420 and at 337 nm. The change is even smaller for lower K^+ concentrations which makes the study of the K^+ dependence of activation nearly impractical.

2. The deactivation process, to exchange K^+ ion for the $(CH_3)_4$-N^+ ion on the enzyme, is not feasible because tryptophanase has a higher affinity for potassium ion than for tetramethylammonium ion.

3. Activation experiments should be completed in less than five hours, otherwise, the enzyme irreversibly loses activity. Scanning stoppped-flow experiments, however, require at least a full day of experimentation.

4. The amount of pyridoxal-p which may remain free in the solu-tion cannot be measured and, thus, a proper baseline cannot be de-termined.

5. Pyridoxal-p reacts with dithiothreitol (DTT), another component of the buffer solution as indicated by changes in absorbance at 390 and 325 nm.

To measure the extent of this reaction, a 50 μM solution of pyridoxal-p in the TMA-Epps buffer at pH 8.0 was titrated with a 0.2 molar solution of dithiothreitol as indicated in Figure IV.3. An equilibrium constant of 15.1 ± 1.0 mM^{-1} was calculated for reaction IV.1 by KINFIT. A possible scheme for this reaction is presented in Figure IV.4. Since the spectral changes associated with this reaction occur in the same wavelength region as those of the enzyme (see Figure IV.3), use of such a buffer system adds complexities to the enzyme spectral changes in the activation experiments.

Because of these problems associated with the TMA-buffer (excess pyridoxal-p, excess DTT), we decided not to use such a system in the stopped-flow reactivation studies.

To carry out the activation experiments, we finally decided to use 18-crown-6. To circumvent the loss of stability of the enzyme in the absence of monovalent cations, the activation process was studied by mixing a solution of the enzyme, freshly deactivated by addition of complexant 18-crown-6 with an excess of K^{+}. This technique proved to be a useful new tool for the study of enzyme activation by monovalent cations. The remainder of this chapter explains the results obtained from such stopped-flow activation studies. Cryptand[2.2.2] was not used in this study because of its effect on the enzyme activity as discussed in Chapter III.
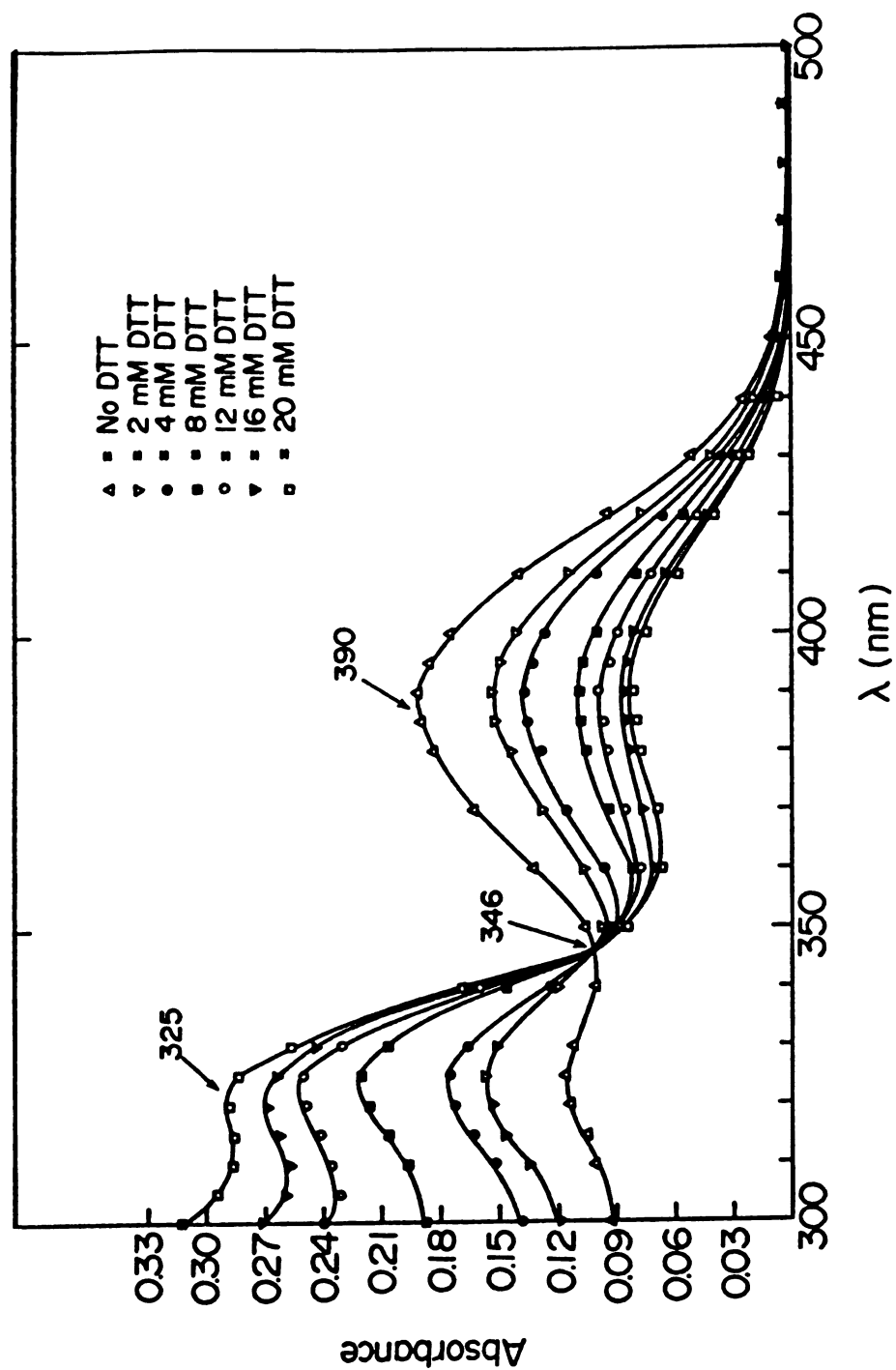
Figure IV.3. Spectral changes obtained during titration of 50 μM pyridoxal-p with dithio-threitol (DTT) in $(CH_3)_4NCl$-Epps buffer at pH 8.0. The spectra were recorded with a Cary 17 spectrophotometer, twenty minutes after addition of each DTT aliquot.

107

(pLp)

$\lambda_{max} = 390$

$+$ CH$_2$—(CHOH)$_2$—CH$_2$

|
SH

|
SH

(DTT)

(Acetal)

$\lambda_{max} = 325$

(Scheme IV.1)

Figure IV.4. A suggested scheme for the reaction between pyridoxal-phosphate (PLP) and dithiothreitol (DTT).

B. Stopped-Flow Studies of Tryptophanase Activation by K^+

B.1. Experimental Procedure

A solution of holotryptophanase in K^+-bicine buffer at pH 8.70 with a total K^+ concentration of 17 mM was prepared as previously described (123, Chapter III). The enzyme had a specific activity of 50 $\mu \cdot mol \cdot min^{-1} \cdot mg^{-1}$ when assayed with 0.6 mM S-orthonitrophenyl-L-cysteine (SOPC) in 50 mM potassium phosphate, pH 8.0, 50 mM KCl, at 30°C (123). Prior to a push, the enzyme was diluted with dialysis buffer to 4.0 $mg \cdot ml^{-1}$, deactivated by 18-crown-6 (18C6) and subsequently pushed against various concentrations of free K^+ as indicated in Table IV.1. A stock 1 molar solution of 18-crown-6 was used to reduce the free K^+ concentration in the enzyme solution. All spectra were scanned over the wavelength range 315-540 nm. The experiments were carried out between 10 and 40 minutes after addition of 18-crown-6 at the ambient temperature of 23±1°C.

B.2. Results

The kinetics of activation were studied in both scanning and fixed-wavelength modes. Figure IV.5 shows the spectral changes that occurred when a solution of freshly deactivated tryptophanase was pushed against a saturating concentration of K^+. Concentrations of the enzyme and free K^+ after mixing were 2.0 $mg \cdot ml^{-1}$ (36 μM) and 33.0 mM, respectively. The spectra show the simultaneous growth of the active enzyme (at 337 nm since pH = 8.70) and the decay of the

Table IV.1. Concentration of Various Species (After Mixing) in the Stopped-Flow Studies of Tryptophanase Reactivation by K^+ (K^+ Jump). E_0 = 2.0 mg.ml^{-1} (36 µM) for all experiments.

18-Crown-6 (mM)	K^+_{free} (initial) (mM)	K^+_{free} (final) (mM)
50.5	0.7	3.0
50.5	0.7	7.5
62.5	0.5	11.6
67.0	0.5	16.0
69.5	0.5	18.7
70.0	0.5	19.2
70.0	0.5	24.2
70.0	0.5	33.0
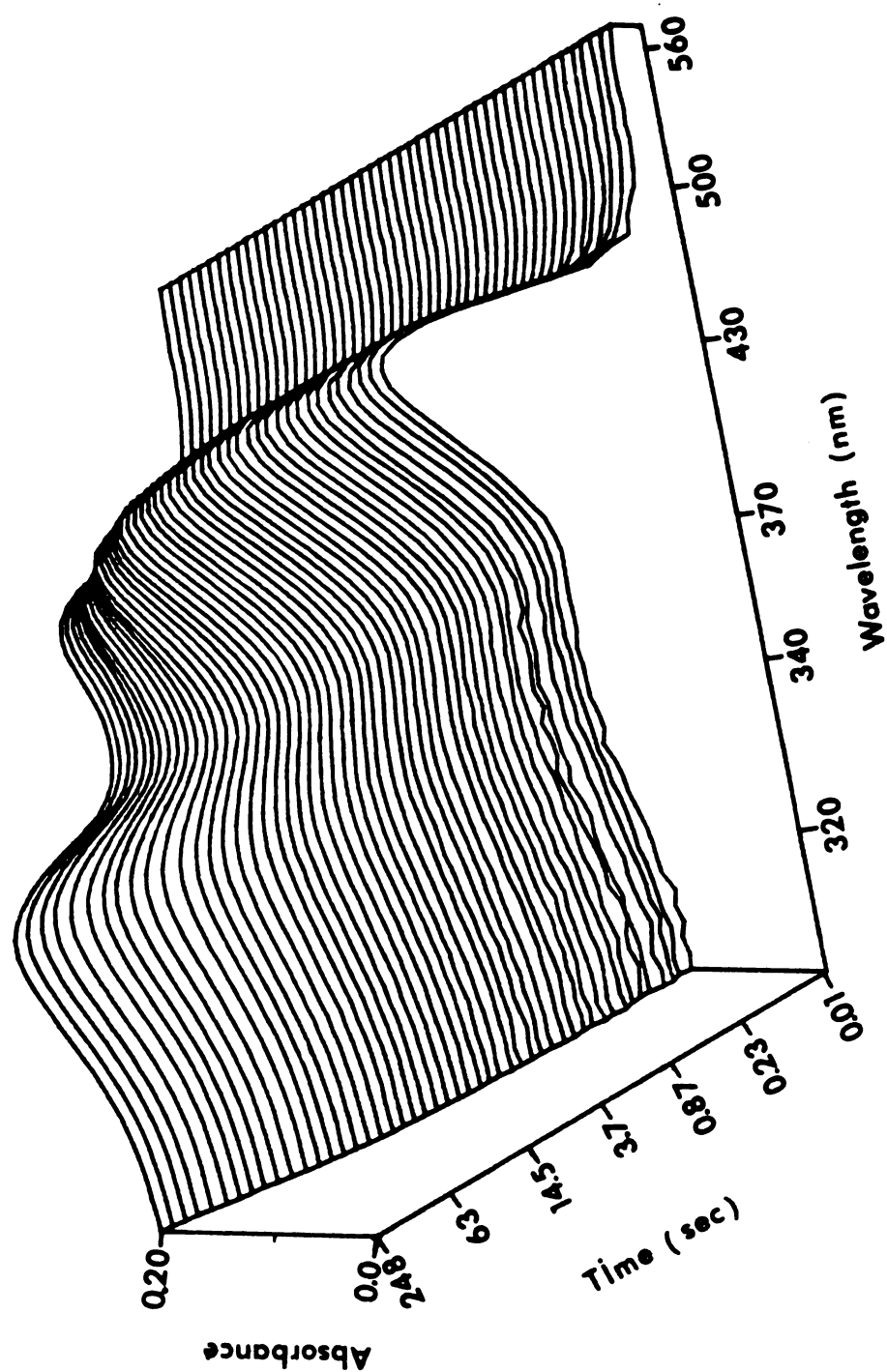
Figure IV.5.   Absorbance-wavelength-time surface for activation of tryptophanase (freshly deactivated by 18C6) by K^+ in bicine buffer at pH = 8.70. Concentrations of the enzyme and K^+ were 2.0 mg·ml^{-1} and 33.0 mM, respectively. t=23±1°C.

"inactive" enzyme (420 nm). The difference spectra taken from Figure IV.5 are compared with similar spectra during K^+ removal (deactivation) in Figure IV.6. As shown in this figure, the overall spectral changes are essentially the reverse of those which occurred during the K^+ removal with one important difference. Even in the presence of saturating amounts of K^+, only about 50 percent of the 337 absorption was receovered and a corresponding fraction lost at 420 nm. Similar experiments by using a Cary 17 spectrophotometer where the activation was allowed to proceed for longer times showed only a small additional recovery (less than 10 percent) in a period of about 1 hour. In spite of this apparent spectral irreversibility, however, separate experiments showed that 100% of the enzymatic activity could be recovered by adding K^+ to the deactivated enzyme. The rate data at 420 and 337 nm were analyzed by the program KINFIT4 using appropriate rate equations.

B.2.1. <u>Absorbance Change at 337 nm</u> - Inspection of the difference spectra, obtained by subtracting the spectrum of the inactive enzyme from other spectra, showed no detectable fast change at this wavelength at the start of the reactivation. The overall process is slower than K^+ removal so that the reaction is not complete in over 4 minutes of data collection time.

At saturating K^+ concentrations (above 16 mM), the growth in absorbance at this wavelength was fit to within random errors by three exponentials with the rate constants k_1, k_2 and k_3 essentially independent of the free K^+ concentration. Equation IV.2 was used

112

Figure IV.6. Selected difference spectra at three different times presenting changes in absorbance observed during the "K⁺ drop" experiment (---) and "K⁺ jump" experiment (——). Concentrations after mixing were, tryptophanase, 2.0 mg/ml; 18-crown-6; 148 mM (---), and free K⁺, 33.0 mM (——). Times of consecutive spectra are 4.0, 12.7 and 130 seconds (---) and 17.8, 63.0 and 248 seconds (——).
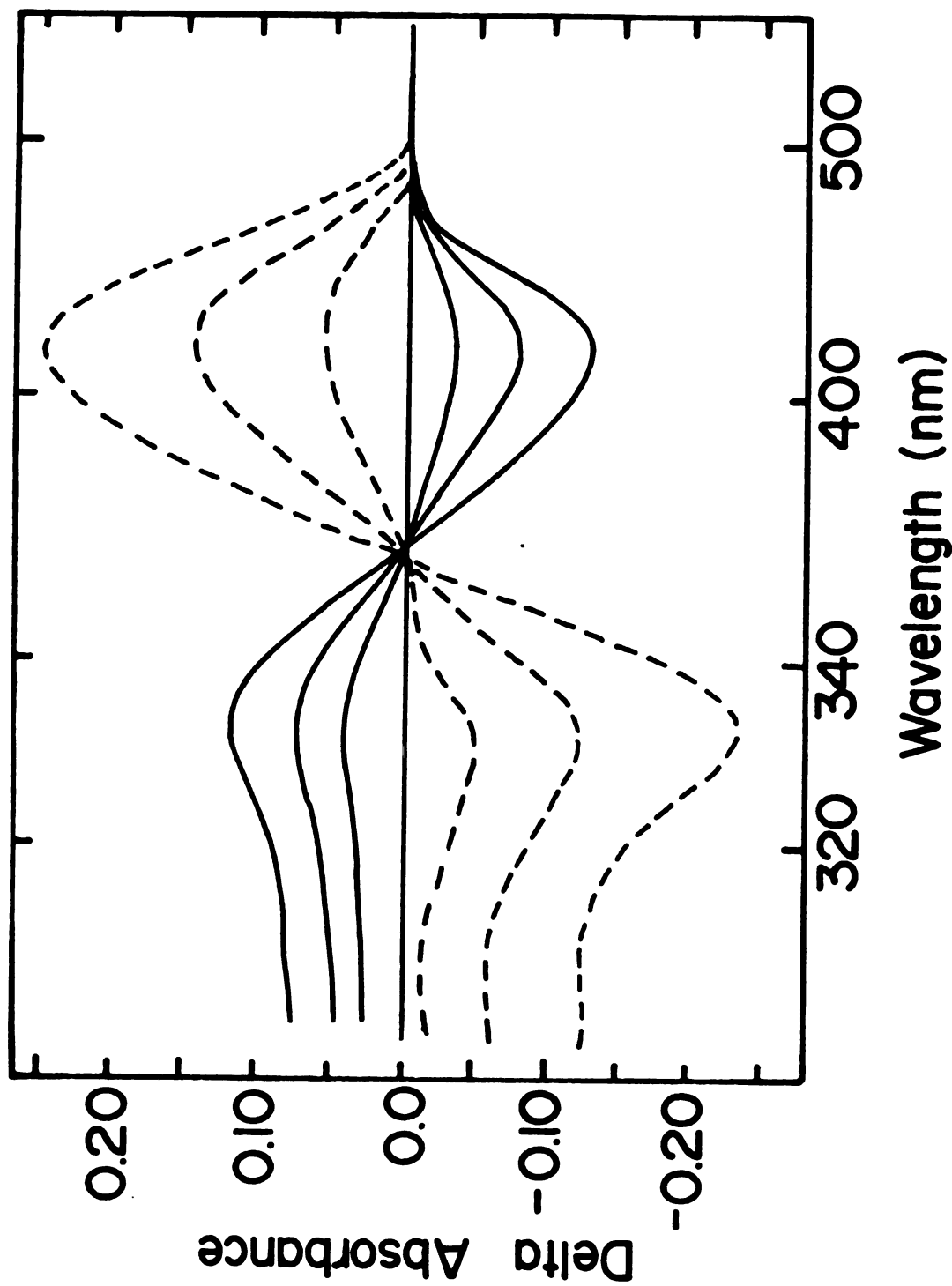
Figure IV.6

to fit the data at saturating K^+ concentrations.

$$A_{obs} = A_\infty - \sum_{i=1}^{3} \Delta A_i \exp(-k_i t) \qquad (IV.2)$$

ΔA_1, ΔA_2, ΔA_3, k_1, k_2 and k_3 were the six adjustable parameters. The following relation was used for A_∞ to reduce by one the number of adjustable parameters for the purpose of data fittings.

$$A_\infty = A_0 + \sum_{i=1}^{3} \Delta A_i \qquad (IV.3)$$

The A_0 values were obtained from the experiments. At a concentration of 16.0 mM free K^+, the values of ΔA_1 and k_1 were fixed at 0.0085 O.D. and 0.39 sec^{-1} (the averages of ΔA_1 and k_1 at saturating K^+ concentrations), respectively, to get a reliable fit. Figure IV.7 shows a computer fit of the data at 337 nm for the enzyme and free K^+ concentrations of 2.0 $mg.ml^{-1}$ and 18.70 mM, respectively (after mixing). At the concentration of 11.6 mM free K^+, the two faster processes decreased in amplitude and/or rate so that a two-exponentials equation similar to Equation IV.2 (i=2) fit the data to within the experimental random errors. At this concentration, one of the exponentials accounted for over 80% of the total change in absorbance. Finally, at the two lowest concentrations of free K^+ (2.3 mM and 7.0 mM), the three phases were inseparable and a single exponential could account for the total change in absorbance. Results of the fitting precedure at saturating K^+ concentrations are tabulated in Table IV.2 while those below saturation are given in Table IV.3.
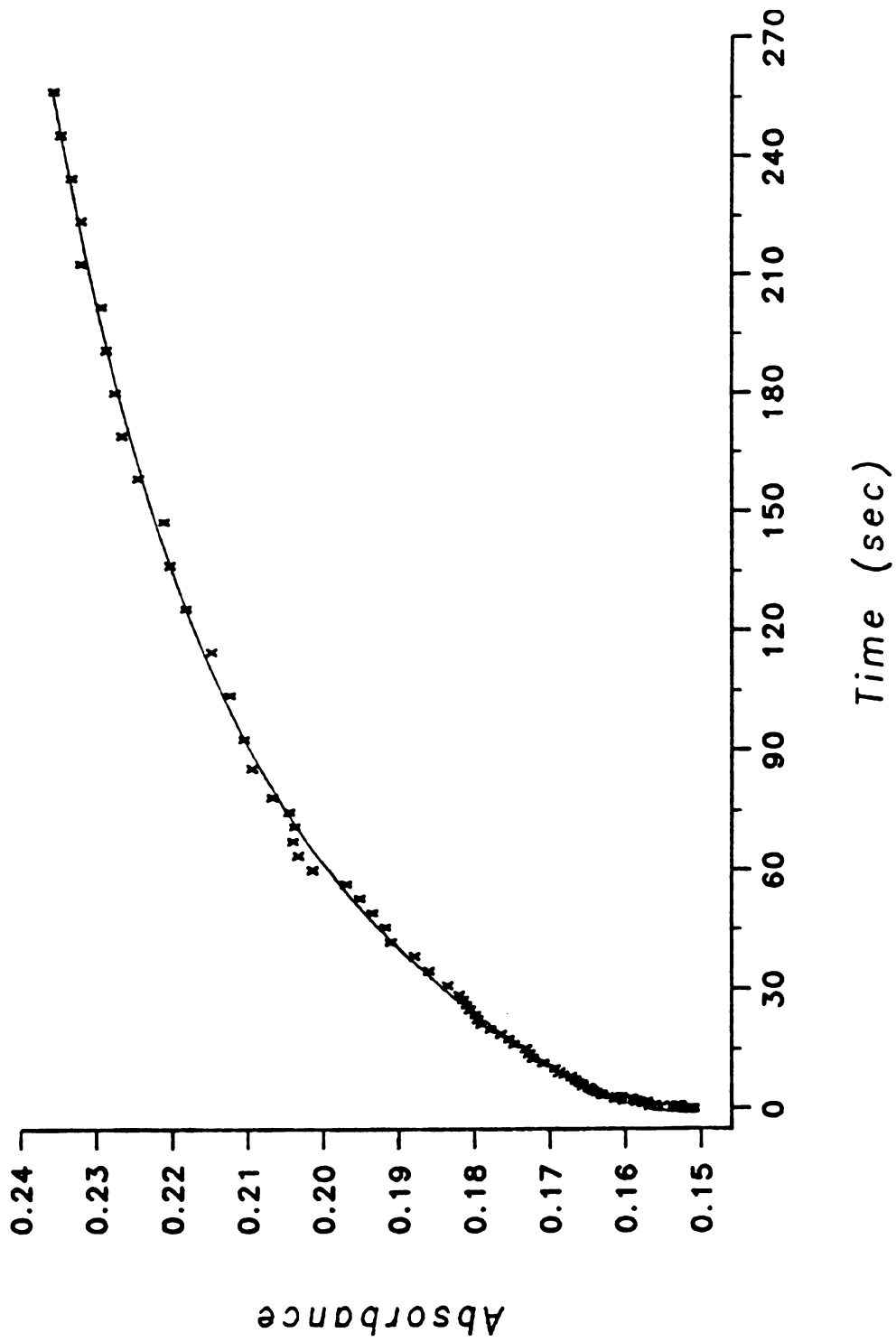
Figure IV.7. Fit of the data at 337 nm for tryptophanase activation by K$^+$ (K$^+$ jump) by Equation IV.2. X's are the data and the solid line is the calculated curve. Concentrations of the enzyme and K$^+$ were; 2.0 mg/ml (36 µM) and 18.7 mM, respectively.

Table IV.2. Kinetic Parameters for the Reactivation of Tryptophanase by K^+ at Saturating Concentrations of the Cation. These Parameters were Obtained by Fitting the Absorbance Changes at Each Wavelength to Equation IV.2. E_0 = 2.0 mg/ml^{-1} (36 μM) after mixing.

Concentration	-----3 Exponentials-----		
K^+_{free}(final) mM	$k_1^{(b)}$,S^{-1}	$k_2^{(b)} \times 10^2$,S^{-1}	$k_3^{(b)} \times 10^3$,S^{-1}
33.0	0.39±.05	2.08±.22	4.72±1.32
24.2	0.38±.03	2.57±.15	5.58±1.31
19.2	0.38±.04	2.21±.12	3.20± .91
18.7	0.57±.14	2.01±.34	3.06±2.09
16.0	0.39[a]	2.06±.28	4.95±1.07

K^+_{free}(final) (mM)	Wavelength (nm)	--- A_1 ---	--- A_2 ---	--- A_3 ---
33.0	337	0.009±.001	0.053±.009	0.065±.004
	420	0.014±.001	0.077±.001	0.060±.001
24.2	337	0.008±.001	0.055±.005	0.050±.002
	420	0.010±.001	0.072±.001	0.057±.001
19.2	337	0.009±.001	0.058±.004	0.071±.006
	420	0.016±.001	0.075±.001	0.049±.001
18.7	337	0.008±.001	0.040±.010	0.066±.011
	420	0.008±.001	0.047±.001	0.065±.001
16.0	337	0.0085[a]	0.028±.007	0.065±.003
	420	0.005±.001	0.049±.001	0.063±.001

[a]Values were fixed, see the text.

[b]k_i are the "apparent" rate constants.

Table IV.3.   Kinetic Parameters for the Reactivation of Tryptophanase by K^+ at Concentrations of the Cation Below Saturation. A Two Exponential Equation (11.65 mM) and a Single Exponential Equation (7.5 and 3.0 mM) were Used in the Fit. E_0 = 2.0 mg.ml^{-1} (36 μM) after mixing.

K^+_{free}(final) (mM)	Wavelength (nm)	$k_1^{(a)}$x10^2, s^{-1}	$k_2^{(a)}$x10^3, s^{-1}
11.65	337	6.59±1.00	7.76±.43
	420	6.88±1.19	8.55±.74
7.5	337	1.37± .04	--------
	420	1.32± .02	--------
3.0	337	1.21± .20	--------
	420	1.12± .04	--------

K^+_{free}(final) (mM)	Wavelength (nm)	$\Delta A_1^{(b)}$	ΔA_2
11.65	337	0.013±.001	0.063±.002
	420	0.012±.001	0.072±.003
7.5	337	0.034±.001	----------
	420	0.053±.001	----------
3.0	337	0.0090±.0003	----------
	420	0.018±.001	----------

[a] k_1 and k_2 are the "apparent" rate constants.

[b] Values are corrected for the slight difference in the enzyme concentration.

B.2.2. <u>Absorbance Change at 420 nm</u> - The absorbance change at the start of the activation at 420 nm is different from that at 337 nm. At saturating K^+ concentrations (above 16 mM), an exponential fast growth was observed at this wavelength (centered at ~430 nm) which lasted about 600 mSec; no significant change occurred at 337 nm during this period as indicated earlier. Figure IV.8 shows the difference spectrum obtained at the end of the fast growth along with a partial time course of the absorbance change at 420 nm. Concentrations of the enzyme and free K^+ after mixing were 2.0 $mg \cdot ml^{-1}$ and 19.2 mM, respectively. The data during this time period were fit to a single exponential by KINFIT (Figure IV.9) and the results are presented in Table IV.4. The absorbance change during the same time at lower potassium concentrations was not large enough to allow a reasonable fit. From the data in Table IV.4, the rate constant k_0 for this process is $9.5 \pm .5$ sec^{-1}.

Following the fast exponential process, the growth of absorbance at 337 nm is quantitatively mirrored by the decay at 420 nm. The data at this wavelength were again fit to Equation IV.2 and the results are reported in Tables IV.2 and IV.3. From the data at saturating K^+ concentrations (Table IV.2), three exponentials with k_1 = 0.43 ± 0.09 sec^{-1}, k_2 = $(2.2 \pm 0.2) \times 10^{-2}$ sec^{-1}, k_3 = $(4.3 \pm 1.1) \times 10^{-3}$ sec^{-1}, and relative amplitudes of ΔA_1 = $7.5 \pm 2.0\%$, ΔA_2 = $44 \pm 8\%$ and ΔA_3 = $49 \pm 8\%$ can be calculated. From the data at the two lowest concentrations of K^+ (Table IV.3), a single rate constant (obtained by averaging the results at both 337 and 420 nm is $1.3 \pm .1 \times 10^{-2}$ sec^{-1}.
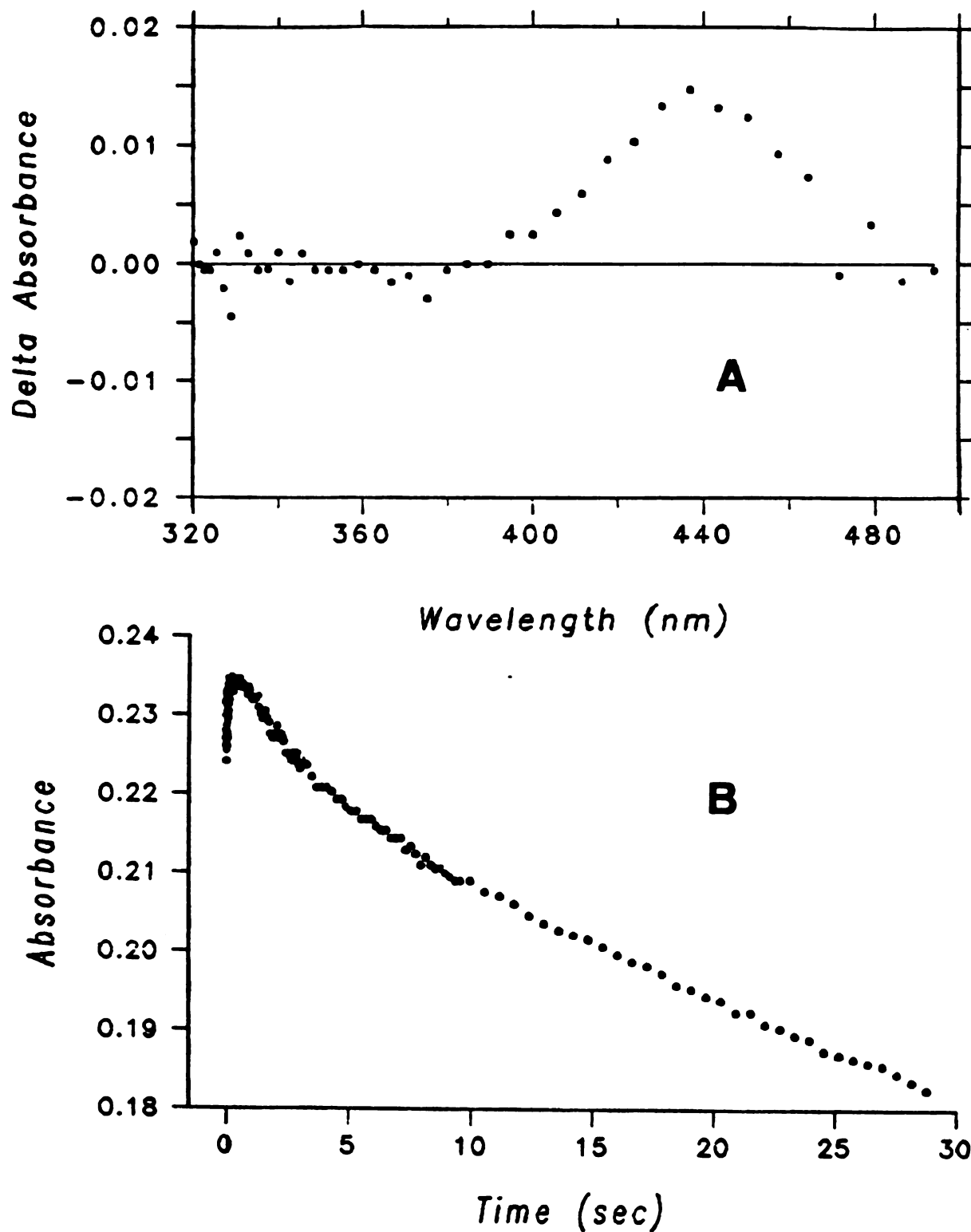
Figure IV.8. (A) Difference spectrum at completion of the fast growth at 430 nm in tryptophanase activation by K^+. (B) Partial time course of the absorbance change at 420 nm. Concentrations were; tryptophanase, 2.0 mg·ml^{-1} (36 μM); K^+, 19.2 mM, respectively.
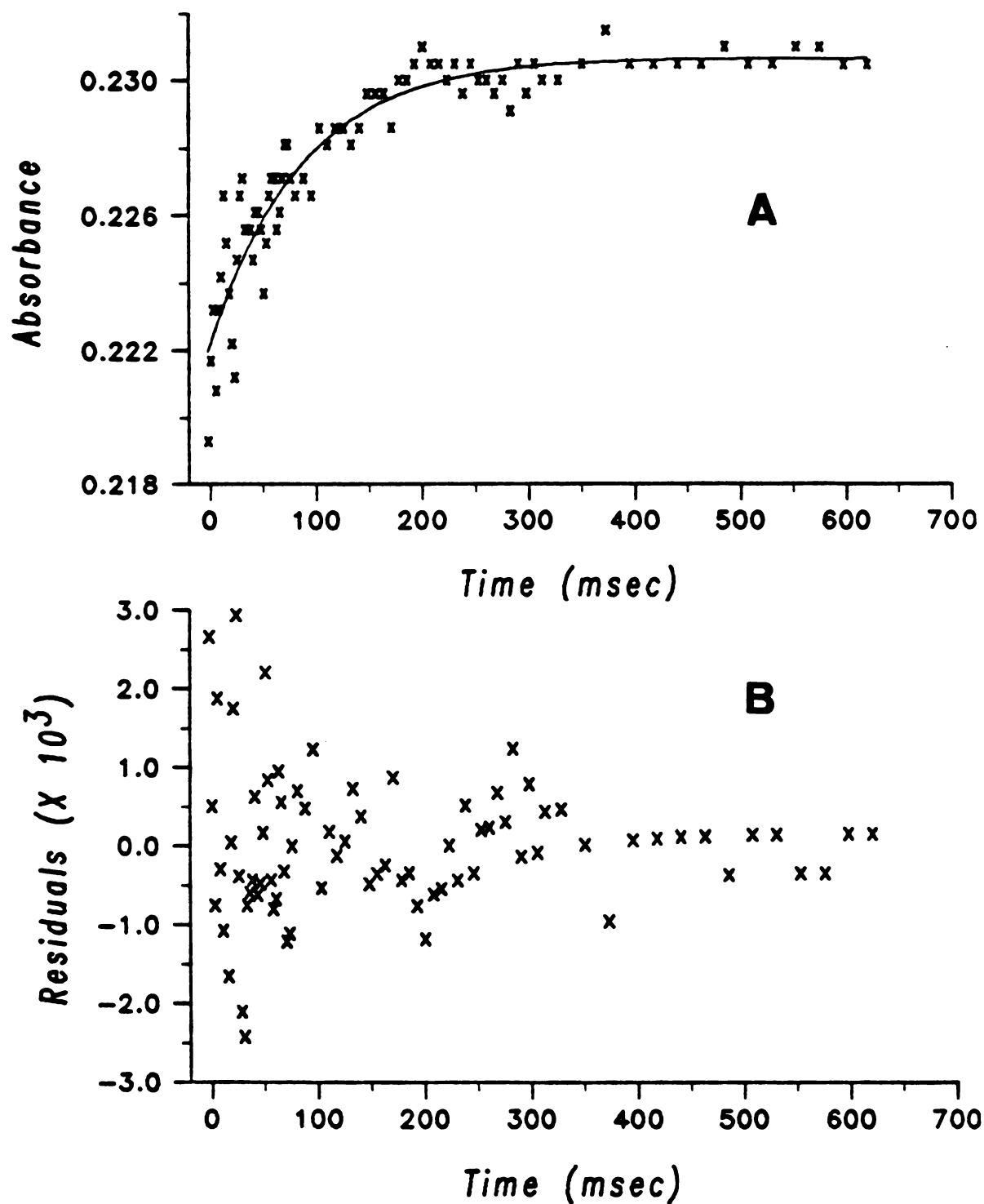
Figure IV.9. (A) Fit of the fast growth at 420 nm (600 mSec) in "K$^+$ jump" by a single exponential. (B) Residuals of the fit. Concentrations were; tryptophanase, 2.0 mg· ml^{-1} (36 µM), K$^+$, 33.0 mM, respectively.

Table IV.4. Kinetic Parameters Obtained from the Fit of the Early
Growth (600 mSec) at 420 nm by a Single Exponential Equa-
tion in Tryptophanase Activation by K^+ at pH= 8.70 (K^+-
Jump). E_0 = 2.0 mg/ml^{-1} (36 μM) after mixing.

K^+_{free}(final), mM	----- A-----	--k_0,S^{-1}--
33.0	0.0090±.0005	9.7± .9
24.2	0.0087±.0003	7.3± .5
19.2	0.0080±.0004	11.5± .9
18.7	0.0044±.0003	8.6±1.0
16.0	0.0036±.0003	10.6±1.8
		AVG=9.5±.5

The variation of the overall amplitude of the absorbance change at 420 and 337 nm with K^+ concentration does not follow a typical saturation function; half-saturation occurs at 9 mM and above 18 mM the value of ΔA is independent of the K^+ concentration.

C. Discussion

In this chapter we have reported some basic kinetics data dealing with the effect of monovalent cation, K^+, on the transformation of inactive tryptophanase into functional holoenzyme. The kinetics of reactivation by K^+ are complex as evidenced by the existence of three distinct phases during the process which can be interpreted in more than one way. Even at saturating concentrations of K^+, [above 16 mM (Table IV.2)], nearly half of the enzyme does not convert to the 337 nm absorber (Figure IV.6). Furthermore, this incomplete recovery of the original absorbance at 337 nm is time-independent. Even after a period of one hour the absorbance at 337 nm is only about half the initial absorbance (less than 10% additional recovery) as indicated earlier. Yet, the enzymatic activity is completely restored in a few minutes. These observations lead to the following possibilities;

i) The enzyme is not homogeneous, i.e., it exists in two different conformational forms and that only one of these forms converts to the 337 nm absorber upon reactivation by K^+.

ii) The holoenzyme dissociates into dimers upon removal of potassium ion and that only one dimer converts to the 337 nm absorber (γ form) upon addition of K^+.

iii) The enzyme remains as a tetramer in the inactive form but only two of the four protomers convert to the γ-form upon reactivation by K^+. The other two subunits convert very slowly, not contributing much to the 337 nm growth over the time of the experiment (over 4 minutes).

The first possibility can be ruled out due to the fact that tryptophanase purification from Escherichia Coli Blt7/A yields essentially 95% homogeneous enzyme as judged by polyacrylamide gel electrophoresis and its high specific activity when assayed with the substrate, S-orthonitrophenyl-L-cysteine (123). It does not seem likely that removal of K^+ ion causes significant inhomogeneity in the enzyme. The dissociation of holoenzyme into dimers (possibility ii) is not feasable under our experimental condition. Morino and Snell (59,60) have shown that dissociation of holotryptophanase into subunits requires strong denaturing agents such as sodium dodecyl sulfate or urea. Furthermore, Raibaud and Goldberg showed that dimeric tryptophanase is not functional under conditions where the tetrameric enzyme is perfectly active (71). These studies, along with the fact that the growth of the quinonoid absorbance (508 nm) upon mixing L-ethionine and saturating concentration of K^+ with the deactivated enzyme is complete in 5 minutes or less (Chapter V), strongly suggest that holotryptophanase is not dissociated into dimers under the reactivation experimental conditions. Dissociation of pyridoxal-p from the holoenzyme in the absence of K^+, which may lead to partial dissociation of the apoenzyme into dimers, does not occur either. This is concluded from the facts that the deactivation rate remained unchanged in the

presence of excess pyridoxal-p (Chapter III) and that the spectrum of pyridoxal-p under similar (to reactivation) experimental conditions did not fit as an absorber in the PCA analysis of the reactivation (Chapter VII). These observations, thus, suggest that tryptophanase remains as a tetramer in the inactive conformation and that two of the four subunits remain "inactive" upon activation by K^+ alone.

The initial fast rise at 420 nm, which amounts to only $\sim$6 percent of the total absorbance change (decay) at this wavelength at the highest K^+ concentration (Table IV.4), is probably due to a change in 420 nm absorbance upon K^+ binding since it shows no change at 337 nm. Alternatively, a small fraction of the enzyme which does not contribute to the absorbance at 420 nm is readily converted to the β form upon addition of K^+ with the rate constant, k_0, $9.5\pm.5$ sec^{-1}. This fraction may be present in the original preparation or it may have been produced by the 18C6 deactivation (perhaps indicated by the very slow exponential changes at the completion of the deactivation, Chapter III). The initial fast first order process (k_1, Table IV.2), which also accounts for only $7.5\pm2\%$ of the overall change at both 337 nm and 420 nm, could then be due to conversion of the form β to the γ-form at 337 nm. This can be represented by;

$$\beta \xrightarrow{k_1} \gamma$$
$$\text{(420 nm)} \qquad \text{(337 nm)}$$
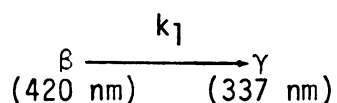
The rate constant for this process obtained in these experiments, $0.43\pm.09$ sec^{-1} (Table IV.2), compares reasonably well with the value 0.80 ± 0.2 sec^{-1} obtained by June et al. (82) for the same process at a

similar pH from the pH jump and drop studies on the spectral forms
of tryptophanase.

The second and third phases in the three exponential process of
reactivation (Table IV.2) have comparable changes in absorbance with
values of ΔA_2 = 44±8% and ΔA_3 = 49±9%, respectively. However. the
rates of the two phases differ by a factor of 5. The apparent first
order rate constants for the two processes are 2.2±.2 x 10^{-2} $\sec^{-1}$
and 4.3±1.1 x 10^{-3} $\sec^{-1}$, giving half-lives of 0.52 min and 2.7 min,
respectively. Above 16 mM, both processes are independent of potas-
sium as indicated earlier. Since both of these phases remove 420 nm
absorbance and simultaneously replace it by 337 nm absorbance, they
cannot represent conversion among various forms of the inactive enzyme
or a single bottleneck step. One way to interpret these results is
given by the two following assumptions;

a) Two sites per subunit saturate in binding by potassium ions
in order to obtain the functional holoenzyme

b) Two inactive (α) forms of comparable concentration exist.

Our results on tryptophanase deactivation in the presence (Chapter
VI) and absence (Chapter III) of L-ethionine strongly suggest that
two potassium ions per subunit are required for activation, consistent
with the binding of two Tl^+ per subunit as reported earlier (77).
To account for this and the second assumption together in the reactiva-
tion of the enzyme by K^+, one possibility is that each of the subunits
of the enzyme converts from α to γ at a "different rate" according to
the following simple model;

$$\alpha_4 \underset{\xleftarrow{}}{\overset{k_2}{\rightleftharpoons}} \gamma_1\alpha_3 \underset{\xleftarrow{}}{\overset{k_3}{\rightleftharpoons}} \gamma_2\alpha_2$$

$$\left(\begin{array}{c}\text{Tetrameric }\alpha\\ \text{inactive}\end{array}\right) \qquad\qquad \left(\begin{array}{c}\text{Tetrameric}\\ \text{50\% }\gamma\text{ recovered}\end{array}\right)$$
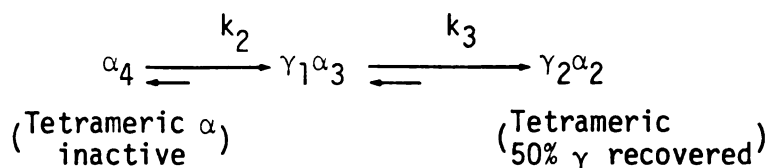
with the rate constants k_2 and k_3 represented in Table IV.2. Even though tetrameric holotryptophanase shows no cooperativity, it has already been demonstrated that the enzyme exhibits a strong "kinetic anticooperativity" in the binding of its cofactor, pyridoxal-p (63). Raibaud and Goldberg showed that a strong structural coupling between the protomers is involved in the binding of the coenzyme; such that fixation of the first two pyridoxal-p molecules to the apoprotomers results in a decrease in the binding rate of the two remaining sub-units (71,72). In view of this, it may also be possible that potassium binding to the first protomer induces a change in the conformation of the second protomer and renders it less reactive to the potassium ion. By "less reactive" it is meant that the rate of potassium binding is slower, i.e., "kinetic anticooperativity" exists in K^+ binding to the enzyme protomers. The "invisible" very slow step, which at saturating K^+ concentration contributes only about 8 percent to the absorbance recovery at 337 nm after a period of 1 hour, could then be due to the two remaining subunits slowly converting into the γ-form according to;

$$\gamma_2\alpha_2 \xrightarrow{\text{very slow}} \gamma_4$$
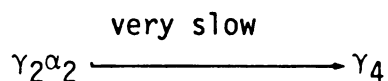
The data in Table IV.2 indicate that above 16 mM free potassium, the activation process is K^+-dependent. This suggests that K^+

binding must either be fast and complete or else occurs after the rate-determining step. From the effect of monovalent cations on the enzymatic activity of tryptophanase, Raibaud and Goldberg suggested that addition of potassium ion to a solution of the enzyme (in the presence of 0.1 M triethanolamine-HCl, pH 7.5) might induce a transition in the tetramer from an inactive form not fixing the cation, to an active form with affinity for the same ion (63), i.e., K^+ binding occurs after such transition. The data obtained in our experiments do not permit us to discriminate between these two possibilities, even though fast K^+ binding seems more probable. As the concentration of free potassium falls below saturation (16 mM) in the reactivation experiments, the three processes gradually decrease in amplitude and/or rate so that a single "effective" rate can account for the overall change in absorbance as indicated in Table IV.3.

D. Conclusions

The results presented here suggest a multistep interconversion of the K^+-depleted (inactive) enzyme into the functional (γ form) holoenzyme. The kinetic results, by themselves, are not sufficient to propose a detailed scheme for this interconversion. Further experiments, such as the enzyme dependence of the activation, and pH-dependence of the process, in particular, are needed to gain more information on the possible individual steps involved in the mechanism. The stability studies indicate that the enzymatic activity, in contrast to the enzyme spectrum, is fully recovered upon reactivation of the enzyme by K^+. This suggests that substrate in addition to K^+

is required to regenerate the spectrum of the enzyme. The stopped-flow results are interpreted in terms of "kinetic anticooperativity" between the subunits of the enzyme upon K^+ binding. Such kinetic anticooperativity has been reported in binding of pyridoxal-phosphate to tryptophanase (72) and aspartate aminotransferase (150).

CHAPTER V

TRYPTOPHANASE ACTIVATION BY K^+ IN THE PRESENCE OF
ETHIONINE-"QUINONOID FORMATION"

A. Introduction

An absorption band centered around 500 nm appears following addition of certain amino-acid inhibitors such as L-ethionine, or true substrates such as L-tryptophan, to several pyridoxal-p dependent enzymes (7). This band is due to a quinonoid complex at the enzyme active site formed by the loss of a labile group from the α-carbon of the inhibitor (or substrate)-pyridoxal-p complex. In the presence of true substrates a leaving group from the β-carbon of the quinonoid complex is labilized causing the disappearance of the 500 nm band as the substrate is converted to products. Morino and Snell (65) demonstrated that a stable quinonoid complex characterized by an intense absorption band with λ_{max} at 502 nm and a prominent shoulder near 470 nm is produced immediately upon mixing the competitive inhibitor, L-alanine, with tryptophanase. They further showed by experiments in ^2H_2O and ^3H_2O that the α-hydrogen of L-alanine was labilized in the process. Watanabe and Snell (149) later identified a number of inhibitors that formed quinonoid complexes with tryptophanase. In this chapter we will focus on the interaction of the inhibitor, L-ethionine, with inactive tryptophanase in the presence of K^+.

Formation of the enzyme-quinonoid complex with ethionine requires activating monovalent cations. Suelter and Snell (77) proposed that in the absence of such cations, ethionine formed a Schiff's base with the enzyme, but that this complex did not proceed to quinonoid until KCl was added.

The K^+-complexing agent, 18-crown-6, was used in the present work to reduce the concentration of K^+ in the enzyme solution prior to the push for subsequent rapid scanning stopped-flow spectrophotometry (see Experimental Section). The purpose of this study was to examine the kinetics of quinonoid formation of the K^+-depleted enzyme with the inhibitor, L-ethionine. A further goal was to correlate the results with those of activation in the absence of the inhibitor (Chapter IV) in an attempt to gain some insight into the mechanism of the interconversion of the active and inactive enzyme forms.

B. Experimental Section

Tryptophanase from E-Coli B/1t7-A was prepared as described previously (123). Holoenzyme in bicine buffer at pH - 8.70 with a total K^+ concentration of 17 mM was prepared from the stock apoenzyme as described in Chapter III. The enzyme had a specific activity of 46.0 $\mu mole \cdot min^{-1} \cdot mg^{-1}$ when assayed with 0.6 mM SOPC as before. A stock 1M solution of 18-crown-6 in dialysis buffer was used to reduce the concentration of free K^+ in the enzyme solution to ~ 1 mM just before the stopped-flow experiments. Similar to reactivation experiments in the absence of the inhibitor (Chapter IV), all experiments

were carried out within 10 to 40 minutes after addition of 18-crown-6 at the ambient temperature of $23 \pm 1°C$. The experiments were performed in two different ways:

i) The enzyme was deactivated by 18-crown-6 (α-form) and then pushed against similar bicine buffer solutions containing in addition; 16 mM L-ethionine (saturating concentration, $K_I = 0.52$ mM) and sufficient KCl to give final free K^+ concentrations of 2.3, 7.0, 12.0, 16.0, 25.0, and 42.0 mM, respectively; (α-Enz) vs. (K^+-Ethionine) experiment.

ii) The enzyme was deactivated by 18-crown-6, then mixed with the inhibitor (16.0 mM before push) and pushed against the bicine solutions with similar free K^+ concentrations as in i; (α-Ethionine) vs.(K^+) experiment.

The results of these studies are described in sections C and D of this chapter, respectively.

C. Activation of Inactive Tryptophanase by a K^+ Mixture-
    (α-ENZ) vs (K^+-ETH)

C.1. Spectral Shape Analysis

Figure V.1 displays a 3D plot of the overall spectral changes from 320 to 550 nm which occur when inactive tryptophanase is mixed with a solution of L-ethionine and K^+. Concentrations of the enzyme, ethionine and free K^+ after mixing were 1.25 $mg.ml^{-1}$, 8.0 mM, and 16.0 mM, respectively. The difference spectra, obtained by subtracting
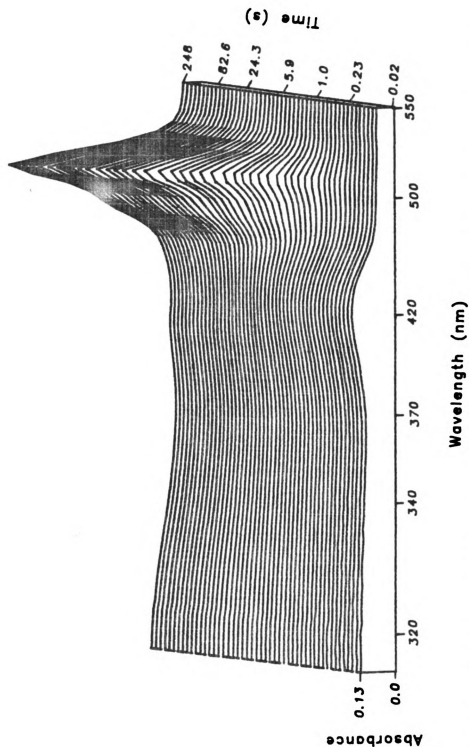
Figure V.1. Absorbance-wavelength-time surface for the reactivation of tryptophanase by a K^+-ethionine mixture (α vs. K^+-Eth.). Concentrations after mixing were; Tpase, 1.25 mg·ml^{-1} (23 µM); Ethionine, 8.0 mM; K_f^+, 16.0 mM. Other conditions are described in the Experimental Section.

the first spectrum collected from the spectra at the various time points, are displayed in Figure V.2. These spectra were selected from 55 spectra collected by the scanning stopped-flow system described in the experimental chapter. The principal changes of absorbance are the decay of the inactive form(s) of the enzyme at 420 nm, and the growth of the quinonoid complex with an intense peak at 508 nm. Due to the fact that the 337 nm absorbing form of the enzyme is not formed under these experimental conditions, the spectral contributions are only from the α-form(s) and quinonoid chromopnores. The changes in absorbance at $\sim$300 nm are precisely parallel to those at 508 nm.

C.2. Kinetics

The kinetics of the reaction were studied in both scanning and fixed wavelength modes by stopped-flow spectrophotometry. Kinetic analyses were done on data collected in the scanning mode as well as on data from the fixed wavelength mode. The scanning mode analyses were done in order to get a more precise estimate of the values of delta-absorbances at each wavelength for comparison. This is due to the fact that the fixed wavelength pushes at various K^+ concentrations may have been at slightly different wavelengths because the scanning monochromotor is mechanically set to a particular wavelength. Non-linear least-squares data fittings were carried out by program KINFIT.
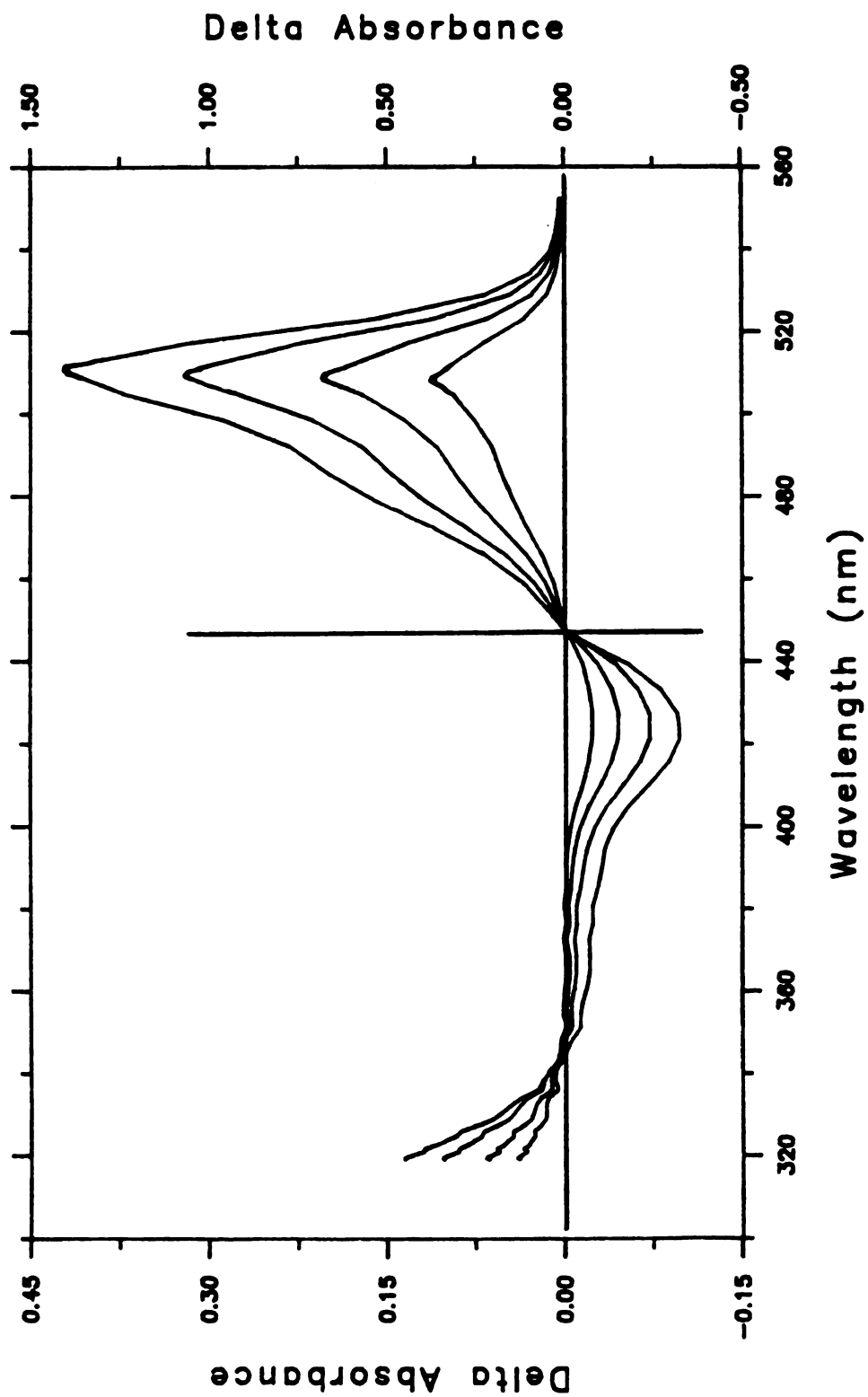
Figure V.2. Selected difference spectra constructed from Figure V.1 by subtracting the spectrum of the inactive enzyme (first spectrum). All conditions were the same as in Figure V.1. Times for the spectra, in sec, from the bottom at 508 nm are: 2.3, 7.0, 27.5, and 248.

C.2.1. <u>Absorbance Change at 508 nm</u> - The change at this wavelength is triphasic at all except the lowest K^+ concentration. The data at this wavelength were best fit to a three "1st-order" exponential equation (similar to Equation IV.2) by KINFIT. The rates of the three processes were sufficiently different for KINFIT to separate them. At the lowest K^+ concentration a two "first-order" exponential equation described the data. A typical fit of the overall absorbance change at this wavelength is shown in Figure V.3. The results of the fit at this wavelength are summarized in Tables V.1A for the rate constants (k_i) and V.2A for the delta-absorbances, ΔA_i.

The results in Table V.1A indicate that the rate constant for the second phase, k_2, is the most sensitive to the K^+ concentration while the rate constant for the last phase, k_3, is relatively independent of K^+. An average value of $(6.79\pm0.63) \times 10^{-3}$ sec^{-1} can be calculated for k_3 at this wavelength. At the lowest K^+ concentration the last two phases were inseparable indicating that the two slower processes have decreased in amplitude and/or rate. The magnitude of the absorbance change for the first process is strongly K^+ dependent while the change contributed by the second phase is practically independent of K^+ (Table V.2A). The delta absorbance for the third phase shows a slight increase at the lower K^+ concentrations.

C.2.2. <u>Absorbance Change at 420 nm</u> - The absorbance change at this wavelength was also triphasic, again, with the exception of the change at the lowest K^+ concentration. The magnitude of the absorbance change at the latter concentration was very small, only 0.008 O.D.
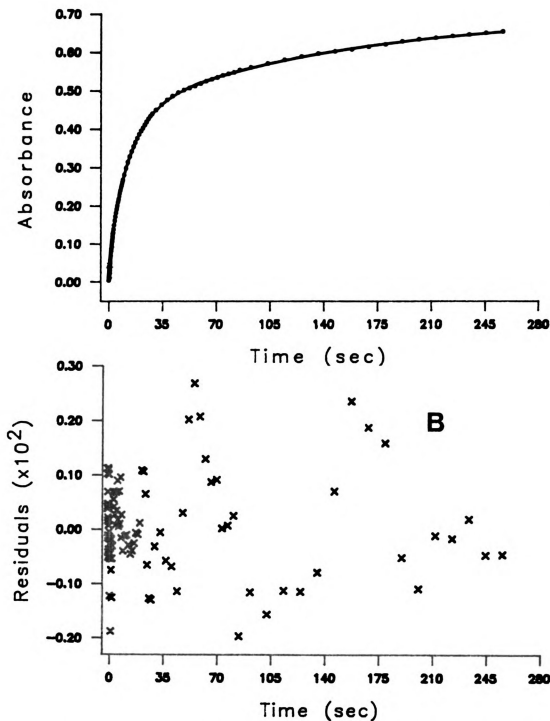
Figure V.3(A). Fit of the data at 508 nm in "α-Enzyme" vs. "K$^+$-Ethionine" experiment by a three "first-order" exponential equation. (K$^+$)$_f$ was 12.0 mM. Other conditions were the same as Figure V.1. B. Residuals of the fit.

Table V.1. Apparent Rate Constants at 508 and 420 nm for the Activation of Tryptophanase by a Mixture of Ethionine and K^+ in Bicine Buffer at pH=8.70. Concentrations of the Enzyme and Ethionine (After Mixing) were 1.25 mg.ml^{-1} (23 μM), and 8.0 mM, respectively. (α-ENZ) vs. (K^+-ETH).

A. λ=508 nm

$[K^+]$,mM	k_1',Sec^{-1}	k_2',Sec^{-1}	k_3',Sec^{-1}
42.0	.88±.05	.151±.006	$(7.73±.13)\times10^{-3}$
25.0	.61±.03	.133±.005	$(6.60±.08)\times10^{-3}$
16.0	.36±.03	.083±.004	$(6.17±.11)\times10^{-3}$
12.0	.41±.03	.070±.002	$(6.37±.10)\times10^{-3}$
7.0	.60±.30	.035±.002	$(7.10±.74)\times10^{-3}$
2.3[a]	.50±.20	.015±.001	-------
			AVG=$(6.79±.62)\times10^{-3}$

B. λ=420 nm

$[K^+]$,mM	k_1',Sec^{-1}	k_2',Sec^{-1}	k_3',Sec^{-1}
42.0	.60±.06	.150±.003	$(6.76±.60)\times10^{-3}$
25.0	.56±.04	.133±.002	$(4.97±.80)\times10^{-3}$
16.0	.40±.02	.106±.003	$(6.35±.50)\times10^{-3}$
12.0	.30±.03	.064±.010	$(8.0±1.3)\times10^{-3}$
7.0	.52±.12	.045±.003	$(5.34±.95)\times10^{-3}$
2.3[b]	.062±.015		-------
			AVG=$(6.28±1.20)\times10^{-3}$

[a]Two exponentials equation used in the fit.
[b]One exponential equation used in the fit.

Table V.2. The Amplitude and Percentage of the Absorbance Changes at 508 and 420 nm for the Activation of Tryptophanase by a Mixture of K^+ and Ethionine (α-ENZ vs. K^+-ETH). Experimental Conditions are the Same as in Table V.1.

A. λ=508 nm

$[K^+]$, mM	ΔA_1	ΔA_2	ΔA_3	$\%\Delta A_1$	$\%\Delta A_2$	$\%\Delta A_3$
42.0	.435±.021	.594±.018	.411±.003	30	41	28
25.0	.303±.018	.608±.015	.368±.005	24	47	29
16.0	.285±.023	.616±.021	.383±.004	21	48	30
12.0	.190±.011	.618±.010	.436±.003	15	48	36
7.0	.104±.010	.478±.022	.417±.018	10	48	42
2.3[a]	.047±.010	.400±.004	-----	10	90[a]	

B. λ=420 nm

$[K^+]$, mM	ΔA_1	ΔA_2	ΔA_3	$\%\Delta A_1$	$\%\Delta A_2$	$\%\Delta A_3$
42.0	.034±.001	.051±.001	.037±.001	28	42	30
25.0	.024±.001	.051±.001	.035±.003	22	46	32
16.0	.022±.001	.057±.001	.036±.001	19	50	32
12.0	.020±.001	.050±.001	.033±.001	18	48	32
7.0	.008±.001	.049±.001	.038±.001	7	52	41
2.3[b]	.006±.001	-----	-----	100[b]	--	--

[a] Two exponentials equation used in the fit.   [b] One exponential equation used in the fit.

($\sim$3 times the noise level at this wavelength), and, thus, the three phases were inseparable. A single "average" rate constant of (6.2 ± 1.5) x 10^{-2} $\sec^{-1}$ was calculated at this concentration by KINFIT. The results of the fit at this wavelength are summarized in Tables V.1B (rate constants) and V.2B (delta absorbances). As can be seen from these tables, the data at this wavelength are quantitatively in agreement with those at 508 nm. Specifically;

(a) k_2 and ΔA_1 are strongly K^+ dependent;

(b) ΔA_2 is independent of K^+;

(c) The rate constant of the third phase, k_3, is independent of K^+. The average value of k_3 at this wavelength, (6.28 ± 1.28) x 10^{-3} $\sec^{-1}$, compares favorably with that obtained at 508 nm, (6.79 ± 0.63) x 10^{-3} $\sec^{-1}$, which indicates that they represent the same process.

A fit of the data at this wavelength for the K^+ concentration of 25.0 mM is shown in Figure V.4.

D. Activation of Inactive-Tryptophanase-Ethionine Complex by K^+ (α-ETH) vs. (K^+)

D.1. Spectral Shape Analysis

The spectral changes were identical to those described in Section C of this chapter. The principal changes of absorbance were again the decay of the inactive form at 420 nm and the growth of the quinonoid complex at 508 nm with no substantial change at 337 nm. However, the
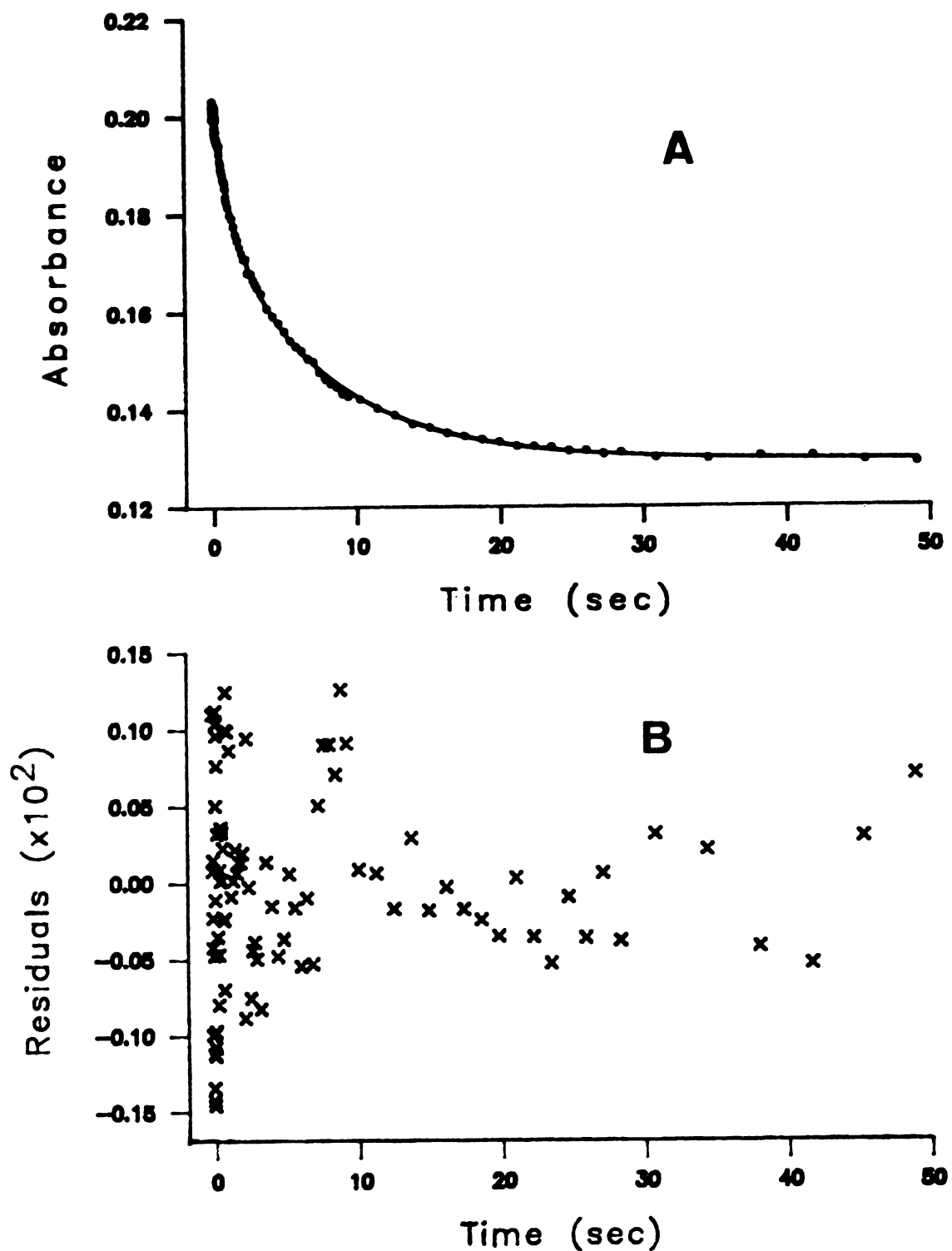
Figure V.4. A. Two-exponential fit to the first 50 seconds of the absorbance-time data at 420 nm in "α-Enzyme vs. K^+-Ethionine" experiment at 25.0 mM free K^+. Other conditions are the same as Figure V.1. Dots (·) are the data and solid line is the calculated curve. (B) Residuals of the fit.

overall process appears to be somewhat slower in this experiment and it is not completely over during the same time period as the α-enzyme vs. K^+-ethionine experiment (Section C). The difference in extrapolated final absorbance between the two experiments at a K^+ concentration of 42.0 mM is about 20 percent of the quinonoid absorbance peak. Similar differences in total absorbance change were also observed at all other K^+ concentrations.

D.2. Kinetics

The kinetics of this experiment were again studied in both scanning and fixed-wavelength modes and the data were analyzed by the program KINFIT4.

D.2.1. _Absorbance Change at 508 nm_ - The absorbance change at this wavelength was again triphasic at and above K^+ concentrations of 12 mM. At a K^+ concentration of 7.0 mM, it appears that the first process decreased in amplitude so that a single exponential could account for the absorbance change of the first two phases (Table V.3A). At the lowest K^+ concentration, the three phases were completely inseparable and a single exponential with a rate constant of $(1.78\pm.02) \times 10^{-2}$ sec^{-1} accounted for the total change in absorbance. The fit of the data at this wavelength for a K^+ concentration of 16 mM is shown in Figure V.5, and the results are summarized in Table V.3A (rate constants) and Table V.4A (delta absorbances).

Comparison of the results in Table V.3A with those in Table V.1A at this wavelength reveals that the rate constants for the first and

Table V.3. Apparent Rate Constants at 508 and 420 nm for the Activation of K^+-depleted-Tryptophanase-Ethionine Complex by K^+ in Bicine Buffer at pH = 8.70. Concentrations of the Enzyme and Ethionine (After Mixing) Were 1.25 mg.ml^{-1} and 8.0 mM, respectively. (α-Ethionine) vs (K^+).

A. λ=508 nm

$[K^+]$,mM	k_1'',Sec^{-1}	k_2'',Sec^{-1}	k_3'',Sec^{-1}
42.0	.70±.03	.086±.003	$(6.95±.13) \times 10^{-3}$
25.0	.50±.02	.073±.002	$(5.16±.21) \times 10^{-3}$
16.0	.40±.02	.064±.002	$(5.32±.06) \times 10^{-3}$
12.0	.43±.02	.086±.012	$(7.30±.15) \times 10^{-3}$
7.0[a]	.13±.01		$(6.77±.09) \times 10^{-3}$
2.3[b]	$(1.78 .02) \times 10^{-2}$		-------
			$AVG=(6.3±1.0) \times 10^{-3}$

B. λ=420 nm

$[K^+]$,mM	k_1,Sec^{-1}	k_2,Sec^{-1}
42.0	.25±.02	$(4.92±.13) \times 10^{-3}$
25.0	.24±.04	$(5.28±.40) \times 10^{-3}$
16.0	.20±.03	$(4.96±.18) \times 10^{-3}$
12.0	.12±.02	$(6.83±1.2) \times 10^{-3}$
7.0[b]	$(1.19±.10) \times 10^{-2}$ ----	
2.3[b]	$(.64±.12) \times 10^{-2}$ ----	
		$AVG=(5.47±.92) \times 10^{-3}$

[a]Two exponentials equation used in the fit.

[b]One exponential equation used in the fit.
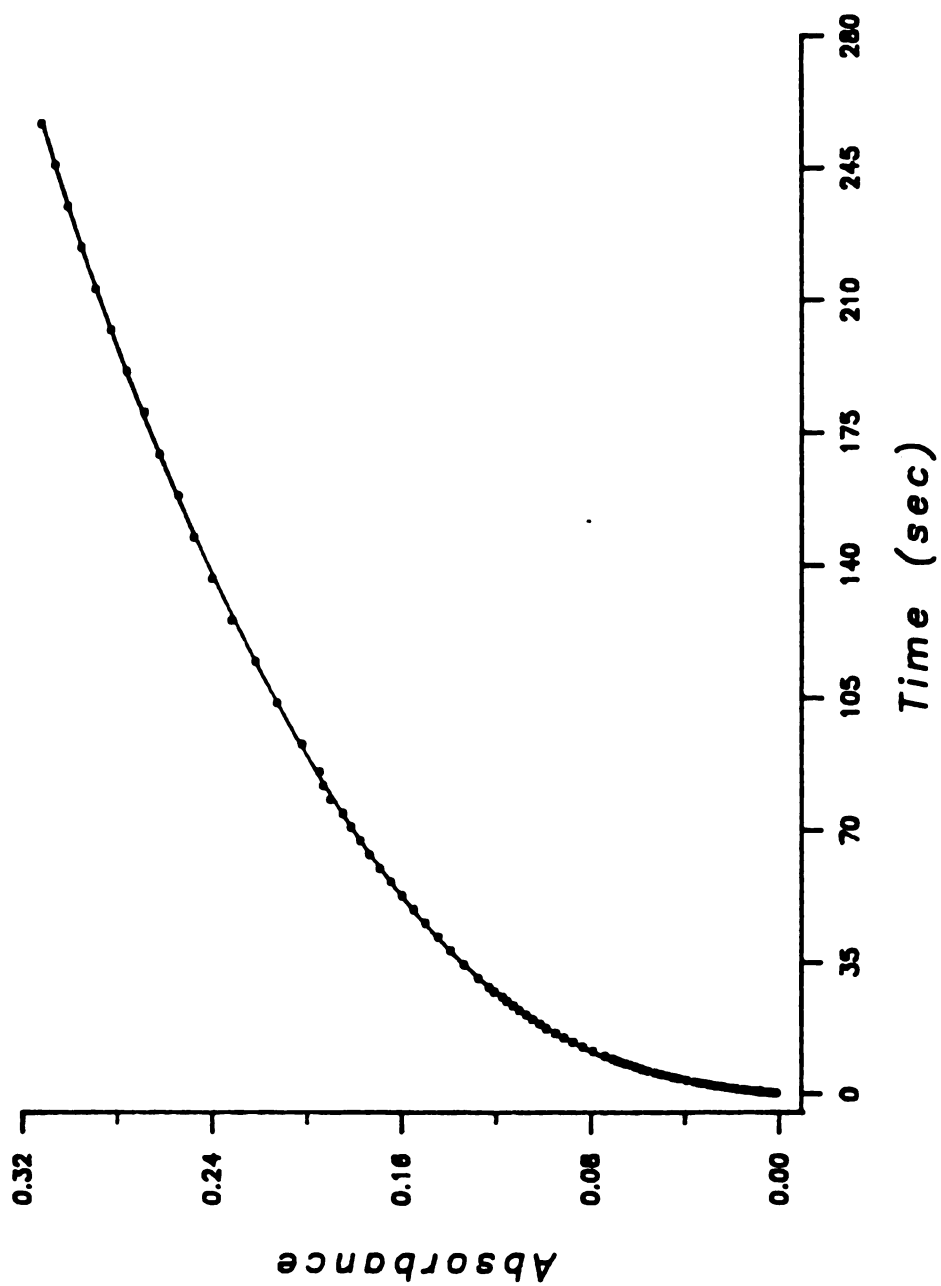
Figure V.5. Three-exponential fit of the data at 508 nm in "α-Ethionine" vs. "K$^+$" experiment at 16.0 mM free K$^+$. Other concentrations were; TPase, 1.25 mg·ml^{-1} (23 μM); L-ethionine, 8.0 mM (after mixing). PH was 8.70. Dots (·) are the data and the solid line is the calculated curve.

Table V.4. The Amplitude and Percentage of the Absorbance Changes at 508 and 420 nm for the Activation of "K$^+$-Depleted-Tryptophanase-Ethionine" Complex by K$^+$ (α-ETH. vs. K$^+$). Experimental conditions are the same as in Table V.3.

A. λ=508 nm

[K$^+$], mM	ΔA_1	ΔA_2	ΔA_3	%ΔA_1	%ΔA_2	%ΔA_3
42.0	.193±.007	.202±.006	.584±.002	20	20	60
25	.180±.007	.176±.006	.614±.005	18	18	63
16.0	.110±.004	.186±.003	.642±.002	12	20	68
12.0	.051±.014	.175±.011	.563±.003	6	22	71
7.0[a]	.056±.001		.507±.002	10[a]		90
2.3[b]	.220±.002		-----	100[b]		--

B. λ=420 nm

[K$^+$], mM	ΔA_1	ΔA_2	%ΔA_1	%ΔA_2
42.0	.026±.001	.059±.001	31	69
25.0	.023±.002	.056±.002	29	71
16.0	.015±.001	.056±.002	21	78
12.0	.008±.001	.055±.003	13	87
7.0[b]	----	.032±.003[b]	--	100
2.3[b]	----	.026±.002[b]	--	100

[a] Two exponentials equation used in the fit. [b] One exponential equation used in the fit.

third phases, k_1'' and k_3'', are essentially the same as k_1' and k_3', however, in contrast to the former experiment (α-Enzyme vs. K^+-Ethionine mixture) k_2'' is independent of potassium. An average value of $0.077\pm.011$ sec^{-1} can be calculated for k_2'' from the data in Table V.3A. Comparing the absorbance changes in the two experiments, presented in Tables V.2A and V.4A, shows ΔA_1 to be similarly K^+ dependent, ΔA_2 is K^+ independent at least above 12 mM, and ΔA_3 shows a gradual increase with increasing K^+ concentration. The significant difference between the two experiments is that in the latter case (α-Enzyme-ethionine vs. K^+) the overall absorbance change is only about 75 to 80% of that in the former experiment (α-Enzyme vs. K^+-Ethionine). Moreover, the absorbance change during the third phase in the latter case contributes more than 60% of the total absorbance change compared to ∿25% in the previous experiment.

D.2.2. <u>Absorbance Change at 420 nm</u> - The absorbance change at this wavelength was biphasic, two first order processes, at K^+ concentrations of 12.0, 16.0, 25.0 and 42.0 mM. The change at the two lower K^+ concentrations was small and a single rate constant was calculated by KINFIT for the overall process in both cases. Results of the analyses at this wavelength are summarized in Tables V.3B (rate constants) and V.4B (absorbance changes).

The results in Tables V.3 and V.4 together reveal the following information regarding this experiment;

    i)   The rate constant for the slower process at 420 nm, k_2, is

           essentially the same as the rate constant for the third

phase at 508 nm, k_3'', (Table V.3).

ii) The relative percentage of the absorbance change due to the slower process at 420 nm, $\%\Delta A_2$ in Table V.4B, is also comparable to the $\%\Delta A_3$ at 508 nm (Table V.4A) and they both show similar K^+ dependence characteristics.

iii) The rate constant for the faster of the two phases at 420 nm, k_1, appears to be an average of the two faster processes at 508 nm, k_1'' and k_2'' (Table V.3).

iv) Finally, the magnitude of the change in absorbance due to the faster process at 420 nm, $\%\Delta A_1$ in Table V.4B, is again strongly K^+ dependent, similar to that at 508 nm (V.4A) and the changes in the α-enzyme vs. K^+-ethionine experiments (Table V.2).

E. Discussion

The results presented in this chapter on activation of tryptophanase in the presence of L-ethionine are again multiphasic. As discussed earlier (Chapter IV), it does not seem likely that inhomogeneity of the enzyme is responsible for the multiphasic kinetics observed in these experiments. Such inhomogeneity would have to be significant, in particular, in these experiments to account for the triphasic behavior of the reactivation. The significant difference between the activation in the presence of ethionine described in this chapter and that in the absence of the inhibitor is that the growth of the quinonoid absorbance upon mixing ethionine and saturating concentration of K^+ with the deactivated enzyme is complete; whereas only about 50 percent

of the original absorbance at 337 nm is recovered in the absence of the inhibitor (Chapter IV). Once again, the results can be interpreted in terms of "kinetic anticooperativity" between subunits of the enzyme. Hereafter, the reactivation of the inactive (α) enzyme by a mixture of K^+ and ethionine (Section C) will be referred to as experiment 1 and reactivation of the inactive-enzyme-ethionine complex by K^+ (Section D) will be referred to as experiment 2 for the sake of brevity.

The variation of the amplitude of the absorbance change at 508 and 420 nm in the first phase of experiment 1, ΔA_1 in Table V.2, shows a saturation behavior that depends on the square of the potassium concentration as indicated in Figure V.6; half-saturation occurs at about 14 mM K^+ concentration. The $(K^+)^2$ dependence again strongly suggests that two sites per protomer need to be saturated by potassium for the appearance of activation. In this experiment, ΔA_1 contributes an average of 25 percent to the overall absorbance change. In addition, ΔA_2 and ΔA_3 contribute about 48 percent ($\sim$50%) and 30 percent ($\sim$25%) to the overall absorbance change in experiment 1 as indicated in the same table. Since the quinonoid growth in this experiment is complete and no enzyme inhomogeneity is believed to be present, the data might indicate that the rate of quinonoid formation depends upon the subunit conformation, i.e., kinetic anticooperativity is responsible for the complex kinetics in these experiments. The contributions of the three phases to the overall absorbance change in experiment 1 suggest that one protomer in the first step, two in the second, and one in the third phase convert to the quinonoid at different rates by virtue of the kinetic anticooperativity.
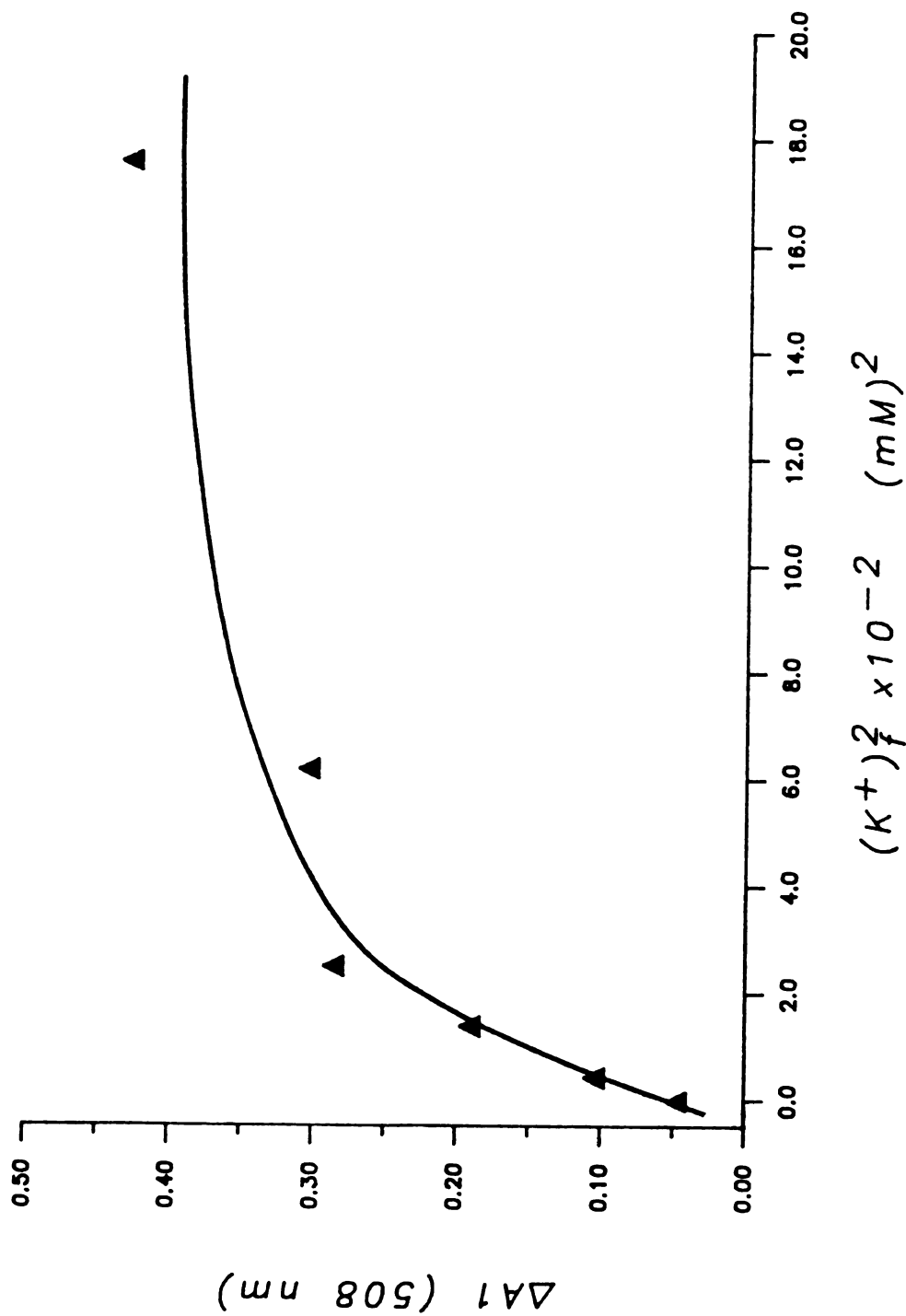
Figure V.6. Dependence of the amplitude of the absorbance change of the fast phase in experiment 1 (α-Enz. vs. K^+-ETH), ΔA_1 in Table V.2, on the square of the free K^+ concentration.

The data in the two experiments do not provide any information about the rates of binding of potassium and ethionine to the inactive enzyme. Such information is not reported in the literature either. However, from our results it is reasonable to assume that both K^+ (2 per protomer) and ethionine binding must be complete before any conversion to the quinonoid occurs; and that each protomer may bind either potassium or ethionine at different rates. For a protomer, represented by α, this can be expressed by the following simple scheme;

$$\alpha + 2K^+ \underset{}{\overset{fast}{\rightleftharpoons}} \alpha K_2^+ + E \underset{}{\overset{fast}{\rightleftharpoons}} \alpha E K_2^+ \qquad (V.1)$$
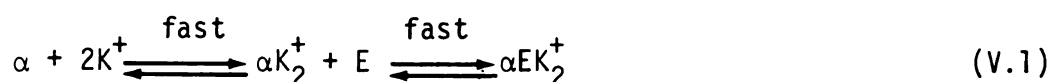
where E represents the inhibitor, L-ethionine.

In the absence of ethionine αK_2^+ can convert to the γ form at 337 nm (Chapter IV); however, in the presence of ethionine the equilibrium lies far to the right. This is supported by the fact that the kinetics of quinonoid growth from the inactive enzyme (this chapter) are different than in the absence of ethionine. The absorbance change during the first phase in experiment 1 could then arise from the conversion of one protomer, bound to both K^+ and ethionine, to the quinonoid at 508 nm with the rate constant, $0.56 \pm .14$ sec^{-1} (Table V.1, k_1') practically independent of the potassium concentration.

The absorbance change during the second phase in experiment 1 has a relatively constant amplitude above 7.0 mM K^+, and contributes about 50 percent to the overall absorbance change as indicated earlier. This

was attributed to the conversion of the two other protomers from the inactive form to the quinonoid. The rate constant for the second phase, k_2' in Table V.1, is directly proportional to the concentration of free K^+ which indicates that one potassium ion is involved in the rate-determining step in this process or in a pre-equilibrium process just before this step. Assuming that two potassium ions should bind to each protomer, the dependence suggests that the two protomers probably bind one of the two potassium ions more strongly than the other. Conversion to the quinonoid does not proceed, however, until the second K^+ ion binds to the complex. If α again represents one of the protomers involved in this process, we can schematically

$$
\alpha + K^+ \xrightarrow{\text{fast}} \alpha K^+
$$

$$
+
$$

$$
E
$$

$$
\Updownarrow
$$

$$
K^+ + \alpha EK^+ \underset{}{\overset{K}{\rightleftharpoons}} \alpha EK_2^+ \overset{k_{\alpha 2}}{\rightleftharpoons} QE\ (508\ nm)
$$

$$(V.2)$$
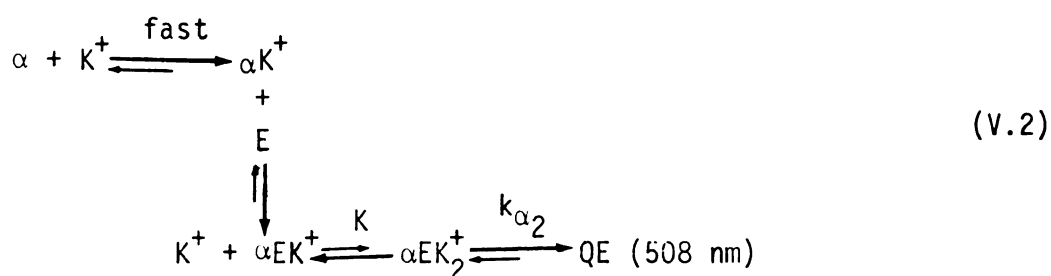
It is likely that k_2' (Table V.1) actually represents two steps, K^+ binding (equilibrium) and conversion to QE (slow). According to Scheme V.2 k_2' can be represented by;

$$
k_2' = k_{\alpha 2} K(K^+)
$$

being directly proportional to the free K^+ concentration as indicated in Table V.1. This scheme also explains the incomplete recovery of

the original absorbance in the absence of ethionine (Chapter IV) since it suggests that the second K^+ binding, which is required for the formation of the quinonoid, occurs only after the ethionine binding. No direct experimental evidence is available, however, to confirm this assumption.

The absorbance change in the last phase of experiment 1 is probably due to conversion of the last inactive protomer (recall that this phase contributes about 25% to the overall absorbance change) into the quinonoid with the rate constant k_3' represented in Table V.1. Once again, the K^+ binding to this protomer must be complete before any quinonoid is formed. From the data in Table V.1 an average value of $6.54 \pm .84 \times 10^{-3}$ sec^{-1}, independent of the K^+ concentration, can be calculated for k_3'. These observations together can be explained by the following simple scheme for the activation of inactive tryptophanase by a mixture of potassium and ethionine (experiment 1).

$$4E \;+\; (\alpha)_4 \;\rightleftharpoons\; (\alpha E)_4$$
$$\Big\Downarrow k_1'$$
$$(QE)(\alpha E)_3$$
$$\Big\Downarrow k_2'$$
$$(QE)_3(\alpha E)$$
$$\Big\Downarrow k_3'$$
$$(QE)_4$$

$$(V.3)$$
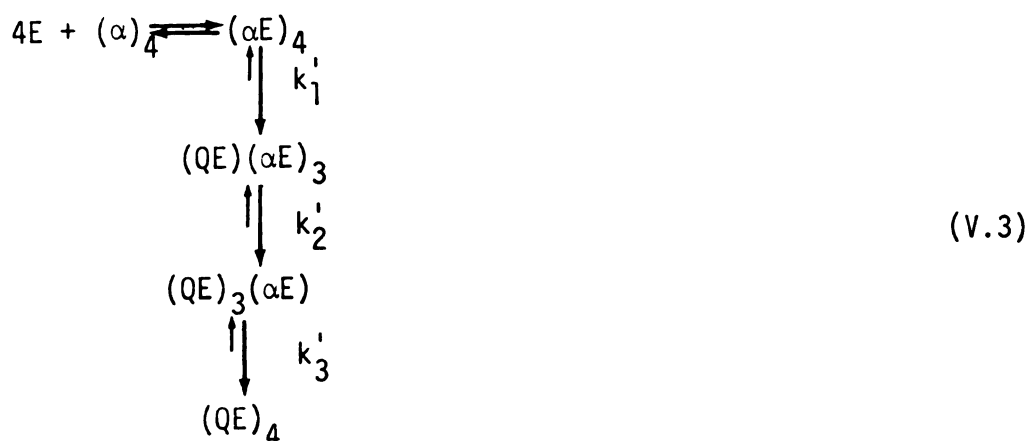
In this scheme potassium ions are involved as described in the text.

In experiment 2 the inactive enzyme was first mixed with ethionine followed by pushing the resulting mixture against potassium in the

stopped-flow system. Mixing of the inactive-enzyme-ethionine complex with K^+ was carried out from 10 to 40 minutes after addition of 18-crown-6, depending upon the time of a particular push. The major difference between the two experiments are that in this case (experiment 2);

i) The overall absorbance change extrapolated to "infinite" time is only about 75 to 80 percent of that in experiment 1 as indicated earlier;

ii) The rate constant for the second phase, k_2'', is independent of potassium concentration, K^+;

iii) The sum of ΔA_1 and ΔA_2 at 508 nm (Table V.4A) compares with ΔA_1 in experiment 1 at the same wavelength (Table V.2A), at least above 12.0 mM free K^+ concentration. Furthermore, at 420 nm, where the absorbance change of the first phase represents the "sum" of the two faster processes at 508 nm (Table V.4B), ΔA_1 (at 420 nm) similarly compares with ΔA_1 in the first experiment. This suggests that the changes in the first "two phases" in this experiment are due to conversion of only one protomer to the quinonoid.

iv) The amplitude of ΔA_3 at 508 nm in this case (Table V.4A) is the same as ΔA_2 of the first experiment at the same wavelength (above 12 mM). This suggests that the change in the third phase of this experiment probably corresponds to that of the second phase in the first experiment. This is further supported by the fact that the amplitudes of ΔA_2 at 420 nm in the two experiments are the same.

To account for these observations, it is proposed that the inactive-enzyme-ethionine complex undergoes a conformational transition in the absence of potassium ions, consistent with the suggestion of Goldberg et al. (63) that the appearance of enzymatic activity of the inactive enzyme by K^+ requires a conformational change in the inactive state of the enzyme. In fact in such a transition the conformational state of each individual subunit might be different from that of the other protomers. If α' represents the conformation of a subunit after such a transition, we can represent the conformational change by;

$$4E + (\alpha)_4 \underset{\longleftarrow}{\overset{fast(1)}{\rightleftharpoons}} (\alpha E)_4 \underset{\longleftarrow}{\overset{(slow)(2)}{\rightleftharpoons}} (\alpha E)(\alpha'E)_3 \underset{\longleftarrow}{\overset{(3)}{\rightleftharpoons}} (\alpha'E)_4$$

$$(V.4)$$
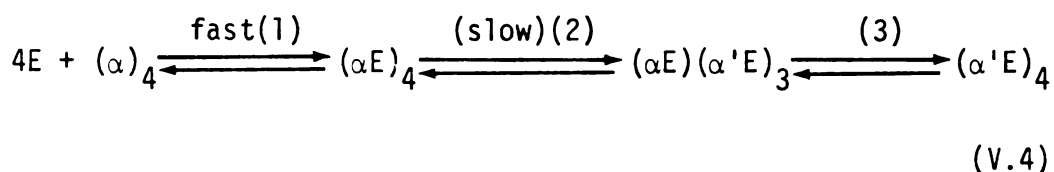
where the equilibrium lies to the right in favor of step 3 in the absence of potassium. The fact that the rate constants for the first process in the two experiments, k_1' and k_1'', $0.56\pm.14$ sec^{-1} and $0.51\pm.12$ sec^{-1}, respectively, are the same, suggests the existence of both forms in equilibrium for at least one of the protomers as given in the last step in Equation V.4. Both of these rate constants probably represent conversion of the same protomer in a similar conformation, i.e., conformation α. In addition, the relative amplitudes of ΔA_1 and ΔA_2 (Table V.4A, above 12 mM) at 508 nm indicates that the equilibrium constant for this step is not far from unity. Since the changes in the first "two phases" in experiment 2 are due to only one protomer as discussed, the second rate constant in the process, k_2'', should represent the conformational change of the same protomer from the $\underline{\alpha'E}$ state to the $\underline{\alpha E}$ state

before conversion to the quinonoid. These changes can be represented by Equation V.5 as;

$$(\alpha E)(\alpha' E)_3 \underset{k_2''}{\overset{K \approx 1}{\rightleftharpoons}} (\alpha' E)_4$$

$$\downarrow k_1'' (=k_1')$$

$$(QE)(\alpha' E)_3$$

$$(V.5)$$
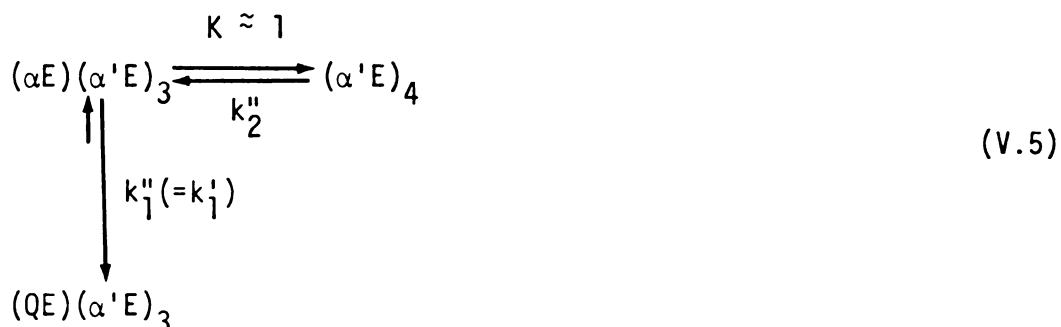
The change in the third phase of experiment 2 at 508 nm (corresponding to the 2nd phase at 420 nm, see Table V.3), which accounts for two subunits (as ΔA_2 in experiment 1), can then be attributed to conversion of two other protomers in the $\alpha' E$ conformation to the quinonoid, either directly with the rate constant k_3'', or via the α conformation. In the latter case the α' to α conformational change should be the rate-determining step. The difference in the overall absorbance change in the two experiments (only 75 to 80% total quinonoid growth in experiment 2 compared to 1) suggests that one of the subunits converts very slowly to the quinonoid in the second experiment. The conversion rate of this subunit is probably further slowed down due to the different conformational states of the other subunits, i.e., the $\alpha' E$ conformations.

The results of the two experiments on the activation of tryptophanase by K^+ in the presence of ethionine can be represented together by the following model;

$$\underbrace{2K^+ \text{ Per subunit}} \qquad\qquad \underbrace{2K^+ \text{ Per Subunit}}$$

$$4E + (\alpha)_4 \underset{}{\overset{(fast)}{\rightleftharpoons}} (\alpha E)_4 \underset{}{\overset{(slow)}{\rightleftharpoons}} (\alpha E)(\alpha'E)_3 \underset{k_2''}{\overset{K \approx 1}{\rightleftharpoons}} (\alpha'E)_4$$

$$\Big\updownarrow k_1' \qquad\qquad \Big\updownarrow k_1''$$

$$(QE)(\alpha E)_3 \qquad\qquad (QE)(\alpha'E)_3$$

$$\Big\updownarrow k_2' \qquad\qquad \Big\updownarrow k_3'' \qquad\qquad (V.6)$$

$$(QE)_3(\alpha E) \qquad\qquad (QE)_3(\alpha'E)$$

$$\Big\updownarrow k_3' \qquad\qquad \Big\updownarrow k_4'' \text{ (very slow)}$$

$$(QE)_4 \qquad\qquad (QE)_4$$
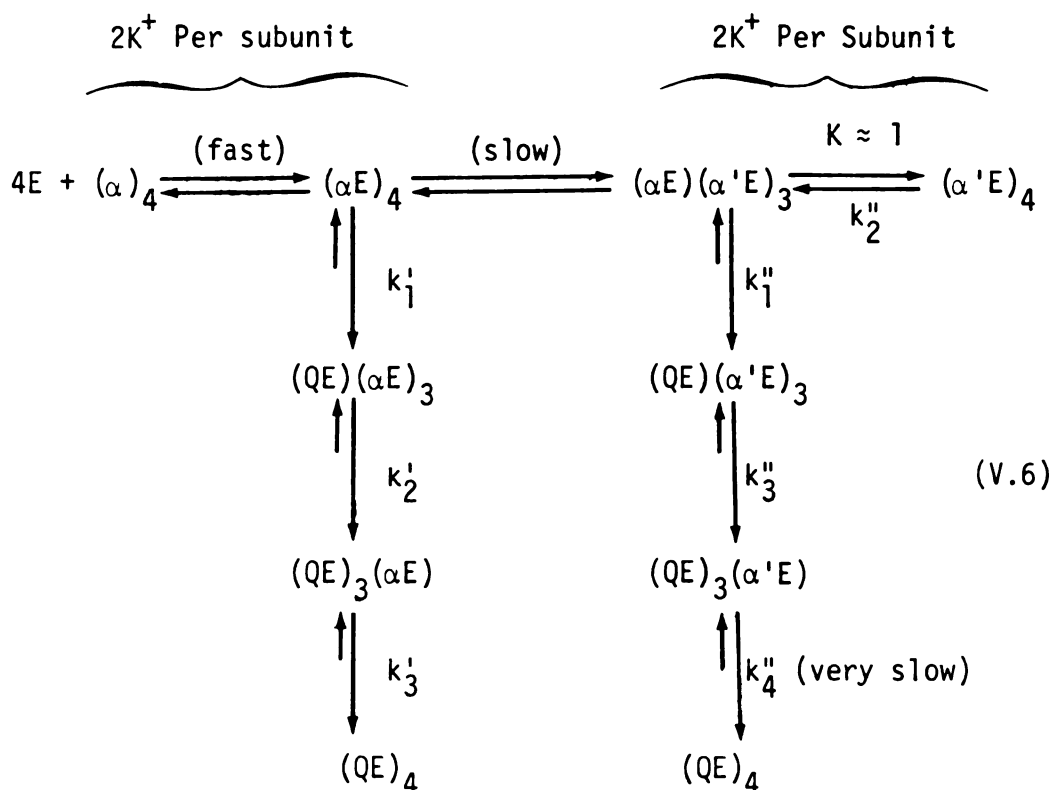
in which the slow equilibrium (conformational change) occurs in the absence of potassium ions. The left side of this model (with the rate constants k_i') represent the first and the right side of the model (with the rate constant k_i'') represents the second experiment, and potassium binding in individual steps are discussed in the text (Schemes V.1, V.2 and V.4).

An alternative model for experiment 2 can also be proposed in which all protomers "anticooperatively" undergo a conformational change to the α state (similar to the first protomer) before conversion to the quinonoid. In this model the α' to α transition should govern the overall rate to account for the differences in the kinetics of the two experiments. The data obtained in these experiments cannot discriminate between these two possibilities.

F. Conclusions

The results presented here provide some reproducible experimental information about the interconversion of inactive tryptophanase into the quinonoid in the presence of L-ethionine. In contrast to the activation by K^+ in the absence of the inhibitor (Chapter IV), growth of the original absorbance is complete (experiment 1) which confirms that substrate or inhibitor in addition to potassium is required to completely reverse the deactivation brought about by depletion of K^+. Our data again suggest that kinetic anticooperativity governs the rate of conversion of the inactive enzyme into the quinonoid. The data agree with the suggestion of Goldberg et al. (63) that, during appearance of the enzymatic activity in the presence of potassium ion, the inactive enzyme undergoes a change in its conformation. Our data are also in agreement with circular dichroic experiments (77) which show formation of a complex between the enzyme and ethionine in the absence of potassium.

A simple model based on the kinetic anticooperativity between the protomers is proposed which describes the results obtained in this chapter. It is worth mentioning here that our data on the deactivation of the enzyme by 18-crown-6 both in the presence and absence of ethionine (Chapters VI and III, respectively) are also in accord with the fact that active holotryptophanase exhibits no cooperativity; as no multiphasic kinetics is observed in those experiments.

CHAPTER VI.

REACTION OF THE "TRYPTOPHANASE-ETHIONINE" COMPLEX
WITH 18-CROWN-6 - "QUINONOID DROP"

A. Introduction

The formation of an intense absorption band around 500 nm due to a
quinonoid structure upon mixing certain amino acid inhibitors or sub-
strates with tryptophanase in the presence of activating monovalent
ions was described in Chapter V. In the absence of activating monovalent
cations this absorption is absent. The goal of this study was to examine
the kinetics of disappearance of this band simultaneously with the
growth of the α-form (the reverse of the process described in Chapter
V) upon reducing the concentration of free K^+. This experiment was an
attempt to get more insight into the mechanism of the interconversion
of the active and inactive enzyme conformers. For this purpose 18-crown-6
was employed as the K^+-complexing agent due to the absence of an effect
on the spectrum or activity of the enzyme as described in Chapter IV.

B. Experimental Section

Holoenzyme from E-Coli Blt7/A with a total K^+ concentration of 17
mM in bicine buffer at pH = 8.70 was prepared as previously described
(123). The enzyme had a specific activity of 49.0 $\mu\text{mole} \cdot \text{min}^{-1} \cdot \text{mg}^{-1}$

when assayed with 0.6 mM SOPC in potassium phosphate buffer at pH 8.0. Prior to the stopped-flow experiments, the enzyme solution was mixed with a solution of L-ethionine to build up the quinonoid. The enzyme and ethionine concentrations were 2.0 mg·ml^{-1} and 16.0 mM, respectively, and the K$^+$ concentration was kept constant at 17.0 mM. This solution was then pushed against the various concentrations of 18-crown-6 indicated in Table VI.1. The experiments were carried out at 23±1°C.

C. Spectral Shape Analysis

The spectral changes as a function of the wavelength and time following mixing of the tryptophanase-quinonoid complex with 18-C$_6$ are presented in Figure VI.1. Concentrations of the enzyme and 18-C$_6$ after mixing were 1.0 mg·ml^{-1} (18 μM) and 190 mM, respectively. Comparison of the quinonoid spectrum at t=0, prior to mixing, with the first spectrum collected after mixing with 18-C$_6$ (∿13 mSec) showed no abrupt changes upon mixing as the two spectra were superimposable. Figure VI.2 displays, in two dimensions, spectra selected from Figure VI.1 as a function of time. As expected, the spectral changes are essentially the reverse of those which occurred during the quinonoid growth from the α-form of the enzyme (Chapter V). Similarly, the change in absorbance at ∿300 nm was parallel to that at 508 nm. The overall absorbance change at 420 nm is much smaller than that at 508 nm as demanded by the relative values of their extinction coefficients.

Table VI.1. Concentrations of K^+ and 18-Crown-6 After Mixing in the Stopped-Flow Studies of the Tryptophanase-Ethionine Complex Disappearance by 18-Crown-6. E_0 = 1.0 mg.ml^{-1} (18 μM) (L-ethionine)$_0$ = 8.0 mM for all pushes after mixing.

[Crown]$_0$, mM	(K^+_{free})final, mM
225	0.30
190	0.39
170	0.48
150	0.69
140	0.84
110	1.13
80	1.63

160
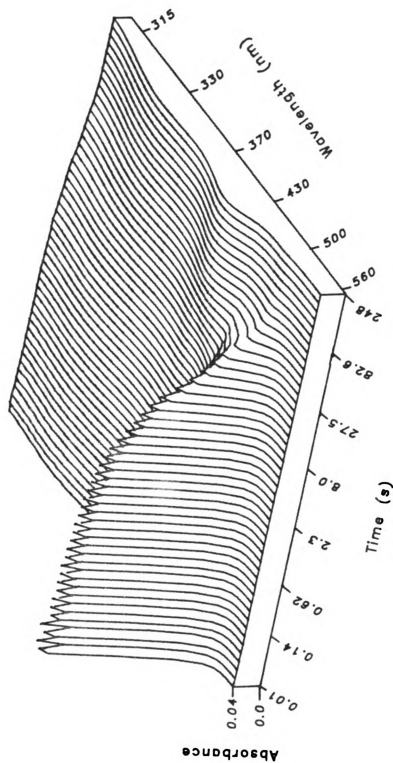
Figure VI.1. Absorbance-time-wavelength surface for the quinonoid disappearance by 18-crown-6. Concentrations after mixing were: tryptophanase, 1.0 mg·ml⁻¹ (18 μM); Crown, 190 mM. Other conditions are described in the text.

Figure VI.2. Selected difference spectra constructed from Figure VI.1 during the reaction of the holoenzyme-ethionine complex with 18-crown-6 (---). Conditions are the same as in Figure VI.1. Times of consecutive spectra are 5.9 and 248 seconds. The solid lines are for the reverse reaction described in Chapter V.

162
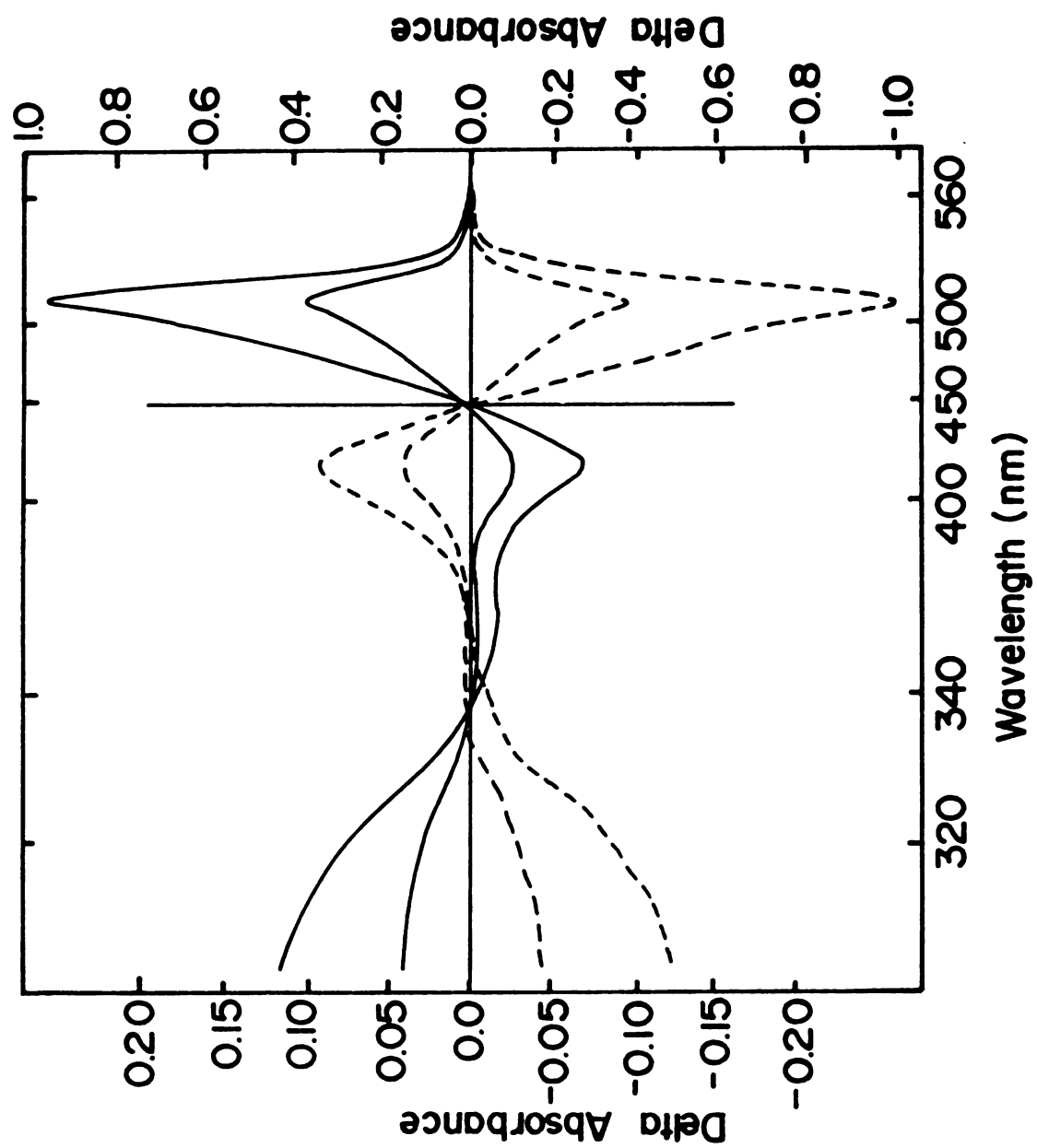
Figure VI.2

D. Kinetics of the Quinonoid Disappearance After Mixing Tryptophanase-
    Ethionine-K^+ Complex with 18-crown-6

D.1. Absorbance Change at 508 nm

The absorbance change at this wavelength is biphasic, with an initial
fast decay lasting about 200 mSec followed by a slower first-order con-
version of the quinonoid to the 420 nm absorbing form(s). The initial
fast phase was analyzed by choosing data points covering about the
first 200 mSec of the reaction. This phase was best fitted by a single
exponential with the program KINFIT4, the results of which are summarized
in Table VI.2A. The rate constant for this phase is independent of the
crown concentration, k_1 = 16.6±2.0 sec^{-1}; however, the amplitude of the
absorbance change was inversely proportional to the square of the free
K^+ concentration. The changes in absorbance in the initial fast phase
at concentrations of 18-crown-6 below 140 mM were too small to allow a
reasonable fit by KINFIT ($\Delta A \sim 0.006$ O.D. at a crown concentration of
140 mM). The analysis also showed that the contribution of the fast
phase to the total absorbance change at 508 nm is about 5% at the highest
crown concentration. Figure VI.3 shows the fit of the initial fast
phase to a single exponential at a crown concentration of 190 mM.

The major contribution to the overall absorbance change (>95%) at
508 nm, however, occurs in the slower phase of the reaction. The rate
of this slow phase is extremely sensitive to the crown concentration
(and thus to the free K^+ concentration) as indicated in Figure VI.4.
The absorbance change in this phase was again described by a 1st-order
process with values of the rate constants being inversely proportional

Table VI.2. Analysis of the Fast Phase of the Quinonoid Disappearance
by 18-Crown-6 in Bicine Buffer at pH=8.70. k_1 is the
observed 1st-Order Rate Constant for the Process.

A. λ=508 nm

[Crown], mM	$(K^+_{free})_{final}$	ΔA	k_1,Sec^{-1}
225	0.30	.072±.001	16.51± .77
190	0.39	.48±.002	16.33±1.82
170	0.48	.035±.002	16.05±3.06
150	0.69	.020±.003	17.57±7.18
140	0.84	.006±.002	-----
			AVG=16.6±2.0

B. λ=420 nm

[Crown], mM	$(K^+_{free})_{final}$	ΔA	k_1,Sec^{-1}
225	0.30	.007±.001	19.1±3.5
190	0.39	.0043±.003[a]	13.1±3.0
170	0.48	.0032±.003[a]	17.1±4.4
			AVG=15.2±1.8

[a]ΔA is very small and it is at the noise level of the experiment.
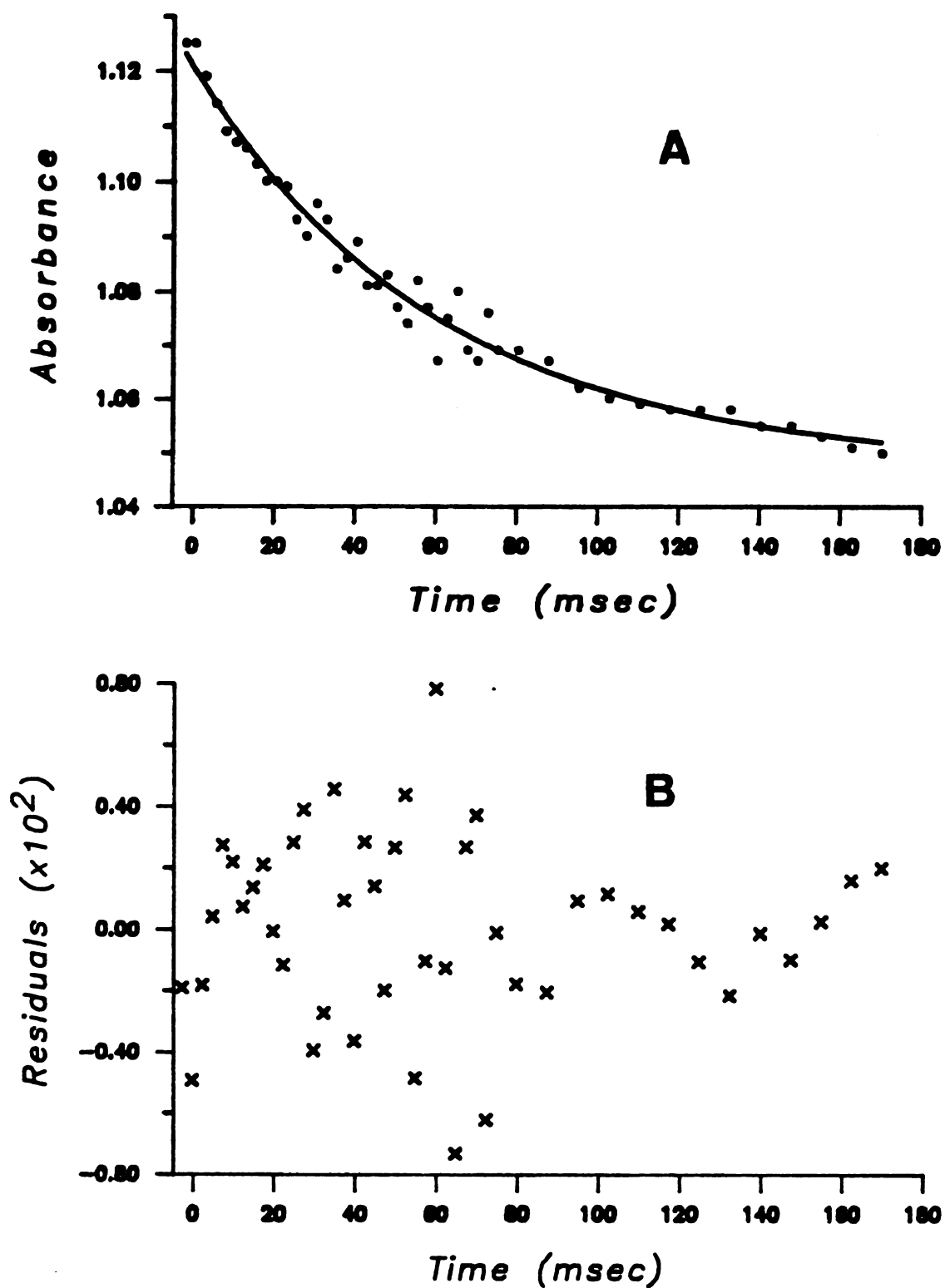
Figure VI.3. (A) Fit of the fast decay at 508 nm by a single exponential during the reaction of the quinonoid complex with 18-crown-6. Conditions are the same as in Figure VI.1. (B) Residuals of the fit.
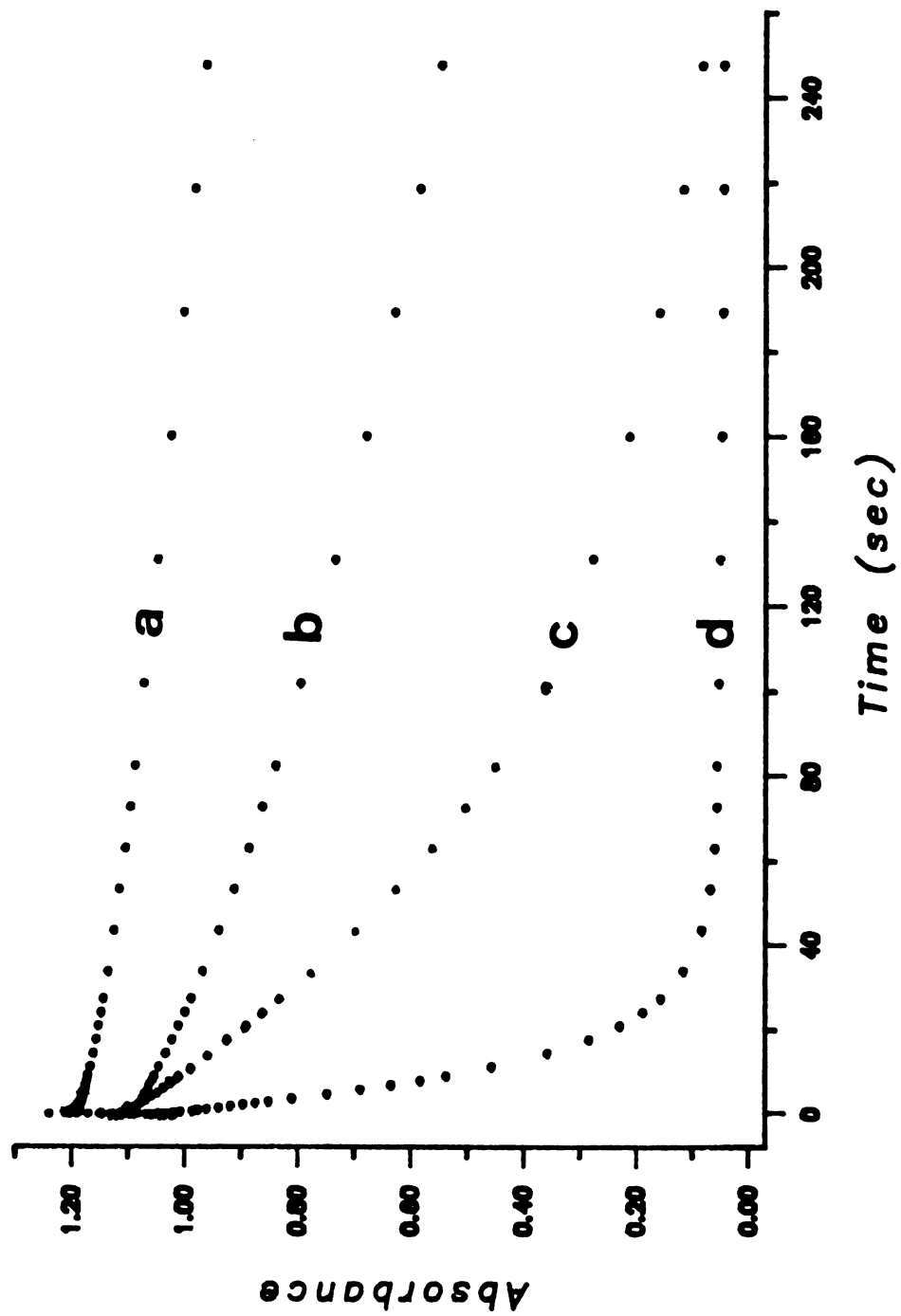
Figure VI.4. Effect of various concentrations of 18-crown-6 on the rate of quinonoid disappearance at 508 nm. Conditions are described in the text. a) 80 mM crown; b) 110 mM crown; c) 140 mM crown; d) 225 mM crown.

to the square of the free K^+ concentration as shown in Figure VI.5. The results of the fit of this phase at 508 nm are summarized in Table VI.3A.

D.2. Absorbance Change at 420 nm

The absorbance change at 420 nm mimics that at 508 nm. An initial fast growth in absorbance which lasted about 200 mSec, was observed at the highest concentration of 18-crown-6, 225 mM, and to a lesser extent at the crown concentrations of 190- and 170-mM. Although the magnitude of this change was very small ($\Delta A \sim 0.007$ O.D. at 225 mM crown), it was systematic enough to be resolved by KINFIT. The change was very well described by a first order process, the results of which are presented in Table VI.2B. Similar to the results at 508 nm, the rate constant for this process is independent of the crown concentration and its average value at this wavelength, $k_1 = 15.2 \pm 1.8$ Sec^{-1}, is essentially the same as that obtained at 508 nm, $k_1 = 16.6 \pm 2.0$ Sec^{-1}. Furthermore, the absorbance change during this phase also contributes only 5-6% to the overall absorbance change at this wavelength, which is in agreement with that at 508 nm.

The slow phase which again gave the major contribution to the overall absorbance change was also fit to a 1st-order process by KINFIT. The rate constants obtained are practically the same as those at 508 nm at all concentrations of 18-crown-6 as indicated in Table VI.3B. Similar to the results at 508 nm, the apparent first order rate constant is inversely proportional to the square of the
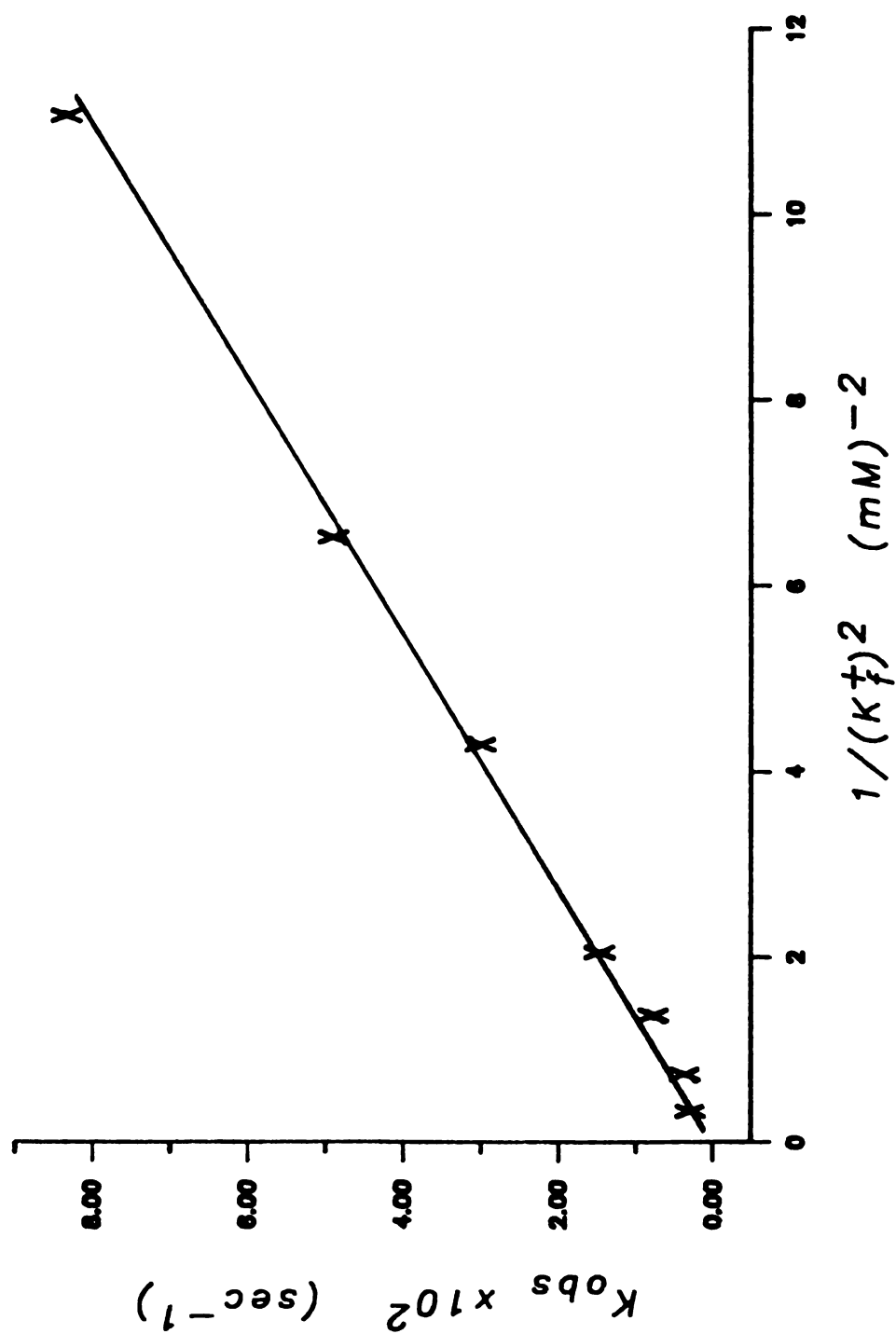
Figure VI.5. Dependence of the pseudo first-order rate constant of the slow phase, k_2 in Table VI.3, on the inverse square of the free K^+ concentration.

169

Table VI.3. Analysis of the Slow Phase of the Quinonoid Disappearance by 18-Crown-6 in Bicine Buffer at pH = 8.70. k_2 is the First-Order Rate Constant for the Process.

A. $\lambda = 508$ nm

$(K^+_{free})_{final}$, mM	ΔA	k_2, Sec^{-1}
.30	1.054±.003	$(8.32±.03)\times10^{-2}$
.39	1.077±.002	$(4.87±.01)\times10^{-2}$
.48	1.087±.001	$(2.98±.01)\times10^{-2}$
.69	1.034±.001	$(1.45±.01)\times10^{-2}$
.84	.920±.001	$(.67±.01)\times10^{-2}$
1.13	.915±.001	$(.36±.01)\times10^{-2}$
1.63	.340±.005	$(.29±.01)\times10^{-2}$

B. $\lambda = 420$ nm

$(K^+_{free})_{final}$, mM	ΔA	k_2, Sec^{-1}
.30	.103±.001	$(8.94±.11)\times10^{-2}$
.39	.103±.001	$(5.33±.03)\times10^{-2}$
.48	.100±.001	$(3.21±.01)\times10^{-2}$
.69	.096±.001	$(1.59±.02)\times10^{-2}$
.84	.084±.001	$(1.08±.02)\times10^{-2}$
1.13	.070±.001	$(.56±.02)\times10^{-2}$
1.63	.027±.001	$(.50±.02)\times10^{-2}$

free potassium ion concentration. Similar to deactivation in the absence of L-ethionine (Chapter III), a very slow decay in absorbance occurs upon completion of the reaction at this wavelength. This change was observed at the three higher concentrations of 18-crown-6 but the magnitude was too small to be analyzed by KINFIT.

E. Discussion

The data presented in this chapter on the reaction of the enzyme-bound quinonoid complex with 18-crown-6 provides some information about the mechanism of the interconversion of the quinonoid complex, absorbing at 508 nm, to the "inactive" α form(s), absorbing at 420 nm. The biphasic growth (at 420 nm) and decay (at 508 nm) in absorbance is certainly indicative of a rather complex mechanism for this interconversion. However, the following simple kinetic scheme (Equations VI.1-3, VI.15) is compatible with the observations described in this chapter.

$$Q \underset{k_{-1}}{\overset{k_1}{\rightleftharpoons}} Q'$$
(VI.1)

where

$$K_1 = \frac{k_1}{k_{-1}} = \frac{(Q')_{eq}}{(Q)_{eq}} \ll 1$$
(VI.2)

Variation of the magnitude of the absorbance change as well as the independence of the observed rate constant to free K^+ concentration during the first 200 mSec of the reaction (fast phase) suggest

that the quinonoid complex is probably present in two different forms, represented here by Q and Q', in equilibrium with each other. The form Q' has a lower affinity than Q for K^+ and is thus present at a very small concentration at saturating K^+ concentrations.

The fast phase of the reaction can then be expressed as the reaction of the minor species (Q', which probably has two K^+ ions loosely bound per subunit) with 18-crown-6 in a fast equilibrium step according to Equation VI.3;

$$Q' \cdot K_2^+ + 2C \underset{}{\overset{K_2}{\rightleftharpoons}} \beta(H^+) + 2K^+C \qquad (VI.3)$$
$$(\lambda_{max}=508 \text{ nm}) \qquad\qquad (\lambda_{max}=420 \text{ nm})$$
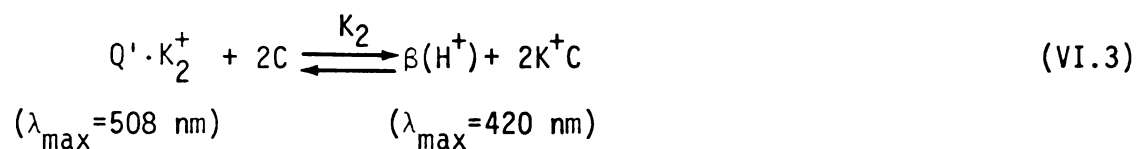
Previous studies by June et al. (25) on the spectral forms of tryptophanase suggest that the form (β) is probably protonated at the pH of this experiment. The rate equation for the fast phase of the absorbance change can then be written as;

$$\frac{d[(Q') + (\beta)]}{dt} = k_1(Q) - k_{-1}(Q') \qquad (VI.4)$$

The mass balance on the enzyme

$$E_t = (Q) + (Q') + (\beta) \qquad (VI.5$$

together with the equilibrium expression of Equation VI.3 allows the rate law to be rewritten as;

$$\frac{d[(Q')+(\beta)]}{dt} = k_1 E_t - \left\{\frac{(k_1 + k_{-1})K_3^2(K^+)^2}{K_2} + k_1\right\}(\beta) \qquad (VI.6)$$

in which K_3 = 115 M^{-1} (110) represents the equilibrium constant for the formation of the K^+-18-crown-6 complex according to Equation VI.7;

$$K^+ + C \underset{\longleftarrow}{\overset{K_3}{\longrightarrow}} K^+C \qquad . \qquad (VI.7)$$

Equations VI.3-VI.7 together give the concentration of (Q') in terms of (β) as;

$$(Q') = \frac{K_3^2(K^+)^2}{K_2}(\beta) \qquad (VI.8)$$

Substituting (Q') in Equation VI.6 yields the following rate law for the fast phase of the reaction;

$$\left\{1 + \frac{K_3^2(K^+)^2}{K_2}\right\}\frac{d(\beta)}{dt} = k_1 E_t - \left\{\frac{(k_1 + k_{-1})K_3^2(K^+)^2}{K_2} + k_1\right\}(\beta) \qquad (VI.9)$$

If we assume that reaction VI.3 lies far to the right (low K^+ affinity in Q'), we can write

$$(Q')_{eq} << (\beta)_{eq} \qquad (VI.10)$$

and therefore

$$\frac{K_3^2(K^+)^2}{K_2} << 1 \qquad (VI.11)$$

This approximation leads to Equation VI.12 for the rate law of the fast phase.

$$\frac{d(\beta)}{dt} = k_1 E_t - k_1(\beta) \qquad (VI.12)$$

Equation VI.12 predicts a first-order process for the fast phase of the quinonoid disappearance with the rate constant, k_1, being independent of the free K^+ concentration, in agreement with the experimental results presented in Table VI.2.

Equation VI.2 together with the equilibrium expression for reaction VI.3 also allows calculation of the equilibrium concentrations of the species. The two equations lead to the following relation;

$$(\beta)_{eq} = \frac{K_1 K_2}{K_3^2(K^+)^2} (Q)_{eq} \simeq \frac{K_1 K_2}{K_3^2(K^+)^2} \cdot E_t \qquad (VI.13)$$

if

$$(\beta)_{eq} << (Q)_{eq}$$

Equation VI.13 can be written in terms of the absorbance change as;

$$(\Delta A)_{fast} = \frac{K_1 K_2 \Delta A_T}{K_3^2} \cdot \frac{1}{(K^+)_f^2} \qquad (VI.14)$$

where ΔA_T represents the overall absorbance change.

Equation VI.14 predicts the magnitude of the absorbance change in the fast phase to be inversely proportional to the square of free K^+ concentration. This is, again, in agreement with the data presented in Table VI.2. From the slope of the fit of the data (absorbance changes at 508 nm in Table VI.2 as a function of inverse square K^+ concentration) a value of $K_1 K_2 = (8.6 \pm .4) \times 10^{-5}$ was determined by KINFIT.

The slow phase of the quinonoid disappearance which contributes over 95 percent to the total absorbance change at both 420 nm and 508 nm can be represented by the following enzyme conformational change;

$$\beta \xrightarrow{\ k_4\ } \alpha \qquad \qquad (VI.15)$$

which gives the rate law;

$$\frac{-d(Q)}{dt} = \frac{d(\alpha)}{dt} = k_4 (\beta)_{eq} \qquad \qquad (VI.16)$$

Substituting for $(\beta)_{eq}$ from Equation VI.13 gives

$$-\frac{d(Q)}{dt} = k_4 \left[\frac{K_1 K_2}{K_3^2 (K^+)^2}\right] (Q) \qquad \qquad (VI.17)$$

The rate law of Equation VI.17 again predicts a first-order inter-conversion of the quinonoid complex (form Q) to the inactive form(s), α, for the slow phase with the pseudo 1st-order rate constant given by;

$$k' = \frac{k_4 K_1 K_2}{K_3^2} \cdot \frac{1}{(K^+)_f^2} \qquad\qquad (VI.18)$$

Equation VI.18 is supported by the experimental data for the slow phase presented in Table VI.3 (see also Figure VI.5). From Equation VI.18 and values of 115 M^{-1} for K_3 (110) and 8.6 x 10^{-5} for $K_1 K_2$ (determined by KINFIT), a value of 1.1±.1 sec^{-1} was calculated for k_4.

The change in the slow phase of the quinonoid disappearance can be further investigated to see whether the (β) to (α) interconversion occurs directly or via the γ (337 nm) form. As indicated earlier, from June et al. (82,89) the β form of the enzyme is mostly protonated at the pH of the experiment, 8.70 (PK_0 for protonation of the β-form is 9.70, see Scheme III in Figure I.4). However, the deprotonated γ-form is dominant at this pH (PK_4 = 6.75 in Scheme III). Furthermore, the values of k_1 (rate constant for the conversion of deprotonated β-form to deprotonated γ-form in the scheme and k_{-3} (rate constant for the conversion of protonated β-form to protonated γ-form in the cheme) were determined by June et al. (82) to be 8.3 sec^{-1} and 0.03 sec^{-1}, respectively. Therefore, the relative magnitude of k_1 and k_{-3} along with the high pH of the experiment suggest that conversion of the protonated β-form to deprotonated γ-form is favored to proceed through the route with the rate constant k_1, if the (β) to (α) interconversion is to proceed through the γ-manifold (Scheme III). If this is the case, then, an effective first-order rate constant for such a process at pH = 8.70 (H^+ = 2.0 x 10^{-9} M) is

$$k_{eff} = \frac{K_{\beta H}}{(H^+)} \cdot k_1 \qquad\qquad (VI.19)$$

Substituting for the values gives;

$$k_{eff} = 0.83 \pm .16 \ Sec^{-1}$$

This value is similar to the value of the rate constant for the slow phase of the quinonoid disappearance by 18-C_6, $k_4 = 1.1 \pm .1 \ sec^{-1}$ and, thus, seems to suggest that the (β) to (α) interconversion proceeds through the γ-manifold. So, the slow phase of the quinonoid disappearance may be explained more precisely by the following process;

$$\beta(H^+) \xrightarrow{\ 1.1 \ sec^{-1}\ } \gamma \xrightarrow{\ 2.8 \ sec^{-1}\ } \alpha \qquad (VI.20)$$
$$(420 \ nm) \qquad\qquad (337 \ nm) \qquad (420 \ nm)$$
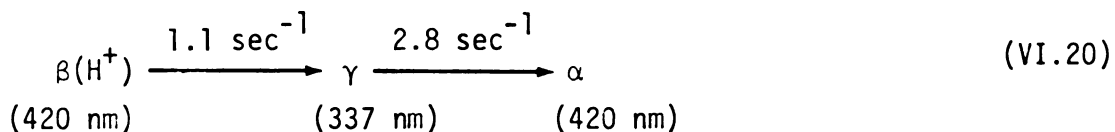
with the first step being rate-limiting with a rate constant $k_4 = 1.1 \pm .1 \ sec^{-1}$. The rate constant for the second step is $2.8 \pm .2 \ sec^{-1}$ determined from the deactivation of the enzyme by 18-crown-6 (Chapter III).

Reaction VI.20 predicts the concentration of the γ-form at steady state to be

$$(\gamma)_{s.s.} = \frac{k_1}{k_2} \ (\beta) \simeq 0.4 \ (\beta)$$

However, since $(\beta)_{eq} << (Q)_{eq}$, one does not expect a significant build up of the γ-form at 337 nm.

F. Conclusions

The simple scheme discussed above satisfactorily explains the results presented in this chapter. The biphasic changes in absorbance at 420 nm and 508 nm are explained in terms of this scheme and the rate constants of 16.6 ± 2.0 sec^{-1} and $1.1 \pm .1$ sec^{-1} are obtained for the fast and slow phases of the quinonoid disappearance, respectively. The inverse second-order dependence of the rate of the slow phase on the concentration of free K^+ again strongly suggests that two potassium ions per subunit are required for activation. This is consistent with the deactivation results discussed in Chapter III and binding of two thallium (I) ions per subunit as reported earlier (77). The data also suggest that the interconversion of the (β) to (α) in the slow phase probably proceeds through the γ-manifold which absorbs at 337 nm. More kinetic experiments at different pH values and enzyme concentrations as well as some information on the nature of the "inactive" enzyme form(s) are, however, needed to present a detailed model clearly.

CHAPTER VII

PRINCIPAL COMPONENT ANALYSIS OF TRYPTOPHANASE
ACTIVATION/DEACTIVATION PROCESSES

A. Introduction

Optical absorption spectroscopy has been widely used in the characterization of tryptophanase spectral forms and catalytic reactions. As described earlier, the holoenzyme has peaks at 337 and 420 nm due to bound pyridoxal-p and at 508 nm due to a bound amino acid substrate or inhibitor that has undergone α-proton abstraction. In this chapter, the method of Principal Component Analysis (PCA), also known as principal factor analysis (PFA), will be described first. This will be followed by its application to the scanning stopped-flow experiments of tryptophanase activation/deactivation by the monovalent cation, K^+, in the presence and absence of the dead-end inhibitor, L-ethionine. The purpose of this study was to determine the number of optically absorbing species present during the reactions and to resolve the scanning data into the individual static spectra and concentration-time profiles of such species in order to propose appropriate mechanisms for the reactions.

B. The Method of Principal Component Analysis (PCA)

As described earlier, in a typical scanning wavelength experiment, a selected wavelength region is rapidly and repeatedly scanned as a function of time while a spectrophotometric response such as absorbance is measured at a fixed number of wavelength channels during each scan. The result is then a PXN data matrix $\underline{A}$ composed of N consecutive spectra measured at P wavelength channels. Such a data matrix is suitable for the application of principal component analysis. Although PCA has been applied to a variety of physical techniques such as analysis of mass spectra (141,142), analysis of potentiometric data (143), studies of multicomponent equilibrium systems (144,145), and band resolution of IR spectra (146), only its application to scanning stopped-flow data is briefly described here. The method is discussed in detail in the Ph.D. dissertation of R. Cochran (98).

Application of PCA to properly weighted data gives the number of absorbers in the system under study and, in ideal cases, can provide complete resolution of the absorber's spectra and their time courses. However, improper weighting of the data can lead to an erroneous estimate of the number of absorbing species. A block diagram that gives the main steps in PCA is shown in Figure VII.1. Principal component analysis does not require any mechanistic assumption, the only assumption required is that the absorbance at every wavelength channel be a linear function of the concentration of the absorbing species (Beer's law). Thus, for errorless data, the element A_{ij} (absolute absorbance measured at ith channel and
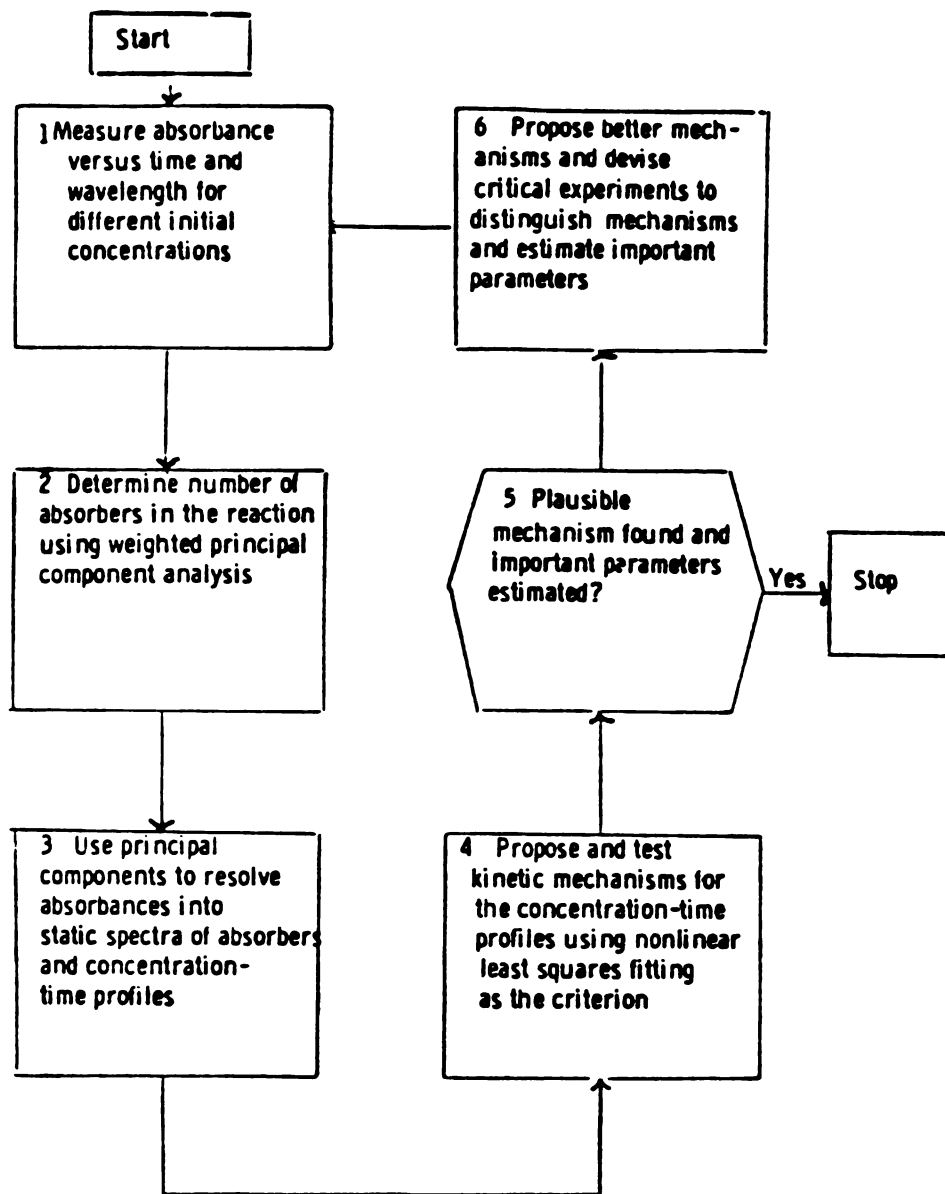
Figure VII.1. Block diagram for main steps in Principal Component Analysis (from Ref. 98).

jth scan) of the matrix $\underline{A}$ is represented as

$$A_{ij} = \sum_{k=1}^{q} f_{ik}\, C_{kj} \qquad (VII.1)$$

where f_{ik} is the molar absorptivity (times the path length of the absorbance cell) of absorber k at wavelength channel i, C_{kj} is the molarity of absorber k at the time of scan j and q is the number of absorbers. Likewise, the experimental matrix $\underline{A}$ can be factored into two matrices; one containing information about the spectral shapes of the absorbers (called the $\underline{F}$ matrix), while the other contains information about the concentration-time profiles of the absorbers (called the $\underline{C}$ matrix). Hence, the experimental matrix can be described by a matrix model as

$$\underline{A} = \underline{F}\,\underline{C}^{T} = \sum_{k=1}^{q} \underline{f}_{k}\, \underline{C}_{k}^{T} \qquad (VII.2)$$

where $\underline{A}$ is the experimental (PXN) matrix. $\underline{F}$ is a (Pxq) matrix defined by $\underline{F} = (\underline{f}_1,\underline{f}_2,..\underline{f}_q)$, where $\underline{f}_j$, called the static spectrum of absorber j, is a P component column vector whose ith element is the product of the cell path length and the molar absorptivity of absorber j at wavelength channel i. $\underline{C}$ is an (Nxq) matrix defined by $\underline{C}=(\underline{C}_1,\underline{C}_2...\underline{C}_q)$, where $\underline{C}_j$, called the concentration vector of absorber j is an N component column vector whose ith element is $C_j(t_i)$, the molarity of absorber j at the time of scan i.

B.1. Application of PCA to Errorless Data

Cochran and Horne (98,139) have shown that two kinds of PCA are useful for kinetics experiments; each requires only the matrix $\underline{A}$ and each gives a lower bound estimate of $\underline{q}$. These two methods are referred to as M and S analyses, respectively.

B.1.1. M Analysis - Second moment matrix PCA, called M analysis, gives for q a lower bound estimate that is required to interpret the experiment. The matrix $\underline{M}$ (PxP) is defined by

$$\underline{M} = \frac{1}{N} \underline{A}\, \underline{A}^T \tag{VII.3}$$

For an errorless experiment, the goal of M analysis is to obtain r_M, the rank of $\underline{M}$, which also equals r_A, the rank of $\underline{A}$ by a standard matrix theorem (147). Since $r_A \leq q$, r_M is a lower limit to the number of absorbers in the reaction. r_M is determined by diagonalizing $\underline{M}$, which is done by solving the eigenvalue problem

$$\underline{\phi}^T \underline{M} \underline{\phi} = \underline{\Delta} \quad , \quad \underline{\phi}^T \underline{\phi} = \underline{I}$$

or

$$\underline{M} \underline{\phi} = \underline{\phi} \underline{\Delta} \tag{VII.4}$$

where $\underline{\Delta}$ is the eigenvalue matrix,

$$\underline{\Delta} = \text{diag} \; (\delta_1, \; \delta_2, \; \ldots, \; \delta_p) \qquad\qquad \text{(VII.5)}$$

with $\delta_1 \geq \delta_2 \geq \delta_3 \ldots \geq \delta_p$, and $\underline{\Phi}$ is a (pxp) matrix whose columns are the p orthonormal eigenvectors:

$$\underline{\Phi}_i \; \underline{\Phi}_j = \delta_{ij} \qquad\qquad \text{(VII.6)}$$

For errorless data, there are two ways to determine r_M:

1. The rank of $\underline{M}$, r_M, is equal to the number of non-zero eigen-values in Equation VII.5; δ_1, δ_2, $\ldots$ δ_{r_M}.

2. r_M is also the lowest value of r for which $\hat{\underline{A}}_r$, the reconstruct-ed experimental surface, defined by

$$\hat{\underline{A}}_{(r)} = \underline{\Phi}_{(r)} \; \underline{\Phi}_{(r)}^T \; \underline{A} \qquad\qquad \text{(VII.7)}$$

is exactly equal to A, where $\underline{\Phi}_{(r)}$ is the (Pxr) matrix whose r columns are the first r eigenvectors of $\underline{M}$. $\hat{\underline{A}}_{(r)}$ is called the prin-cipal component estimate of $\underline{A}$. The fact that $\hat{\underline{A}}_{(r_M)} = \underline{A}$ for an error-less experiment is shown in Appendix A of R. Cochran's Ph.D. disser-tation (98).

B.1.2. S Analysis - Sample covariance matrix PCA, or S analysis, gives for q the number of absorbers whose concentrations change in-dependently of one another during the experiment. $\underline{S}$ is defined by

$$\underline{S} = [1/(N-1)](\underline{A} - \overline{\underline{A}})(\underline{A} - \overline{\underline{A}})^T \qquad \text{(VII.8)}$$

where $\overline{A}_{ij} = \dfrac{1}{N} \displaystyle\sum_{k=1}^{N} A_{ik}$ is the average absorbance at wavelength channel i. An $\underline{S}$ analysis gives r_S, the rank of $\underline{S}$, which is also the rank of $(\underline{A} - \overline{\underline{A}})$. The procedure to determine r_S is similar to that of M analysis, i.e., the rank of $\underline{S}$ equals the number of non-zero eigenvalues of $\underline{S}$ and is also the lowest value of r for which $(\widehat{\underline{A}}_{(r)} - \overline{\underline{A}})$ defined by

$$(\widehat{\underline{A}}_{(r)} - \overline{\underline{A}}) = \underline{\phi}'_{(r)} \, \underline{\phi}'^{T}_{(r)} \, (\underline{A} - \overline{\underline{A}}) \qquad \text{(VII.9)}$$

is an exact r principal component estimate of the experimental $(\underline{A} - \overline{\underline{A}})$ difference surface.

B.2. Effect of Random Measurement Errors-Actual Case

B.2.1. Inclusion of Error in the Absorbance Model - Each experimentally measured absorbance has a random measurement error associated with it which must be considered in order for PCA to give correct results. Thus a more realistic model for $\underline{A}$ than Equation VI.2 is defined by

$$\underline{A} = \underline{F} \, \underline{C}^T + \underline{\varepsilon} \qquad \text{(VII.10)}$$

where $\underline{A}$ is the matrix of measured absorbance, and $\underline{\varepsilon}$ is a (PxN) error matrix whose element ε_{ij} is the random measurement error of the

absorbance measurement A_{ij}.

To complete this model, it is necessary to make some reasonable statistical assumptions about the error matrix $\underline{\varepsilon}$. Cochran and Horne (98,139) assumed that the noise in absorbance measurements obtained by the scanning stopped-flow used in this study can be approximately factored into two major contributions: (1) a time-dependent component which is minimized by signal averaging, and (2) a position dependent component which depends upon the position of a channel in the spectrum and its nominal absorbance. They thus proposed that the i,jth element of $\underline{\varepsilon}$, which is assumed to have an expectation value of zero, has variance in the form of Equation VII.11,

$$Var(\varepsilon_{ij}) = \sigma_{ij}^2 = X_i Z_j \tag{VII.11}$$

where X_i is a function of the peak position (or wavelength channel number) and Z_j is a function of the spectrum (group) number.

The Z_j contribution in our case is attributable to the nature of the data collection scheme used in our stopped-flow instrument. In order to optimize the allocation of a finite number of computer storage locations and at the same time scan the full dynamic range of a reaction, the stopped-flow system averages a number of consecutive scans and stores the average as a single spectrum. The number of scans averaged into each stored spectrum is increased with time during the reaction; so at early times, where fast changes occur in the reaction, there is little or no averaging while at

longer times, where the changes are slow, the signal to noise ratio
is greatly improved by increased averaging. The averaging scheme
is fully described in Coolen's Ph.D. dissertation (134). Using
this scheme, Coolen points out that the Z_j contribution for this in-
strument is given by Equation VII.12

$$Z_j = g^{(1-n_j)} \hspace{4cm} \text{(VII.12)}$$

where g is the group factor (modulus for increasing the averaging)
and n_j is the stored group number.

The X_i component in Equation VII.11 accounts for three major
noise contributions to the absorbance at channel i: (1) the wave-
length corresponding to this channel (mainly photomultiplier tube
noise); (2) the actual value of absorbance; and (3) the rate of
change of absorbance with wavelength at the particular channel i.
The last contribution originates from errors in the precise wave-
length reproducibility at each channel due to mechanical vibrations
of the mirror system used.

A method previously used to calculate the values of X_i for each
channel was to use a flat absorber, e.g., a neutral density filter.
However, while the method accounted for the X_i contribution originat-
ing from the photomultiplier tube response, it failed to correct
X_i for contributions arising from the latter two sources. To cor-
rect for this, a new method was adopted by F. Halaka which uses two
"scanning" experiments that represent the major reactant chromophore(s)
and those of the final products with no reaction occurring in either

experiment. These two "weight" files must be collected with the same scanning parameters used for the reaction under study (i.e., same wavelength region and number of points per spectrum), but without averaging. An "average weight" is then calculated from the standard deviations in each weight experiment for every wavelength channel by Equation VII.13

$$W_i^{av} = \frac{1}{\sigma_i^{av}} = \frac{1}{[1/2(\sigma_{1i}^2 + \sigma_{2i}^2)]^{1/2}} \tag{VII.13}$$

where σ_{1i} and σ_{2i} are the standard deviations of channel i from the two weight experiments. This new method gives a much better weight for each channel over the previous one because it accounts for the characteristics of the scanning monochromotor used in this study. That is, if a chromophore has a sharp peak, the "sides" of the peak are most sensitive to irreproducibility in the scan synchronization and to scanning mirror mechanical artifacts and hence have the highest measurement errors. This new method particularly should be a good approximation for reactions that do not produce intermediates with spectral shapes greatly different from those of reactants or products.

B.2.2. <u>Weighted Principal Component Analysis</u> - The model for variance given by Equation VII.11 leads to statistically weighted absorbance matrices defined as

$$\underline{A}_W = \underline{L} \, \underline{A} \, \underline{T} \tag{VII.14}$$

$$\overline{\underline{A}}_W = \underline{L} \; \overline{\underline{A}} \; \underline{T} \tag{VII.15}$$

where $\underline{L} = \text{diag} \; (1_1, 1_2, \ldots 1_p)$ and $I = \text{diag} \; (t_1, t_2 \ldots t \;)$. As pointed out by Cochran and Horne (140), the elements of $\underline{L}$ and $\underline{T}$ are given by

$$\underline{L} = a^{1/2} \; \underline{X}^{-1/2} \tag{VII.16}$$

$$\underline{T} = b^{1/z} \; \underline{Z}^{-1/2} \tag{VII.17}$$

where a and b are arbitrary constants (set equal to 1) and X's and Z's are defined by Equation VII.11.

With the above definitions of weighted absorbance matrices, Equations VII.3 and VII.8 become, respectively,

$$\underline{M}_W = \frac{1}{N} \; \underline{A}_W \; \underline{A}_W^T \tag{VII.18}$$

and

$$\underline{S}_W = \frac{1}{N-1} \; (\underline{A}_W - \overline{\underline{A}}_W) \; (\underline{A}_W - \overline{\underline{A}}_W)^T \tag{VII.19}$$

and principal component analysis is performed using $\underline{M}_W$ and $\underline{S}_W$ to determine the essential ranks, m and s, of $\underline{M}_W$ and $\underline{S}_W$, respectively.

The inclusion of $\underline{\varepsilon}$ in Equation VII.10 makes the matrices $\underline{M}$ and $\underline{S}$ of full rank P. In other words, the eigenvalues in Equation VII.5 are all non-zero. For statistically weighted PCA, Cochran

points out that the weighted sum of the squares of the residuals, defined by Equation VII.20 gives the condition for the value of r that equals the essential rank of $\underline{M}_W$, m.

$$Q_r = \sum_{i=1}^{P} \sum_{j=1}^{N} L_i T_i \, (\hat{A}_{ij}(r) - A_{ij})^2 \qquad\qquad (VII.20)$$

When r=m, the value of the function $Q_r/(N-r)(p-r)$, should be approximately unity (140). This function also approaches unity for weighted S analysis when r=s, and $\hat{A}_{ij}(r)$ and A_{ij} in Equation VII.20 are replaced with the appropriate difference surfaces.

Similar to the errorless case, the essential rank, m, in weighted M analysis is also determined by finding the lowest value of r for which $\hat{\underline{A}}_{(r)}$, now defined by

$$\hat{\underline{A}}_{(r)} = (\underline{L}^{-1} \, \underline{\phi}_{(r)} \, \underline{\phi}^T_{(r)} \, \underline{L}) \, \underline{A} \qquad\qquad (VII.21)$$

fits the experimental matrix $\underline{A}$ to within its random errors. Likewise in S analysis, s is the lowest value of r for which $(\hat{\underline{A}}_{(r)} - \overline{\underline{A}})$ defined by

$$(\hat{\underline{A}}_{(r)} - \overline{\underline{A}}) = (\underline{L}^{-1} \, \underline{\phi}'_{(r)} \, \underline{\phi}'^T_{(r)} \, \underline{L}) \, (\underline{A} - \overline{\underline{A}}) \qquad\qquad (VII.22)$$

fits the experimental difference surface $(\underline{A} - \overline{\underline{A}})$ to within its random errors. In Equations VII.21 and VII.22, $\underline{\phi}$ and $\underline{\phi}'$ are the eigenvector matrices of $\underline{M}_W$ and $\underline{S}_W$, respectively.

The most straightforward procedure for determining when $\hat{\underline{A}}_{(r)}$ fits

$\underline{A}$ to within experimental error is to examine the residual surface $(\hat{\underline{A}}_{(r)} - A)$. For a fit to within random experimental errors, points on the weighted residual surface should fluctuate randomly about zero and thus the residuals should not be highly patterned when plotted vs time or wavelength. If there is no pattern we have chosen the value of r equal to the essential rank.

B.3. PCA Determination of Real Components

As described earlier, the two kinds of principal component analysis, M analysis and S analysis, yield, respectively, the minimum number of absorbers required to interpret the experiment (m) and the minimum number of absorbers whose concentrations must have changed independent of one another during the experiment(s). In addition, PCA provides a tool by which one can test whether a proposed spectral shape or a concentration profile fits as one of the column vectors of the $\underline{F}$ and $\underline{C}$ matrices in Equation VII.2. This is called "Target Testing". If the measured static spectra of known reactants, products, and catalysts fit and account for the m required absorbers, then one has resolved the experiment.

The starting point uses an identical but more useful equation than Equation VII.21 for $\hat{\underline{A}}_{(r)}$ given by

$$\hat{\underline{A}}_{(r)} = \underline{L}^{-1} \, \underline{\phi}_{(r)} \, \underline{\Omega}_{(r)} \, \underline{\psi}_{(r)}^{T} \, T^{-1} \tag{VII.23}$$

where

$$\underline{\Omega}_{(r)} = \text{diag}(\omega_1, \omega_2, \ldots, \omega_r) \tag{VII.24}$$

$$\omega_j = (N\delta_j)^{1/2}$$

and

$$\underline{\Psi}_{(r)} = (\underline{\psi}_1, \underline{\psi}_2, \ldots, \underline{\psi}_r) = \underline{A}^T_w \, \underline{\phi}_{(r)} \, \underline{\Omega}^{-1}_{(r)} \tag{VII.25}$$

where the r columns of $\psi_{(r)}$ contain the first r eigenvectors of M'_w, defined by (appendix A in Ref. (98))

$$M'_w = (1/p) \, \underline{A}^T_w \, \underline{A}_w \tag{VII.26}$$

The model for M analysis estimate of $\underline{F}$ and $\underline{C}$ is

$$\hat{\underline{A}}_{(m)} = \hat{\underline{F}} \, \hat{\underline{C}}^T \tag{VII.27}$$

where $\hat{\underline{A}}_{(m)}$ is given by Equation VII.23 and $\hat{\underline{F}} \, \hat{\underline{C}}^T$ is an error-containing estimate of $\underline{F} \, \underline{C}^T$ in Equation VII.10. Equation VII.27 is used to estimate for each absorber the shape of its static spectrum, the shape of its concentration profile, and its contribution to the measured experimental (absorbance-wavelength-time) surface.

Equations VII.23 and VII.27 together give

$$\hat{\underline{A}}_{(m)} = \hat{\underline{F}} \, \hat{\underline{C}}^T = \underline{L}^{-1} \, \underline{\phi}_{(m)} \, \underline{\Omega}_{(m)} \, \underline{\psi}^T_{(m)} \, \underline{T}^{-1} \tag{VII.28}$$

solved for $\hat{\underline{F}}$, Equation VII.28 gives

$$\hat{\underline{F}} = (\underline{L}^{-1} \, \underline{\phi}_{(m)}) \, \underline{U} \qquad\qquad \text{(VII.29)}$$

where $\underline{U}$ is an (mxm) matrix defined by

$$\underline{U} = \underline{\Omega}_{(m)} \, \underline{\psi}^T_{(m)} \, \underline{T}^{-1} \, \hat{\underline{C}} \, (\hat{\underline{C}}^T \, \hat{\underline{C}})^{-1} \qquad\qquad \text{(VII.30)}$$

solved for $\hat{\underline{C}}$, Equation VII.28 gives

$$\hat{\underline{C}} = (\underline{T}^{-1} \, \underline{\psi}_{(m)}) \, \underline{V} \qquad\qquad \text{(VII.31)}$$

where $\underline{V}$ is an (mxm) matrix defined by

$$\underline{V} = \underline{\Omega}_{(m)} \, \underline{\phi}^T_{(m)} \, \underline{L}^{-1} \, \hat{\underline{F}} \, (\hat{\underline{F}}^T \, \hat{\underline{F}})^{-1} \qquad\qquad \text{(VII.32)}$$

Resubstitution of Equations VII.29 and VII.31 into Equation VII.28 gives the following condition on $\underline{U}$ and $\underline{V}$,

$$\underline{U} \, \underline{V}^T = \underline{\Omega}_{(m)} \qquad\qquad \text{(VII.33)}$$

It follows from Equations VII.29-33 that if the m^2 elements of either $\underline{U}$ or $\underline{V}$ are known, then both $\hat{\underline{F}}$ and $\hat{\underline{C}}$ can be computed directly from Equations VII.29 and VII.31, respectively.

Thus, the strategy for obtaining $\hat{\underline{F}}$ and $\hat{\underline{C}}$ is to estimate enough elements of $\underline{U}$ and $\underline{V}$ separately so that all of $\underline{U}$ and $\underline{V}$ are given by

Equation VII.33. By partitioning $\underline{U}$ and $\underline{V}$,

$$\underline{U} = (\underline{U}_1, \underline{U}_2, \dots \underline{U}_m) \qquad \underline{V} = (\underline{V}_1, \underline{V}_2, \dots \underline{V}_m) \qquad \text{(VII.34)}$$

where each $\underline{U}_j$ and $\underline{V}_j$ is an m component column vector, Equations VII.29 and VII.31 become respectively

$$\hat{\underline{f}}_j = (\underline{L}^{-1} \, \Phi_{(m)}) \, \underline{U}_j \qquad j = 1, 2, \dots, m \qquad \text{(VII.35)}$$

$$\hat{\underline{C}}_j = (\underline{T}^{-1} \, \psi_{(m)}) \, \underline{V}_j \qquad j = 1, 2, \dots, m \qquad \text{(VII.36)}$$

which shows that the jth columns of $\underline{U}$ and $\underline{V}$ depend only on the jth static spectrum and concentration vector, respectively.

For a given reaction there is usually a set of suspected absorbers. For example, in an enzyme-catalyzed reaction the suspected absorbers are any light-absorbing substrates, inhibitors and enzymes that were mixed to initiate the reaction. Equations VII.35 and VII.36 can then by used as models against which suspected static spectra or kinetic profile can be tested. If a suspected absorber is one of the m linearly independent absorbers in the experiment, its static spectrum and concentration vector must satisfy Equations VII.35 and VII.36, respectively. Cochran and Horne (98) presented the least squares criterion for determining whether a suspected absorber fits as one of the m linearly independent absorbers. In Equation VII.35, we see that every spectral shape that fits to within random error as one of the components, provides an estimate of the jth column of $\underline{U}$,

$\underline{U}_j$, and hence gives m elements of $\underline{U}$. Finding all the m static absorbers, i.e., all $\hat{f}_j$'s, provides all the m^2 elements of the matrix $\underline{U}$ and from Equation VII.33 the matrix $\underline{V}$ can then be directly computed. Equation VII.31 can then be used to compute directly from the matrix $\underline{V}$ the concentration vectors of the m linearly independent absorbers, i.e., all $\hat{C}_j$'s, and thus completely resolve the experiment. Similar arguments hold for every concentration profile that fits, within the least squares conditions, as one of the components in the experiment. For an "absorber" in the experiment, even if a limited wavelength region is used for the spectral shape proposed (in case the complete spectrum is not available), the spectral shape of that absorber which best fits that surface, is calculated for the entire set of experimental wavelength channels by PCA.

A note of caution is also necessary regarding the correct interpretation of the term "absorber". The fit of a suspected absorber as one of the m linearly independent absorbers shows that the experiment can be interpreted by using the suspected absorber as one of the absorbers, however, it does not prove that the suspected absorber is an "absorber" in the experiment. In other words, the term "absorber" may in fact refer to several species that are not independent in their rates (S analysis), concentration-time profiles (M analysis), or spectral shapes. An example of the first case (linearly dependent rates) was previously given in Chapter II. The following example is intended to show the effect of linear dependence of the latter two points on the determination of the number of "absorbers" by PCA.

Suppose we have a two absorber reaction that follows the simple

kinetic mechanism

$$A_1 + A_2 \xrightarrow{\;k_1\;} \text{non-absorbing products} \tag{I}$$

with the initial concentrations of A_1 and A_2 in the experiment being equal

$$(A_1)_0 = (A_2)_0 \tag{II}$$

Mechanism (I) imposes the constraint

$$\frac{d}{dt}[A_1] = \frac{d}{dt}[A_2] \tag{III}$$

and Equations (II) and (III) together give the constraint

$$[A_1]_t = [A_2]_t \tag{IV}$$

so that $\underline{A}_1$ and $\underline{A}_2$ are linearly dependent. Performing M analysis PCA on such a system would give m to be unity even though there are two absorbers. Even if the static spectra $\underline{f}_1$ and $\underline{f}_2$ are linearly independent, they do not individually satisfy Equation VII.35, and by testing them as proposed static spectra one would correctly conclude that A_1 and A_2 are not linearly independent absorbers in the reaction. In fact the information in the experiment lumps A_1 and A_2 together as one absorber. This can also be seen by noting that Beer's law contribution to this experiment may be written as

$$\underline{F} \ \underline{C}^T = \underline{f}_1 \ \underline{C}_1^T + \underline{f}_2 \ \underline{C}_2^T \tag{V}$$

but Equations (IV) and (V) together would give

$$\underline{F} \ \underline{C}^T = (\underline{f}_1 + \underline{f}_2) \ \underline{C}_1^T \tag{VI}$$

from which it can be seen that the combination $\hat{f}_{jprop} = (\underline{f}_1 + \underline{f}_2)$ would fit as a proposed static spectrum for an "absorber".

Detailed discussion of PCA along with more examples and its application to the stopped-flow studies of LADH-catalyzed reduction of NDMA by NADH can be found in R. Cochran's Ph.D. dissertation (98). Also, application of the technique along with the results obtained on reduction of cytochrome oxidase by MPH is discussed in the Ph.D. dissertation of F. Halaka (99). The application of the steps summarized above to the present work is discussed below.

C. Principal Component Analysis of Tryptophanase Deactivation by 18-C_6

The characteristics of this reaction are discussed in Chapter III. PCA was performed on data collected in the wavelength region 300-500 nm. The data contain information on the spectral shapes and kinetic profiles of the active and inactive enzyme. We here describe the steps taken to resolve the independent components in this region.

C.1. Number of Absorbers

Figure VII.2 presents the three dimensional wavelength-time-absorbance experimental surface obtained on mixing 6.0 mg/ml tryptophanase in the presence of K^+ with 300 mM 18-crown-6. Principal component analysis surfaces were reconstructed for $\underline{r}$ values from 1 to 5 (Equation VII.23). Careful visual comparison of the reconstructed absolute surfaces, $\hat{\underline{A}}_{(r)}$, with the experimental data surface, $\underline{A}$ showed that the surface was quantitatively reproduced by three absorbers. Figure VII.3A shows the reconstructed surface for r=3 (this is to be compared with Figure VII.2). For comparison, the reconstructed surface with one eigenvector (r=1) is displayed in Figure VII.3B, which clearly indicates that it does not reproduce the experimental surface.

Inspection of the residual surfaces, $(\hat{\underline{A}}_{(r)} - \underline{A})$, which should be random at r=m, provides a better visual comparison of the fit. In Figure VII.4A, the residual surface is shown for r=3, which confirms the assignment of $\underline{r}_m$=3 since the residuals are small and fluctuate around zero. The small and relatively non-random pattern observed for the late time spectra of the surface may be indicative of yet a fourth absorber which contributes slightly to the surface at the last phase of the reaction. The residuals constructed by using two eigenvectors are shown in Figure VII.4B for comparison. S-analysis of the same data indicated that there are also three components that independently change their concentrations with time, $\underline{r}_s$=3. This, again, was concluded from examination of the reconstructed absorbance surfaces and residuals. In addition, the

198
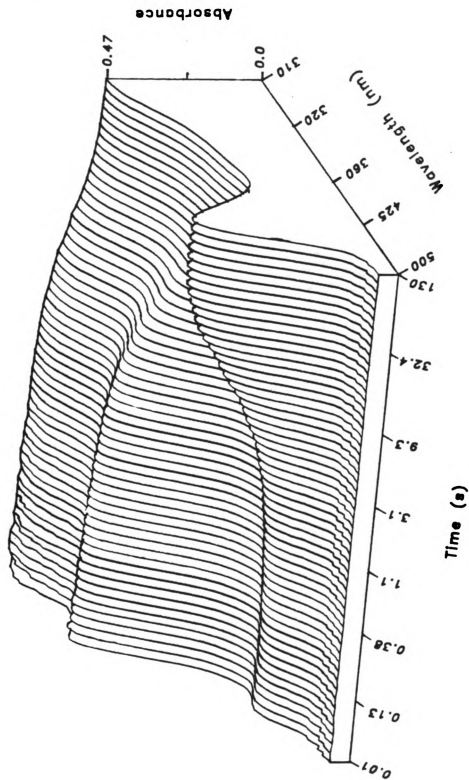
Figure VII.2. Experimental abosrbance-wavelength-time surface for the deactivation of 3.0 mg.ml⁻¹ tryptophanase by 150 mM 18-crown-6 (concentrations after mixing). Medium was 15 mM Bicine buffer containing total K⁺ concentration of ~17 mM, pH = 8.75, T = 24±1°C.
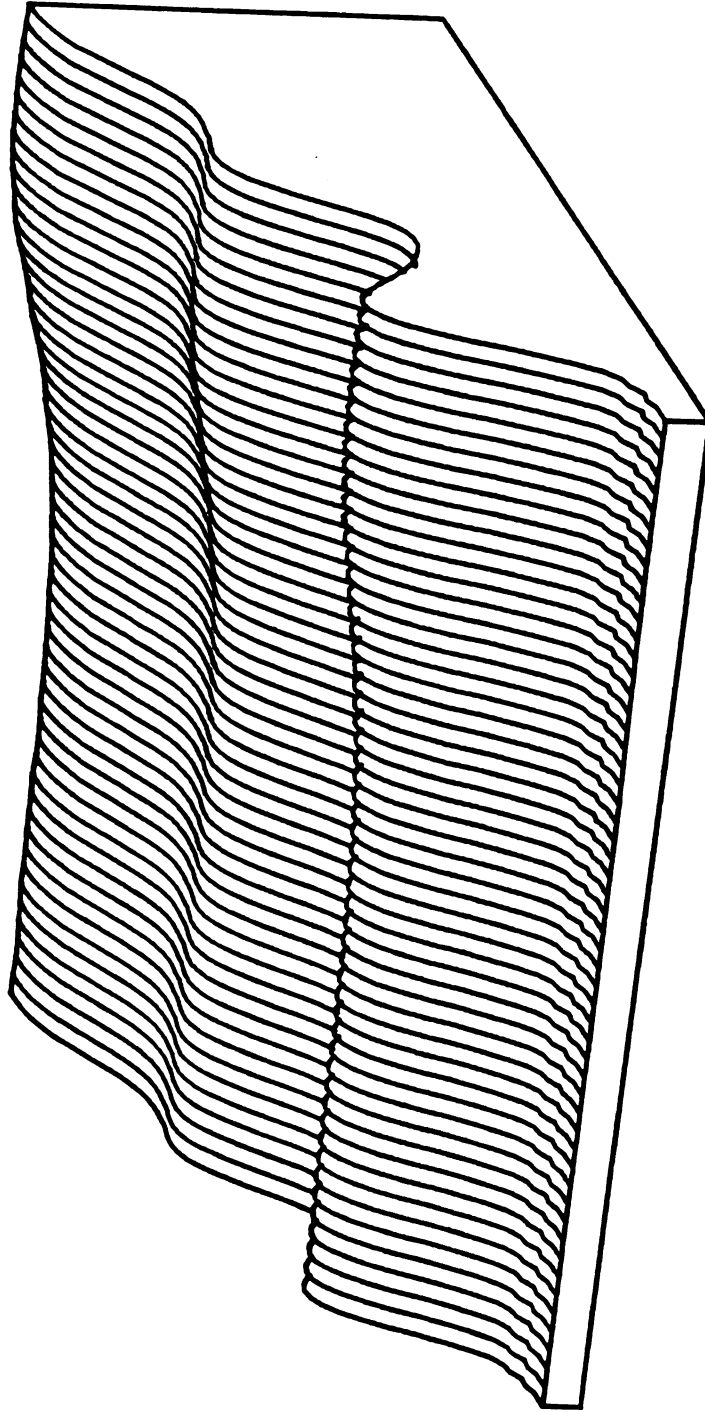
Figure III.3B. Reconstructed surface of the data in Figure VII.2 using only one M-analysis eigenvector for the data in Figure VII.2.
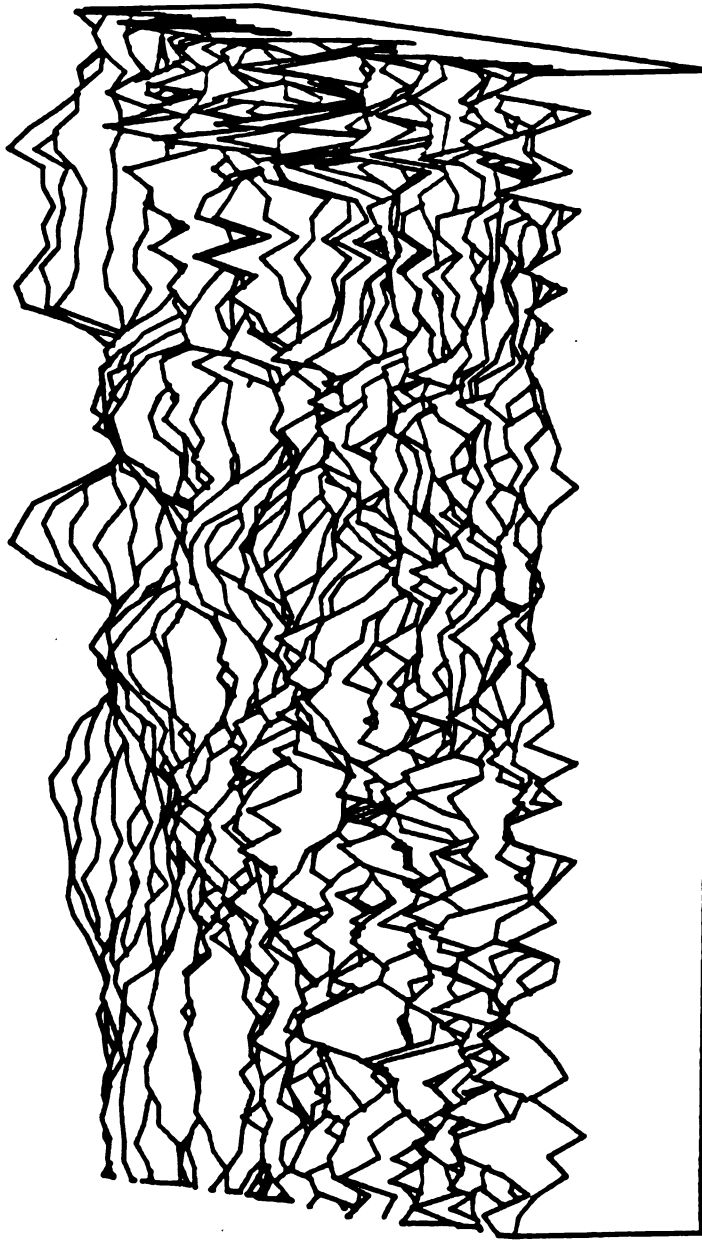
Figure VII.4A. Residual surface ($\hat{\underline{A}}_{(3)} - \underline{A}$), resulting from subtracting the matrix in Figure VII.3A from the data in Figure VII.2. $\hat{\underline{A}}_{(3)}$ refers to a reconstructed matrix using 3-eigenvectors, $\underline{A}$ is the experimental surface.
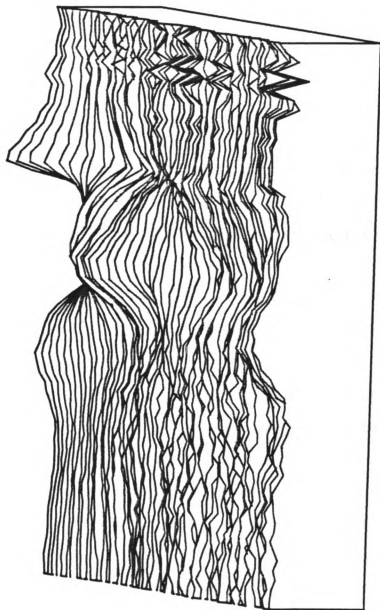
Figure VII.4B. Residual surface $(\hat{\underline{A}}_{(2)} - \underline{A})$.

of the function $Q_r/(N-r)(p-r)$ for $\underline{r}_s$ = 1,2,3 and 4 were 20.5, 4.4,

1.6 and 0.9, respectively, indicating $\underline{r}_s$ = 3.

Thus, M-analysis indicates that a minimum of three absorbers
with spectrophotometric responses are present in the reaction. The
possible target absorbers for the fitting of the eigenvectors are;
the active 337 nm absorber, the 420 nm inactive species, and the
slow growth at ∿382 nm at the completion of deactivation.

C.2. Concentration Profiles of Individual Absorbers

In this step one may fit to the M-analysis eigenvectors for the
whole experiment, either the static spectra, or the kinetic profiles
of the suspected absorbers. A measured static spectrum or concen-
tration profile that fits the absorbance surface may be counted as
belonging to one of the $\underline{m}$ absorbers in the experiment. We shall
focus here on the fit of proposed concentration profiles to the M-
analysis eigenvectors.

The M-analysis fits to the proposed concentration profiles of
the 337 and 420 nm species, two of the suspected absorbers, are shown
in Figure VII.5. The concentration profile of the third suspected
absorber at 385 nm was obtained by simulating the time course with
a rate constant of 1.4×10^{-2} Sec^{-1}, as determined by KINFIT at
this wavelength (Chapter III). Fit of the simulated time course to
the M-analysis eigenvectors showed that this species is one of the
three absorbers in the experiment.

204

Figure VII.5. (A) M-analysis fit of the 337 nm concentration
profile from the data in Figure VII.2. X's are
the proposed time course and the solid line is
the estimated points. Three eigenvectors were
used in the fit. (B) Same fit to the concen-
tration profile at 420 nm.
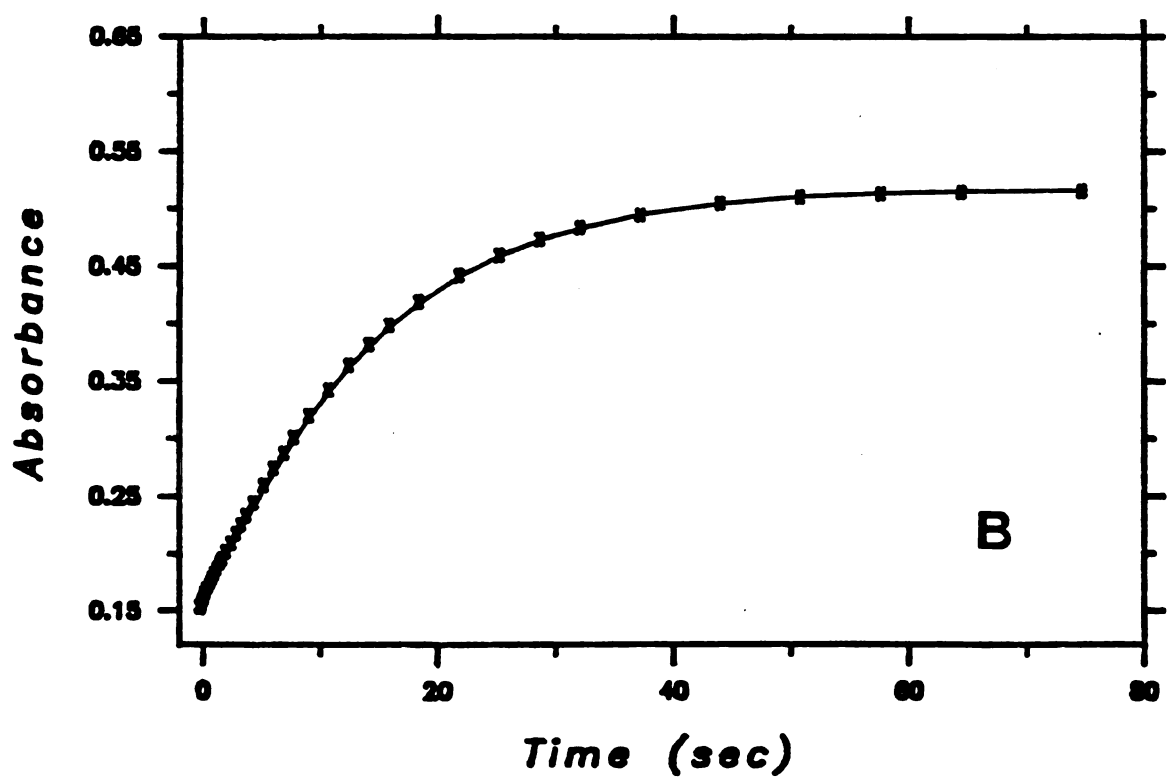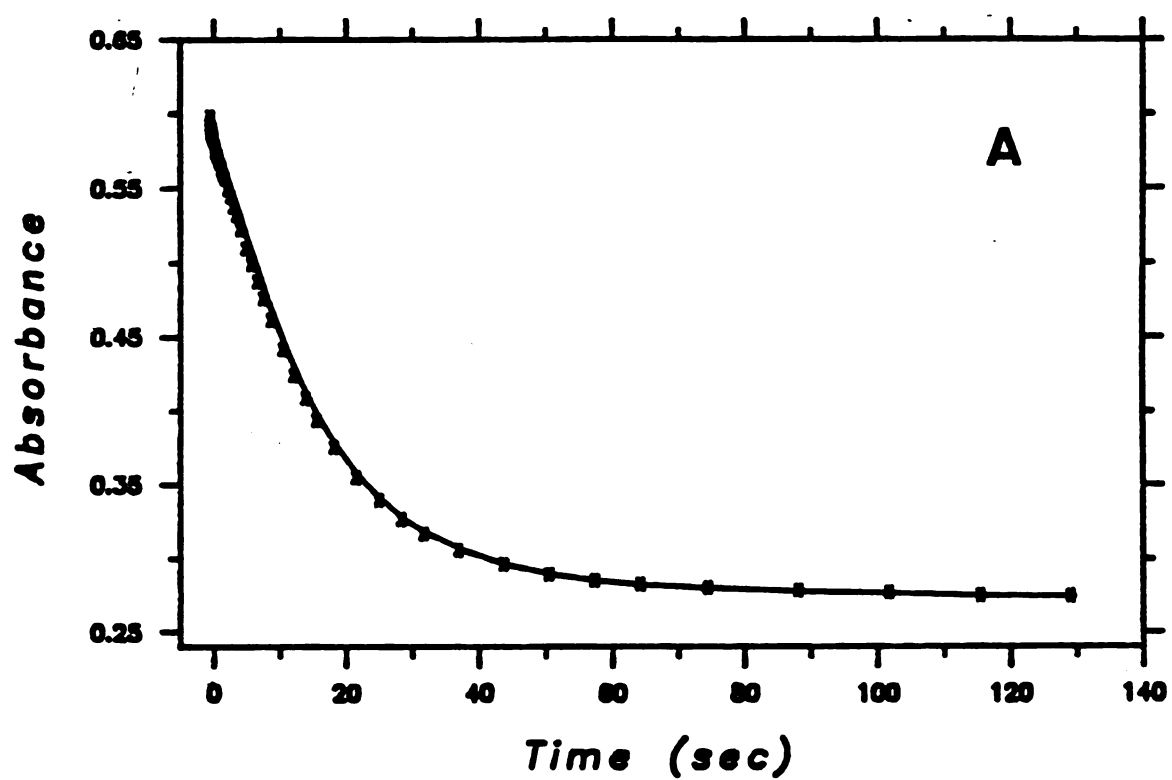
Figure VII.5.

C.3. Spectra of Individual Absorbers

Since it was possible to account for all the $\underline{m}$(=3) eigenvectors in M-analysis, it was a straightforward problem to calculate the individual spectra of the three absorbers. The results are shown in Figure VII.6 for the three absorbers. The spectra of the 337 and 420 nm are in general agreement with those previously reported. Also, the estimated spectrum of the final product shows a maximum around 382 nm, in agreement with the experimental observation of a small growth at this wavelength at the end of the deactivation.

D. PCA Analysis of the Reactivation of Deactivated Enzyme with K^+

The characteristics of this reaction are discussed in Chapter IV. Principal component analysis was performed at two free-K^+ concentrations of 12 mM and 33 mM, respectively. The experimental absorbance-wavelength-time data surface is shown in Figure VII.7 for the reactivation of 2.0 mg/ml deactivated (K^+-free) tryptophanase by 33.0 mM free K^+.

D.1. Number of Absorbers

M-analysis gave for the rank of $\underline{M}$ a value of 3. The values of the function $Q_r/(N-r)(p-r)$ in Equation VII.20 were 917.9, 12.8, and 2.7 for the first three eigenvectors. Even though the value of this function for the fourth eigenvector was 1.2, suggesting a value

Figure VII.6. Estimated static spectra of the three absorbers in Figure VII.2 (a) 337 nm absorber, (b) 420 nm absorber, (c) the final product. The spectra are normalized to maximum absorbance.

Figure VII.6

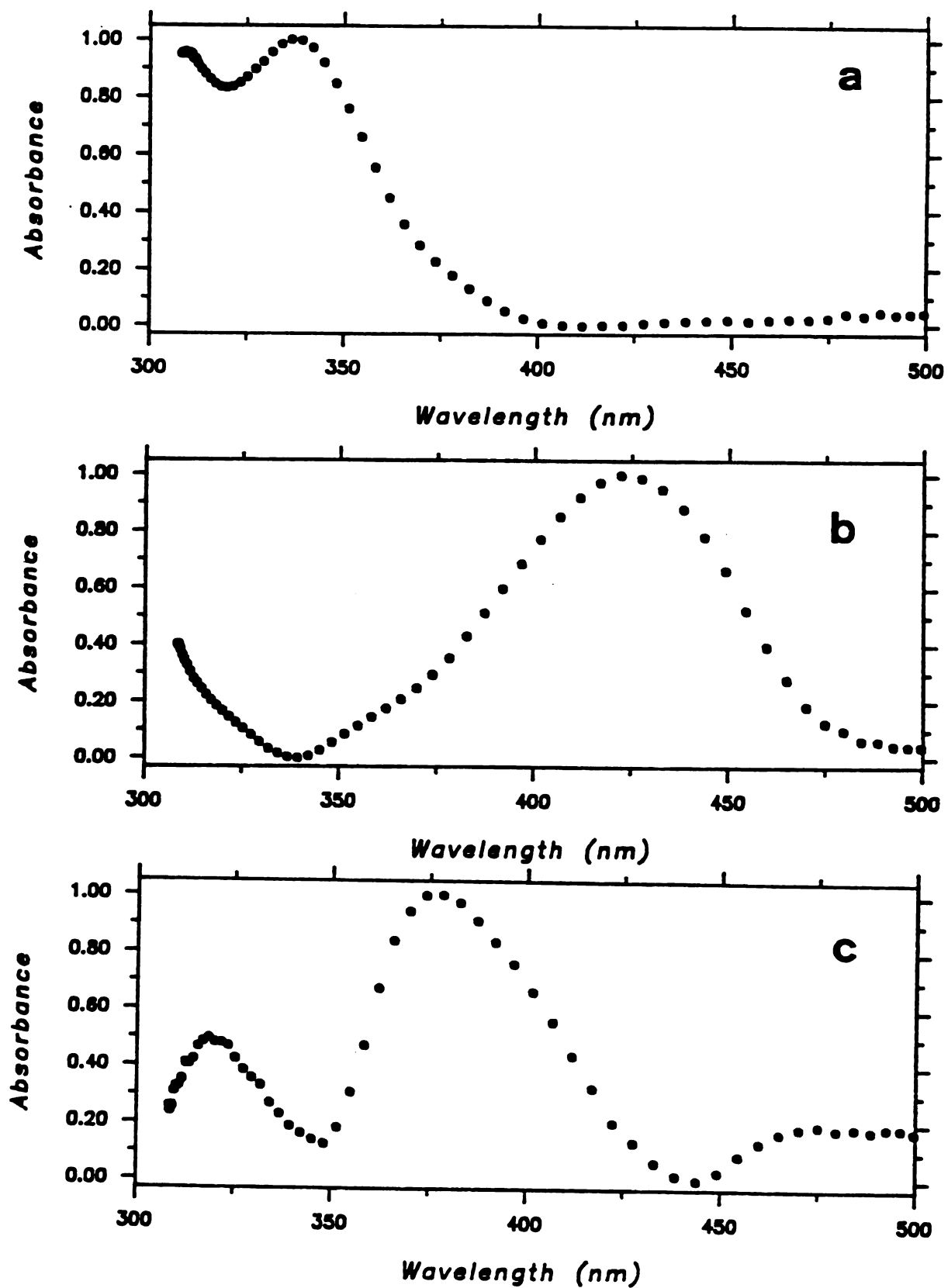of 4 for the rank of $\underline{M}$, the value $\underline{r}_m$ = 3 was assumed to be correct. This was concluded from examination of the reconstructed absorbance surfaces. For $\underline{r}_m$ = 3, the reconstructed surface, $\hat{\underline{A}}_{(3)}$, faithfully reproduces the data in Figure VII.7. This is further supported by examination of the residual surfaces for $\underline{r}_m$ = 2 and 3, which are shown in Figures VII.8A and VII.8B, respectively. It can be seen that for $\underline{r}_m$ = 3, the residual surface is random and non-patterned. S-analysis of the same data indicated that there are only two components that independently change their concentration with time, thus $\underline{r}_s$ = 2. This, again, was concluded from examination of the reconstructed difference surfaces, $(\hat{\underline{A}}_{(r)} - \overline{\underline{A}})$, and residuals. The residual surface for $\underline{r}_s$ = 2 is shown in Figure VII.8C.

The suspected absorbers to be used in fitting the eigenvectors in this case (M-analysis) are; the active enzyme (337 nm), the inactive species (420 nm), the exponential fast growth at 420 nm (first 600 mSec of the reaction, see Chapter IV), and pyridoxal-p which may have possibly been released from the deactivated enzyme.

D.2. Individual Absorbers

The concentration profiles of the 337- and 420 nm species were found to fit as two of the M-analysis eigenvectors. However, the fits of the exponential fast growth at 420 nm and the spectrum of the 382 nm absorber were unsatisfactory. Also, the static spectrum of pyridoxal-p obtained under the same experimental condition did not fit as one of the M-analysis eigenvectors. It should also be mentioned that no intermediate was observed in the reaction over
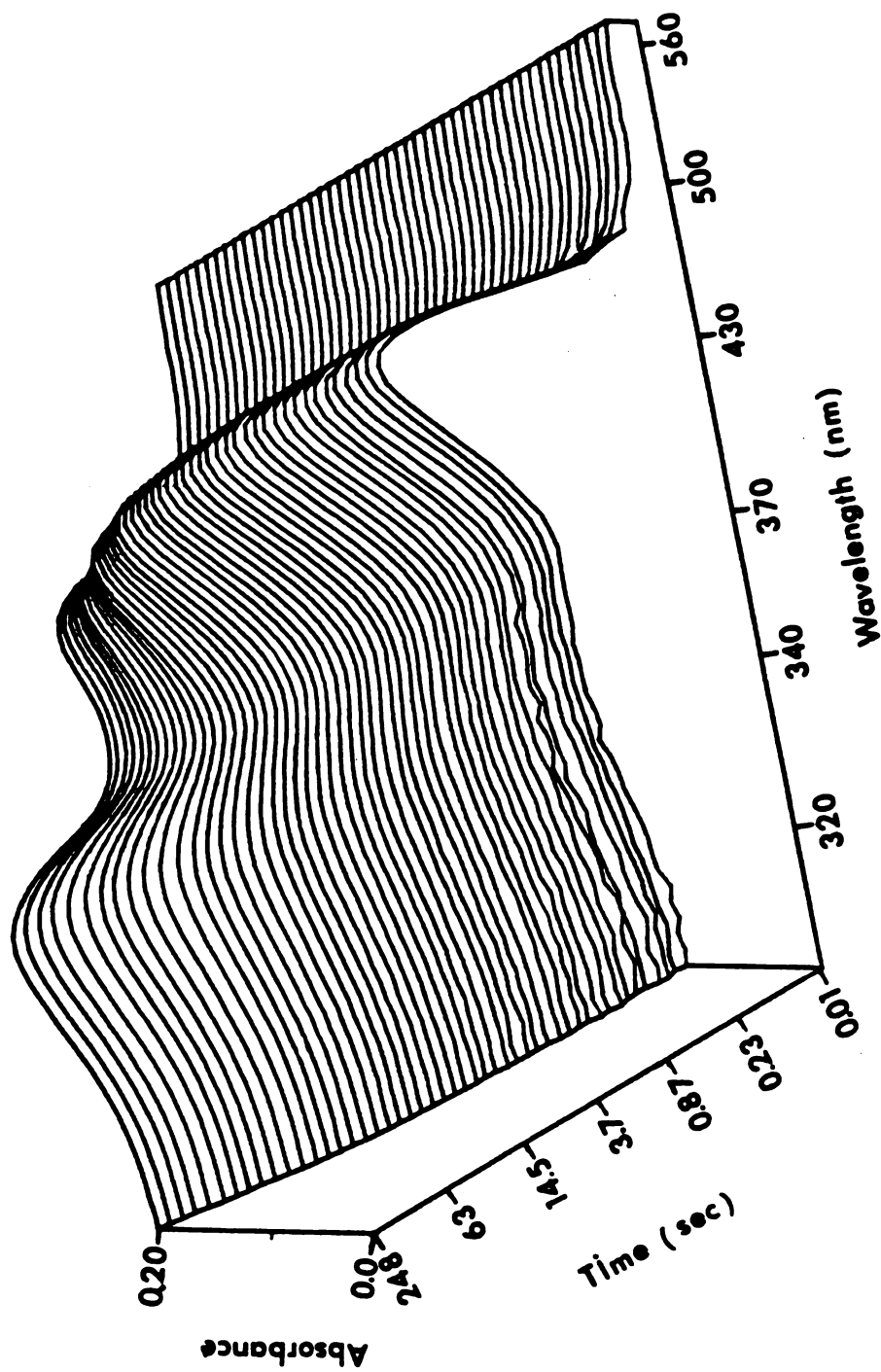
Figure VII.7. Experimental absorbance-wavelength-time surface for the reactivation of 2.0 mg.ml^{-1} tryptophanase by 33.0 mM free K$^+$ at pH=8.70. Cell path length=1.85 cm, t=23±1°C.
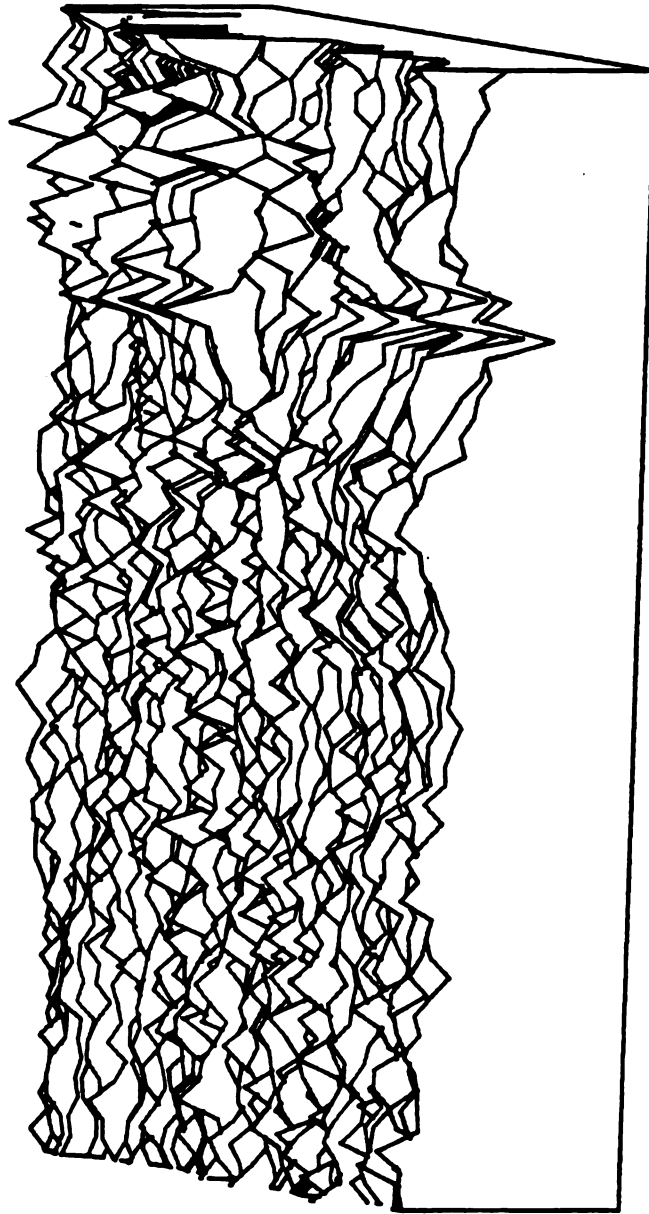
Figure VII.8B. Residuals ($\hat{\underline{A}}_{(3)}$ – $\underline{A}$) of the data presented in Figure VII.7.

the wavelength region used in this experiment, thus, ruling out the possibility of an intermediate being the other absorber in the experiment.

The results probably suggest that K^+ binding to the inactive enzyme to some extent perturbs the spectrum of the enzyme, so that in fact two absorbers with maxima close at 420 nm contribute to the absorbance surface. Since the 337 and 420 nm absorbing species are found to be two of the absorbers in M-analysis, we can also check their individual static spectra against S-analysis eigenvectors to see if the two absorbers have linearly independent rates. Such a fit was found to be unsatisfactory in either case, indicating that the time rate of the concentration of the 337 nm absorber is linearly dependent on that of the 420 nm species.

For a two absorber system that reacts via the mechanism

$$A_1 \xrightarrow{k} A_2$$

where $\underline{f}_1$ and $\underline{f}_2$ (static spectra) are linearly independent, M-analysis gives $\underline{r}_m = 2$ whereas S-analysis gives $\underline{r}_s = 1$ because of the constraint

$$\dot{\underline{c}}_1 + \dot{\underline{c}}_2 = 0$$

In such a case, Cochran has shown that the combination $\underline{f}_{proposed} = (\underline{f}_1 - \underline{f}_2)$ would fit as an "absorber" with a linearly independent rate in S-analysis (98). To check this, $(\underline{f}_{337} - \underline{f}_{420})$ was proposed as an absorber and was tested against S-analysis eigenvectors. The

fit is shown in Figure VII.9, indicating that the proposed spectral shape is an absorber with a linearly independent rate. Thus, we can conclude that the 337 nm form is directly produced from the 420 nm species upon reactivation by K^+. Once again, this is in agreement with the experimental observation that no intermediate was detected in the experiment and that the growth of the absorbance at 337 nm is quantitatively mirrored by the decay at 420 nm.

E. **PCA on the Reactivation of Deactivated Enzyme with a (K^+- Ethionine Mixture)**

The characteristics of this reaction are discussed in Chapter V. The major changes in this experiment are at 420 nm (due to inactive enzyme) and 508 nm (due to formation of the quinonoid structure). PCA was performed on data collected in the wavelength region 320-550 nm at two free K^+ concentration of 16 and 42 mM. The results were found to agree with each other. The experimental absorbance-wavelength-time data surface is shown in Figure VII.10A for the re-action of 2.0 mg/ml deactivated enzyme with a K^+-ethionine mixture containing 16 mM free K^+ and 8 mM L-ethionine (after the push).

E.1. **Number of Absorbers**

M-analysis gave again a value of 3 for the rank of $\underline{M}$. This was concluded from a reconstruction of the absorbance surfaces with r = 2 and r = 3 (Figure VII.10B). It can be seen that for r = 3, the reconstructed surface faithfully reproduces the data in Figure VII.10A.
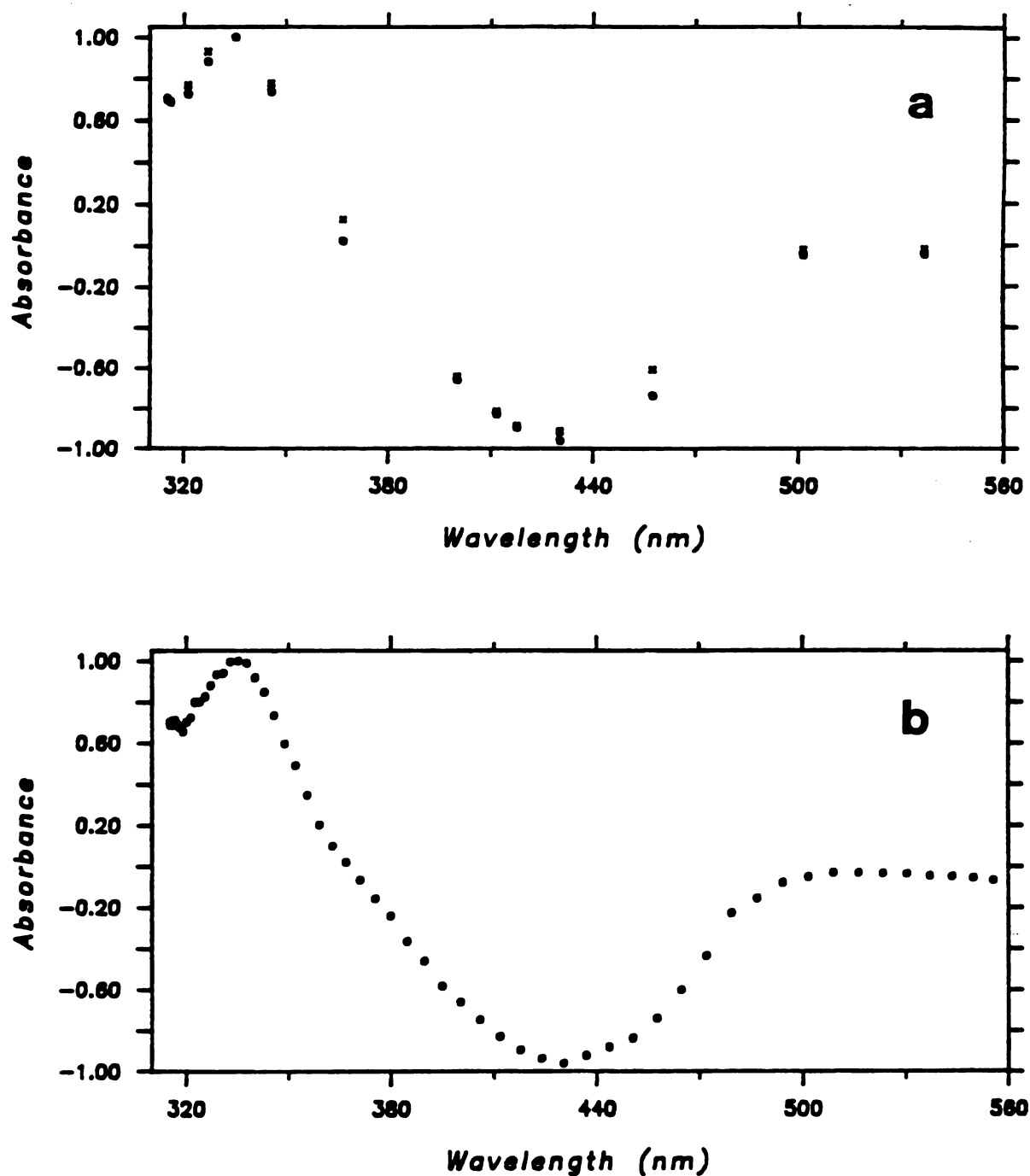
Figure VII.9. (A) S-analysis fit of the $\underline{f}_{prop} = (\underline{f}_{337} - \underline{f}_{420})$ in trypto-
phanase reactivation by K^+ using two eigenvectors. X's
are the proposed spectrum and ●'s are the estimated
points. (B) Estimated spectrum $(\underline{f}_{337} - \underline{f}_{420})$. The $\underline{f}$'s
are the static spectra of the two absorbers.
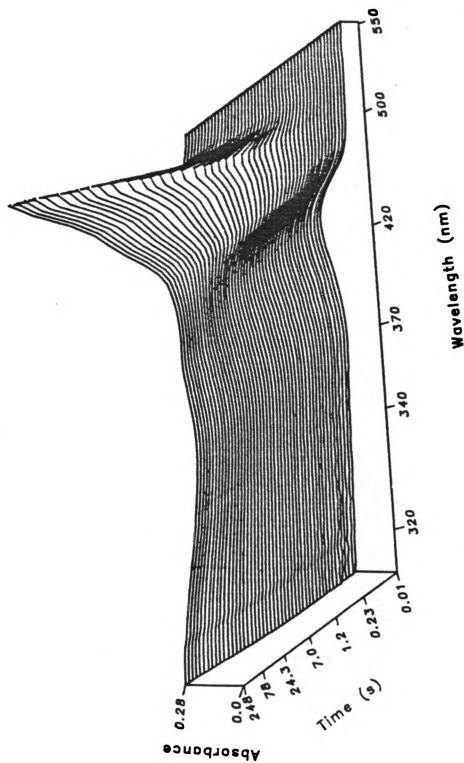
Figure VII.10A. Experimental absorbance-wavelength-time surface for the reaction of 2.0 mg.ml^{-1} deactivated (K$^+$ free) tryptophanase by a K$^+$-Ethionine mixture containing 16.0 mM free K$^+$ and 8 mM L-Ethionine. pH = 8.75 (Bicine). t = 23±1°C.
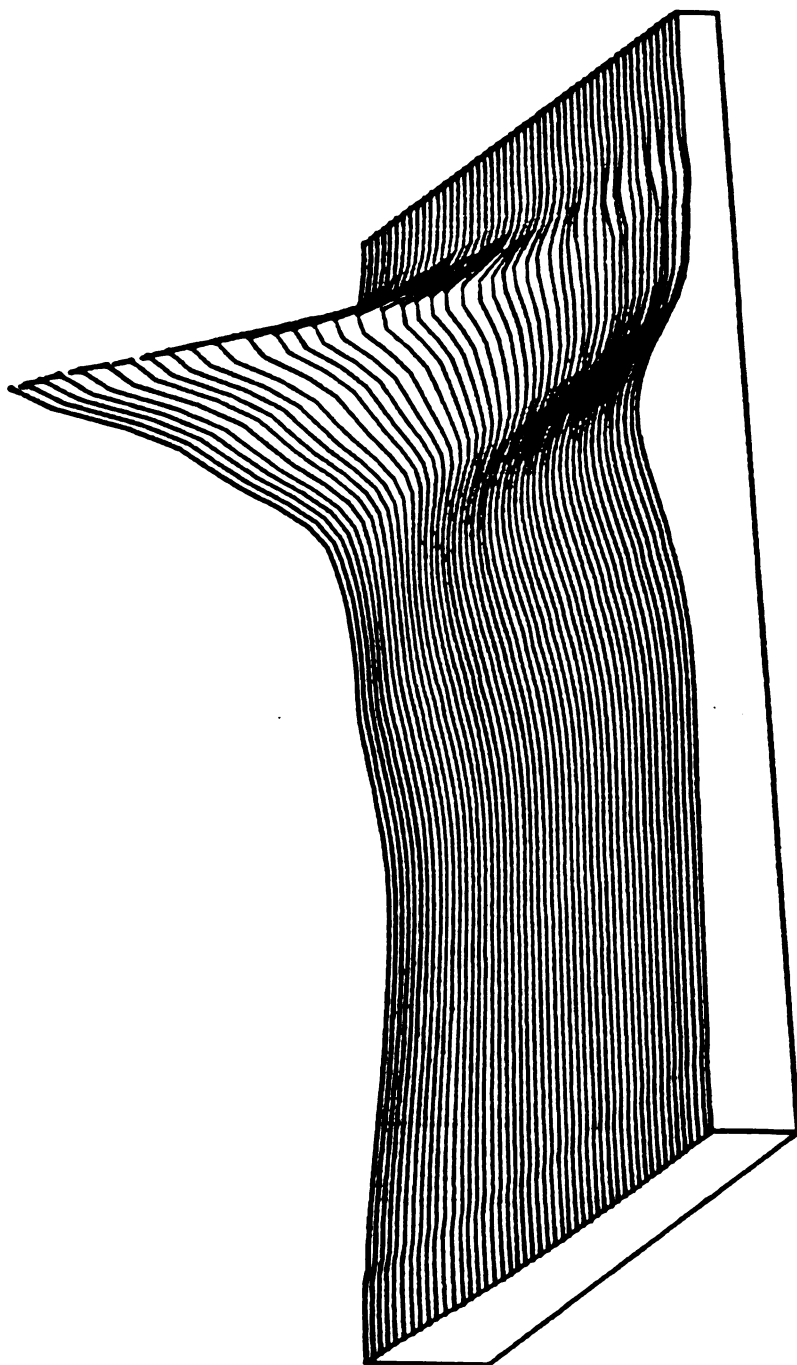
Figure VII.10B.   PCA reconstructed surface of the data presented in Figure VII.10A using three eigenvectors in M-analysis.

Furthermore, examination of the residual surfaces for $r_M = 2$ and $r_M = 3$, shown in Figure VII.11A and Figure VII.11B, respectively, confirms the assignment, $r_m = 3$. Also, the values of the function $Q_r/(N-r)(p-r)$ were 2972.2, 34.3, and 1.5 for the first three eigenvectors. The value of this function for the fourth eigenvector was 0.90, indicating that $r_m = 3$. S-analysis of the same data indicated that there are also three components that independently change their concentrations with time, thus $r_s = 3$. This, again, was concluded from examination of reconstructed absorbance surfaces, shown in Figures VII.12A and Figure VII.12B for the experimental difference surface and three eigenvector reconstructed difference surface, and residuals, shown in Figures VII.13A and VII.13B for $r_s = 2$ and $r_s = 3$, respectively. This value of r_s was further confirmed by the values of $Q_r/(N-r)(p-r)$ for $r_s = 1$ to 4, which were 59.5, 5.3, 1.4 and 0.6, respectively, indicating $r_s = 3$. The possible absorbers in this case are the quinonoid species, the 420 and 337 nm absorbing species and pyridoxal-p.

E.2. Individual Absorbers

Since L-ethionine is a dead-end inhibitor, it binds the enzyme without further reaction. Thus, the final spectrum collected in a scanning experiment (infinity spectrum) was used as the proposed spectrum for the quinonoid. This spectrum was found to fit as one of the M-analysis eigenvectors (Figure VII.14). The fit of the spectra of pyridoxal-p and the 337 nm absorber were, however unsatisfactory. The fit to the 420 nm absorbing spectrum
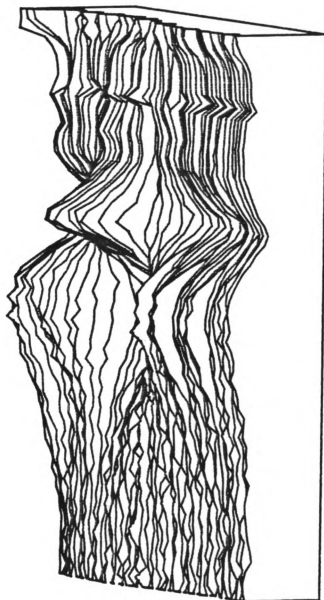
Figure VII.11A. Residuals $(\hat{\underline{A}}_{(2)} - \underline{A})$ of the data presented in Figure VII.10A.

221
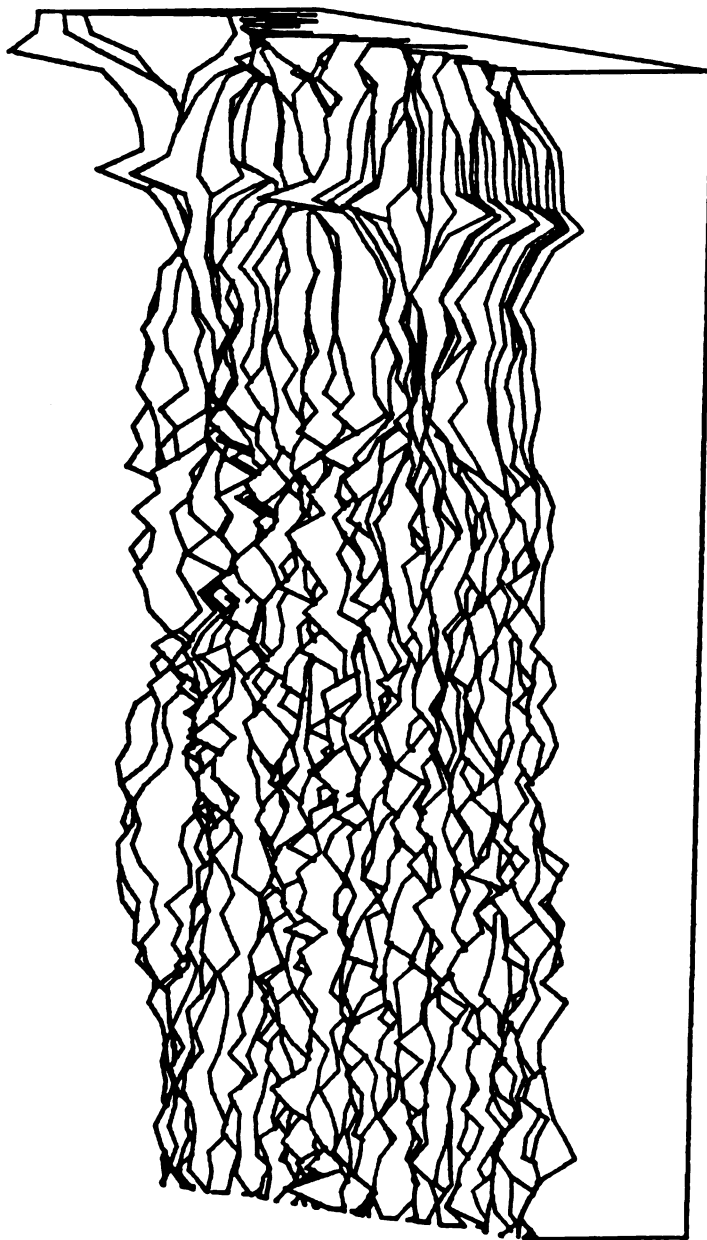
Figure VII.11B. Residuals ($\hat{\underline{A}}_{(3)}$ − $\underline{A}$) of the data presented in Figure VII.10A.
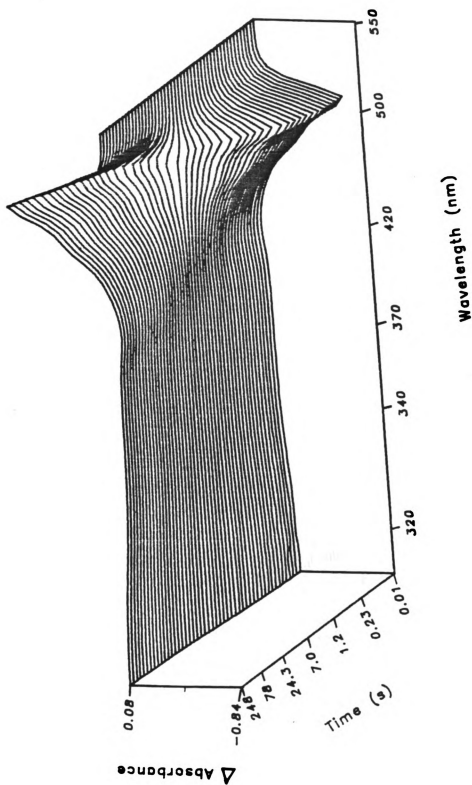
Figure VII.12A. Experimental difference surface of the data represented in Figure VII.10A. Δ Absorbance refers to $(\underline{A} - \overline{\underline{A}})$ where $\overline{A}_{ij} = \frac{1}{N} \sum_{k=1}^{N} A_{ik}$ is the average absorbance at the wavelength channel i.
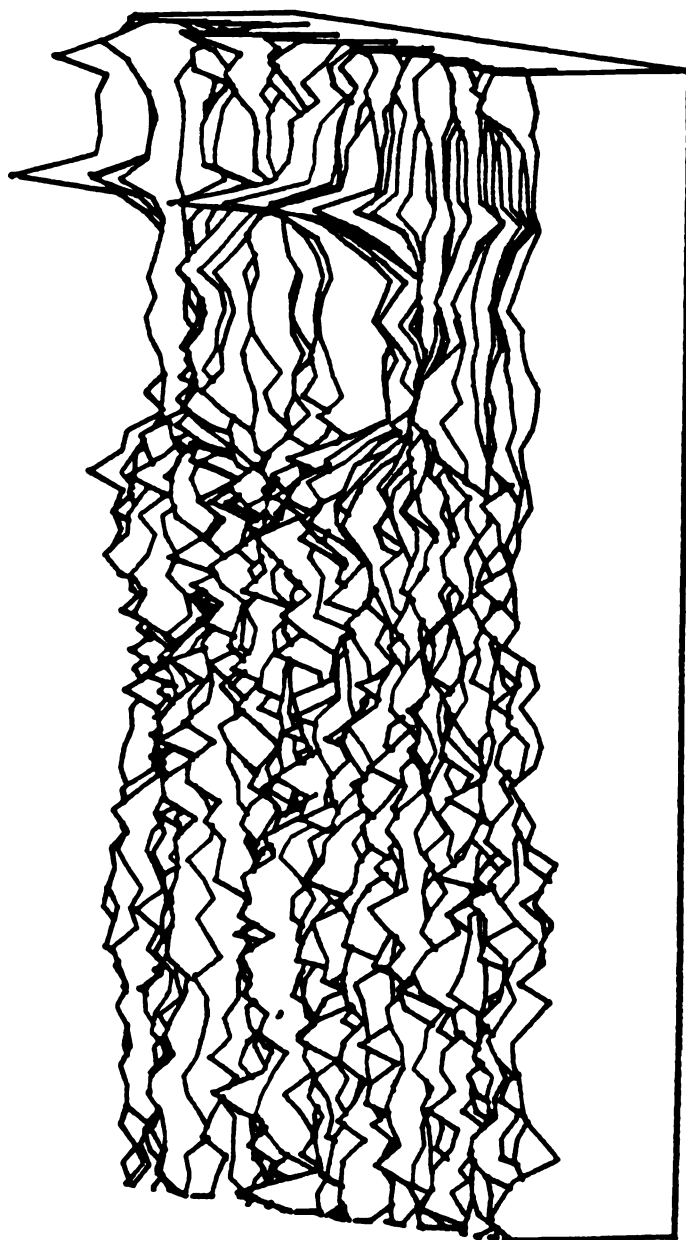
Figure VII.13B.   Three eigenvectors S-analysis residuals of the data represented in Figure VII.10A.
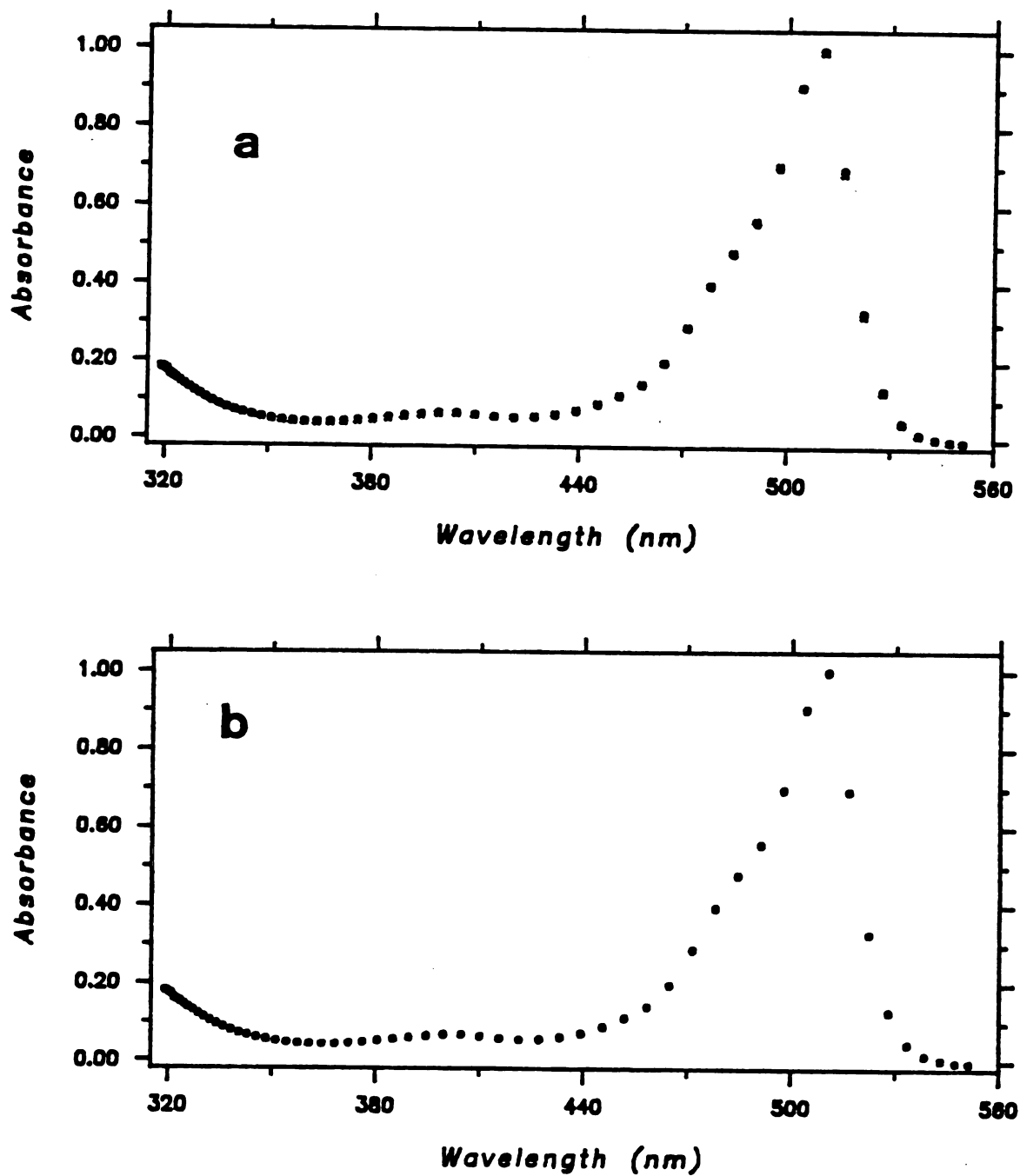
Figure VII.14. (A) M-analysis fit of the quinonoid spectrum from the data presented in Figure VII.10A. Three eigenvectors were used in the fit. (B) Estimated spectrum. The spectra are normalized.

was acceptable, but it was not as good as the quinonoid fit. The same fit using four eigenvectors, however, was completely randomized. This may be explained in two ways:

1. The experiment contains four independent absorbers.
2. The K^+-free enzyme may have partially formed a Schiff's base with the inhibitor, L-ethionine.

The first possibility can be ruled out based on the discussions in the previous section (E.1). However, formation of a Schiff's base between K^+-free enzyme and the substrate has already been reported for tryptophanase (77). Such a reaction is accompanied by a change in the circular dichroic spectrum but no major change in the absorption spectrum of the enzyme occurs. Therefore, the proposed spectrum used in the fit may in fact be a composite spectrum of two absorbers, namely the K^+-free enzyme and the enzyme-ethionine complex, each of which has a maximum at or near 420 nm.

The S-analysis fit to the quinonoid spectrum was also satisfactory, indicating that it is one of the absorbers with a linearly independent rate. The K^+-free enzyme and the enzyme Schiff's base complex may be the other two probable absorbers in S-analysis. More information about the nature of the absorber(s) at 420 nm is needed in order to sufficiently and completely resolve these data.

F. Conclusions

The work presented here demonstrates the application of PCA to three different stopped-flow experiments. In the deactivation with

18-crown-6, PCA provides resolution of the independent spectral shapes of the components of tryptophanase. These spectral shapes, which were deduced from PCA without any mechanistic assumption, agree well with the reported assignments for the components of the enzyme. In the M-analysis for the reactivation experiment, three independent absorbers are required to allow reproduction of the absolute experimental surface. S-analysis gave only two components that change concentration independently with time. This was interpreted by postulating that K^+ binding to the inactive 420 nm perturbs the spectrum of the enzyme which in turn is dictated as two absorbers in PCA analysis. In the reactivation experiment with L-ethionine present, three independent absorbers were again the minimum number required by both M- and S-analysis. The quinonoid species was found to be one of the absorbers in each case. The K^+-free enzyme and the enzyme (K^+-free)-ethionine Schiff's base complex are suggested as the other two absorbers.

A final point regarding the power of the PCA method is worth mentioning here. In fitting a suspected absorber to the PCA eigenvectors, one does not need the spectrum of the absorber over the whole wavelength region of the experiment. However, once a given absorber has been shown by principal component analysis to appear in the experiment, its spectral shape across the entire wavelength region of the experiment is estimated by PCA. This is particularly useful in cases where only a limited range of wavelength channels is available for the proposed spectrum.

CHAPTER VIII

SUGGESTIONS FOR FUTURE WORK

The work presented here demonstrated the potential of using crown-ethers (and to some extent cryptands) as complexing agents for inorganic monovalent cations in studies of enzyme activation/deactivation by such cations. Application of this work to other enzymatic systems which require these cations, such as β-tyrosinase, should further test the usefulness of this new method for the studies of enzyme activation-deactivation by monovalent cations. Structural information coupled with the kinetic data on activation/deactivation of the enzyme by monovalent cations should provide an in depth picture of the specific role of the cation in the enzyme structure as well as its role in enzyme catalysis. Binding of 2 K^+ ions per subunit of tryptophanase as shown in this work proves a specific role for the cation, rather than a nonspecific conformational effect.

Since the spectral forms of tryptophanase are pH-dependent as discussed in the text, the activation/deactivation experiments should be carried out at several pH values. The practical pH range in such studies is, however, limited because of the fact that the 420 nm form of the active enzyme dominates the absorption spectrum (absorbing in the same wavelength range as the inactive enzyme. Thus, the

overall absorbance change is drastically reduced (83).

The enzyme concentration dependence of the activation and de-activation (in the presence of ethionine) should also be examined to see what effect the enzyme concentration might have on the rate constants. Application of PCA to this and other systems mentioned above should be useful in understanding the activation mechanism of these enzymes. PCA, when supplied with sufficient target absorbers (spectral shapes or concentration profiles), can completely resolve scanning stopped-flow experiments.

It is known that tryptophanase forms a Schiff base, αS, with ethionine in the absence of activating monovalent cations. Even though the absorption spectrum of the inactive enzyme and the Schiff base are similar, their CD spectra are different (77). In order to clearly propose a reliable model for the enzyme activation by the cation, some experimental data on the rate of such SB formation is needed. Such information cannot be obtained by uv-visible studies; however, circular dichroism can yield such information, provided that the scanning rate of the instrument is fast enough to follow the Schiff's base formation.

Finally, attempts on crystallizing tryptophanase, ideally in both active and inactive states, to get the x-ray structure of the enzyme is suggested.

REFERENCES

REFERENCES

1. Mahler, H. R. and Cordes, E. H., (1971), *Biol*. *Chem*., 2nd ed. Harper & Row Publishers, New York.

2. Kennedy, B., (1979), Ph.D. Dissertation, Michigan State University.

3. Metzler, D. E., and Snell, E. E., (1952), J. Biol. Chem. 198, 363-373.

4. Martell, A. E., Proceedings of Symposium on Pyridoxal Catalysis, 1979, Toronto, Canada, 163.

5. Metzler, D. E., (1977) Biochemistry; The Chemical Reactions of Living Cells, Academic Press, New York.

6. Matsuo, Y., (1957), J. Am. Chem. Soc., 79, 2011-2015.

7. Jenkins, W. T., and Sizer, I. W., (1957), J. Am. Chem. Soc. 79, 2655-57.

8. Churchich, J. E., (1965), Biochemistry, 4, 1405-10.

9. Klein, S. M., and Sagers, R. D. (1966), J. Biol. Chem. 241, 206-9.

10. Snell, E. E., Adv. Enzymol. Relat. Areas Mol. Biol., (1975), 42, 287.

11. Fasella, P. (1967) Ann. Rev. Biochem. 36, 185.

12. Snell, E. E. and Dimari, S. J. (1970), The Enzymes, Vol. 2, 3rd ed. 335.

13. Boyer, P. D., (1970). Academic Press, New York, P335.

14. Matsuo, Y. and Greenberg, D. M. (1959), J. Biol. Chem. 234, 507.

15. Fischer, E. H. and Krebs, E. G., (1966), Federation Proc. 25, 1511.

16. Hughes, R. C., Jenkins, W. T., and Fischer, E. H., (1962), Proc. Natl. Acad. Sci, U.S. 48, 1615.

17. Schirch, L. G., and Mason, M., (1963) J. Biol. Chem. 238, 1032.

18. Dempsy, W. B. and Snell, E. E. (1963), Biochemistry, 2, 1414.

19. Metzler, D. E., M. Ikawa and Snell, E. E., (1954), J. Am. Chem. Soc. 76, 648.

20. Braunstein, A. E., and M. M. Shemyakin, (1953) Biokhimiya, 18, 393.

21. Snell, E. E., (1958) Vitamines and Hormones, 16, 77.

22. Braunstein, A. E., (1960). The Enzymes, ed. P. D. Boyer, H. Lardy, and K. Myrback, Vol. 2, 113.

23. Perault, A. M., B. Pullman, and C. Valdemoro, (1961) Biochem. Biophys. Acta, 46, 555.

24. Schleicher, E., Mascaro, K., Potts, R., Mann, D. R., and Floss, H. G., (1976), J. Am. Chem. Soc. Vol 984, 1043.

25. June, D. S., (1979), Ph.D. Dissertation Thesis, Michigan State University.

26. Wada, H. and Snell, E. E., (1962), J. Biol. Chem., 237, 145.

27. Snell, E. E. (1970) Vitamins and Hormones, 28, 265.

28. Ivanov, V. I. and Karpeisky, M. Y., (1969), Advance in Enzymology, 32, 21.

29. Schnackerz, K. D. and Snell, E. E. (1983), J. Biol. Chem. 258, 4839-4841.

30. Dunathan, H. C., (1966), Proc. Natl. Acad. Sci, U.S.A. 55, 712.

31. Dunathan, H. C., (1971) Adv. Enzymol., 35, 79.

32. Corey, E. J., and Sneen, R. A. (1956) J. Am. Chem. Soc., 78, 6269.

33. Vederas, J. C. and Floss, H. G. (1980). Acc. Chem. Res. 13, 455-463.

34. Tsai, M. D., Weintraub, H. J. R., Byrn, S. R., Chang, C. and Floss, H. G., (1978), 17, 3183-3188.

35. Harris, C. M., Johnson, R. J., and Metzler, D. E., (1976) Biochem. Biophys Acta, 421, 181.

36. Metzler, C. M., Cahill, A., and Metzler, D. E. (1980), J. Am. Chem. Soc. 102, 6075-6082.

37. Johnson, R., and Metzler, D. E., (1970) Methods. Enzymol., 18A, 433.

38. Morozov, Yu. V., Bazhulina, N. P., Cherkashina, L. P. and Karpieski, M. Ya., (1967) Biofizika, 12, 397.

39. Morozov, Yu. V., Bazhulina, N. P., and Karpeiski, M. Ya, (1967), Biofizika, 12, 454.

40. Davis, L. and Metzler, D. E., (1972) The Enzymes (Boyer, P. D.) Vol. 7, 33-74.

41. Nencki, M. (1875), Ber. 8, 336.

42. Kühne, M. (1875), Ber., 8, 206

43. Hopkins, F. G., and Cole, W. S. (1903), J. Physiol., 29, 451.

44. Hopkins, F. G., and Cole, W. S. (1901), J. Physiol., 27, 418.

45. Happold, F. C. and Hoyle, L. (1935), Biochem. J., 29, 1218.

46. Happold, F. C. and Struyvenberg, A. (1954) Biochem. J. 58, 379.

47. Wada, H., (1958) Proc. Intem. Symp. Enz. Chem. Maruzen, Tokyo, 148.

48. Wood, W. A., Gunsalus, I. C., and Umberit, W. W., (1947), J. Biol. Chem. 170, 313.

49. Happold, F. C., (1950) Adv. in Enzymol. Relat. Subj. Biochem. Vol. 10, 51-82.

50. Wada, H. (1964) Tryptophan Metabolism, Vol. 1, Sekai Hoken Tsushinsha, Ltd., Osaka, Japan, 77-92.

51. Snell, E. E., (1975). Adv. Enzymol. Relat. Area. Mol. Biol., 42, 287.

52. DeMoss, R. D. and Moser, K. (1969), J. Bact. 98, 167.

53. Newton, W. A., and Snell, E. E. (1962), Proc. Nat. Acad. Sci. U.S.A., 48, 1431-1439.

54. Yanofsky, C., and Crawford, I. P. (1959) Proc. Nat. Acad. Sci. U.S., 45, 1016.

55. Newton, W. A., and Snell, E. E. (1965), J. Bact. 89, 355.

56. Neuton, W. A., and Snell, E. E. (1964). Proc. Nat. Acad. Sci. U.S., 51, 382.

57. Kagamiyama, H., Wada, H., Matsubara, H. and Snell, E. E., (1972), J. Biol. Chem., 247, 1571.

58. Newton, W. A. and Morino, Y. and Snell, E. E. (1965), J. Biol. Chem. 240, 1211.

59. Morino, Y. and Snell, E. E. (1967), J. Biol. Chem., 242, 5591-5601.

60. Morino, Y. and Snell, E. E. (1967), J. Biol. Chem., 242, 5602.

61. London, J. and Goldberg, M. E. (1972), J. Biol. Chem. 247, 1566.

62. Morino, Y. and Snell, E. E. (1967), Biochem. J., 57, 1692-1699.

63. Hogberg-Raibaud, A., Raibaud, O. and Goldberg, M. E. (1975) J. Biol. Chem. 250, 3352.

64. Deeby, M. C. and Yanofsky (1981) J. Bacteriol. 147, 787-796.

65. Morino, Y. and Snell, E. E., (1967) J. Biol. Chem. 242, 2800.

66. Kagamiyama, H., Morino, Y. and Snell, E. E. (1970) J. Biol. Chem. 245, 2819.

67. Gopinathan, K. P., and DeMoss, R. D., (1968) Biochem. 7, 1685.

68. Watanabe, T. and Snell, E. E. (1972) Proc. Natl. Acad. Sci. U.S. 69, 1086.

69. Raibaud, O. and Goldberg, M. E. (1973) J. Biol. Chem. 248, 3451.

70. Skyzynia, C., London, J. and Goldberg, M. E. (1974), J. Biol. Chem. 249, 2325.

71. Raibaud, O., and Goldberg, M. E. (1976) J. Biol. Chem. 251, 2820.

72. Raibaud, O., and Goldberg, M. E. (1976) J. Biol. Chem., 251, 2814.

73. Boyer, P. D., Lardy, H. H. and Phillips, P. H. (1942), J. Biol. Chem. 146, 673-682.

74. Suelter, C. H. (1970) Science, 168, 789-795.

75. Suelter, C. H. (1974). In Metal Ions in Biological Systems, Vol. 3, High Molecular Complexes. H. Segel, Editor Marcel Dekker, Inc. 201-251.

76. Toraya, T., Nihira, T. and Fukui, S. (1976) Eur. J. Biochem. 69, 411-419.

77. Suelter, C. H. and Snell, E. E. (1977) J. Biol. Chem. 252, 1852-57.

78. Nowak, T. and Suelter, C. H. (1981) Molecular and Cellular Biochem. 35, 65-75.

79. Matsuo, Y. (1957), J. Am. Chem. Soc., 79, 2011-2015.

80. Heinert, D., and Martell, A. E. (1962) J. Am. Chem. Soc., 84, 3257-3263.

81. June, D. S., Kennedy, B., Behbahani-Nejad, I., Pierce, T., Halaka, F.,El-Bayoumi, A., Suelter, C. H., and Dye, J. L. (1979), J. Am. Chem. Soc. 101, 2218.

82. June, D. S., Suelter, C. H., and Dye, J. L., (1981) Biochemistry, 20, 2707.

83. June, D. S. (1979) Ph.D. Dissertation, Michigan State University, East Lansing, Michigan.

84. Matsushima, Y. and Martell, A. E. (1967) J. Am. Chem. Soc., 89 1322-1330.

85. Morino, Y. and Snell, E. E. (1967), J. Biol. Chem. 242, 2793-2799.

86. Hall, A. N., Lesson, J. A., Rydon, H. N. and Tweedle, J. C., (1960) Biochem. J., 74, 209.

87. Suelter, C. H., Coolen, R. B., Papadakis, N., and Dye, J. L., (1975), Anal. Biochem. 69, 155-163.

88. Hillebrand, G. G., Dye, J. L., and Suelter, C. H. (1979) Biochem, 18, 1751-1755.

89. June, D. S., Suelter, C. H. and Dye, J. L. (1981) Biochemistry, 20, 2714.

90. Elias, S. (1983) Ph.D. Dissertation, Michigan State University, East Lansing, Michigan.

91. Papadakis, N., Coolen, R. B., and Dye, J. L. (1975) Anal. Chem. 47, 1644.

92. Coolen, R. B., Papadakis, N. Avery, J. Enke, C. G., and Dye, J. L. (1975) Anal. Chem. 47, 1649.

93. Suelter, C. H., Coolen, R. B., Papadakis, N., and Dye, J. L. (1975). Anal. Biochem. <u>69</u>, 155.

94. Cox, R. P., andHollaway, M. R. (1977) Eur. J. Biochem. <u>74</u>, 575.

95. Halaka, F. G., Babcock, G. T. and Dye, J. L. (1981) J. Biol. Chem., <u>256</u>, 1084.

96. Ho, G. H., Dye, J. L., and Suelter, C. H. (1981), J. Biochem. Biophys. Meth. <u>4</u>, 287-298.

97. Dye, J. L. and Feldman, L. H. (1966) Rev. Sci Instrum. <u>37</u>, 154.

98. Cochran, R. N. (1977) Ph.D. Dissertation, Michigan State University, East Lansing, Michigan.

99. Halaka, F. G., (1981), Ph. D. Dissertation, Michigan State University, East Lansing, Michigan.

100. Behbahani-Nejad, I., Suelter, C. H. and Dye, J. L. (1983), Current Topics in Cellular Regulation, Vol. <u>24</u>, 219.

101. Moore, C. and Pressman, B. C. (1964) Biochem. Biophys. Res. Comm. <u>15</u>, 562.

102. Izatt, R. M., Nelson, D. P., Rytting, J. H., Haymore, B. L. and Christensen, J. J. (1970), J. Am. Chem. Soc., 13:7, 1619.

103. Pederson, C. J. (1967), J. Am. Chem. Soc., <u>89</u>, 7017.

104. Pederson, C. J. (1971) J. Org. Chem., <u>36</u>, 254.

105. Dietrich, B., Lehn, J. M. and Sauvage, J. P. (1969), Tetrahedron Lett., 2885.

106. Lehn, J. M. (1978) Acc. Chem. Res., <u>11</u>, 49.

107. Van Eck, B., (1983) Ph.D. Dissertation, Michigan State University, East Lansing, Michigan

108. Dye, J. L., DeBacker, M. G. and Nicely, V. A. (1970), J. Am. Chem. Soc. <u>92</u>, 5226.

109. Dye, J. L., Lok, M. T., Tehan, F. J., Coolen, R. B., Ceraso, J. M. and DeBaker, M. G., (1971) Ber. Bunsenges Phys. Chem. <u>75</u> 659.

110. Izatt, R. M., Rytting, J. H., Nelson, D. P., Haymore, B. L., and Christensen, J. J. (1969) Science, <u>164</u>, 443.

111. Eisenman, G., Ciani, S. M., Szabo, G., _ibid_, 1289.

112. Tosteson, D. C., _ibid_, 1269.

113. Pederson, C. J. (1970) J. Am. Chem. Soc., <u>92</u>, 391.

114. Lehn, J. M. and Sauvage, J. P. (1971) Chem. Comm. <u>440</u>.

115. Dietrich, B., Lehn, J. M. and Sauvage, J. P. (1973) Chem. Comm. <u>15</u>.

116. Wong, K. H., Konizer, G., and Smid, J. (1970) J. Am. Chem. Soc. <u>92</u>, 666.

117. Bush, M. A., and Truter, M. R. (1972), J. Chem. Soc., 340.

118. Wing, R. M., and Eiss, R. (1970) J. Am. Chem. Soc.; <u>92</u>, 1929.

119. Christensen, J. J., Eatough, D. J., and Izatt, R. M. (1974), Chem. Rev., <u>74</u>, No. 3.

120. Shaltiel, S. and Er-el, Z. (1973) Proc. Nat. Acad. Sci, U.S.A. <u>70</u>, 778.

121. Axen, R., Porath, J. and Ernback, S. (1967) Nature, 214, 1302.

122. Watanabe, T., and Senell, E. E. (1972) Proc. Natl. Acad. Sci, U.S.A. <u>69</u>, 1086-1090.

123. Suelter, C. H., Wang, J., and Snell, E. E. (1976) Anal. Biochem., <u>76</u>, 221-232.

124. Lowry, O., Rosenbrough, H., Farr, N. J., and Randall, R. J. (1951) J. Biol. Chem. <u>193</u>, 265-275.

125. Boyland, E., Manson, D., and Nery, R. (1962) J. Chem. Soc. (London) 606-612.

126. Gokel, G. W., Cram, D. J., Liotta, Col. Harris, H. P. and Cook, F. L., (1974), J. Org. Chem., <u>39</u>, 2445.

127. Hartridge, H. and Roughton, F. J. W. (1923), Proc. R. Soc. Lond. Ser. A., <u>104</u>, 376.

128. Chance, B. (1940) J. Franklin Inst., <u>229</u>, 455.

129. Crouch, S. R., Holler, F. J. and Notz, P. K. (1977) Appl. Spec. Rev., <u>13(2)</u>, 165.

130. Malmstadt, H. V. (1979), Topics in Automated Chemical Analysis, Vol. 1, Holsted Press, N.Y., 1979.

131. Dye, J. L. and Feldman, L. H. (1966) Rev. Sci. Inst., 37, 154.

132. Ho, G. H., (1976) Ph.D. Dissertation, Michigan State University, East Lansing, Michigan.

133. Papadakis, N. (1974), Ph.D. Dissertation, Michigan State University, East Lansing, Michigan.

134. Coolen, R. B. (1974), Ph.D. Dissertation, Michigan State University, East Lansing, Michigan.

135. Wiskend, H. K. (1964) in Rapid Mixing and Sampling Techniques in Biochemistry, Appendix I, p. 356.

136. Nakamura, T. (1971) J. Biochem., 70, 691.

137. Dye, J. L., and Nicely, V. J. (1971) J. Chem. Educ., 48 443.

138. Cochran, R. N., Horne, F. H., Dye, J. L., Ceraso, J. and Suelter, C. H. (1980) J. Phys. Chem. 84, 2567.

139. Cochran, R. N., Horne, F. H. (1980) J. Phys. Chem. 84, 2561.

140. Cochran, R. N., Horne, F. H. (1977) Anal. Chem. 49, 846.

141. Rozett, R. W. and Peterson, E. M., (1975) Anal. Chem. 47, 1301.

142. Ritter, G. L. Lowry, S. L., Isenhour, T. L., and Wilkins, C. L., (1976) Anal. Chem., 48, 591.

143. Vadasdi, K., (1974). J. Phys. Chem. 78, 816.

144. Kankare, J. (1970) J. Anal. Chem. 42, 1322.

145. Sylvester, E. A., Lawton, W. H. and Maggio, M. S. (1974) Technometrics, 16, 353.

146. Bulmer, J. T.,and Shurrell, H. F., (1973) J. Phys. Chem. 77, 256.

147. Bellman, R. (1970) Introduction to Matrix Analysis, 2nd ed. McGraw-Hill, New York.

148. Lamb, D. L., Izatt, R. M., Christensen, J. J., and Eatough, D. J., (1979). In "Coordination Chem. of Macrocyclic Compounds" (G. A. Melson, ed.), pp. 145-218, Plenum, New York.

149. Watanabe, T. and Snell, E. E. (1977). J. Biochem. 252, 1852-1857.

150. Arrio-Dupont, M. (1972) Eur. J. Biochem. 30, 307-317.